Engineering Stable Bacteriophage Dosage Forms Active Against Antibiotic-Resistant Bacteria for Respiratory Delivery and Food Safety Applications

by

Nicholas Benjamin Carrigy

A thesis submitted in partial fulfillment of the requirements for the degree of

Doctor of Philosophy

Department of Mechanical Engineering
University of Alberta

Abstract

The topic of this thesis is the engineering of stable bacteriophage dosage forms that are active against antibiotic-resistant bacteria for applications in respiratory delivery and food safety. Experimental methods and theoretical models are developed to test and understand the effects that various factors have on the biological stability and delivery of bacteriophages manufactured and aerosolized by various techniques.

Chapter 1 provides an introduction to the engineering of stable spray dried biologic powder for respiratory delivery. Descriptions of the processes that spray dried powder undergoes during development, manufacturing, and delivery are discussed. Processes covered include purification and formulation, atomization, solvent evaporation and particle formation, particle collection and analysis, aerosolization, and lung deposition. Additionally, particle engineering models, amorphous glass stabilization, spray dryer process models, and development of a supplemented phase diagram are reviewed.

Chapter 2 describes the development of a solid dosage form of anti-*Campylobacter* bacteriophages produced by spray drying. The effect that various factors such as purification technique, temperature, formulation, and atomization method have on bacteriophage inactivation are explored. Development of a method for packaging, shipping, and storing the powder at ambient temperature without inactivating the bacteriophage is detailed. The main inactivating stress is shown to be desiccation. The use of amorphous shell forming excipients is proposed to counter this stress and increase biological stability. Two fully amorphous formulations, trileucine and trehalose, and pullulan and trehalose, prove to outperform the standard leucine and trehalose formulation commonly used in the literature. Particle formation mechanisms are proposed for the different formulations tested.

Chapter 3 provides further characterization of the fully amorphous dry dosage form containing pullulan and trehalose in terms of manufacturability, physical stability, device compatibility, and aerosol performance. A multi-component analytical particle formation model is developed to estimate the time that a microdroplet evaporates prior to co-solidification into an amorphous solid phase at the surface. The model is used to predict normalized volume equivalent diameter to reasonable accuracy relative to experimental measurements performed with a monodisperse droplet chain. A radial glass transition temperature model is developed and the model predictions are shown to qualitatively match experimental modulated differential scanning calorimetry measurements on spray dried powder. The solid dosage form is promising for respiratory delivery, as aerosol performance using a dry powder inhaler is better than many commercial solid dosage forms. The powder is also found to be physically stable in propellant loaded into a pressurized metered-dose inhaler.

Chapter 4 provides a comparison of three commercial inhalation devices for the delivery of anti-tuberculosis bacteriophage D29 liquid lysate as an aerosol. A jet nebulizer, vibrating mesh nebulizer, and soft mist inhaler are compared in terms of bacteriophage inactivation and active bacteriophage delivery rate. A mathematical model of liquid recirculation in the jet nebulizer is used to quantify the renebulization and repeated baffle impaction processes the bacteriophage is exposed to in the device. The soft mist inhaler is shown to quickly deliver active bacteriophage, which is useful for self-administration. The vibrating mesh nebulizer is shown to be the best option for delivering large amounts of bacteriophage aerosol for animal studies.

Chapter 5 describes the delivery of active bacteriophage D29 aerosol to the lungs of mice using a nose-only inhalation device adapted for use with a vibrating mesh nebulizer. A dose simulation technique, involving experimental work aerosolizing a tryptophan tracer through the device with

simulated mouse inhalation, is combined with theoretical modeling to predict the dose reaching the lungs of mice. *In vivo* measurements of bacteriophage D29 delivery to the lungs of mice with the nose-only inhalation device are shown to match model predictions. Prophylactic respiratory delivery of active bacteriophage D29 is found to offer significant protection to mice that are subsequently exposed to *Mycobacterium tuberculosis* aerosol.

Chapter 6 summarizes the main conclusions of this research, the new contributions to knowledge, and provides recommendations for future work.

Preface

Chapter 1 is primarily from the published book chapter,

> "Carrigy NB, Vehring R. 2019. Engineering stable spray dried biologic powder for inhalation. Chapter 12 in *Pharmaceutical Inhalation Aerosol Technology, Third Edition,* ed. Hickey AJ, da Rocha SRP. New York: Marcel Dekker, Inc. pp. 291-326."

I wrote the book chapter and my supervisor RV provided edits and feedback.

Chapter 2 will be submitted as 2 journal papers and was partially published as a conference paper,

> "Carrigy NB, Liang L, Wang H, Kariuki S, Nagel TE, Connerton IF, Vehring R. 2018. Mechanistic modeling expedites the development of spray dried biologics, pp. 1551-1558 in *Proceedings of 21st International Drying Symposium.* Cárcel JA, Clemente G, García-Pérez JV, Mulet A, Rosselló C. (eds.) València, Spain: Editorial Universitat Politècnica de València."

I planned the study and carried out the literature review, formulation, atomization, spray drying, packaging, shipping from Canada, scanning electron microscopy, titer analysis, and interpretation of results including statistical analysis, and wrote the first draft of the manuscript. LL performed amplification, purification, air drying, plaque assays, titer reporting, and shipping from England. HW performed Raman spectroscopy. SK and TN provided consultation and coordinated work in Kenya. IC, TN, and RV supervised the study. Rick Conrad helped with adding the potentiometer and negating the safety controls in the B-90 spray dryer.

Chapter 3 is primarily from the published journal paper,

> "Carrigy NB, Ordoubadi M, Liu Y, Melhem O, Barona D, Wang H, Milburn L, Ruzycki CA, Finlay WH, Vehring R. 2019. Amorphous pullulan trehalose microparticle platform for respiratory delivery. *International Journal of Pharmaceutics.* 563:156-168."

I designed the study, conducted the literature review, developed the multi-component analytical particle formation model and the radial glass transition temperature model, completed spray drying experiments and associated scanning electron microscopy, performed aerosol performance measurements, supervised work by other co-authors, analyzed the results, and wrote the first draft of the manuscript. MO developed and ran the multi-component numerical particle formation model, YL and OM performed the monodisperse droplet chain experiments including image analysis, DB carried out the modulated compressed bulk density measurements, HW performed

the pressurized metered-dose inhaler measurements and Raman spectroscopy, LM did the modulated differential scanning calorimetry experiments, CAR trained me on next generation impactor measurements and WHF is his supervisor. RV supervised and provided feedback.

Chapter 4 is primarily from the published journal paper,

> "Carrigy NB, Chang RY, Leung SSY, Harrison M, Petrova Z, Pope WH, Hatfull GF, Britton WJ, Chan H-K, Sauvageau D, Finlay WH, Vehring R. 2017. Anti-tuberculosis bacteriophage D29 delivery with a vibrating mesh nebulizer, jet nebulizer, and soft mist inhaler. *Pharmaceutical Research.* 34:2084-2096."

I carried out the literature review, wrote the paper and designed the study, shipped the lysate to Sydney, performed all dilution stability and aerosolization titer reduction experiments including the plaque assays, developed the mathematical models for nebulization cycle count and titer delivery rate and conducted the associated experiments, and completed statistical analysis. RYC and SSYL provided me with training on plaque assays and generated some of the required stock materials, MH performed amplification, lysate plaque assay prior to shipping to Sydney, and six week refrigerated lysate storage stability, ZP and WHP generated the lysate and shipped it from Pittsburgh to Edmonton, GFH, WJB, and HKC supervised, WHF supervised and provided the nebulizers and soft mist inhaler and helped with results interpretation, and my supervisor RV helped with study design and results interpretation. Helena Orzanscka performed UV-Vis assays.

Chapter 5 is primarily from the submitted journal paper,

> "Carrigy NB, Larsen SE, Reese V, Pecor T, Harrison M, Kuehl PJ, Hatfull GF, Sauvageau D, Finlay WH, Coler RN, Vehring R. Prophylaxis of *Mycobacterium tuberculosis* H37Rv infection in a preclinical mouse model via inhalation of nebulized bacteriophage D29. *Antimicrobial Agents and Chemotherapy.* Submitted April 26, 2019."

I performed all aspects except as follows: SEL performed *in vivo* work at the Infectious Disease Research Institute and helped with writing associated sections; VR and TP were assistants of SEL, and RNC was her supervisor. MH amplified the lysate and DS supervised her. PK suggested the chosen plenum flow rate and suggested design modifications. GH provided advice on study design. WHF lent the unmodified nose-only inhalation device and explained its operation. RV helped with study design and results interpretation. Helena Orzanscka performed UV-Vis assays.

Acknowledgements

My supervisor Prof. Reinhard Vehring has provided constructive advice and feedback regarding my research throughout my degree. He has provided mentorship, introduced me to important contacts in academia and industry, and allowed me to attend international conferences and a six-month research exchange at the University of Sydney in Australia, all of which I am thankful for. My thanks and appreciation go to my fellow Particle Engineering Group members for sharing ideas, friendship, and support. I also thank Luba Slabyj for checking grammar.

Thank you to my supervisory committee members Prof. Warren Finlay and Prof. Dominic Sauvageau for helping guide my progression through the degree and for providing feedback, equipment, and resources invaluable to my research.

My sincere gratitude goes to my research exchange supervisor at the University of Sydney, Prof. Hak-Kim Chan, and members of the Advanced Drug Delivery Group, for being very welcoming and for providing a different perspective on my research.

I am grateful for the help of my many co-authors in academia and industry, MecE shop staff, and nanoFAB staff.

I would also like to thank my caring, supportive family: Colin, Janice, and Alec, as well as my other relatives.

I appreciate the support of my funding sources including the Killam Trust which provided an Izaak Walton Killam Memorial Scholarship, the Natural Sciences and Engineering Council of Canada which provided an Alexander Graham Bell Canada Graduate Scholarship and a Michael Smith Foreign Study Supplement, Alberta Innovates – Technology Futures which provided a Graduate Student Scholarship, and the University of Alberta that provided Queen Elizabeth II scholarships, an Andrew Stewart Memorial Prize, and a Doctoral Recruitment Scholarship.

Table of Contents

List of Tables

List of Figures

1 Introduction

Sections 1.2-1.15 have been published in the book chapter "Carrigy NB, Vehring R. 2019. Engineering stable spray dried biologic powder for inhalation. Chapter 12 in Pharmaceutical Inhalation Aerosol Technology, Third Edition, ed. Hickey AJ, da Rocha SRP. New York: Marcel Dekker, Inc. pp. 291-326."

1.1 Thesis Objectives and Structure

The overarching objective of my research was to improve the way in which bacteriophage dosage forms are manufactured and delivered in respiratory and food safety applications. The term dosage form refers to the physical form of the product intended for end use. Chapters 2 and 3 focus on solid dosage forms while Chapters 4 and 5 focus on liquid dosage forms. The challenges and scopes of my research are outlined below.

Chapter 2

Challenge: Develop a dry bacteriophage dosage form for use in chicken feed to improve food safety in Kenya.

Scope: Demonstrate that anti-*Campylobacter* bacteriophage CP30A can be spray dried, shipped, and stored at ambient temperature without substantial inactivation.

Chapter 3

Challenge: Design an inhalable dry biologic dosage form for use in developing countries without cold-chain capabilities.

Scope: Demonstrate that pullulan trehalose formulation can be spray dried to a respirable powder and effectively dispersed from a dry powder inhaler.

Chapter 4

Challenge: Determine the best type of device for delivering a liquid dosage form of anti-tuberculosis bacteriophage.

Scope: Compare a vibrating mesh nebulizer, soft mist inhaler, and jet nebulizer for delivering anti-tuberculosis bacteriophage D29 aerosol.

Chapter 5

Challenge: Use bacteriophage to eliminate tuberculosis in the lungs.

Scope: Demonstrate that inhaled bacteriophage D29 aerosol can provide prophylactic protection against *Mycobacterium tuberculosis* in the lungs of mice.

While the research focus was on bacteriophage, which are parasitic viruses of bacteria (discussed further in Chapters 2, 4, and 5), the methods are expected to be applicable to other types of biologics. The research was multidisciplinary, requiring mechanical engineering theory and implementations, knowledge of materials science and pharmaceutical science, and novel developments of particle engineering and aerosol science techniques, with microbiology applications. For example, spray dryer process modeling using a mass and energy balance as well as a material phase diagram were used to determine spray drying conditions to stabilize bacteriophage, a new particle engineering model was developed to characterize co-amorphous solidification during spray drying and to explain improved biological stability with novel excipient formulations, a novel aerosol recirculation model was developed to help explain bacteriophage inactivation with a jet nebulizer, and hygroscopic theory and aerosol deposition modelling were applied to characterize aerosol losses in a nose-only inhalation device modified to delivering bacteriophage D29 aerosol to mice via a vibrating mesh nebulizer.

The following sections provide details regarding manufacturing stable spray dried biologic powder and are important in order to understand Chapters 2 and 3. Aerosolization and lung deposition of liquid dosage forms, an important component of Chapters 4 and 5, is briefly discussed in sections 1.9-1.10. The conclusions of this thesis are given in Chapter 6.

1.2 Abstract: Engineering Stable Spray Dried Biologic Powder for Inhalation

Recent developments in the engineering of spray dried biologic powder for inhalation are reviewed, with a focus on theories and methods for developing dispersible powders with long-term ambient storage stability. First, an overview of the applications and advantages of spray drying biologics is provided. This is followed by detailed descriptions of the various stages spray dried biologics for inhalation undergo during development, manufacturing, and delivery: purification and formulation, atomization, solvent evaporation and particle formation, particle collection and analysis, aerosolization, and lung deposition. The discussion of solvent evaporation and particle formation includes a review of particle engineering models for designing particles with desired characteristics such as surface enrichment, solid state, and aerodynamic diameter. Amorphous glass stabilization theories and stability testing methods are then reviewed. Subsequently, a spray dryer process model is derived using a mass and energy balance to predict the outlet temperature and relative humidity for different process parameters. Using moisture uptake data, this process

model is coupled to a non-equilibrium supplemented phase diagram derived using plasticization data for a trehalose-water system. Use of the supplemented phase diagram allows for the design of biologic powder with long-term physical stability at ambient temperature storage without requiring many experiments.

1.3 Background to Spray Drying

In 1865, Charles A. La Mont of New York claimed invention of a method of desiccating egg-batter into fine particles, whereby the egg-batter is forced into a spray using a 'powerful blast of air' and made to 'fall through a current of heated air' [1]. A similar patent regarding drying and concentration of liquid and solid substances in general was granted in 1872 [2]. These patents appear to be the first descriptions of the process now known as spray drying, which can be defined as the atomization of feed formulation (either solution or suspension) into a hot drying gas to evaporate the solvent, thereby creating dry particles from the solute materials.

The schematic of a typical laboratory-scale spray dryer, given in Figure 1.1, shows some details of the process. In this setup, the feed is pumped to a twin-fluid atomizer which generates droplets that are dried in a drying chamber and collected in a collection bottle using a cyclone. The applications and advantages of spray drying are discussed in the following paragraphs.

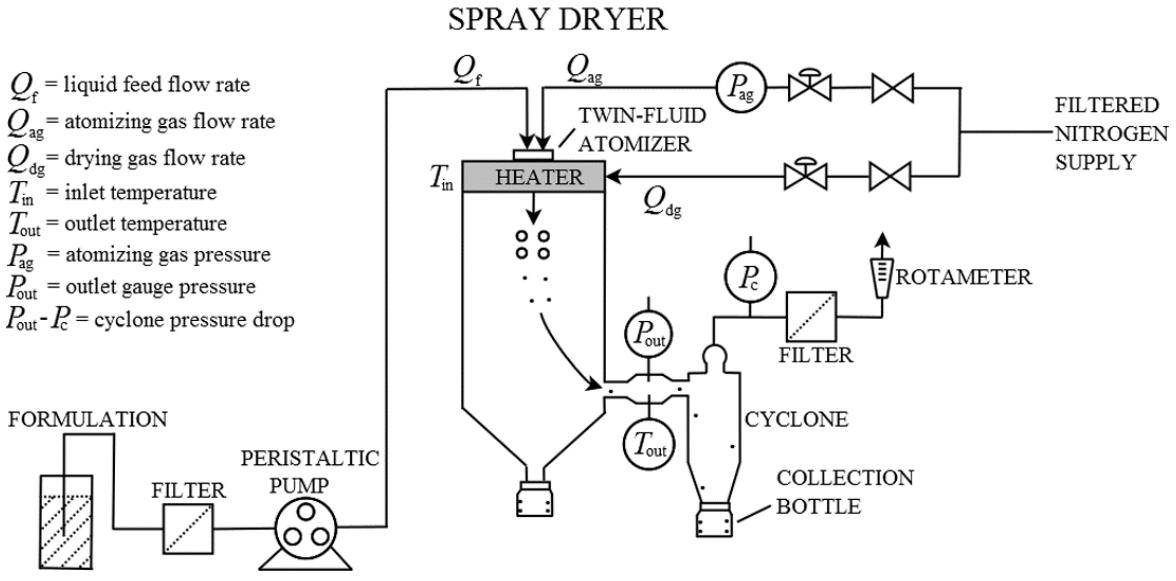

Figure 1.1: Schematic showing an example setup for a laboratory-scale open-loop spray dryer.

Spray drying is the most commonly used technique for microencapsulation in the food industry [3-4] and for dehydration of dairy products [5]. Indeed, a milk spray dryer in New Zealand can generate nearly 10 tons of milk powder per hour [6]. Spray drying is also widely used for producing dry and stable food additives and flavors [3-4,7-8], fruit and vegetable juices [4,9-10], coffee and tea [11], probiotic bacteria [12-18], and nutraceuticals [19]. Spray drying to produce particles with thick shells can be used for prolonged scent release and volatile retention [8], as well as for protecting oil from oxidation [3,20]. Other industries that use spray drying include, but are not limited to, the pharmaceutical, ceramic, polymer, detergent, pesticide, mining, and chemical industries [4,11,21]. Spray drying is even being considered for water recovery on the International Space Station [22-23].

The success and widespread use of spray drying is due largely to it being a continuous, fast, scalable, bottom-up approach that allows for particle properties such as particle size and distribution, surface composition, roughness, and particle density to be controlled [24], with comparatively low cost [3-4,14,25-30]. By contrast, lyophilization does not allow for the level of control over particle properties that spray drying provides, as generally, secondary milling or sieving is required [31-32]. Additionally, lyophilization is a lengthy batch process and requires infrastructure for freezing and generating sub-atmospheric pressures.

The removal of water associated with drying reduces weight and volume, which can reduce transportation costs and make handling and storage easier [33]. Additionally, many studies have demonstrated superior thermal stability of biologics in dry dosage forms as compared to liquid dosage forms [34-39], which is associated with decreased water-mediated degradation. An improved shelf-life could eliminate the need for cold-chain infrastructure, which can fail and lead to vaccine wastage, and is not available everywhere in developing countries [36,37,39-49]. There is also a risk of transmitting blood-borne diseases when needles are used, and this can be addressed by instead using inhaled vaccine delivery, which has the additional benefits of eliminating needle pain, needle-stick injuries, and needle disposal issues [36,40,44-46,50]. The potential for dry dosage forms to have long-term ambient temperature storage stability may also allow for easier stockpiling and distribution during pandemics [31,48-49,51].

Spray dried vaccines intended for inhalation include influenza vaccines [34-35,52-54], a pneumonia vaccine [55], a measles vaccine [56], Newcastle disease vaccines for poultry [57-58],

a listeria vaccine [59], a hepatitis B vaccine [60], and various tuberculosis vaccines [61-67]. By offering immediate protection at the exposure site for diseases transmitted by aerosol, inhaled vaccine powder affords comparable or greater mucosal immunity than does liquid subcutaneous or intramuscular vaccine delivery, and may even result in systemic immunity [35,40,53-54,60-61]. Indeed, large trials with measles vaccine delivered by nebulizer have demonstrated higher antibody titers with the inhalation route as compared to injection [68-71]. However, there is a general concern about adverse reaction to foreign material depositing in the lung [72-75]. This is particularly the case for the delivery of lipid-based vectors [61,75] and delivery to asthmatics [45,50], or immunocompromised patients [45]. Smokers may also be at risk [76]. The adjuvant-like response generated by inhaled powder may eliminate the need for an adjuvant in the formulation [54,60,64], which is important as little is known about the safety of adjuvants in the lung [40]. There are also safety and toxicity concerns with inhaling residual organic solvents sometimes used in spray dried formulations [77]. Whilst spray dried vaccines can be resuspended for injection rather than direct inhalation [37,39,48,78-79], enhancements to stability can be lost upon reconstitution as can the advantages of needle-free delivery; moreover, reconstitution creates a need for a sterile rehydration medium, which can complicate preparation and transportation [80].

Biologics are gaining market share relative to small molecules, with 52% of the top 100 product sales expected to be biologics by the year 2022 [81], and it is thus expected that there will be many applications other than vaccines where spray drying biologics can prove beneficial. Research has shown that monoclonal antibodies (mABs), which have been the most frequently approved biologics recently [82], can be successfully spray dried [83-87], and work has been done to scale-up the spray drying process for bulk mAB storage applications [38,86]. Currently commercially available inhalable biologics include colistin methosulfonate, bovine pulmonary surfactants, Pulmozyme® (recombinant human DNase), and AFREZZA® (fast-acting insulin) [31,88]. Spray drying has been used for generating materials in regulatory-approved inhaled products such as for EXUBERA® inhaled insulin [89], Tobramycin Inhalation Powder [90], BEVESPI AEROSPHERE® [91-92], and the topically applied biologic RAPLIXA® [26]. Further details are available in the literature regarding spray drying insulin [89,93-95] and tobramycin [90,96], which have been rendered room-temperature stable for years by glass stabilization, a process discussed later in this chapter. The most common application of spray drying in the pharmaceutical industry, however, is the generation of an amorphous form of the excipient lactose to improve compaction

properties of tablets [21]. There is also much interest in using spray drying to generate amorphous solid dispersions to deliver poorly water-soluble drugs [97-101].

Another application of spray drying in the pharmaceutical industry is for controlled release of a drug or biologic substance in the lungs. The morphology of the spray dried particles, for example, thickness and surface area, can affect the dissolution and diffusion of material through the outer layer of the particle [24]. Due to the small size of spray dried particles for inhalation, release is rapid unless the solubility and diffusion are very low; hence, slowly biodegradable polymers with high molecular mass are typically used [24]. Of the many materials available, poly(lactic-*co*-glycolic acid) (PLGA) is the most commonly used [24]. Nano-PLGA particles (that can be delivered to the lungs within lactose microparticles) are too small to be efficiently phagocytosed by alveolar macrophages and have been used for controlled release of an antibody [102]. Other biologics for which PLGA has been used to provide controlled release include spray dried antigen [64,103] and interleukin [104]. A review of the use of PLGA for inhalation applications is available elsewhere [105].

Spray dried biologics may be able to address the rise in antibiotic resistance and the slow development of new antibiotics. Examples of such biologics include bacteriophage [106-121], antimicrobial peptides [122-123], and bacterial cell wall hydrolases [122]. Pulmonary delivery of bacteriophage to mice [118,124] and humans [108,125] has generally produced positive results with few if any side effects. Spray dried bacteriophage powder has been produced with high titer [126-129] and has demonstrated long-term stability with refrigerated [128] and room temperature storage [126].

Successful development of stable spray dried biologic products can be a challenging task. In the following sections, the main stages in engineering spray dried biologics for inhalation are discussed, with a focus on the development of dispersible powders with long-term stability. This discussion includes detailed descriptions of: (1) purification and formulation, (2) atomization, (3) solvent evaporation and particle formation, (4) particle collection and analysis, (5) aerosolization, (6) lung deposition. Then, theoretical and practical aspects of glass stabilization and stability testing are discussed. Finally, the development of a spray dryer process model and non-equilibrium supplemented phase diagram is demonstrated.

1.4 Purification and Formulation

After isolation and initial characterization, biologics are typically purified and formulated with stabilizers before spray drying. The degree of purification and formulation is typically much less in the laboratory than in the development of commercial products and it should be considered that impurities can affect stability and particle formation. The purification process will also vary between biologics. For mABs, the purification process may involve clarification with disk-stack centrifuge, multiple filtration steps, low-pH virus inactivation, and multiple chromatographic steps including Protein A capture [130-132]. Purification can come at a substantial cost, due in part to the high price of the resin used in chromatography [132]; thus, alternatives such as high performance tangential flow filtration and aqueous two-phase processing have been suggested [133-134]. However, cost analysis has indicated that alternatives may not be warranted [131]. The interested reader is directed elsewhere for more information regarding biologic purification [130-138].

Purified biologics usually cannot be spray dried on their own without substantial inactivation and hence require stabilizing excipients. Ideally, the excipients would not involve materials from animals as these could be contaminated with viruses [139]. The function and concentration of each excipient in the formulation as well as the selection and control of the manufacturing process must be justified to regulatory agencies [140], and, hence, a mechanistic understanding of what each excipient in the formulation does and how the process parameters affect the final product is clearly of interest. Additionally, a mechanistic approach allows the number of experiments required to develop a product with target characteristics to be reduced [31,97,141]. However, rather than mechanistic modeling, past experience and statistical design of experiments (DoE) are often used for determining formulation and process parameters for spray drying [12,34,51,93,95,142-146]. Unfortunately, DoE has limited ability to translate the results across scales and formulations and may require many experiments [97].

Factors that can inactivate biologics during formulation and processing include shear [15,31,147-151], osmotic stress or ionic strength [31,121,152-153], electric fields [154-155], UV light [106,156-159], heat [15,31,41,121,153,159-160], desiccation (which can be related to osmotic stress and ionic strength) [15,31,41,159,161], pH [31,41,106,121,153], and pressure [31,160].

Minimizing these stresses during formulation and spray drying can be crucial to developing an effective biologic product.

Pre-adapting bacteria to environmental stresses such as heat, osmotic pressure, and starvation may help to increase their stress resistance and survival during spray drying [14-15]. Bacteria harvested during the stationary phase may be more resistant to drying [14]. Damage or strain history may be important to consider. Viruses have been adapted for use at different temperatures [162-163].

Increasing the stress resistance at the interior of large biologics such as viruses, bacteria, or red blood cells, may require getting stabilizers into the biologic [24,48,164]. Placing the biologic in a hyperosmotic solution containing the stabilizer may be useful in this regard, but this depends on the permeability of the membrane and whether or not the biologic possesses active transport mechanisms to bring in or expel substances [48,164-165]. Adding compounds to increase membrane fluidity and to take advantage of phase transitions at elevated temperatures may also be helpful for getting stabilizers into the biologic [48,164].

Usually, a major stress on biologics during spray drying is desiccation, which can be addressed by adding a suitable glass stabilizer to the formulation. While many sugars can be used for glass stabilization, those that participate in the Maillard reaction (such as lactose) should be avoided [36]. Trehalose is an excellent glass former and stabilizer and does not participate in the Maillard reaction, although it is not yet approved for inhalation. For reconstitution purposes, it may be important to consider that solution viscosity increases with dissolved trehalose concentration [166] and that high viscosity would result in the need for larger needles which are more painful [38]. Generally, better stabilization is achieved with trehalose than with sucrose [166]. Glass stabilization with trehalose is discussed further later in this chapter.

Spray drying amorphous disaccharide glass stabilizers on their own tends to result in cohesive, solid particles, which are not very flowable or dispersible, typically exhibiting low collection yields in spray dryers. A crystalline shell former, such as leucine, can be used to decrease particle cohesiveness and to lower particle density, thereby improving flowability and dispersibility [24]. The combination of trehalose and leucine has commonly been used in the literature [52,126,128-129,167-168] and has been shown to provide the best stabilization of certain biologics out of different formulations tested, whilst producing a dispersible powder [126,128-129,167].

The pH of aqueous leucine solution is ~5.98, near the isoelectric point, where formally there is no surface charge [169]. The surface activity, solubility, and particle morphology will depend on pH, which should be considered when adding a buffer to the formulation.

For leucine to increase dispersibility, it should be present in high concentration on the surface of the spray dried particles. A high concentration on the surface requires high initial saturation of the leucine relative to the other materials, which may be undesirable if the particles need to consist of a high mass fraction of the active (biologic) [24]. Trileucine has therefore been considered as an alternative, as it reaches a high concentration at the surface at lower feed concentrations, due to a lower solubility in water and higher surface activity [24,170]. The wrinkled structure of trileucine particles, which may be associated with the shell being too thin to maintain a spherical shape [171], is expected to result in a high emitted dose from carrier-free dry powder inhalers [170-171] and potentially less flow dependence [172].

The solvent used for preparing biologic formulations for spray drying is typically water. Spray drying with propellant [173] and ethanol [173-175] as solvents, among others [100], can be performed using a closed-loop (drying gas recycling) configuration, allowing for the spray drying of substances with low aqueous solubility as well as potentially for improved thermal efficiency and particle morphology. However, it is crucial to check that the biologic is stable or can be stabilized in the chosen solvent [176] and inhaled toxicity of residual solvent in the particles must be considered in non-aqueous systems [77]. Emulsion formulation preparation may involve the use of a high-shear mixer and a high-pressure homogenizer before spray drying [91], and the effect of the preparation method on the biologic activity should be tested. The formulation of biologics is discussed further in Chapter 15.

Prior to entering the atomizer, the formulation, which is termed the feed, should be well-mixed to ensure that the biologic material is evenly distributed in the solvent. Some larger biologics may entangle or settle if not properly mixed. On a laboratory-scale, mixing can be performed using a magnetic stirrer [12]. The effect of the container and the feed lines on biologic activity should also be tested, as it is known, for example, that proteins, because of their amphipathic nature, can adsorb to surfaces such as on plastic and glassware, in a protein- and material-dependent manner [177-185]. The feed can be cooled prior to drying if required for biologic stability; however, this may affect particle size, as discussed in the next section.

1.5 Atomization

In a spray dryer, an atomizer is used to generate droplets from the liquid feed formulation. The droplets subsequently dry to produce solid particles. This section reviews characteristics of commonly used atomizers, the generated shear stress and air-liquid interfacial stress on biologics, and the use of surfactants and other excipients to displace biologics from the surface of atomized droplets. The interested reader is directed to textbooks for background information regarding the atomization process [11,186-187].

Commercial spray dryers commonly use rotary or twin-fluid atomizers [33,188]. Rotary atomizers impinge a liquid jet onto the center of a rotating disk, which discharges the liquid radially by its rotational motion [186]. The particle size can be controlled by the rate of rotation, but wider drying chambers are needed for higher rotation rates [189]. The disk is typically rotated using a gas-driven turbine for a smaller disk or an electric motor for a larger disk [188]. Very high production rates are possible in production-scale rotary atomizers (up to 40 kg s^{-1}) [186], with little risk of clogging [187]. Whilst rotary atomizers tend to produce more uniform droplets than twin-fluid atomizers, the latter are preferable for developing particles for delivery to the lungs due to the smaller size of the droplets produced [188].

Twin-fluid atomizers use the energy from a high-pressure atomizing gas to break the liquid feed into a spray of droplets. The droplet diameter is related to the ratio of the mass flow rates of atomizing gas and liquid feed [141,188]. An increase in feed viscosity, for example when using a higher dissolved solids content or reducing feed temperature, will tend to produce larger droplets [11,186,188]. Production-scale twin-fluid atomizers are available, such as the Schlick-05 [190]. Large amounts of compressed gas may be required in open-loop configurations and so on scale-up closed-loop configurations, where the atomizing and drying gas are recycled, may be desirable [189].

The wide distribution of droplet sizes produced by twin-fluid atomizers may not be desirable in some pharmaceutical inhalation applications. To address this concern, as well as to study the particle formation process and to generate plenty of uniform particles for analytical work, the use of monodisperse atomizers in research spray dryers has become increasingly common [171,173,191]. Whilst further work is required to scale-up these monodisperse atomizers to

accommodate higher throughput rates, they can be useful in applications where only small quantities of biologic powder need to be developed.

Shear stress can be present in the pressurized liquid flow through the liquid channel of twin-fluid atomizers [31], as well as past the exit of the orifice [18]. Shear stress during atomization is typically considered low enough not to cause biologic inactivation [31,192]. However, in one study less inactivation was observed using a pilot scale rotary atomizer as compared to a pilot scale twin-fluid atomizer, which was hypothesized to be related to a characteristic shear rate that was three orders of magnitude higher for the twin-fluid atomizer [18]. Another study found that using higher atomizing gas pressure with a twin-fluid nozzle led to more biologic inactivation [193]. Whilst these studies point toward shear stress as being a cause of inactivation, this has not been proven because the biologic was assayed from the produced powder rather than from the droplets generated by the atomizer. A filter could be attached to the atomizer to capture and assay atomized droplets [194].

It has been suggested that using larger initial droplet sizes will result in less stress on the biologic, since less energy is needed to break up the liquid jet into larger droplets [41]. Another consideration is that with decreasing droplet size, the surface area to volume ratio of the air-liquid interface increases. Proteins will tend concentrate at the air-liquid interface during drying due to their large size, which prevents quick diffusion away from the receding interface (this is discussed further in the next section). The accumulation and adsorption at the air-liquid interface can lead to the unfolding and exposure of the hydrophobic interior of the protein to the air-phase, which can further lead to hydrophobic aggregation and inactivation by the irreversible loss of the native structure of the protein [31,148-149,195-196]. The surface accumulation effect may be enhanced by the fact that proteins are typically amphiphilic and hence essentially surface-active macromolecules [179,184-185,197].

It is widely accepted that surfactants can displace proteins at the surface and decrease aggregation and inactivation during processing [185,195-202]. The accumulation of surfactants on the droplet surface is a process that occurs transiently during droplet evaporation. In addition to transport from the bulk to the surface and adsorption onto the surface, high molecular mass surfactants will take time to orient at the surface [203]. Some surfactants can accumulate on the surface and decrease surface tension in the millisecond time scale (within the droplet lifetime typically encountered in

laboratory-scale spray drying), although most surfactants will not reach an equilibrium surface tension within this time scale [203-204]. Addition of even small amounts of surfactant can lead to smooth, spherical particles [24,198,202-205]. A concern with using surfactants is that they may solubilize some membrane components for certain biologics [56].

Leucine and trileucine, discussed previously, are potential alternatives for displacing the biologic at the surface. Trileucine decreases surface activity in solution in a concentration-dependent manner and competes with protein on the air-liquid interface, which can decrease denaturation and aggregation of protein [170]. Further details regarding surface enrichment are given in the following section.

1.6 Solvent Evaporation and Particle Formation

This section reviews the basic particle engineering concepts needed to understand the particle formation process, including solvent evaporation, surface enrichment, time available for crystallization, and aerodynamic diameter. Crystallization and shell deformation processes are discussed, as is the development of more complex particles.

The low humidity and high temperature of the drying gas drives evaporation of the solvent from the atomized droplets. The evaporation process involves coupled heat and mass transfer [11,171]. The drying droplet surface stays near the wet bulb temperature of the drying gas (which is much lower than the nominal drying gas temperature) for most of the evaporation process [11]. Evaporative cooling results in the outlet drying gas temperature decreasing with increasing feed flow rates. Computational fluid dynamics (CFD) can be used to model spatial distributions of temperature [206] and evaporation rate in spray dryers [188]. CFD has shown that particles caught up in eddies may be exposed to the high inlet temperature without evaporative cooling to provide protection [188]. For small droplets, solvent evaporation and particle formation commonly take place in co-current drying chambers, in which atomized droplets and drying gas flow in the same direction. For large droplets, a counter-current configuration can be used to increase the time for solvent evaporation; however, in this configuration the hottest air contacts the driest particles [11], which may not be suitable for heat-sensitive biologics.

The radial recession of the droplet surface due to evaporation causes solute to increase in concentration near the surface, unless the solute can diffuse quickly to the interior of the droplet.

A commonly used particle formation model for this process is the Vehring-Foss-Lechuga (VFL) model [171], which is based upon assumptions of one-dimensional spherical symmetry and no convection except Stefan flow. The VFL model does not account for surface activity, shell deformation, or non-constant evaporation rates during initial temperature equilibration and the falling rate period [171]. In reality, the evaporation rate depends upon the local temperature and relative humidity, solute concentration according to Raoult's law, and the diameter according to the Kelvin effect, among other factors [207].

The ratio of surface concentration to mean concentration of the solute in the droplet is termed surface enrichment [24]. The surface enrichment can be considered a function of the Péclet number, Pe_i, which is proportional to the ratio of evaporation rate, κ, to the diffusion coefficient, D_i, of the solute (i) in the solvent [171]:

$$Pe_i = \kappa / (8D_i) \tag{1.1}$$

The steady state evaporation rate can be predicted using hygroscopic theory [171,207] if tabulated data is not available. The diffusion coefficient can be predicted from the Stokes-Einstein equation [208]:

$$D_i = kT / (3\pi\mu d_{mol,i}) \tag{1.2}$$

where k is the Boltzmann's constant, T is the temperature of the droplet, μ is the dynamic viscosity of the droplet, and the molecular diameter $d_{mol,i}$ can be estimated from the bond length and structure of the solute molecule.

The evaporation rate and diffusion coefficient may need to be modeled as functions of time. In co-solvent systems one solvent may evaporate faster than the other, resulting in a transient evaporation rate [24]. Near the end of the droplet lifetime, the solute concentration increases, which increases the viscosity of the droplet and decreases the diffusion coefficient, and, hence, a model has incorporated a time-dependent viscosity in Equation (1.2) [208].

The droplet surface recedes faster than the dissolved or suspended components with a Péclet number greater than 1 diffuse, resulting in surface enrichment of those components [24]. Components with Péclet numbers less than 1 remain relatively evenly distributed [24]. If phase transition (crystal nucleation) occurs, the local dissolved solute concentration is lowered, which

can be modeled as a sink condition [209]. The mobility of the nucleated material is drastically reduced resulting in negligible diffusion and a very large Péclet number [24].

Small solute molecules, for example disaccharide sugars such as trehalose, have lower Péclet numbers than large solute molecules such as proteins or most other biologics. Thus, the biologic will tend to reside on the surface of the particle (exhibit high surface enrichment), and be exposed to surface stresses at the air-liquid interface, unless there is an excipient that will out-compete the biologic to reside on the surface.

In Figure 1.2, the surface enrichment, E_i, defined as the ratio of surface concentration, $C_{s,i}$, to mean concentration, $C_{m,i}$, in the droplet, is shown to increase with Péclet number. This figure, which is useful for a first estimate of the radial distribution of components in the particle, shows the constant surface enrichment that would result at the end of the droplet lifetime, were there no solidification event, and is a good approximation within the range shown [210]. To model the change in surface enrichment over time, more complex analytical models have been developed, which extend the VFL model to larger Péclet numbers, and which can be used to estimate the shell thickness at the time of saturation [210].

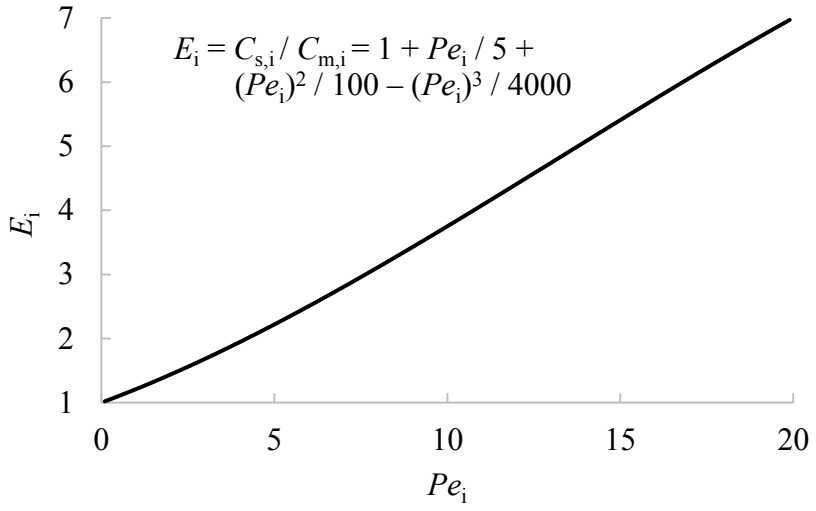

Figure 1.2: Surface enrichment, E_i, versus Péclet number, Pe_i, according to the steady-state VFL model, given by Vehring *et al.* [171]. Large molecules such as polymers and biologics have large Péclet numbers and hence high surface enrichment, whilst amino acids and disaccharide sugars typically have low Péclet numbers and hence low surface enrichment.

In spray drying, nucleation and crystallization or precipitation generally occur first at the surface, where the local concentration is high enough to overcome the local saturation concentration. By performing a mass balance on the solute and assuming a constant evaporation rate, it can be shown that the time for the solute to reach saturation at the surface, $\tau_{sat,i}$, is given by [24]:

$$\tau_{sat,i} = \tau_D \left[1 - (S_{0,i}E_i)^{2/3}\right] \quad (1.3)$$

where the droplet lifetime, τ_D, is given by [24]:

$$\tau_D = (d_0)^2 / \kappa \quad (1.4)$$

where d_0 is the initial diameter of the droplets emitted by the atomizer. As most atomizers emit polydisperse sprays, a range of these characteristic times will be present. The droplet lifetime can be used to predict whether the drying chamber of a given spray dryer provides enough residence time for droplets of a particular diameter to complete the drying process.

Also required in Equation (1.3) is the initial saturation ratio, $S_{0,i}$, which is given by [24]:

$$S_{0,i} = C_{0,i} / C_{sat,i} \quad (1.5)$$

where $C_{0,i}$ is the initial concentration of dissolved solute in the solvent, and $C_{sat,i}$ is the saturation concentration of the dissolved solute in the solvent.

The difference between the droplet lifetime and the time to reach saturation is termed the time available for crystallization, also known as the precipitation window, $\tau_{p,i}$, and is given by [24]:

$$\tau_{p,i} = \tau_D - \tau_{sat,i} = (S_{0,i}E_i)^{2/3} (d_0)^2 / \kappa \quad (1.6)$$

Whether the solute forms crystals that grow within this time available for crystallization depends on many factors. Time is required for crystal nucleation, growth, and polymorph transitions, which proceed according to the Ostwald step rule [24]. Many factors can affect the times required, including droplet temperature, which tends to increase the rate of nucleation [209]. Studies have suggested a critical supersaturation (in the range of 1-10), which depends on material properties, must be reached for spontaneous nucleation to occur [211-212].

If the time available for crystallization is not long enough for the crystals to reach equilibrium, a mixture of different polymorphs will result [24]. The presence of the most stable form increases

the rate that the less stable polymorphs convert to the most stable form [24]; such a system would likely be unstable on storage. Additionally, if the time available for crystallization is too short, some or all of the solute may not grow crystals and instead will precipitate in a disordered, higher energy state, termed amorphous [141]. A mixture of amorphous and crystalline states of the same material may also not be stable on storage. Once the amorphous phase starts to crystallize, expelled water can enter the remaining amorphous matrix and speed up the rate of conversion to crystalline form, which could cause rapid product failure [24]. Physically unstable systems like these are difficult to scale-up, as residence times may be different in large spray dryers [24]. As the time available for crystallization is shorter for smaller droplets, leading to crystals not having the same time to grow [24], production of potentially unstable systems like these may be a particular concern for polydisperse sprays. Additionally, at the center of a droplet, water evaporation is slower and crystals may have more time to grow [213]. Studies have quantified the growth of larger and broader crystals with increased time available for crystallization [173,208,212] and have demonstrated the formation of larger crystals growing from smaller crystals on microparticles in a high humidity environment [213]. Controlling crystal size is important since it affects rugosity and hence particle cohesiveness and dispersibility [214].

Certain materials can be used to inhibit or delay the onset of crystallization [84,213,215-216]. Inhibiting crystallization can lead to glass stabilization with materials that normally crystallize quickly like mannitol [84], although decreased yield may be present without a crystalline shell [215]. Delaying crystallization can lead to smaller crystals and a smoother surface [213].

Buffer, ions, and impurities will increase in concentration during the evaporation process and may be enriched on the surface. Any changes in pH could affect the biologic and will affect protein solubility [217] and hence particle formation. Increases in ionic concentration during evaporation can exert osmotic stresses on the biologics. Small amounts of impurities can substantially decrease crystal growth rates [218].

Trehalose and leucine have been studied extensively as excipients for particles containing biologics. In trehalose and leucine systems, it is desirable to dissolve the trehalose in the liquid feed with a low initial saturation ratio so that it will precipitate near the end of the drying process into an amorphous solid suitable for stabilization of biologics. By contrast, leucine should be dissolved in the liquid feed with a high initial saturation ratio, leading to a long time available for

crystallization, which allows crystals to grow at the surface of the drying droplet and form a shell that decreases particle cohesiveness. The shell is typically not exclusively composed of leucine, but can nevertheless lead to acceptable dispersibility [126]. As the leucine shell forms early in the evaporation process, whilst the droplets are relatively large, hollow particles, with low particle density, ρ_p, result; it has been shown that more void space and lower particle density result with increasing time available for crystallization [208,212]. The particle density can be predicted from measurements of volume equivalent diameter, d_v, (e.g. by estimating the hydrodynamic diameter using scanning electron microscopy for a large number of particles) and aerodynamic diameter, d_a, (e.g. using aerodynamic particle sizing techniques such as impactors), using the relationship obtained by equating the settling velocities [24,219]:

$$d_a = d_v \, (\rho_p / \rho_*)^{1/2} \tag{1.7}$$

where ρ_* is a reference density equal to 1000 kg/m^3.

The aerodynamic diameter of the dry particles can be predicted via a mass balance [24,141]:

$$d_a = d_0 \, (C_0 / \rho_*)^{1/3} \, (\rho_p / \rho_*)^{1/6} \tag{1.8}$$

where C_0 is the concentration of the solute in the feed and d_0 is the initial droplet diameter emitted from the atomizer. These equations assume spherical droplets and particles and neglect the Cunningham slip correction factor [141]. These equations are useful during scale-up to ensure particle size is not greatly affected by changing feed concentrations and initial droplet diameters [24]. The aerodynamic diameter is an important factor for estimating the lung dose of the emitted aerosol using extrathoracic deposition models, as discussed later in this chapter.

Models are available to predict the shell thickness and particle density of spray dried particles, which operate on the assumption that the shell forms immediately upon the saturation concentration being reached on the surface, and that the shell density is the mass-averaged true density of the materials [210]. Further work is required to develop more exact models not requiring these simplifying assumptions.

Leucine shells may deform substantially [168], provided impurities do not interfere with this process [194]. Experimental and theoretical studies of shell deformation processes are available in the literature [220-230]. One prevailing theory argues that elastic shell deformation occurs when

capillary forces in menisci that form between nanoparticles (which could perhaps apply to small crystals of leucine) overcome stabilizing electrostatic forces between nanoparticles [220].

Another related important aspect of particle formation that has yet to be incorporated into particle engineering models for spray drying applications is the role of surface activity in surface enrichment, which may be relevant for trileucine shell formation.

Trileucine forms a non-crystalline thin shell or coating that cannot support a spherical shape and deforms substantially. Like trileucine, polymers and other large molecular mass compounds have restricted molecular motions and hence tend to not crystallize or crystallize much slower than low molecular mass compounds [218].

More complex approaches can be used to produce low density particles by spray drying. Volatile salts or other templating agents can be sublimated to form voids, typically by incorporating a secondary drying step [24,90,174,231]. Templating has been used to produce PulmoSphere™ particles [232], which are part of the commercial Tobramycin Inhalation Powder, administered with the TOBI® Podhaler™ [90]. These particles are stable for 3 years at 30°C and 75% relative humidity (stored in a blister pack), result in less variable dosing, and require only low inspiratory efforts [90,96,232]; however, further excipients are needed for glass stabilization. PulmoSphere™ particles incorporate distearoylphosphatidylcholine (which is endogenous to the lungs) as a shell former and can be suspended for use with pressurized metered-dose inhalers, nebulizers, or liquid instillation [96,232].

1.7 Particle Collection

Cyclones are the most commonly used equipment in industry for collecting spray dried microparticles [33,195]. A cyclone is typically situated just downstream of the drying chamber, its use allowing for the capture of the particles in a collection bottle (see Figure 1.1).

The low yield typically encountered in laboratory-scale spray dryers with small batch sizes is generally improved upon scale-up [80]. Losses due to wall deposition upstream of the cyclone typically occur for large or highly surface-charged particles, whilst losses of small particles typically occurs at the exit of the cyclone [188]. A dual cyclone design has been implemented for accommodating the increased drying gas flow rate during scale-up [38].

Use of pure spray dried trehalose typically results in a low yield due to its cohesive nature. Particles can also agglomerate in cyclones [233]. CFD has been used to model particle trajectories as a means of evaluating spray dryer designs that may minimize wall deposition and agglomeration [206,234-236]. Fragile particles may fracture or deform when impacting the cyclone wall (termed attrition), which has been related to the inlet velocity of the cyclone [233]. Attrition may damage biologics residing on the surface of microparticles, but such damage has not been quantified.

Conditions in the collector should be controlled to ensure consistent powder properties. External surface thermometers have been used to estimate the temperature in the collection bottle [95]. The collector can be thermostated using a water bath [237], which can also be used to control the relative humidity in the collection bottle and hence the moisture content in the powder.

In standard laboratory-scale spray dryers, the collection bottle is typically quickly removed and capped after the run is completed to minimize thermal degradation and entry of moisture into the bottle from the surroundings. There may be time-dependent degradation in the collection bottle for large batch sizes without bottle replacement [95]. In these instances, collectors can be changed intermittently. For aseptic systems, a valve can shut off flow to the collection bottle, allowing for replacement of the collection bottle in a clean room at set time intervals during continuous operation.

After collection, a secondary drying step (for example, in a vacuum desiccator, convection-tray dryer, or fluidized bed system) may be used to lower the moisture content of the powder or to remove residual organic solvent [100,188,238]. Decreasing moisture content by using a secondary drying step may be more suitable than using a higher drying gas temperature for heat-sensitive biologics [238]. A secondary moisture-equilibration step, for example, using a humidity-controlled chamber or saturated salt solution, can be used to target a desired moisture content. Moisture equilibration is discussed further later in this chapter.

1.8 Particle Analysis

Whilst mechanistic models can be used to predict the properties of the freshly spray dried particles, the analysis discussed in this section should be performed to verify the predicted results. Analysis can also be performed at different time points during stability studies. Many analytical techniques are available and not all can be discussed here.

Techniques available for quantifying the amount of amorphous and crystalline material present in spray dried powder are reviewed in the literature [239]. Such analysis is important since, as discussed previously, partially crystalline excipients should be avoided, as these can act as a template to increase the rate of crystallization. One method for quantitative crystallinity measurement is Raman spectroscopy, in which an infrared laser is directed at the powder, and the intensity of the portion of light that is inelastically scattered to a different wavelength is measured [126,168,240-242]. Crystalline material results in narrow spectral lines, whilst amorphous material results in a broader scattering pattern. Since small masses of powder are typically used for analysis, relative humidity control is important during Raman spectroscopy to prevent water uptake and solid-state change. Although interfering fluorescence may not be a large concern for high purity small molecule drug powders [241], biologics may not be highly purified during preliminary development and, hence, it may be more difficult to perform quantitative Raman spectroscopy, due to residual fluorescence. Still, Raman spectroscopy has been used to screen excipients for providing long-term stability to spray dried mABs [83]. Powder X-ray diffraction is an alternative to Raman spectroscopy for solid phase analysis, but it is more difficult to quantify small masses of amorphous material in a primarily crystalline powder [241].

Modulated differential scanning calorimetry (MDSC) can be used to determine the glass transition temperature of the powder [128,243]. Enthalpic relaxation heat flow measured by MDSC can be used to assess the amorphous content in a partially crystalline sample [244]. Dynamic vapor sorption can be used to determine the moisture uptake behavior of the powder [126-128]. These techniques are discussed in more detail later in this chapter.

X-ray photoelectron spectroscopy, also known as electron spectroscopy for chemical analysis, can be used to measure the elemental surface composition of spray dried powders [87,126,170-171,174,196,199-200,202,204,212,245-248]. The elemental surface composition can be useful for determining the ratios of excipients on the surface and for comparison to theoretical surface enrichment described previously. This is, however, strictly speaking a near-surface method, and, hence, the measurements may not be able to accurately measure a coating thinner than the penetration depth of the instrument [24]. Alternatively, time-of-flight secondary ion mass spectroscopy can provide qualitative near-surface composition measurements [246].

Scanning electron microscopy is commonly used to examine microparticle morphology, which is then compared to expectations from particle formation theory. Scanning electron microscopy can also be used for estimating crystal size [212]. If the interior of the particle is of interest, particles can be cut with ion-beam milling and then the cross section can be viewed using scanning electron microscopy [93,141,173,208,212,249-250]. This method also yields shell thickness [208,250]. X-ray photoelectron spectroscopy on ion-beam milled particles can potentially determine if the radial internal distributions of materials match particle formation theory [212]. Milling, when performed at multiple locations [141], can also verify predications of void space from particle formation models. For example, it has been shown using ion-beam milling that for polydisperse powders, large particles may contain void space whereas smaller particles do not [141], in agreement with theoretical predictions. Compressed bulk density can also be used to predict if there are internal voids or porous materials [141]. Porosity may decrease with increasing surface corrugation [249].

A unique feature of spray dried biologics is that it is generally necessary to quantify the level of biological activity in the collected powder. This can be done with bioassays, which are often more variable and costly than chemical assays such as those used for small-molecule antibiotics [31]. Additionally, bioassays are generally performed in the liquid state and hence a method of rehydration is necessary. Therefore, any possible inactivation due to spray drying may not be able to be separated from inactivation due to rehydration. The activity of biologics after rehydration has been shown to be affected by temperature [14-15,251-256], rate or duration of rehydration [15,251,253,256-258] (likely related to osmotic stress), resuspension medium composition [15,156,251,256,258], exposure to UV radiation [156], and powder composition [258]. Biologics can leak if rehydration causes phase change [252,259-262].

A generalized method for resuspending spray dried biologics for bioassay is not available. It can be assumed that the rehydration method resulting in the lowest overall spray drying and rehydration inactivation most closely represents the inactivation due to spray drying, provided there is no increase in biologic activity in the resuspension media, for example, due to cell division. For dry powders meant for inhalation, however, it may be most relevant to resuspend in a medium representative of the fluid in the lungs, provided one can perform an accurate bioassay in such a medium. Reconstitution may occur in mucus in the upper respiratory tract and surfactant in the lower respiratory tract, both of which contain anti-microbial molecules [263]. *In vitro* studies in

mucus or surfactant may therefore be useful for testing biologic reconstitution survival in a realistic medium [263].

1.9 Aerosolization

This section reviews considerations regarding the use of various inhalation devices for delivering biologics. Spray dried powder is usually intended for delivery with a dry powder inhaler (DPI), but powder can also be suspended for delivery from nebulizers, pressurized metered-dose inhalers (pMDIs), or soft mist inhalers (SMIs). Device selection depends on the intended use of the biologic and the dose to be delivered.

Not surprisingly, the most common method for aerosolizing dry powder is to use a DPI. Loading the powder may require filling into a capsule, which is a well-established technique in industry [25,89] and should be done in a temperature- and humidity-controlled environment. Triboelectric charging can be an issue for powder filling, and, hence, it may be beneficial to retain some moisture in the powder and filling environment. Cohesive powders can also be difficult to fill. Advantages of using DPIs include the obviation of any need for on-site reconstitution, which might otherwise require the transport of sterile liquid (not desirable for use in developing countries, as discussed previously), less administration time than with nebulizers [96], and the possible elimination of any need for adjuvants in vaccine preparation (as discussed previously).

Nebulizers are commonly used for aerosol delivery as they allow for the delivery of large doses without the need for breath coordination and refilling is simple; however, nebulizers can be bulky, comparatively expensive, and require electricity. Biologics have been shown to sustain acceptable losses of activity after aerosolization from nebulizers [264]. However, this is not always the case, as use of certain biologic and nebulizer combinations can result in substantial inactivation [265]. The use of jet nebulizers can be particularly damaging to biologics, a problem that may be due to the hydrodynamic shear stress during droplet production and the repeated baffle impaction and recirculation that the biologic is exposed to in the device [265]. With nebulizers, the inhaled volume of aerosol may vary between patients, leading to variability in the dose reaching the lungs. Accordingly, it is suspected that the administration of measles vaccine to children in Mexico using nebulizers with disposable paper cups led to variable dosing. Nevertheless, this means of measles aerosol vaccine delivery has proven successful [68-71,266]. Nebulizers can also be used to deliver

aerosol vaccines to people in a tent or other enclosure [267-268]; this practice is also expected to result in dose variability.

Biologics have been spray dried and resuspended in pMDIs [269-270], which may be particularly useful for administration in developing countries [31]. Bacteriophage can sustain acceptable losses of activity after aerosolization from a pMDI [31]. To minimize extrathoracic deposition, and to allow for the same pMDI to be used with multiple patients, which may be useful for vaccine delivery in developing countries, face masks and valved holding chambers can be used. However, it has been demonstrated that the fraction of air inhaled through the holding chamber rather than the environment determines the dose, and that this fraction is related to potential face mask leaks [271]. Therefore, if face masks are not held tightly onto the face, for example, because the same face mask or holding chamber is used for multiple patients and cross-contamination needs to be avoided, then a low and variable lung dose may be expected [271].

SMIs may also be useful for administering biologics; indeed, an SMI insulin product is being developed [272]. It has been demonstrated that inactivation of anti-tuberculosis bacteriophage D29 with an SMI was relatively small, comparable to that with a vibrating mesh nebulizer, and much less than with a jet nebulizer (see Chapter 4 [273]).

The use of CFD and analytical models can help to determine the strain rates encountered in commercial aerosolization devices [274], and hence to predict if biologic inactivation will result. Transmission electron micrographs taken after aerosolization and powder resuspension may be compared to images taken of the initial formulation to determine if visible damage is present and related to inactivation of the biologic [275], but it is difficult to find the biologic when imaging if the biologic is not in high number [193]. Inactivation due to aerosolization should be considered when selecting the inhalation device and the loaded dose. The loss of aerosol due to extrathoracic deposition and the inactivation after deposition in the lungs also plays a role when determining dose, as discussed in the following section.

1.10 Lung Deposition

This section reviews the use of deposition modeling and idealized *in vitro* models for predicting the lung dose of inhaled aerosol, and loss of biologic activity upon deposition in the lungs, both of which are useful for determining the nominal dose to deliver.

Aerosol must pass through the extrathoracic region prior to entering the lungs [207]. It logically follows that extrathoracic deposition models are particularly useful for estimating the lung dose of inhaled aerosol [207,276-277]. Different extrathoracic deposition profiles are expected for different patient age groups [207,276-277]. Much less data is available on extrathoracic deposition in pediatrics than in adults [277], a paucity that can have implications for vaccine delivery to children in developing countries. Furthermore, different particle sizes for children than for adults may be required for optimal lung deposition, because of differences in extrathoracic dimensions (including smaller airways in children) and inhalation flow patterns [276]. In some cases lung dose per unit body surface area may be a better parameter than total lung dose for predicting whether or not the intended effect will be achieved [276,278]. Infants are nasal breathers and hence a pMDI with attached valved holding chamber and face mask is sometimes used for aerosol delivery, but again a proper face mask seal is crucial for delivering a high dose [271].

In vitro extrathoracic deposition models typically neglect aerosol exhalation and neither consider hygroscopic particles nor the effect of disease on airway dimensions or the effect of coughing on deposition [276]. CFD can be useful for modeling local deposition patterns and may include effects of hygroscopic growth and condensation of the aerosol in the airways [277].

Among many other parameters, the particle size of the aerosol emitted from inhalation devices is important for predicting lung deposition. The size of individual dried particles can be predicted from particle formation theory. However, for DPI delivery, the particle size distribution of the aerosol is affected by incomplete process yield, size selective retention in the filling process and inhalation device, and incomplete dispersion of the powder. The particle size emitted from different aerosolization devices, and the biological activity within certain size ranges, can be measured using an impactor or multistage liquid impinger [126-128]. Idealized geometries, which are available for infants [271,279], children [280-281], and adults [282-284], can be included upstream of the impactor or a filter to quantify extrathoracic deposition and to better estimate the dose and particle size distribution that enters the lungs. Ideally, environmental chambers are used to maintain representative temperature and relative humidity when performing these *in vitro* measurements [141]. Airway surface liquid concentration models can then be used to extend the particle size specific information to predict deposition and biologic concentration in different lung generations [264].

Upon deposition in the lungs, biologics are subject to degradation mechanisms, which are discussed in more detail elsewhere [285]. Some biologics may be able to evade lung defense mechanisms for long enough to produce the desired effect. For example, bacteriophage D29 can infect tuberculosis inside macrophage before being inactivated [286].

Once the biologic aerosol is likely to achieve the desired effect in the lungs, the product development process can proceed. It is in most cases necessary to stabilize the biologic so that the aerosolization device and biologic combination has a reasonable shelf life. Glass stabilization, discussed in the next section, is the preferred method for stabilizing labile biologics.

1.11 Glass Stabilization

This section discusses an important aspect of ensuring the stability of desiccated biologics during storage, glass stabilization. Other physical and chemical degradation pathways such as deamidation and oxidation can occur in the solid state and these are discussed in detail elsewhere [177,287].

As discussed previously, the fast evaporation process in spray drying can result in precipitation of dissolved material into a high energy, disordered, glassy state if the time available for crystallization is too short or the material does not have a natural tendency to crystallize. Glasses, amorphous materials that exhibit a glass transition at the temperature where the time for relaxation to a lower viscosity equals the typical time scale of an experiment (usually ~100 seconds), are essentially very high viscosity liquids (10-12 orders of magnitude higher after vitrification than in the initial liquid state) [288]. The solid-like behavior of glasses is due to reduction in molecular motions and long relaxation times [288]. Amorphous solids are more soluble (with quicker dissolution) than their lower energy state more structured crystalline counterparts and have a higher thermal expansion coefficient [289-290]. Amorphous solids may have some short-range molecular order, but do not have the long-range order present in crystalline solids [289-290]. Water molecules may freely diffuse through the solid phase of glassy solids [288]. Unlike small molecules, which are generally more stable in crystalline form, amorphous excipients provide better stabilization of biologics [36].

Some organisms can survive severe dehydration by accumulating disaccharides such as trehalose and sucrose [291]. This characteristic is thought to be related to the ability of these disaccharides

to form glasses. The most common mechanisms hypothesized to explain the stabilization upon desiccation by glass stabilizers have been water (hydrogen bond) replacement and vitrification [31,35,47,195,260,291-293].

Water replacement stabilization theory has been suggested on the grounds that lysozyme or bovine serum albumin lyophilized with trehalose produces a similar infrared spectrum to hydrated trehalose (but different than trehalose lyophilized on its own), and this 'hydration' by trehalose correlates with stabilization [292,294]. Essentially, the effect of the protein on the sugar structure is hypothesized to have the same effect as water [292]. More specifically, this is believed to mean that hydrogen bonds between polar amino acids and water are replaced by hydrogen bonds between the amino acids and the stabilizing sugar, preventing denaturation of the protein (associated with exposure of inner hydrophobic structure) due to drying [31,47,291-292].

Vitrification stabilization primarily considers immobilization of the biologic in the glassy matrix. Reduced molecular mobility decreases denaturation, and physical separation may decrease aggregation [31,47,291]. These two theories are not mutually exclusive as glass formation is thought to be a necessary condition for hydrogen bond replacement [294]. However, vitrification on its own may be insufficient for glass stabilization. For example, it has been shown that even though dextran forms a glassy matrix, it is not very good at providing glass stabilization [291]. In fact, the larger the molecular mass of dextran, the less it stabilizes, despite an increasing glass transition temperature, from which it has been hypothesized that steric hindrance in large molecular mass dextran interfered with hydrogen bond replacement [291]. Furthermore, studies have shown that small molecular mass glass formers stabilize better than large molecular mass glass formers (even though glass transition temperature increases almost linearly with molecular mass), a difference thought to be related to the greater ability of small glass formers to directly interact by hydrogen bond replacement because of their lower free volume [17,291,293]. Whilst physical stability requires that the glassy matrix not undergo a glass transition and become less viscous or crystallize, the above argument clearly demonstrates that storage well below the glass transition temperature is not all that is required for stability. If a glass transition and subsequent excipient crystallization event occurs, biological inactivation may result [295], because crystallization would lead to a loss of hydrogen bonds with the biologic.

From the above arguments, the reason trehalose is a good glass stabilizer and preserver of biologics may in part be due to it being small enough to effectively provide hydrogen bond replacement, whilst being large enough that it has a sufficient glass transition temperature to ensure it remains amorphous when stored at ambient temperature, low humidity conditions. Moreover, trehalose molecules have many locations available for hydrogen bonding [166]. It has been suggested that the sugar-protein ratio in a formulation should be designed based on the number of bonding sites on the protein that need to be replaced [243].

Despite its relatively small size, trehalose may not be able to replace all hydrogen bonds with the protein; hence, adding a small amount of even lower molecular mass compound, such as sorbitol, may fill some of the remaining excess free volume and allow for additional hydrogen bonding to the protein to improve stability. The use of small amounts of plasticizers such as glycerol may improve stability despite lowering the glass transition temperature [185,296-297]. This effect is thought to be related to the slowing down of the fast dynamics of short-range relaxations, which appear to be more important for long-term biological stability than long-range relaxation occurring at glass transition, as short-range relaxations occur well below the glass transition temperature [185,298-299]. The use of incoherent neutron scattering and isothermal microcalorimetry may be useful for modeling these relaxations in screening studies [87,299]. Isothermal microcalorimetry instruments can be used to measure heat flow from many powders simultaneously and with great sensitivity, a feature that may prove useful for screening, and for indicating the rate of reactions within the powder, including those between components, as part of excipient compatibility testing.

Isothermal microcalorimetry can be adapted to perform relative humidity (RH)-perfusion microcalorimetry in order to assess suitable storage conditions by predicting long-term chemical and physical stability [300-302]. Heat flow is measured upon exposure of the powder to different relative humidity streams. This measurement can be performed at several temperatures so that the effect of both temperature and relative humidity can be determined [302]. Using RH-perfusion microcalorimetry it has been observed that at an increase in energy of interaction (not associated with phase or morphology change) between water vapor and glass occurs at a threshold relative humidity (hydration limit), which is thought to relate to water vapor saturating binding sites within the amorphous phase, as the water content at this relative humidity is near the monolayer value from Brunauer-Emmett-Teller theory [237]. The hydration limit is thought to represent the

amorphous analogue of the deliquescence point of crystalline material [237]. Below the hydration limit the water vapor, which may freely diffuse in the amorphous solid matrix, is soluble in the solid, and above the hydration limit additional absorbed water vapor acts as solvent on the amorphous solid, since the heat of water sorption approaches the enthalpy of condensation of water [237]. If so, the supersaturated solution above the hydration limit may initiate crystal growth [300].

A minimum in oxidation rate is expected at the (monolayer) hydration level [288]. Essentially, the monolayer of water may block reaction sites [288]. Other studies have suggested that retaining some residual moisture in the powder may improve stability. Decreased aggregation with 2-3% moisture relative to 1% moisture has been demonstrated for lyophilized mAB powder [243], and better stability without secondary drying in a lyophilizer from 3% moisture to 1% or less moisture has been demonstrated for spray dried measles vaccine [56].

It has been suggested that the hydration limit may relate to a zero mobility temperature [300], and that a system specific mobility temperature may eventually replace the empirical T_g - 50 rule of thumb [288], which assumes long-term physical stability is present when the powder is stored 50°C below the wet glass transition temperature [303]. Indeed, some materials such as amorphous indomethacin crystallize relatively quickly well below the glass transition temperature, which is thought to be due to the large molecular mobility and the quick relaxation of amorphous phases [304-305]. Ultimately, the chemical nature of the formulation determines the stability in a glassy matrix [288]. Stability testing, discussed in the next section, can experimentally demonstrate whether glass stabilization is successful.

1.12 Stability Testing

Stability testing is essentially stress testing required by regulatory agencies to determine the storage conditions and shelf-life of spray dried biologic products. The stability testing requirements are not well-defined for all biologic products. One should speak with regulators early in the development process as different procedures may apply for different biologics [139,306].

The analytical techniques described in the Particle Analysis section, in particular bioassays, should be performed at each time point in the stability tests. Performing different analytical measurements at the same time can be important for determining causes of instability. For example, if biologic inactivation is found to occur at a specific time point, moisture content measurement by Karl

Fischer titration may indicate increased moisture content (which could be due to a leak in the packaging), solid state analysis may indicate crystallization has occurred (because of an increased moisture content), and scanning electron microscopy may indicate that the morphology of the dried particles has changed (through moisture-induced crystallization events).

There are many different types of stability tests that can be performed to determine when the product fails. Typically, regulatory agencies require long-term and accelerated stability testing, the methods and protocols for which can be found elsewhere [307-311].

Long-term, or real-time, stability measurements are used to determine the shelf-life of the product and should be performed until degradation is seen or the target shelf-life is passed [309-312]. Using multiple samples is particularly important for biologics, as there can be large variability [313]. Long-term stability tests are typically conducted monthly for the first 3 months and then at 3-month intervals thereafter until the end of the first year, every 6 months until the end of the second year, and annually thereafter [309]. For Climate Zones I and II, 25°C is the long-term stability temperature for room temperature storage, while for Climate Zones III and IV it is 30°C [310]. There are no general recommendations for acceptable loss of biological activity [309]. In many instances, a biphasic loss on storage is observed [41,51,56] that may be related to damage from the spray drying process [14].

In accelerated stability tests, the product is stressed at higher temperature, typically for shorter periods of time, to increase degradation rates [311]. The theory of accelerated degradation kinetics is discussed elsewhere [313]. Since the loss of biologic activity and other changes to the powder such as solid phase changes may be non-linear functions of temperature and time, extrapolation of accelerated to long-term stability may not be simple. For example, the time until physical instability is observed for a given difference between wet glass transition temperature and storage temperature is expected to have a non-linear relationship, but the exact relationship is material dependent and usually not known *a priori*.

Cyclic temperature stress testing provides evidence of instability not seen in isothermal long-term and accelerated stability tests and is useful in development and troubleshooting [310,312]. Quicker degradation may result during cyclic stress testing than isothermal testing.

Small chambers can be used for accelerated and cyclic stability studies, whereas long-term stability studies may be performed in walk-in chambers engineered to provide a uniform temperature exposure; these may be fitted with temperature readouts and alarms [310]. In preliminary laboratory work, spray dried powder can be stored over saturated salt solution in a desiccator to control relative humidity, and the desiccator placed in the stability chamber at a set temperature [237]. Relative humidity ranges for saturated salt solutions are available in the literature [314-315]. However, this method can require much storage space and does not test the effect of interactions of the powder with the container, for example, those associated with leachables and extractables, which should be tested [41,309]. Additionally, the ability of the proposed packaging to protect against humidity should be tested [309].

In preliminary stability testing, representative simulated packaging may be used. It is often overlooked that bottles, vials, and bags are semipermeable to water vapor [311] and should not be used on their own to package spray dried biologics, as high relative humidity storage can inactivate biologics in spray dried powder [128]. Thus, for preliminary stability measurements, spray dried powder can be packaged with desiccant, which is designed to act like a moisture buffer that slows down the effects of moisture ingress; this is due to the large internal surface area of the desiccant to which water can adsorb [316]. Molecular sieve desiccant possesses a high moisture sorption capacity at low relative humidity, whereas silica gel desiccant is useful for protection from higher relative humidity because of a more linear relationship between moisture sorption capacity and relative humidity [317]. Larger quantities of dry desiccant or powder will lower the relative humidity in the container, through larger moisture sorption capacity [317].

The change in relative humidity within packaging over the time of a stability test can be estimated from moisture sorption isotherms and the moisture vapor transmission rate of the packaging system, along with ambient conditions [317]. In practice, it is typical for moisture to transfer quickly from the dosage form to the desiccant until the relative humidity is equilibrated; thereafter, external moisture will slowly enter the packaging and increase the water content of the powder and desiccant over time [317].

It may be of interest to store the powder at a low, but optimized non-zero moisture content since very dry powder may lead to increased degradation and electrostatic charging can make filling and handling difficult [33,47,188]. The simplest method for equilibrating moisture for passive relative

humidity control is to place the materials in an environmental chamber that is set to the desired relative humidity and temperature [316]. The moisture adsorbed to the packaging material and desiccant and in the headspace of the packaging material should be equilibrated to the desired level prior to packaging. The desiccant is most crucial to equilibrate, as it generally has the highest moisture capacity. Equilibration can be verified by placing the desiccant in a sealed container (such as a bottle) within the environmental chamber and measuring the relative humidity in the bottle with a hygrometer [316]. A supplemented phase diagram can be used to choose moisture equilibration parameters, as discussed later in this chapter.

Biologic powders have been packaged to protect against moisture using heat-sealed aluminum foil bags containing desiccant [49,52]. It is crucial that there are no humidity excursions during the stability testing period, which can last on the order of years; hence, double packaging and double heat sealing are recommended. In addition to desiccant, for some biologics, it may be useful to add antioxidant and perform a nitrogen purge when packaging [59,255]. Instead of an external antioxidant pack, excipients such as ascorbic acid can be added to the spray drying formulation to work as an oxygen scavenger [18].

1.13 Process Modeling

In this section, thermodynamic modeling of a spray drying process is used to predict the outlet temperature and relative humidity for different inlet conditions. This is important since the outlet temperature and relative humidity are key factors in determining the biological and physical stability of the developed particles. The process model presented here is similar to those presented in the literature [97,318]. It is developed by applying a mass and energy balance on the spray dryer under steady state conditions. The following paragraphs contain a brief derivation of the process model.

For incompressible liquids and ideal gases at constant pressure, the relation between enthalpy, h, and temperature, T, at two locations (here, 'in' and 'out') is given by:

$$h_{out} - h_{in} = c_p \, (T_{out} - T_{in}) \tag{1.9}$$

where c_p is the specific heat capacity. For this equation to be valid c_p must be constant, and, thus, this equation alone does not adequately describe the enthalpy change when phase change is present, such as when there is evaporation, in which case, latent heat must also be considered.

The steady state conservation of energy equation developed considering a control volume around the spray dryer, neglecting energy changes associated with kinetic energy and elevation, is given by:

$$\dot{m}_{ag}h_{ag,in} + \dot{m}_{dg}h_{dg,in} + \dot{m}_{w}h_{w,in} = \dot{Q}_{loss} + \dot{m}_{ag}h_{ag,out} + \dot{m}_{dg}h_{dg,out} + \dot{m}_{w}h_{w,out} \quad (1.10)$$

where $\dot{m}$ refers to mass flow rate, the subscript 'ag' represents atomizing gas, 'dg' drying gas, and 'w' liquid feed solvent (considered as water here). Unless sufficient insulation is used, the spray dryer cannot be considered adiabatic and the heat loss, $\dot{Q}_{loss}$, is non-zero. Using the enthalpy relation in Equation (1.9) and considering latent heat of evaporation, $\Delta h_{w,evap}$, Equation (1.10) can be rearranged as:

$$\dot{Q}_{loss} = \dot{m}_{dg}c_{p,dg}\,(T_{in} - T_{out}) - \dot{m}_{w}\Delta h_{w,evap} \quad (1.11)$$

where the sensible heat associated with the liquid feed and atomizing gas have been omitted for the sake of simplicity. It is assumed that the drying gas is at 0% relative humidity, the effect of dissolved solids can be neglected, c_p of the drying gas is constant over the ranges tested, and the gas is incompressible and ideal as stated previously. For closed-cycle systems, which are often used after scale-up, the model may differ, particularly if the inlet drying gas has a non-zero relative humidity [97].

The dryer heat loss decreases the temperature the droplet or particle is exposed to and increases the relative humidity and hence moisture content of the produced powder [31]. The heat loss can be most easily modeled empirically; here, the case where the heat loss can be approximated as a linear function of the outlet temperature is considered:

$$\dot{Q}_{loss} = \alpha\, T_{out} + \beta \quad (1.12)$$

where α and β are experimentally determined constants.

Combining Equations (1.11) and (1.12) gives:

$$\alpha\, T_{out} + \beta = \dot{m}_{dg}c_{p,dg}\,(T_{in} - T_{out}) - \dot{m}_{w}\Delta h_{w,evap} \quad (1.13)$$

which can be rearranged to:

$$T_{out} = (\dot{m}_{dg} c_{p,dg} T_{in} - \dot{m}_w \Delta h_{w,evap} - \beta) / (\dot{m}_{dg} c_{p,dg} + \alpha) \quad (1.14)$$

The outlet relative humidity, RH_{out}, can be calculated according to:

$$RH_{out} = (P_w / P_{w,sat}) \times 100\% \quad (1.15)$$

where the water vapor partial pressure, P_w, is given by:

$$P_w = P_{out} \times (\dot{m}_w / M_w) / [(\dot{m}_w / M_w) + (\dot{m}_{dg} / M_{dg}) + (\dot{m}_{ag} / M_{ag})] \quad (1.16)$$

where P_{out} is the pressure at the outlet which can be measured (see Figure 1.1) and predicted empirically for different process conditions, the powder moisture content is neglected, and M refers to molecular mass. The saturation vapor pressure, $P_{w,sat}$, can be determined as a function of T_{out}, for example, according to the Antione equation for water vapor pressure [319]:

$$P_{w,sat} = 10 \text{ ^ } \{7.113 - [1685.6 / (T_{out} - 43.154)]\} \quad (1.17)$$

where T_{out} is in units of Kelvin and $P_{w,sat}$ is in units of kilopascals.

The relative humidity calculated using Equation (1.15) can be verified by replacing the outlet temperature probe used in typical commercial laboratory-scale spray dryers with a combined temperature and relative humidity probe. Note that the outlet temperature and relative humidity may differ from the temperature and relative humidity in the collection bottle. External surface thermometers can be used to measure the temperature of the collection bottle [95]. A common method for controlling the temperature and hence relative humidity in the collection bottle is to use a water bath [237].

From Equations (1.14) and (1.15), the outlet temperature and outlet relative humidity can be modeled for various inlet temperatures and gas flow rates. The process model plots in Figure 1.3 illustrate this relationship. As expected, higher drying gas flow rate and higher inlet temperature lead to higher outlet temperature and lower outlet relative humidity, whilst higher liquid feed flow rate leads to lower outlet temperature (due to evaporative cooling) and higher outlet relative humidity.

The necessary use of lower process temperatures with biologics leads to higher relative humidity for the same drying gas and feed flow rates, which corresponds to greater moisture uptake in the

powder. Process modeling is useful for predicting how scenarios like this will affect the properties of the powder. This is possible by using the outlet relative humidity to predict the moisture content in the powder, and to relate this to stability, as discussed further in the next section.

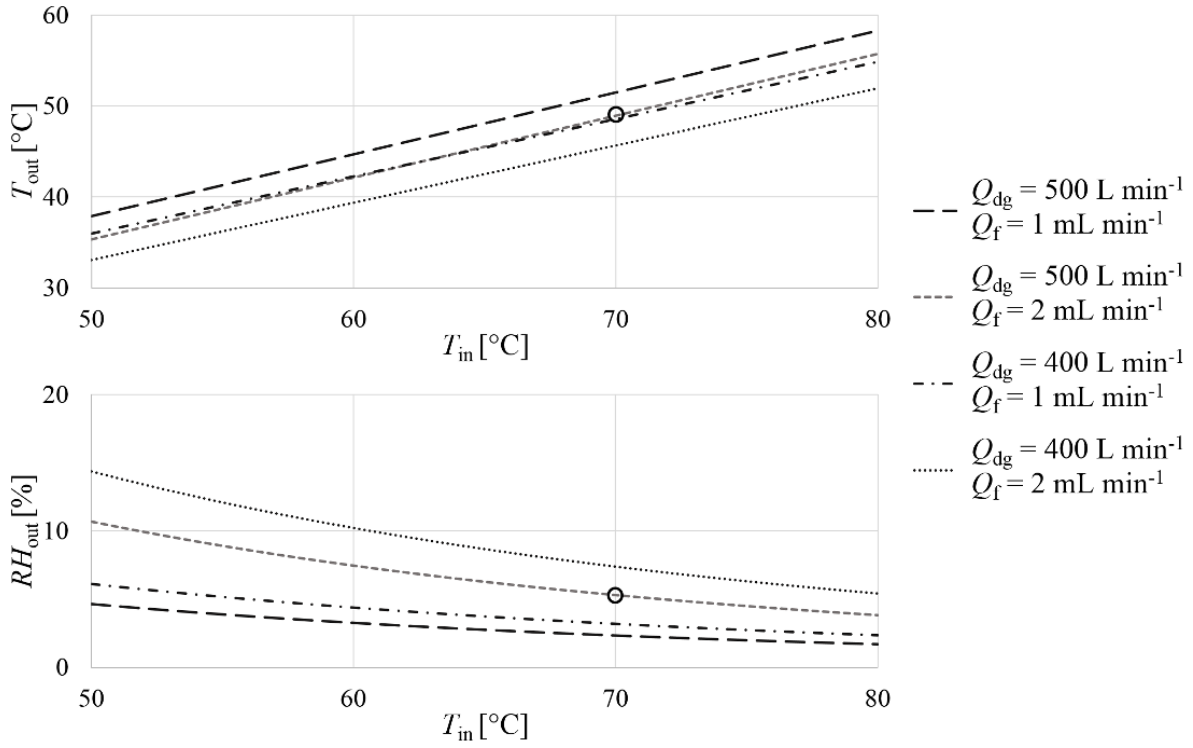

Figure 1.3: Outlet temperature and outlet relative humidity for different inlet temperatures, drying gas flow rates, and liquid feed flow rates based on a spray dryer process model developed for the laboratory-scale spray dryer in Figure 1.1. The experimentally determined constants are $\alpha = 4.7 \times 10^{-3}$ kW/K and $\beta = -1.4$ kW. Chosen process parameters used in Figures 1.4 and 1.5 are indicated by circles.

1.14 Supplemented Phase Diagram

A supplemented phase diagram can be used to predict the physical and possibly the biological stability of powder for different storage conditions. The first step in developing the supplemented phase diagram is to determine the moisture uptake of the powder for different relative humidity levels. The relationship between equilibrium moisture content and relative humidity can be obtained experimentally, for example, using dynamic vapor sorption and Karl Fischer instruments. Equilibrium moisture uptake for amorphous trehalose can also be estimated from the literature [320-323], but more data at low relative humidity levels is desirable.

The glass transition temperature of an amorphous powder decreases with increasing moisture content, an effect known as plasticization [288]. The glass transition temperature can be determined using MDSC. The use of a sinusoidal heating rate overlaid on a ramp heating rate in MDSC allows for the distinction between reversible and non-reversible heat flow for easier detection of glass transitions [243]. Lower heating rates in MDSC are more representative of real-time stability and give lower glass transition temperature values [324], but take longer to perform and provide weaker signals that may be difficult to detect. It is important that the pan and lid are hermetically sealed during MSDC measurements, otherwise, the dry glass transition temperature (only relevant to 0% relative humidity storage) will be measured; unfortunately, this mistake is often made in the literature.

When the glass transition temperature is known only for individual components within a powder containing a well-mixed amorphous glass, the glass transition temperature of the mixture, $T_{g,mix}$, can be estimated using the Gordon-Taylor equation [325]:

$$T_{g,mix} = (w_1 T_{g,1} + K w_2 T_{g,2}) / (w_1 + K w_2) \quad (1.18)$$

where $1 = w_1 + w_2$, with w referring to mass fraction. Equation (1.18) can also be used to predict the glass transition temperature of a single amorphous excipient for different moisture contents. An estimate for the constant K is 7.5 for trehalose (subscript 1) and water (subscript 2), when trehalose is assumed to have a dry glass transition temperature $T_{g,1} = 387$ K and water is assumed to have a glass transition temperature $T_{g,2} = 138$ K [326].

Summaries of the wet glass transition temperature of trehalose for different moisture contents are given in the literature [323,327]. Figure 1.4 gives the wet glass transition temperature of trehalose for different relative humidity levels predicted by the Gordon-Taylor equation using the constants given previously, along with the corresponding moisture content. The predictions are more accurate at higher relative humidity levels. Note that the glass transition temperature here is only for the moist trehalose component of a particle. For a mixture of amorphous components or partially ordered shell or coating the glass transition temperature may vary with the radial dimension of the particle [24]. At the same moisture content, sucrose has a much lower glass transition temperature than trehalose, and therefore may not be as suitable of a glass stabilizer for storage at room temperature [323,326].

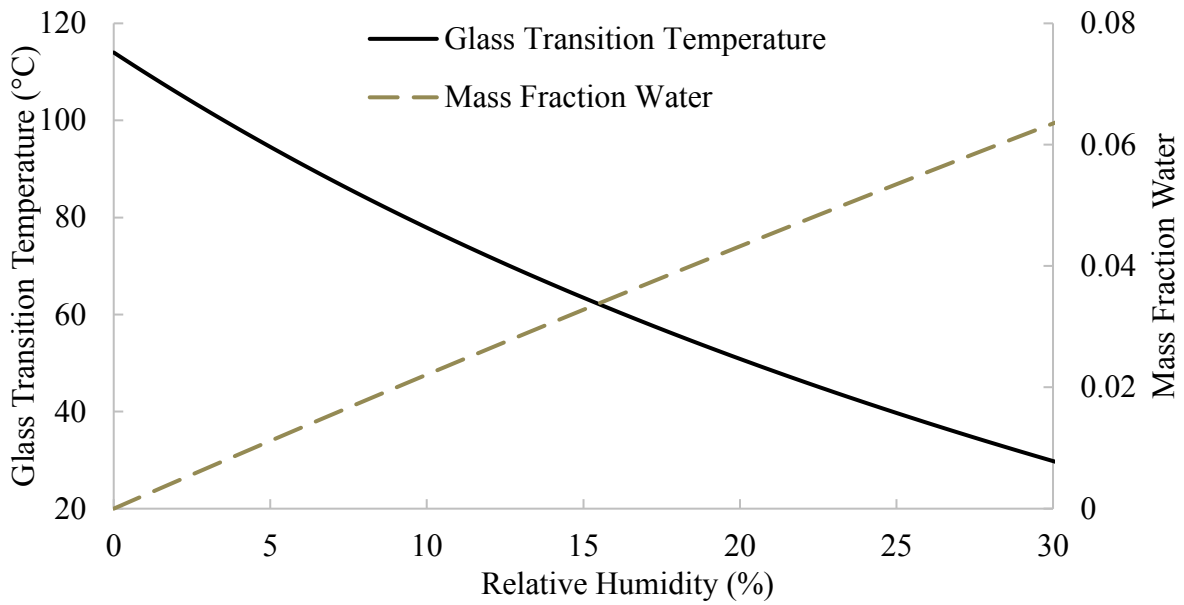

Figure 1.4: Glass transition temperature and mass fraction of water in amorphous trehalose equilibrated at different relative humidity levels. Glass transition temperature was predicted using the Gordon-Taylor equation (1.18) for a trehalose-water system using $K = 7.5$ [326], whilst the mass fraction of water is determined from Roe *et al.* [323]. The values expected at the spray dryer outlet for the process parameters chosen in Figure 1.3 are indicated by circles.

A non-equilibrium supplemented phase diagram conveniently combines the previously discussed factors of temperature, moisture, and time into a single graph, enabling predictions of physical stability for an amorphous powder [31]. With this approach, the stability of the biologic in the amorphous matrix formulation can be estimated prior to any experiments, saving development time and resources. Figure 1.5 shows a supplemented phase diagram for the spray drying of trehalose with the process conditions presented in Figure 1.3, plasticization data from Figure 1.4, and a storage condition of 5% relative humidity and 30°C.

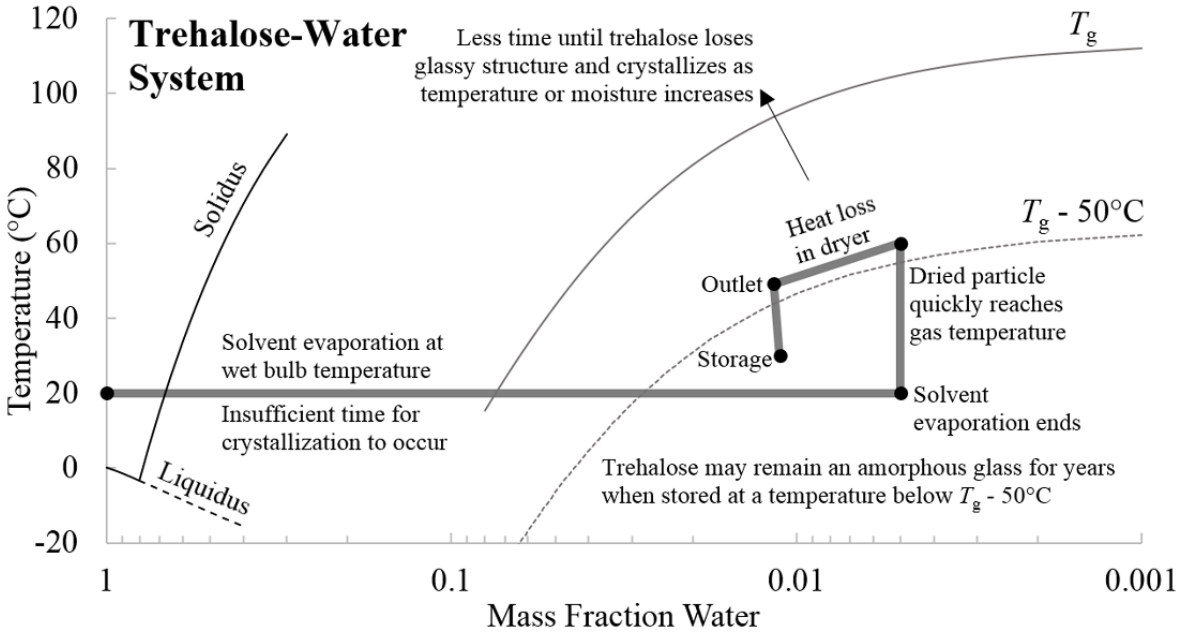

Figure 1.5: Non-equilibrium supplemented phase diagram for a trehalose-water system. The solidus and liquidus were approximated from data available in Chen *et al.* [327] and Roe *et al.* [323]. The thick line represents an approximation of the spray drying process from atomization to storage for the parameters chosen in Figure 1.3. The plasticization curve (glass transition temperature for different mass fractions of water) was developed using values from the Gordon-Taylor equation as per Figure 1.4. The storage condition is 5% relative humidity and 30°C.

The drying occurs very quickly, as the droplet lifetime predicted from Equation (1.4) is very small, on the order of milliseconds for the spray dryer in Figure 1.1, and, thus, the dried particles form early in the dryer. The quick evaporation occurs at a temperature much lower than the drying gas temperature due to evaporative cooling and can be approximated by the wet bulb temperature [31]. It is assumed that after evaporation ends, the particle temperature quickly increases to the surrounding gas temperature [31]. Further modeling would be required to determine the surrounding gas temperature at the location in the dryer where the particles are at the end of the droplet lifetime (only an estimate is given in Figure 1.5). As further heat loss occurs during the drying process, the relative humidity will increase accordingly, as cooler air has a lower saturated vapor pressure according to Equation (1.17). This increase in relative humidity may lead to more moisture in the powder near the outlet and in the collection bottle than further upstream. The collector temperature is usually assumed to be the same as the outlet temperature [31], but it is

likely lower without external control. The collector temperature can be raised to decrease relative humidity in the collector and hence decrease the moisture content in the powder, as explained previously.

The storage temperature is typically lower than the outlet temperature. A rule of thumb is that the wet glass transition temperature of the biologic powder should be 50°C above the storage temperature for long-term stability to be expected [303]. The relative humidity of the powder and packaging material should be designed as per Figures 1.4 and 1.5, to ensure the correct moisture content is achieved to meet this requirement. It can be seen that leaks that raise the moisture content of the powder (move the storage condition to the left in the supplemented phase diagram) can detrimentally affect long-term physical stability. Additionally, following different process paths on this diagram may lead to different levels of biologic inactivation. As explained previously, the use of a system-specific mobility transition temperature may eventually replace the T_g - 50 rule of thumb [288].

Long-term room temperature stability of bacteriophage in a leucine and trehalose powder stored under dry conditions has been demonstrated [126]. Stability without refrigeration is a particularly useful attribute with respect to distribution of biologics to developing countries. While dry storage is simple and practical in many applications, it may not be optimal for all biologics, as previously explained. When a powder is required to have stability at comparatively high relative humidity, the use of a high glass transition temperature polymeric excipient such as pullulan can prevent trehalose from crystallizing at high relative humidity and temperature, improving the storage stability in those conditions [320]. Excellent chemical and aggregation stability of salmon calcitonin and human growth hormone stored at high relative humidity has been demonstrated with trileucine [170].

Further to the supplemented phase diagram, a thermodynamic design space can be developed within which good stability and manufacturability is expected [97,140,328]. The design space consists of constraints to parameters such as inlet and outlet temperature, drying gas flow rate, and feed flow rate. The outlet temperature is constrained to a maximum based on thermal degradation and to a minimum based on relative humidity considerations [97]. Hot-bench experiments, whereby visible observations for cohesiveness, discoloration, or melting are made on a small amount of powder spread over a metal strip with a known thermal gradient along its length have

been suggested to define a maximum temperature the powder can be exposed to [97]. A constraint on the minimum ratio of the feed flow rate to drying gas flow rate has been suggested to ensure an acceptable throughput is achieved [97]. For twin-fluid atomizers, the atomizing gas flow rate may be constrained by the feed flow rate and particle size considerations.

Physical instability can lead to biological instability [295], and many studies have demonstrated more loss of biologic activity with increasing drying gas temperature [12,14,95,146,193,255,329]. Developing a thermodynamic design space for biological stability in addition to physical stability is a subject for future work.

1.15 Summary to Engineering Spray Dried Biologic Powder for Inhalation

Applying engineering principles to the spray drying process expedites the development of stable spray dried biologic powder for inhalation that may eliminate the need for cold chain infrastructure and thus increase market access in developing countries. Formulation using leucine or trileucine as shell-forming excipients and trehalose as a glass stabilizer are promising combinations for the development of dispersible and stable spray dried biologic powders.

Scale-up and aseptic spray drying have proven feasible with some spray dried biologics produced at a manufacturing scale having already reached the market.

Twin-fluid atomizers can produce particles with sizes suitable for inhalation and typically result in an acceptable level of shear stress on the biologic. Inactivation of biologics at the air-liquid interface may occur in the drying process and can be decreased through the use of suitable excipients.

The droplet evaporation and particle formation processes are relatively well understood. Particle engineering models are available to predict the characteristics of spray dried particles, including the surface enrichment and radial distributions of different excipients, solid state, and particle size. Once dried, the particles are typically collected into a collection bottle using a cyclone, from which samples can be taken and analyzed using various particle analysis techniques to verify the predictions from particle engineering models.

The separation of biologic inactivation due to spray drying and rehydration of the powder for bioassay is difficult, and the use of rehydration media representative of lung fluid can be

informative. Aerosolization of spray dried biologic powder can be performed with DPIs, and suspension of spray dried biologic powder in a suitable liquid medium allows for aerosolization with nebulizers, pMDIs, and SMIs. Since biologic inactivation due to aerosolization is variable between strains and inhalation devices, it needs to be tested on a case-by-case basis. A comprehensive analysis of losses, including extrathoracic deposition and device losses such as face mask leaks or device retention, should be undertaken when designing the dosage form and choosing the dose.

Trehalose is often a suitable excipient for glass stabilization of biologics. The reason trehalose is a good glass stabilizer appears to be related to its high glass transition temperature, high hydration number, and small size, which allows for direct replacement of hydrogen bonds lost by the biologic during desiccation. The RH-perfusion microcalorimetry technique may be particularly useful for predicting long-term physical stability of spray dried powder and may eventually replace the use of the T_g - 50 rule of thumb for predicting long-term physical stability. When performing long-term stability studies, it is crucial to ensure the packaging maintains a suitable relative humidity for the duration of the study. The use of moisture equilibrated desiccant for passive relative humidity control may be useful in this regard.

The conditions that powder is exposed to at the outlet of a spray dryer can be predicted using a process model derived from a mass and energy balance on the spray dryer. The temperature and relative humidity to which the droplets and particles are exposed throughout the spray drying process can be overlaid on a supplemented phase diagram, which is developed from plasticization data for the glass stabilizer. Use of this diagram allows for prediction of long-term stability and manufacturability early in product development.

Suggested directions for future work include determining material properties and characterizing the inhalation toxicology of alternative excipients, characterizing the mechanisms of biologic inactivation in response to selected stresses, and characterizing the use of excipients to stabilize against these specific stresses. Additionally, investments in aseptic spray drying, clinical trials, and the development of straightforward regulatory guidelines will contribute to the engineering and commercialization of more spray dried biologic products for inhalation.

2 Amorphous Shell Formers Improve the Biological Stability of Spray Dried Anti-*Campylobacter* Bacteriophage

This chapter has been partially published in "Carrigy NB, Liang L, Wang H, Kariuki S, Nagel TE, Connerton IF, Vehring R. 2018. Mechanistic modeling expedites the development of spray dried biologics, pp. 1551-1558 in Proceedings of 21st International Drying Symposium. Cárcel JA, Clemente G, García-Pérez JV, Mulet A, Rosselló C. (eds.) València, Spain: Editorial Universitat Politècnica de València." Additional material is given in Appendix A.

2.1 Abstract

A spray drying process was developed to stabilize bacteriophage for use as an anti-*Campylobacter* powder additive to chicken feed in Kenya. Three factors contributed to a greater proportion of bacteriophage remaining active after spray drying: the use of a twin-fluid atomizer rather than a vibrating mesh atomizer, purification by centrifugation and dilution of the bacteriophage lysate, and the use of excipient formulations containing a high glass transition temperature amorphous shell former rather than a crystalline shell former. Both trileucine, a surface-active tripeptide, and pullulan, a high molecular mass polysaccharide, were demonstrated through experiment to be suitable amorphous shell formers for stabilizing anti-*Campylobacter* bacteriophage. Neither of these excipients has been tested with bacteriophage before. Particle formation mechanisms are proposed to explain why the amorphous shell formers stabilize the bacteriophage against the main inactivating stress, desiccation at the surface of the microparticles. For bacteriophage formulation with trileucine and trehalose, the combined effects of formulation, spray drying, ambient temperature shipping of the powder from Canada to England, and 1 month of dry room temperature storage resulted in a titer reduction of only 0.6 ± 0.1 log(pfu/mL). The powder did not require cold chain shipping, so it may prove useful for the delivery of efficacious bacteriophage and decreasing the incidence of foodborne illness in Kenya associated with *Campylobacter* in poultry. The proposed amorphous shell platform may also be advantageous for stabilizing biologics in other spray drying applications in the food and pharmaceutical industries.

2.2 Introduction

Campylobacter jejuni is a species of gram-negative bacteria that causes foodborne illness worldwide [330]. *C. jejuni* is prevalent in the gut of chickens and can be present at high

concentrations in raw meat with an attendant high risk of cross-contamination, and can persist in improperly cooked chicken [330-333]. In Kenya, *C. jejuni* is one of a number of foodborne bacteria that pose a substantial threat of mortality to children [334-336]. This study aims to address this issue through the development of a stable spray dried bacteriophage (phage) dry powder that can be added to chicken feed to decrease the levels of *Campylobacter* bacteria in chicken gut in Kenya.

Phages are parasitic viruses that are ubiquitous in the environment, their presence dependent on the availability of suitable bacterial hosts. Anti-*Campylobacter* phages have been demonstrated to be active against *Campylobacter* bacteria from chickens [332, 337-339], including antibiotic-resistant strains [340], which are becoming increasingly prevalent [341]. Phages have a low inherent toxicity since one species of phage typically infects only a narrow-spectrum of bacteria, thus not substantially impacting other community members of the microbiota [342-345].

Spray drying involves the atomization and subsequent drying of liquid formulation into a solid powder. Dry powder has less weight and volume compared to liquid, which can reduce transportation costs and storage space requirements [346]. Additionally, water-mediated degradation is minimized, thereby improving the thermal stability of biologics [347-352]. This greater stability can obviate the need for refrigeration and cold chain infrastructure for shipping, which is important for use in developing countries (see Chapter 1 [353]). Compared to another commonly used method for powder production, lyophilization, spray drying is a relatively low-cost process, which is also important for its successful implementation in developing countries [354-361]. Additionally, lyophilization is a lengthy batch process that is difficult to scale-up and typically requires milling or sieving to adjust the particle size [362-363], whereas spray drying is a fast, continuous, and scalable process for producing powder with controlled particle size, distribution, and density, as well as surface composition, roughness, and flowability [364].

It is imperative that phage remain active (capable of infecting bacteria) in order to have the desired effect; indeed, early attempts at phage therapy were sometimes unsuccessful due to the use of inactive preparations [342,365]. Therefore, an important aspect of spray dried phage product development is minimizing titer reduction (phage inactivation) due to processing, storage, and shipping. Factors that can inactivate biologics, such as phages, include shear, desiccation, osmotic shock, light, heat, and pH (see Chapter 1). It is usually not known *a priori* which factors lead to substantial titer reduction for a specific phage, and therefore experimental measurements to isolate

the factors causing titer reduction are required. Importantly, data in the literature indicates that it is feasible to spray dry phage to a high titer [366-367], and to achieve long-term stability under refrigerated [368] and room temperature dry storage [369] conditions.

The most commonly used excipient combination in spray dried phage formulation is trehalose with leucine. Matinkhoo *et al.* [366] spray dried *Burkholderia* phages in a leucine and trehalose formulation using a Büchi B-90 and found ~0.8 log(pfu/mL) titer reduction for *Myoviridae* phage KS4-M and ~0.4 log(pfu/mL) titer reduction for *Myoviridae* phage KS14. Leung *et al.* [367] observed ~1.3 log(pfu/mL) titer reduction due to leucine and trehalose formulation and spray drying of *Podoviridae* phage PEV2 active against *Pseudomonas* using a Büchi B-290. In a follow-up study [368], it was demonstrated that formulation with 80% trehalose and 20% leucine outperformed formulations containing different excipient ratios or mannitol in terms of titer reduction after one year of refrigerated storage at 0% or 22% relative humidity. They also demonstrated that spray dried phage PEV2 and *Myoviridae* phage PEV40 formulated using leucine and trehalose were stable for one year at refrigerated or 20°C storage using vacuum packaging [369]. Chang *et al.* [370] demonstrated that, out of many different excipients (trehalose, lactose, mannitol, glycine, leucine, PEG3000, and Pluronic F-68) and mass fractions tested with *Podoviridae* phage PEV1, the leading formulation contained 17 mg/mL trehalose and 8 mg/mL leucine, for which only 0.2 log(pfu/mL) titer reduction was observed.

In this paper, anti-*Campylobacter* phages (*Myoviridae)* were spray dried using trehalose with leucine, as well as novel formulations. The causes of phage titer reduction were explored and the effect of shipping and 1 month of dry room temperature storage on the biological stability was determined. A particle formation mechanism was proposed to explain why certain dry powder formulations stabilize phage better than others.

2.3 Materials and Methods

2.3.1 Process Overview

The process of spray drying phage requires a number of steps, each with factors that could affect the resulting titer of the phage in the produced powder. Therefore, tests (see Figure 2.1) were performed to determine the effects that various factors (such as phage type, amplification media, purification procedure, shipment temperature, formulation method, spray dryer type, and powder resuspension method) had on the titer reduction. Experiments in this study were split between

Nottingham, England, where phage lysate preparation and plaque assays took place, and Edmonton, Canada, where formulation, spray drying, and packaging took place. The different numbered steps in the production and assay of spray dried phages are indicated in Figure 2.1 and are discussed briefly, along with the factors tested for each numbered step, in the following paragraphs. The paths followed for the various numbered steps in each set of experiments are indicated in Sections 2.3.2-2.3.8.

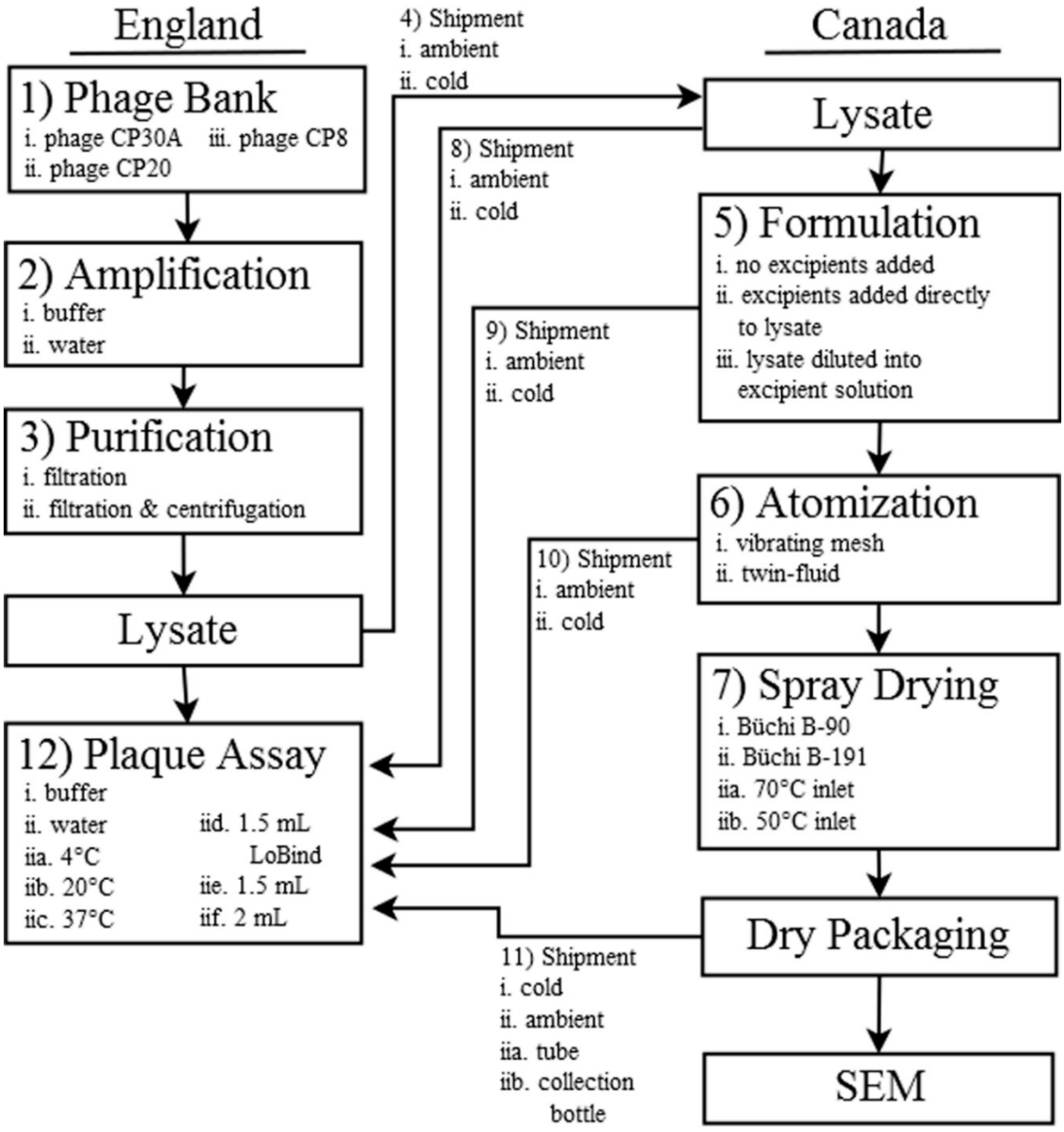

Figure 2.1: Block diagram of the experimental steps involved in the production and assay of spray dried phage powder along with the tested factors.

Phage stock (1): Phages CP30A (vB_CjeM_CP30A; NCBI nucleotide accession JX569801) and CP8 (vB_CjeM_CP8; NCBI nucleotide accession JX569801) are group III (CP8unalikevirus) with genome sizes of approximately 140 kb; CP20 (vB_CcoM_CP20; NCBI nucleotide accession MK408758) is group II (Cp220likevirus) based on a genome size of approximately 175 kb [371]. All are *Eucampyvirinae* of the family *Myoviridae* that infect *Campylobacter jejuni* and/or *Campylobacter coli.* These phages were isolated from chicken excreta and are present in chicken gut [337,345,371-376]. A transmission electron micrograph (TEM) of phage CP30A is given in Figure 2.2.

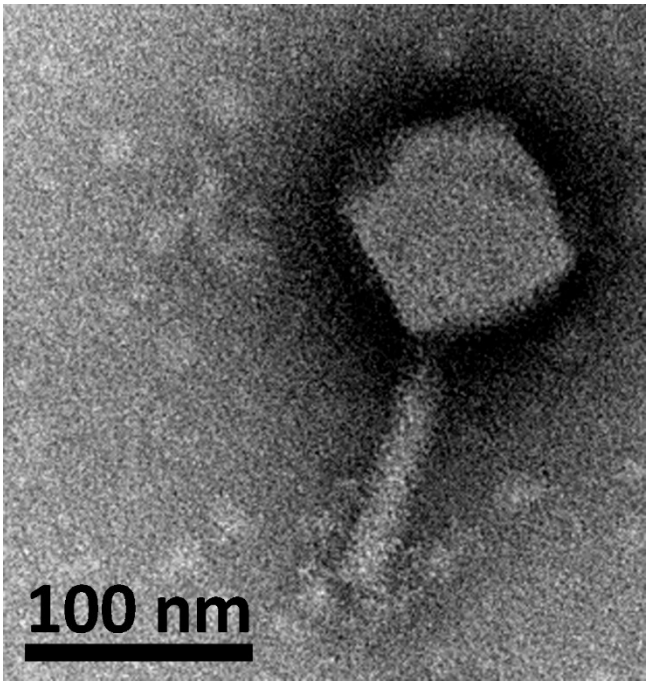

Figure 2.2: TEM image of phage CP30A prepared using the method described in Chapter 4 [377].

Amplification (2): High titer phage lysates, typically ~9.5 $\log_{10}$(pfu/mL), were generated by adding 100 µl of phage at 7 $\log_{10}$(pfu/mL) to 500 µL of bacterial suspension at 8 $\log_{10}$(cfu/mL). This mix was then transferred to 5 ml of melted NZCYM overlay agar, which was pre-tempered to 50°C, and poured onto NZCYM agar plate. After overnight incubation at 42°C under microaerobic conditions, the plates were then flooding with either i) buffer or ii) water. The host strain was isolated from United Kingdom broiler flocks in a previous study [337]. The propagation process is discussed in detail elsewhere [378].

Purification (3): The amplified lysate was passed through a 0.22 μm filter. The filtered lysate was either (i) used as is or (ii) 30 mL at a time was purified by centrifugation at 3.4 x 10^5 m/s^2 [35,000 x g] for 120 minutes at 4°C. After centrifugation, the supernatant was drained and the pellet was resuspended in 30 mL of reverse osmosis water. The resuspension had a solids content less than 0.5 mg/mL, as measured post-evaporation of suspensions on pre-weighed microscope slides.

Lysate shipment (4): An aliquot of the lysate was titered using plaque assay while the remainder was shipped from England to Canada either (i) ambient (without cold packs) or (ii) cold (with cold packs, initially at a temperature of ~4°C). In both cases, shipment occurred with the tube containing the lysate within another secondary tube that was surrounded by foam peanuts in a Styrofoam box.

Formulation (5): Either (i) no further excipients were added to the lysate, (ii) further excipients were added directly into the lysate, or (iii) an excipient solution was made and the lysate was added at a dilution ratio of 1:100 to the excipient solution. Further details regarding the excipients tested are given in later sections.

Atomization (6): Atomization was performed using either (i) a vibrating mesh nebulizer (Aerogen Solo; Model no. 06675745, Lot 60201509300103, Ref AG-AS3350-US; Aerogen Ltd., Dangan, Galway, Ireland) with Pro-X Controller (S/N AP-1510412, Ref AG-PX-1050-IN; Aerogen Ltd., Dangan, Galway, Ireland) or (ii) a custom twin-fluid atomizer. Atomization occurs within the spray dryer, but separate measurements were also performed atomizing the formulated lysate directly onto a filter, as detailed in Section 2.3.3.

Spray drying (7): Spray drying was performed using either (i) a modified Büchi B-90 spray dryer (Büchi Labortechnik AG; Flawil, Switzerland) that uses the vibrating mesh nebulizer, or (ii) a modified Büchi B-191 spray dryer (Büchi Labortechnik AG, Flawil, Switzerland) that uses the custom twin-fluid atomizer. For the Büchi B-191 spray dryer, two different inlet temperatures were tested: (a) 70°C, and (b) 50°C. Process schematics of the spray dryer installations are given in Figure 2.3. An enclosure and a fume hood were used for biohazard control in the respective spray dryers. In the modified Büchi B-90 design, the liquid feed was inserted directly into the reservoir of the vibrating mesh nebulizer prior to the run. This custom configuration with the nebulizer outside the spray dryer minimizes heat exposure of the liquid feed prior to atomization. The modified design also includes a potentiometer to adjust the collecting voltage. Increasing

collecting voltage decreases outlet temperature, potentially due to ion wind caused by the electrostatic collector affecting dryer heat loss. A hygrometer (MI70 Measurement Indicator, serial #J0430061 with HMP77B humidity and temperature probe, serial #J0520002; Vaisala, Vantaa, Finland) was placed past the filter to measure temperature and relative humidity; the use of psychrometrics further allows for prediction of the relative humidity at the outlet. The collected powder was scraped from the collecting electrode onto collection paper and then transferred into a tube. In the modified Büchi B-191 design the formulation was fed to the custom twin-fluid atomizer using a peristaltic pump (Model no. 7528-30, Masterflex L/S, with pump head model no. 77200-60, Easy-load II; Cole-Parmer, Vernon Hills, IL, USA). The powder was collected into a collection bottle using a cyclone. A comparison of titer reduction with the two spray dryers is described in Section 2.3.4.

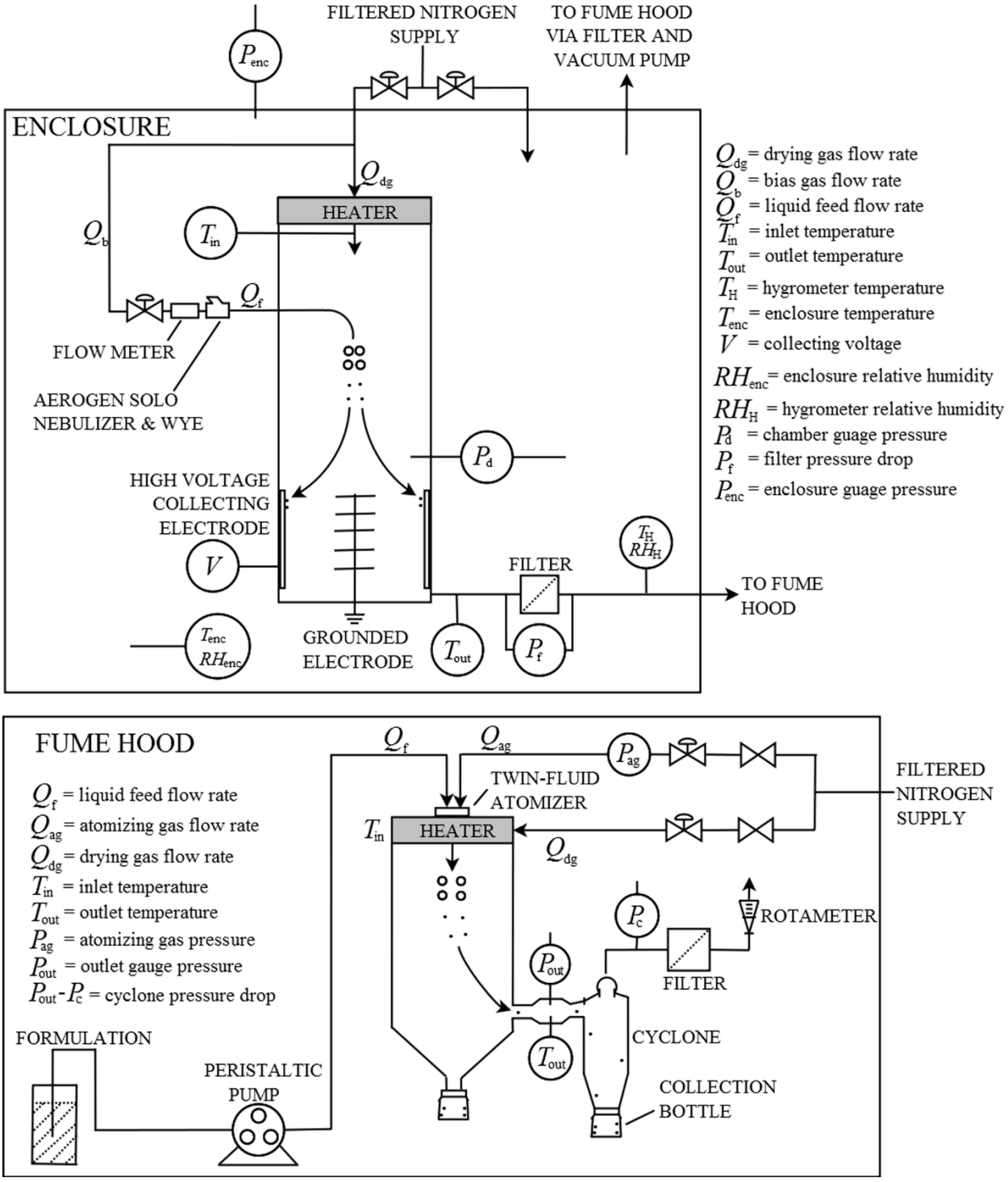

Figure 2.3: Process schematics of the spray dryer installations for the modified Büchi B-90 (top) and modified Büchi B-191 (bottom, as per Chapter 1). Important variables are denoted.

Lysate return shipment (8): The lysate was shipped from Canada to England either (i) ambient (without cold packs) or (ii) cold (with cold packs). In both cases, shipment occurred with the tube containing the lysate within a secondary bag that was surrounded by packing paper and placed in a Styrofoam box within a cardboard box. This lysate is termed a "Lysate Control".

Formulation return shipment (9): The formulated lysate was shipped from Canada to England either (i) ambient (without cold packs) or (ii) cold (with cold packs). Packaging was the same as for the lysate return shipment. This formulated lysate termed a "Feed Control".

Atomization return shipment (10): The atomized liquid was shipped from Canada to England either (i) ambient (without cold packs) or (ii) cold (with cold packs). Packaging was the same as for the lysate return shipment. These measurements were performed for the tests detailed in Section 2.3.3.

Dry packaging and shipment (11): Dry packaging was performed either (a) by placing the powder in 5 mL tubes (Catalogue no. 0030119487, lot G1710906; Eppendorf AG, Hamburg, Germany) and using double heat-sealed, double-bagged aluminium foil bags (Prod no. 139-313; Ted Pella, Inc., Redding, CA, USA) with molecular sieve desiccant packs (Cat no. 1523T76; McMaster Carr, Aurora, OH, USA), as per Figure 2.4, or (b) by shipping the entire collection bottle instead of a tube. Heat sealing was performed using an impulse sealer (No. 912951, type AIE-300; American International Electric, Inc., City of Industry, CA, USA). The packaging components were first placed in a nitrogen-purged enclosure for 4-10 hours to remove moisture. For the Büchi B-90, dry packaging occurred within the enclosure (see Figure 2.3). For the Büchi B-191, after spray drying the collection bottle (see Figure 2.3) was removed, quickly capped, and placed in the nitrogen-purged enclosure, where the powder was added to the tube and heat sealing took place. The packages were shipped from Canada to England either (i) ambient (without cold packs) or (ii) cold (with cold packs). The shipment occurred with the packages surrounded by packing paper and placed in a Styrofoam box within a cardboard box. In these as well as other shipping experiments, the temperature during shipment was monitored and recorded (TempTale 4 USB MultiAlarm; Sensitech Canada, Markham, ON, Canada). A portion of the powder was kept in Canada for scanning electron microscopy (SEM) (Zeiss Sigma FESEM, Oberkochen, Germany) while another portion was optionally kept for Raman spectroscopy to determine solid phase using a custom device developed by Wang *et al.* [379], or for stability studies, as discussed in later sections. The SEM settings throughout this study were 5000x magnification, an in-lens detector, a working

distance of ~7 mm, and an accelerating voltage of 2-5 kV. A gold coating of ~10 nm was applied prior to imaging.

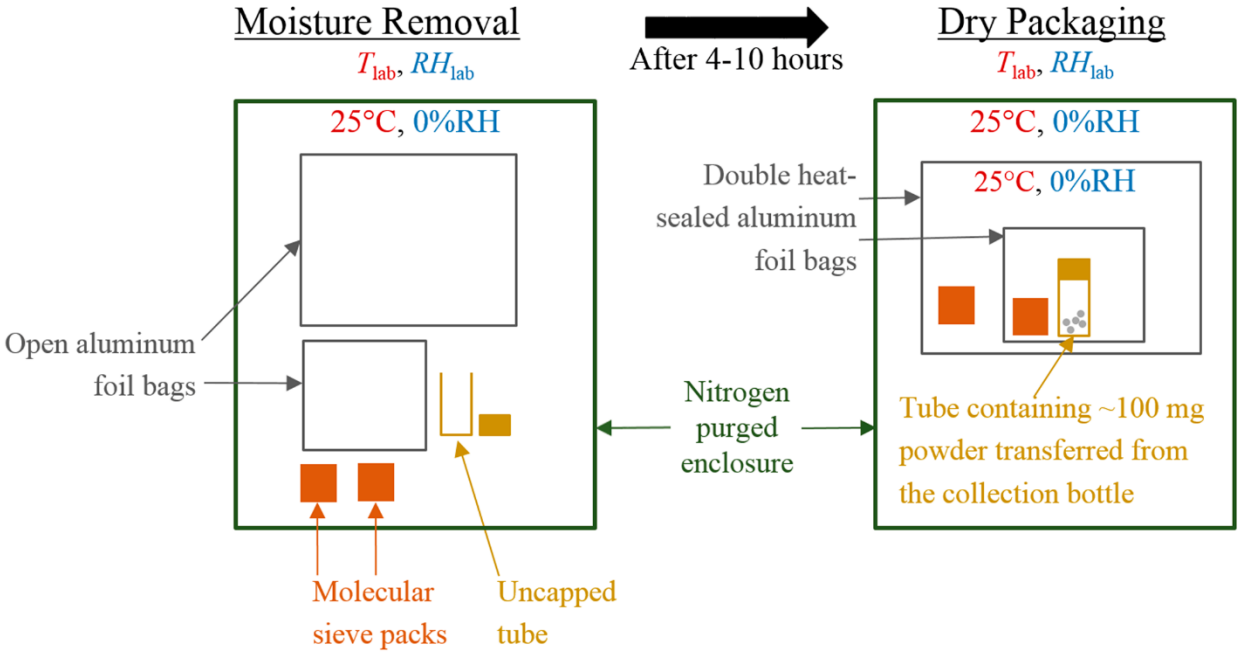

Figure 2.4: Dry packaging method. Full resolution color image available online.

Plaque assays (12): Plaque assays were performed using *C. jejuni* as the host strain. Spot assays were performed in triplicate at multiple dilution levels. For powder, it was necessary to resuspend into liquid at a concentration of 30 mg/mL prior to performing plaque assay to determine titer. Either (i) buffer, or (ii) water was used as the resuspension media and for the dilution series. The temperature of the media for powder resuspension was either (a) 4°C, (b) 20°C, or (c) 37°C. The tube that was used for powder resuspension was either the 5 mL tube shipped with the dry packaging (unless otherwise indicated), or (d) 1.5 mL Eppendorf Safe-Lock Tubes (Catalogue no. 0030120086; Eppendorf AG, Hamburg, Germany), (e) 1.5 mL Eppendorf Protein LoBind Tubes (Catalogue no. 0030108116; Eppendorf AG, Hamburg, Germany), or (f) 2.0 mL Eppendorf Safe-Lock Tubes (Catalogue no. 0030120094; Eppendorf AG, Hamburg, Germany). The titer is reported in units of $\log_{10}$ of plaque-forming units per millilitre: $\log_{10}$(pfu/mL).

2.3.2 Phage Stability in Solution

Phage titer in solution is known to decrease with increasing thermal stress [380], which could be important for shipping and liquid control measurements. Therefore, the first set of experiments

were to measure the stability of the liquid lysate at different temperatures over time. Measurements were performed with phage CP30A amplified in either buffer (path 1i-2i-3i in Figure 2.1) or water (path 1i-2ii-3i), or formulated with buffer having L-leucine (Code 125121000, lot A0269620; Acrōs Organics, NJ, USA) and D-(+)-trehalose dihydrate (Cat. no. BP2687; Fisher BioReagents, NH, USA) added directly (path 1i-2i-5ii, without shipping). The dissolved solids contents were chosen as 7.5 mg/mL leucine and 22.5 mg/mL trehalose as this is similar to the leading formulations for spray drying phage in the literature, as explained previously. These dissolved solids contents of leucine and trehalose are commonly used in this study and the formulation is referred to as F1.

Phage CP30A in F1 was shipped within a tube in a Styrofoam box without temperature control from England to Canada and back, either using buffer or water amplification media. These measurements were to determine if it is feasible to perform lysate control and feed control measurements with each spray drying experiment. The paths followed were: 1i-2i-3i-4i-8i-12i, 1i-2ii-3i-4i-8i-12i, 1i-2i-3i-4i-5ii-9i-12i, and 1i-2ii-3i-4i-5ii-9i-12i.

Further experiments were carried out to determine whether the formulated (F1) lysate was stable with vortexing. Specifically, phage CP30A lysate with leucine and trehalose (path 1i-2i-5ii, without shipping) was vortexed (Clifton Cyclone Vortex Mixer; Camlab Limited, Cambridge, UK) for different amounts of time (5, 10, 20, 40, 60, and 120 seconds) at a constant rotational speed of 2800 rpm used for plaque assay (path 12i). These were compared to a control without vortexing and a second control prepared by repeating pipetting. The lysate itself was assumed to be stable since it is regularly vortexed during amplification and purification.

Prior to entering the atomizer the feed formulation should be well-mixed to ensure that the biologic material is evenly distributed in the solvent, since some larger biologics may entangle or settle if not properly mixed, e.g. by stirring. Experiments were performed to determine if phage settling would occur without stirring during the timeframe of a typical spray drying experiment by taking samples of F1 from the top, middle, and bottom of the liquid in a 50 mL polypropylene Falcon tube (Catalogue no. 06-443-19; Fisher Scientific, Ottawa, ON, Canada) around 25 minutes into a spray drying run. The path followed was 1i-2i-3ii-4ii-5iii-9ii-12iib.

2.3.3 Phage Atomization

The spray rate from the twin-fluid atomizer is controlled by a peristaltic (positive displacement) pump and therefore can be controlled by the pump settings in a manner that is relatively independent of the fluid properties. Calibration with water found that an rpm setting of 8.3 corresponded to a spray rate of 1 mL/min, with a linear relation found between the variables. An atomizing gas flow rate of 1.5×10^{-4} kg/s and a spray rate of 1.7×10^{-5} kg/s were used. The air-to-liquid ratio, defined as the ratio of the mass flow rates of atomizing gas and liquid feed, was thus 8.8. From the air-to-liquid ratio and data for the present atomizer given by Hoe *et al.* [381], an initial droplet diameter of ~9 μm was predicted. Using a model presented by Boraey *et al.* [382], and the formulation compositions given in Section 2.3.1, the aerodynamic diameter at the onset of shell formation was predicted to be ~2 μm. Particles of this size can be collected with the cyclone in the Büchi B-191. For the vibrating mesh nebulizer, there is no atomizing gas. The spray rate (volume output per unit time) of the vibrating mesh nebulizer depends on properties of the liquid such as the viscosity and density and therefore was not directly controlled. Dry microparticles of similar size are expected to be produced with the Büchi B-90.

One potential cause of titer reduction is shear stress during atomization. A characteristic shear rate on the order of 1×10^{5} s^{-1} was expected for the twin-fluid atomizer according to a model presented by Ghandi *et al.* [383]. In the literature [367], phage have remained active after atomization at similar shear rates. In the present study, atomized droplets were assayed without much solvent evaporation in order to isolate shear stress from desiccation stress as much as possible. This aim was achieved using the method shown in Figure 2.5, whereby atomization occurred directly onto a filter (Respirgard II bacterial/viral filter, ref 303EU, lot 12127233; Vital Signs, Inc., Englewood, CO, USA) under conditions that allow for full humidification of the filter space without much evaporation from the droplets. For example, based on flow rates of water and air entering the filter space, it can be calculated that about 13% of the droplet volume will be evaporated to fully humidify the atomizing gas, nitrogen, for the twin-fluid atomizer. Therefore, phage may not concentrate on the surface of the droplets, desiccation and surface-induced titer losses are minimized, and the observed titer reduction is due primarily to shear stress. A custom adapter made from rigid opaque material simulating plastic (Objet VeroGray RGD850; Stratsys, Ltd., Eden Prairie, MN, USA), using a PolyJet 3D printer (Objet Eden 350V High Resolution 3D Printer; Stratsys, Ltd., Eden Prairie, MN, USA), connected the filter to the twin-fluid atomizer.

The atomized liquid remained suspended on the filter fibers. For both atomizers, 3 mL of filtered phage CP30A lysate in formulation F1 was completely atomized onto the filter and 10 mL of buffer was used for resuspension of the atomized droplets from the filter, the resuspended liquid was mixed by swirling the filter, and the liquid was drawn using a micropipette into a tube that was shipped for assay. The difference in titer between the initial lysate (path 1i-2i-3i-5ii-12i or 1i-2ii-3i-5ii-12i, not shipped) and the aerosol captured on the filter (paths indicated in the following sentences) was termed titer reduction. The variables tested were amplification media (2i and 2ii), shipping temperatures (4i and 10i, 4ii and 10ii), and atomization method (6i and 6ii). Specifically, measurements were performed with the following kept constant: 1i-3i-5ii-12i, while the following were the varied paths for each experiment: 2i-4i-6i-10i, 2i-4ii-6i-10ii, 2ii-4i-6i-10i, 2ii-4ii-6i-10ii, 2i-4i-6ii-10i, 2i-4ii-6ii-10ii, 2ii-4i-6ii-10i, 2ii-4ii-6ii-10ii.

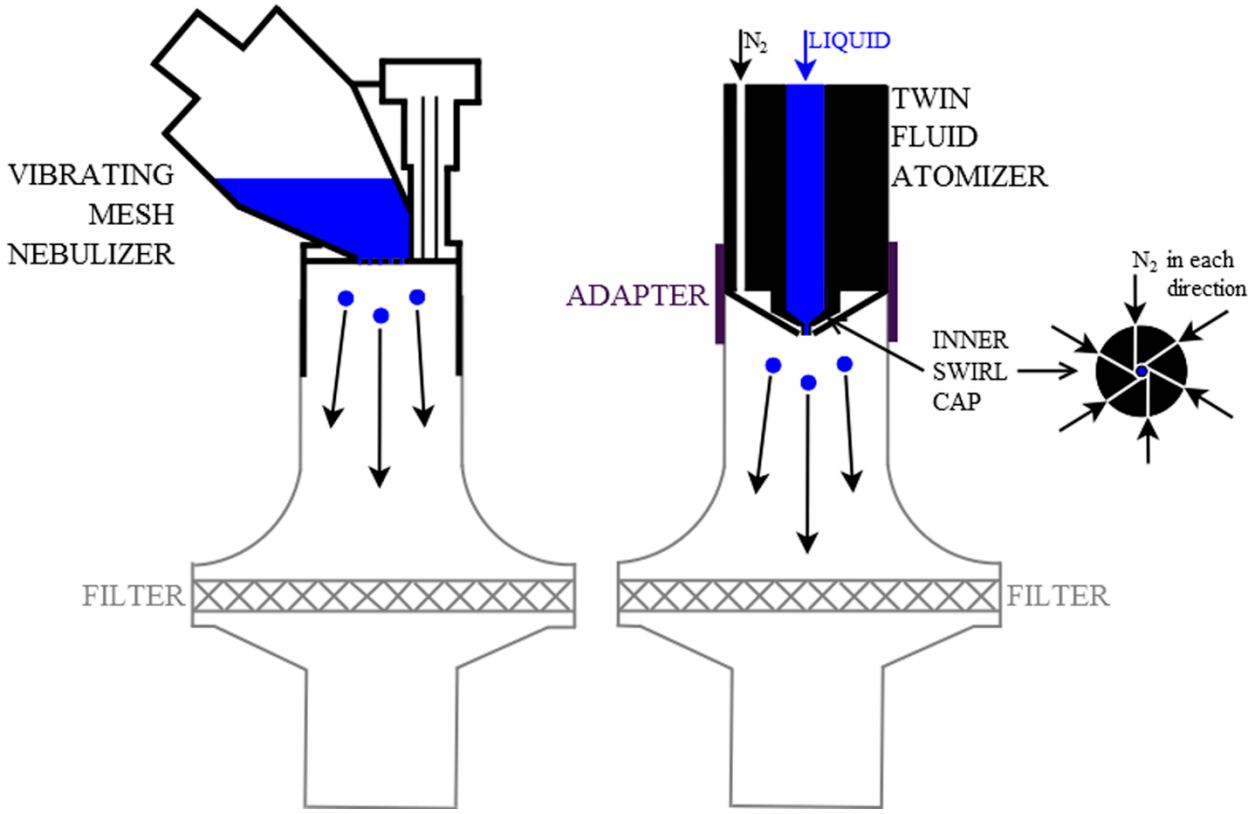

Figure 2.5: Schematic of the experiments used to determine the titer reduction due to atomization for an Aerogen Solo vibrating mesh nebulizer (left) and a custom twin-fluid atomizer (right). Full resolution color image available online.

2.3.4 Spray Dryer Comparison

A comparison of titer reduction due to spray drying with different dryer types was performed and compared to the titer reduction due to atomization in order to isolate the effect of stresses other than shear stress during atomization on phage titer reduction (such as desiccation stress). For both spray dryers an inlet temperature of 70°C was used, which is similar to literature values that resulted in phage not being inactivated to a great extent by spray drying [366-369]. The surface temperature of the atomized droplets is typically assumed to remain near the wet bulb temperature due to evaporative cooling [384]; therefore, thermal inactivation of the phage is not expected during initial stages of solvent evaporation. The drying gas flow rate was 425 L/min for the B-191 and 100 L/min for the B-90. The spray rate was set to 1 mL/min for the B-191 and measured to be 0.1 mL/min for the B-90. Using the process model described in Chapter 1 and Appendix A, the predicted outlet temperature and outlet relative humidity values were 49°C and 2.9% relative humidity for the B-191 and 44°C and 1.6% for the B-90. The moisture content in the powder was thus expected to be ~0.7% for the B-191 and ~0.4% for the B-90 based on trehalose moisture uptake data from Chapter 1. Both of these moisture contents are suitable for long-term physical stability (retention of amorphous structure) of trehalose for dry room temperature storage conditions, according to a trehalose-water supplemented phase diagram in Chapter 1. This is important since the trehalose must remain amorphous to ensure glass stabilization; crystallization of trehalose has been shown to inactivate phage [385].

The powder was packaged dry prior to shipping as described previously in Figure 2.4. The paths tested were similar to those for atomization experiments to allow for a comparison. Specifically, the paths tested were: 1i-2ii-3i-4i-5ii-7i-11iia-12i, 1i-2i-3i-4i-5ii-7ii-11iia-12i, 1i-2i-3i-4ii-5ii-7ii-11iia-12i, 1i-2ii-3i-4i-5ii-7ii-11iia-12i, and 1i-2ii-3i-4ii-5ii-7ii-11iia-12i. The titer reduction was compared to the lysate prior to shipping.

2.3.5 Effect of Phage Type, Formulation, and Inlet Temperature on Spray Drying Titer Reduction

It was not known whether phage CP30A is more susceptible to spray drying titer reduction than phages CP20 or CP8, nor whether the inlet temperature or the use of a buffer would have an effect on phage titer. Therefore, tests were performed with the varied factors including phage type, addition of trisodium citrate-citric acid buffer to F1 or not, and the use of 50°C versus 70°C inlet temperature (all other spray drying parameters were the same as in Section 2.3.4). For all of these

cases centrifugation and dilution were used with cold liquid shipping and ambient powder shipping. Thus, the path variables varied were 1i vs. 1ii vs. 1iii, 7iia vs. 7iib, and the addition of buffer or not in 5iii. The other path variables were kept constant at 2ii-3ii-4ii-11iia-12i. The relevant lysate controls were tested with cold shipping. The effect of a different batch (new lysate and shipment) was tested for purified and diluted CP30A in F1 and for unpurified and undiluted CP30A in F1, both using water for amplification (2ii). For formulations CP30A and CP20, an additional run at an inlet temperature of 70°C was performed with dilution but not purification (3i rather than 3ii).

Another factor tested was whether buffer (12i) or water (12iib) should be used for assay. These were tested with phage CP30A in F1 for an inlet temperature of 70°C and with centrifugation (3ii) but no dilution (5ii rather than 5iii).

To test whether the transfer of powder from the collection bottle to the tube was causing titer reduction, the entire collection bottle was dry shipped (11iib) following the path 1i-2ii-3i-4ii-5ii-7iia-11iib-12i. This was compared to previous measurements which followed the same path except with dry shipping powder that had been transferred from the collection bottle into a tube (11iia). Additionally, the effect of cold powder shipping (11i) was tested and compared to ambient temperature powder shipping (11iia).

For phages CP30A and CP20, additional measurements were performed by spray drying ‘Neat’, i.e. spray drying the lysate without the addition of any excipients. These can be considered control measurements to determine if excipients were improving the titer reduction or not. The paths for these measurements were 1i-2ii-3i-4ii-5i-7iia-10b-12i and 1ii-2ii-3i-4ii-5i-7iia-10b-12i. The dissolved solids content in the ‘Neat’ formulations was determined by air drying on a microscope slide, as described previously. This measurement was compared to the solids content after using centrifugation to further purify the lysate (3ii).

The effect of various excipients dissolved directly into the lysate (5ii) using filtered (3i) CP30A (1i) amplified in water (2ii) on spray drying titer reduction was examined. The formulations tested were F1 with the addition of 2% glycerol (Product no. G7893, lot SHBG4522V; Sigma-Aldrich, St. Louis, MO, USA) by weight based on a study by Ohtake et al. (2010), 5% trileucine (Product no. L0879, lot BCBP2254V; Sigma-Aldrich, St. Louis, MO, USA) and 95% trehalose based on a

study by Lechuga-Ballesteros et al. (2010), and 5% pullulan (Product no. J66961, lot N21D031; Alfa Aesar, Tewksbury, MA, USA) and 95% trehalose based on studies by Teekamp *et al.* [386] and Leung *et al.* [387]. The trileucine and pullulan contents were minimized to keep costs as low as possible, which was an additional reason for the chosen path for these experiments. Control measurements were performed using 100% trehalose, using either a dissolved excipient concentration of 30 mg/mL or 500 mg/mL.

To determine whether desiccation is a major cause of titer reduction, phage lysates were air-dried in a Petri dish (92 mm diameter; Sarstedt, Leicestershire, UK). These experiments were performed for purified and unpurified CP30A, with and without direct addition of leucine and trehalose. The paths followed were 1i-2ii-12i with 3i-5i, 3i-5ii, 3ii-5i and 3ii-5ii varied.

The produced powder was viewed under SEM to determine if centrifugation and dilution, which lower impurity levels (impurities are mainly from the bacteria and media used for amplification), affect particle morphology, and whether a change in titer reduction is a consequence. Additionally, TEM was performed on desiccated purified phage CP20 amplified in water (path 2ii) to determine if these phages tended to be intact or not.

2.3.6 Effect of Shipping and Increased Total Dissolved Solids Content

To verify that shipping was not the cause of titer reduction the protocol indicated in Figure 2.6 was implemented. The path for the development of these powders was 1i-2ii-3ii-4ii-5iii-7iia-11iia-12iib, based on the best conditions from previous sections. The LT formulation here consisted of 20 mg/mL leucine and 100 mg/mL trehalose. The same large batch of spray dried phage powder was aliquoted into 4 tubes which were packaged into separate aluminium foil packages, termed LT(1), LT(2), LT(3), and LT(4), using the method described in Figure 2.4. Package LT(1) was shipped and assayed soon after spray drying, package LT(2) was shipped soon after spray drying but not assayed for 3 weeks, package LT(3) was shipped to England soon after packaging, then shipped back to Canada, then shipped back to England, and then assayed at the same time as LT(2) and LT(4), while package LT(4) was kept in Canada and sent in a later shipment to England for assay. Comparison of LT(1) and LT(2) titer reduction indicates whether 3 weeks of dry storage causes phage inactivation, comparison of LT(3) to the other packages indicates whether multiple shipments cause titer reduction (e.g. due to shaking during shipping and handling), and comparison of LT(1) and LT(4) titer reduction indicates whether differences between shipments causes

differences in phage titer reduction (assuming 3 week dry storage is achieved). The temperature during shipments was monitored and recorded, as described previously. Upon receiving the dry packages, they were stored at room temperature in the laboratory.

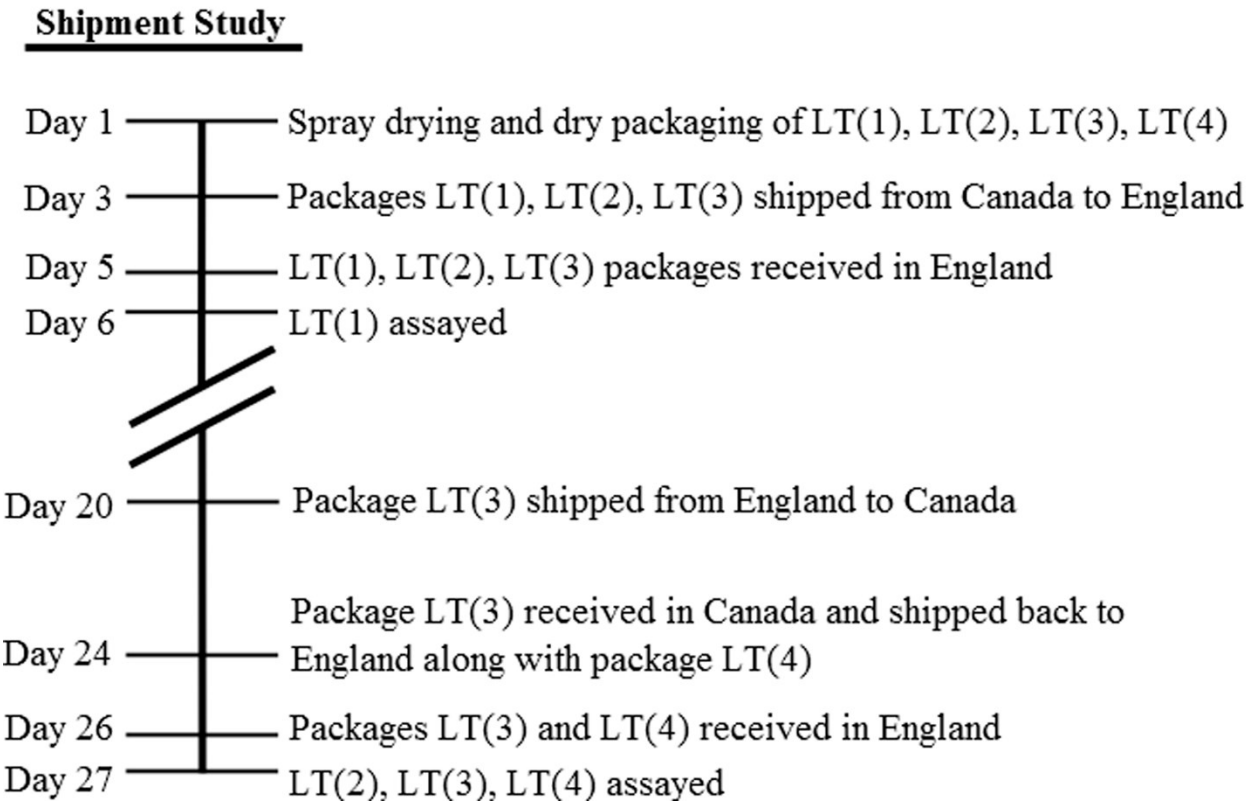

Figure 2.6: Timeline of the shipment study. Measurements were performed using different shipments containing powder (composed of 20 mg/mL leucine, 100 mg/mL trehalose, and phage CP30A) from the same batch aliquoted into different tubes shipped in different packages.

2.3.7 Effect of Powder Resuspension and Leucine Content

As discussed in Chapter 1, for biologics requiring liquid media for assay, biological inactivation by spray drying cannot be separated from inactivation by powder resuspension. This lack of separation is problematic because factors such as temperature, rehydration rate and duration, and rehydration media can potentially affect the resulting titer (see Chapter 1). To quantify the effects of temperature and rehydration media, two formulations were tested: F1 (7.5 mg/mL leucine and 22.5 mg/mL trehalose), and F2 (12 mg/mL leucine and 18 mg/mL trehalose); for these powders the packaging contents were equilibrated at 4% relative humidity using a Steady State / Stability Test Chamber (Model no. CEO910W-4; Lunaire Environmental, Williamsport, PA, USA) rather

than 0%, and silica gel desiccant (Catalogue no. 2189K16; McMaster Carr, Aurora, OH, USA) was used rather than molecular sieves. Formulations F1 and F2 were spray dried and shipped from Canada to the UK and subsequently aliquoted into tubes of different volumes or materials (paths 12iid, 12iie, 12iif) before resuspension at temperatures of 4°C (path 12iia) and 37°C (path 12iic) prior to plaque assay. A resuspension concentration of 30 mg/mL was used throughout.

2.3.8 Effect of Amorphous Shell Former and Room Temperature Stability Testing

Measurements were performed using pullulan and trileucine as amorphous shell formers to stabilize the phage. This was compared to the use of leucine as a shell former. The glass stabilizer trehalose made up the bulk of the powder in each of these cases. As in previous methods, the best conditions from previous sections were used, including centrifugation for purification and dilution of the lysate into the excipient solutions. Additionally, a higher solids content was used to attempt to displace the phage from the surface of the microparticles, by allowing for earlier shell formation. For example, at the time leucine reaches saturation at the surface, the droplet is predicted to be 70% of its initial diameter (35% of its initial volume) for the 30 mg/mL formulation and 97% of its initial diameter (92% of its initial volume) for the 120 mg/mL formulation. The path for these powders was 1i-2ii-3ii-4ii-5iii-7iia-11iia-12iib.

The formulations tested and compared were 20 mg/mL pullulan (high molecular mass, high glass transition temperature amorphous shell former) with 100 mg/mL trehalose (bulk glass stabilizer), 20 mg/mL leucine (crystalline shell former) with 100 mg/mL trehalose, 4 mg/mL Pluronic F-68 (Product no. P7061, lot 70M011718V; Sigma-Aldrich, St. Louis, MO, USA) surfactant (surface-active film former) with 100 mg/mL trehalose, 4 mg/mL trileucine (surface-active, low aqueous solubility, high glass transition temperature amorphous shell former) with 100 mg/mL trehalose, and controls of 20 mg/mL pullulan alone, 20 mg/mL trehalose alone, and 100 mg/mL trehalose alone. The dissolved solids content for trileucine was limited by the solubility. Pluronic F-68 was tested at the same solids content as trileucine as it has a similar surface activity at this concentration.

The titer of the developed powders was measured after processing and after 1 month of dry room temperature storage. For trileucine, the powder was allowed to dissolve for 5 days prior to assay. The dry packaging described in Figure 2.4 was used for storing the powders.

2.3.9 Statistics

Results are generally presented as mean ± standard deviation. Titer results are based on spot assays performed in triplicate. The standard deviation in titer reduction was obtained by error propagation for subtraction formulae, with the individual standard deviations representing the errors. Statistical comparisons utilized the Student's t-test without assuming equal variance, at a significance level of 0.05.

2.4 Results

2.4.1 Phage Stability in Solution

The stability of the phage CP30A lysate over time is presented in Table 2.1. All lysates were stable at 4°C as the titer at day 90 was not significantly less than the titer at day 0 ($p > 0.05$). Filtered phage CP30A lysate was relatively stable when stored at 30°C in water, buffer, or formulation F1, but titer reduction was apparent at day 40. A storage temperature of 40°C did not lead to a significant titer reduction in buffer at day 3 ($p > 0.05$) but led to 1 log(pfu/mL) titer reduction at day 10. A storage temperature of 50°C (data not shown) led to no significant difference in titer in buffer or water after 6 hours ($p > 0.25$).

Table 2.1: Titer, in log(pfu/mL), of amplified phage CP30A in different filtered liquid solutions and at different temperatures over time. The standard deviation ranged from 0.0 to 0.2. "N.M." indicates not measured.

		Time (days)							
Solvent	**Temperature (°C)**	0	1	3	5	10	20	40	90
Buffer	4	9.4	9.5	9.5	9.4	9.4	9.4	9.4	9.3
	20	9.4	9.4	9.5	9.4	9.3	9.4	9.2	9.1
	30	9.4	9.5	9.6	9.4	9.3	9.2	9.1	9.0
	40	9.4	9.4	9.3	8.7	8.4	8.0	5.8	N.M.
Water	4	9.3	9.1	9.3	9.3	9.2	9.4	9.3	9.2
	30	9.3	9.2	9.2	9.3	9.1	9.1	8.7	8.0
F1	4	9.2	9.0	9.2	9.3	9.1	9.3	9.3	9.2
	30	9.3	9.0	9.2	9.2	9.1	9.2	8.6	7.9

There was no significant reduction in titer ($p > 0.1$) after shipping CP30A lysate or CP30A in F1 within a tube in a Styrofoam box without temperature control from England to Canada and back, either using buffer or water amplification media. This stability indicated that it is feasible to perform lysate and feed control measurements with shipped liquid.

There was ≤ 0.3 log(pfu/mL) titer reduction due to vortexing the liquid phage lysate, with no trend observed in relation to the vortexing time within the tested range of 5 to 120 seconds.

There was no significant difference in titer ($p > 0.2$) between samples taken from the top, middle, and bottom of the liquid feed tube approximately half-way through a spray drying run, indicating that indeed phage are evenly distributed in the liquid feed tube during spray drying without stirring.

2.4.2 Phage Atomization

The lysate titer prior to shipping was 9.7 ± 0.2 log(pfu/mL) and 9.5 ± 0.2 log(pfu/mL) for water and buffer amplification media, respectively. The titer reduction due to atomization (including the effect of shipping) is presented in Table 2.2. In no case did shipping cold versus at ambient temperature make a significant difference in titer ($p > 0.05$). Additionally, in no case did using buffer versus water make a significant difference in titer reduction ($p > 0.2$). The average (aggregate) titer reduction for the twin-fluid atomizer, 0.3 log(pfu/mL), was less than that for the vibrating mesh atomizer, 0.8 log(pfu/mL). As a consequence, the twin fluid atomizer was generally used for further measurements and it was concluded that shear stress during twin-fluid atomization is not a major cause of titer reduction for phage CP30A. The twin-fluid atomization titer reduction was less than the value of ~0.75 log(pfu/mL) reported in the literature [367] for phages PEV2 and PEV40, where similar shear rates were calculated to be used, but where greater droplet diameter reduction and hence desiccation may have occurred. The vibrating mesh atomization titer reduction was greater than the value of 0.4 log(pfu/mL) for anti-tuberculosis *Siphoviridae* phage D29 in isotonic saline calculated from Chapter 4, indicating that phage CP30A in F1 is more susceptible to titer reduction with this device than phage D29, which could potentially be due to differences in susceptibility between phage families.

Table 2.2: Titer reduction due to atomization of phage CP30A lysate in F1.

Atomizer	Solvent	Shipping Method	Titer Reduction [log_{10}(pfu/mL)]
Vibrating Mesh	Buffer	Cold	0.6 ± 0.2
		Ambient	1.0 ± 0.2
	Water	Cold	0.6 ± 0.2
		Ambient	0.8 ± 0.2
Twin-fluid	Buffer	Cold	0.3 ± 0.3
		Ambient	0.3 ± 0.2
	Water	Cold	0.3 ± 0.2
		Ambient	0.4 ± 0.2

2.4.3 Spray Dryer Comparison

A comparison of spray drying phage CP30A using different spray dryer types is given in Table 2.3. The use of cold versus ambient liquid shipping and buffer versus water as the solvent made no significant differences in titer reduction ($p > 0.2$). For water solvent and the ambient liquid shipping method, use of the B-191 spray dryer resulted in significantly less titer reduction than use of the B-90 spray dryer ($p < 0.025$), thus providing some evidence that attrition during cyclone collection with the B-191 was not a major cause of titer reduction, as the B-90 spray dryer does not have a cyclone. Non-significant differences ($p > 0.5$) in titer reduction occurred when the effects of atomization (results in Section 2.4.2) were subtracted from the overall titer reductions, indicating that another common factor (desiccation) may be a more substantial cause of titer reduction. The results of testing various other factors that could cause inactivation by spray drying are given in the following sections. Since the B-191 resulted in less titer reduction, it was used for all further spray drying experiments. The outlet temperatures matched predictions from the process models within 2°C for both spray dryers.

Table 2.3: Titer reduction due to spray drying filtered phage CP30A in F1. Titer reduction excluding atomization refers to the titer reduction due to spray drying minus the titer reduction due to atomization given in Table 2.2. Initial lysate titers are the same as in Section 2.4.2.

Spray Dryer	**Solvent**	**Liquid Shipping Method**	**Titer Reduction [$\log_{10}$(pfu/mL)] Relative to Lysate Control**	**Titer Reduction [$\log_{10}$(pfu/mL)] Excluding Atomization**
Büchi B-90	Water	Ambient	2.8 ± 0.2	2.1 ± 0.3
Büchi B-191	Buffer	Cold	2.1 ± 0.2	1.9 ± 0.3
		Ambient	2.3 ± 0.2	2.0 ± 0.3
	Water	Cold	2.2 ± 0.2	2.0 ± 0.3
		Ambient	2.3 ± 0.2	2.0 ± 0.3

2.4.4 Effect of Phage Type, Formulation, and Inlet Temperature on Spray Drying Titer Reduction

Experimental results regarding the effect that various factors have on titer reduction are given in Table 2.4. The use of phages CP20 or CP8 tended to lead to greater titer reduction than the use of phage CP30A, indicating that none of the tested anti-*Campylobacter* phages were resilient to spray drying. As phage CP30A (path 1i) appeared to be the most stable, it was used for further measurements.

Table 2.4: Titer reduction, in $\log_{10}$(pfu/mL), due to spray drying with different phage types, formulations, and inlet temperatures. The number preceding the letter notation refers to the mg/mL of that excipient dissolved in the liquid feed; for example, 7.5L 22.5T refers to formulation with 7.5 mg/mL leucine and 22.5 mg/mL trehalose as feed excipients. Notation: L = leucine; T = trehalose; B = trisodium citrate-citric acid buffer; LLL = trileucine; P = pullulan; Neat = unpurified lysate only. PC indicates purification included centrifugation (path 3ii); "D" indicates 1:100 dilution was used (path 5iii); "CS" indicates cold powder shipping (path 11i); "WA" indicates water was used for assay (path 12iib); "DB" indicates a different batch was tested; "CB" indicates the entire collection bottle containing the powder was shipped for assay (path 12iib); and "N.M." indicates not measured. The formulations were described in more detail in Section 2.3.5.

Phage Type	Formulation	Inlet Temperature (°C)	Titer Reduction Relative to SD 'Neat'	Titer Reduction Relative to Lysate Control	Titer Reduction Relative to Feed Control
CP30A	7.5L 22.5T -PC,WA	70	-1.0 ± 0.2	1.5 ± 0.2	1.7 ± 0.2
	7.5L 22.5T -PC,D	70	-0.9 ± 0.2	1.6 ± 0.1	1.7 ± 0.1
	7.5L 22.5T -PC,D,DB	70	-0.7 ± 0.2	1.8 ± 0.2	2.0 ± 0.1
	7.5L 22.5T -PC	70	-0.7 ± 0.2	1.8 ± 0.1	2.0 ± 0.1
	7.5L 22.5T -CB	70	-0.6 ± 0.2	1.9 ± 0.1	N.M.
	7.5L 22.5T -PC,D	50	-0.6 ± 0.2	1.9 ± 0.1	2.1 ± 0.1
	7.5L 22.5T 1.5B -PC,D	70	-0.5 ± 0.2	2.0 ± 0.2	-0.1 ± 0.1
	7.5L 22.5T	50	-0.4 ± 0.1	2.1 ± 0.1	2.1 ± 0.1
	7.5L 22.5T -PC,CS	70	-0.4 ± 0.2	2.1 ± 0.2	2.3 ± 0.2
	7.5L 22.5T -D	70	-0.3 ± 0.2	2.2 ± 0.1	1.9 ± 0.2
	7.5L 22.5T G	70	-0.3 ± 0.2	2.2 ± 0.2	N.M.
	7.5L 22.5T -DB	70	-0.2 ± 0.2	2.3 ± 0.1	N.M.
	7.5L 22.5T 1.5B-PC,D	50	-0.1 ± 0.2	2.4 ± 0.2	1.5 ± 0.2
	Neat	70	N/A	2.5 ± 0.1	2.5 ± 0.1
	1.5LLL 28.5T	70	0.0 ± 0.2	2.5 ± 0.2	N.M.
	1.5P 28.5T	70	+0.1 ± 0.2	2.6 ± 0.2	N.M.
	30T	70	+0.1 ± 0.2	2.6 ± 0.2	N.M.
	500T	70	+0.5 ± 0.2	2.9 ± 0.2	N.M.
CP20	7.5L 22.5T -PC,D	50	-1.2 ± 0.2	1.7 ± 0.1	1.6 ± 0.1
	7.5L 22.5T -PC,D	70	-1.0 ± 0.3	1.8 ± 0.2	2.0 ± 0.2
	7.5L 22.5T 1.5B -PC,D	50	-0.4 ± 0.2	2.4 ± 0.1	-1.2 ± 0.1
	7.5L 22.5T -D	70	-0.4 ± 0.2	2.4 ± 0.1	2.6 ± 0.2

	7.5L 22.5T 1.5B -PC,D	70	-0.3 ± 0.2	2.5 ± 0.1	-0.5 ± 0.3
	Neat	70	N/A	2.8 ± 0.2	2.9 ± 0.2
CP8	7.5L 22.5T -PC,D	70	N.M.	2.1 ± 0.1	2.0 ± 0.1
	7.5L 22.5T -PC,D	50	N.M.	3.0 ± 0.2	2.8 ± 0.2
	7.5L 22.5T 1.5B -PC,D	50	N.M.	3.0 ± 0.3	0.6 ± 0.3
	7.5L 22.5T 1.5B -PC,D	70	N.M.	3.0 ± 0.3	0.7 ± 0.3

Similar results were generally achieved using an inlet temperature of 70°C versus 50°C, indicating that heat stress due to the drying gas inlet temperature was not a likely cause of titer reduction. Indeed, in Section 2.4.1 it was shown that the phages are stable at 50°C in buffer for at least 6 hours, which is higher than the expected droplet temperature in the dryer for an inlet drying gas temperature of 70°C, and which is greater than the residence time in the dryer for these experiments. For all further measurements a temperature of 70°C (path 7iia) was used, as this results in a drier powder.

Without phage, F1 (7.5L 22.5T) excipient solution had a pH of 6.5; with dilution of purified phage lysate into the excipient formulation the pH decreased to 6.0-6.3 depending on the phage type. The addition of 1.5 mg/mL trisodium citrate-citric acid buffer (denoted 1.5B in Table 2.4) increased the pH to 7.2 in each case, indicating the buffer capacity was sufficient. However, the results in Table 2.4 indicate that this buffer substantially inactivated the phage in liquid, as the feed control for cases with trisodium citrate-citric acid buffer had a greater titer reduction relative to the lysate control, typically 1-3 log(pfu/mL) greater. Therefore, for all further measurements, this trisodium citrate-citric acid buffer was not used.

The use of purification and dilution resulted in significantly less titer reduction due to spray drying ($p < 0.025$), ~0.5 log(pfu/mL), than adding the excipients directly to the phage lysate for an inlet temperature of 70°C and F1 formulation. Additionally, the use of water for assay resulted in less titer reduction than the use of buffer. Therefore, for further spray drying measurements in the following sections, purification (path 3ii) and dilution (path 5iii) were used during formulation, and water was used for assay (path 12iib).

The use of cold phage powder shipping did not decrease the titer reduction relative to the use of ambient phage powder shipping. Shipment of the entire collection bottle resulted in less titer reduction than shipment of phage transferred from the collection bottle to the tube; however, it proved impractical to ship a collection bottle for each measurement and therefore ambient temperature shipping of tubes (path 11iia) was used for further experiments. Spray drying different batches did not lead to a significant difference in titer reduction ($p > 0.1$).

The solids content in the 'Neat' lysate (path 3i-5i) was ~19 mg/mL as measured by air drying on a microscope slide. This value is relatively large compared to the total dissolved excipient concentration of 30 mg/mL in F1. Comparing SEMs (Figure 2.7) of the powders containing components dissolved directly into the lysate without purification or dilution (path 3i-5ii) to the SEMs of the powders formulated using purification of the lysate and subsequent dilution into excipient solution (path 3ii-5iii) indicated that the morphology of the spray dried microparticles was affected by the impurities in lysate. Microparticles containing pullulan and trehalose, trileucine and trehalose, or trehalose alone appeared similar to the Neat formulation, as purification and dilution were not used and the large, slowly diffusing impurities may concentrate on the surface during drying and have a large impact on shell formation and hence particle formation. The phage would be expected to typically be on or near the surface, and hence biologic stabilization is also likely to be affected by impurity enrichment at the surface. Indeed, purification and dilution tended to decrease the titer reduction for spray drying with F1, and a similar morphology for F1 was observed as in the literature for powders that achieved long-term biological stability at 20°C [369]. The use of trileucine or pullulan with trehalose did not improve the titer reduction relative to the 'Neat' case when centrifugation and dilution were not used to decrease the impurity content. However, they did outperform the use of trehalose alone, perhaps because earlier shell formation decreases surface inactivation of the phage. More encouraging measurements where purification and dilution are used to decrease impurity levels and allow for trileucine and pullulan to stabilize the biologic are presented in Section 2.4.7.

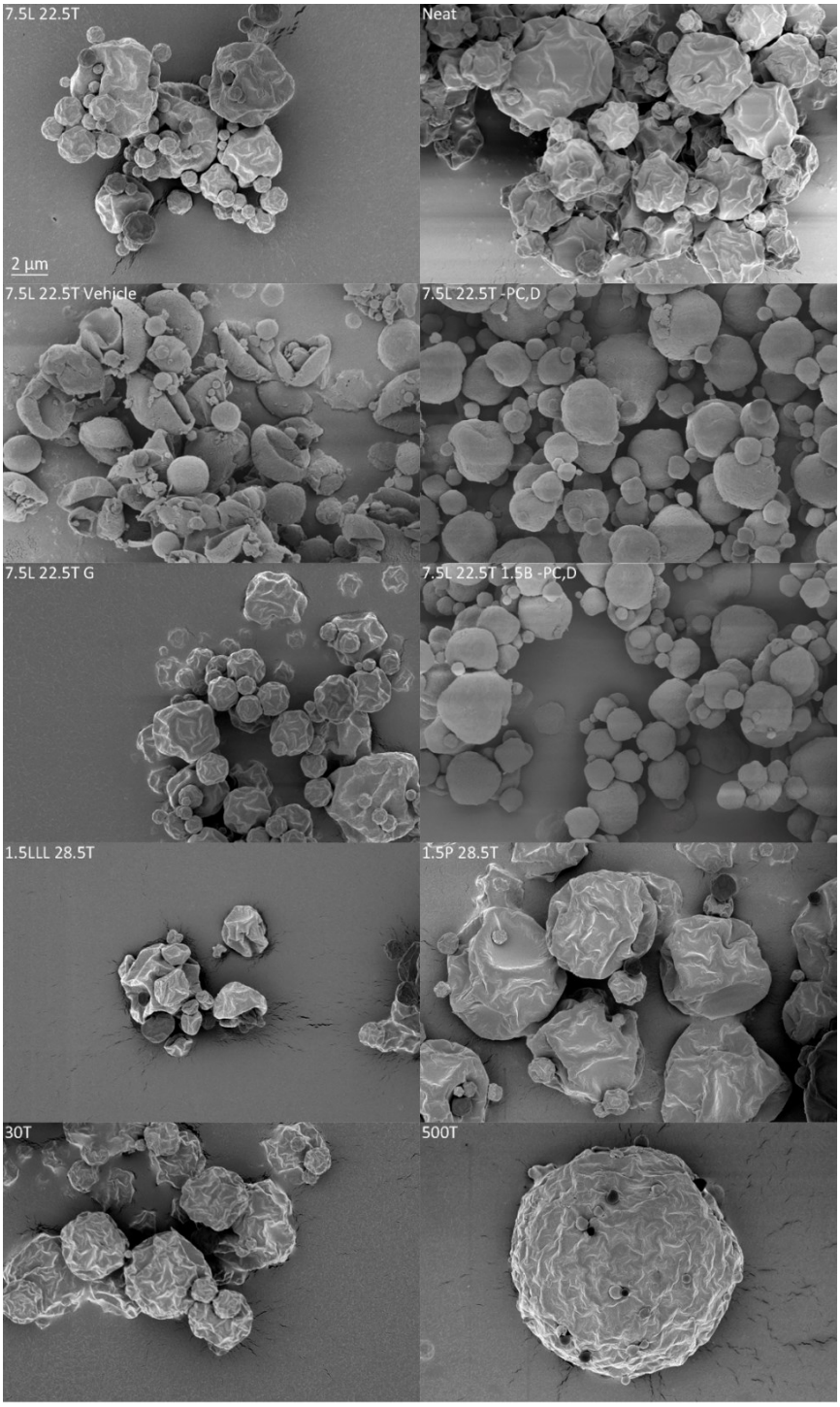

Figure 2.7: SEMs of spray dried powders containing phage CP30A for select 70°C inlet temperature cases from Table 2.4. The microparticles appeared similar for a 50°C inlet temperature and for different phage types. "Vehicle" refers to spray drying without the addition of phage lysate and "–PC,D" refers to cases where purification and dilution were used. The same scale bar applies to all images.

The titer reduction due to air drying in a Petri dish was 2.0 ± 0.1 log(pfu/mL) for unpurified CP30A, 1.8 ± 0.3 log(pfu/mL) for unpurified CP30A in F1, 3.5 ± 0.2 log(pfu/mL) for purified CP30A, and 2.0 ± 0.2 log(pfu/mL) for purified CP30A in F1. As the purified lysate performed worst, it is apparent that leucine and trehalose, and impurities, both provide some stabilization during drying. Excluding atomization titer reduction (based on data from Section 2.4.2), the titer reduction due to spray drying was not significantly different than the titer reduction due to air drying in a Petri dish for either of the unpurified lysate cases ($p > 0.2$). The non-significant differences comparing air drying in a Petri dish to spray drying (excluding atomization titer reduction) provides evidence that desiccation stress is the main cause of titer reduction during spray drying. This is not unexpected as literature indicates that many phages are susceptible to desiccation stress [388].

As desiccation stress appeared to be the main cause of titer reduction due to spray drying, TEM images of desiccated phage CP20 were taken (Figure 2.8). It was observed that many desiccated phages had burst capsids and leaked DNA, which could be the mechanism by which desiccation damages the phages. A caveat is that it was necessary to use a stain to obtain sufficient contrast in TEM, and the stain could potentially affect the desiccation-resistance of the phage. TEM also indicated that some phages appeared disfigured. It is possible that disfigured phages, which could, for example, be damaged during the centrifugation recovery step in amplification, are more readily inactivated during spray drying than undamaged phages.

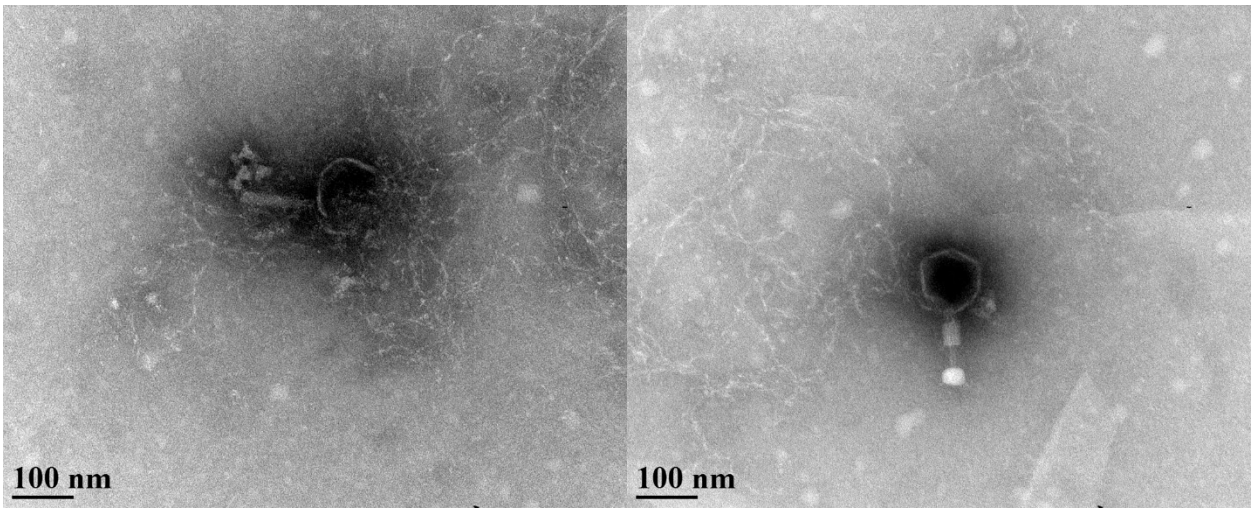

Figure 2.8: TEM showing DNA leaks from burst capsids of desiccated phage CP20. The TEM method is described in Chapter 4.

2.4.5 Effect of Dry Shipping and Increased Total Dissolved Solids Content

The temperature during shipment of dry phage CP30A powder packages LT(1), LT(2), and LT(3) from Canada to England was 22.7 ± 7.1°C (measured every 4 minutes), with a maximum excursion of 37.7°C. The temperature during shipment of LT(3) from England to Canada was 22.1 ± 1.7°C, with a maximum excursion of 23.9°C. The temperature during shipment of LT(3) and LT(4) from Canada to England was 21.6 ± 3.6°C, with a maximum excursion of 29.3°C.

The titer reduction for the phage powder in the packages detailed in Figure 2.6 were 1.9 ± 0.1 log(pfu/mL) for LT(1), 2.0 ± 0.2 log(pfu/mL) for LT(2), 2.0 ± 0.1 log(pfu/mL) for LT(3), and 2.1 ± 0.1 log(pfu/mL) for LT(4). There were no significant differences in titer reduction between any of these powders ($p > 0.05$). This indicates that shipping the powder three times instead of once was not a cause of additional titer reduction and that 3 weeks of dry ambient temperature storage was not a cause of titer reduction. This implies that titer reduction is occurring during processing or early storage (the ~5 days between spray drying and assay). Indeed, a bi-phasic titer reduction has been reported for biologic powder, in which the inactivation rate is greater early during storage, as those biologics that barely remain active after spray drying may inactivate soon after processing (or early in storage) [389-391]. Phages that are disfigured by amplification (as was observed under TEM, images not shown) could thus be more readily inactivated. However, the end goal of this project was to develop a powder that maintains stability for the time it takes to ship the powder,

put it in the chicken feed, and have the chickens eat it, which may be greater than 5 days; therefore, it is desirable for the powder to retain sufficient activity following the bi-phasic transition period. Hence, further measurements with different formulations were tested to attempt to decrease the titer reduction following this period (Section 2.4.7).

2.4.6 Powder Resuspension and Leucine Content

The results of spray drying F1 (7.5 mg/mL leucine and 22.5 mg/mL trehalose) and F2 (12 mg/mL leucine and 18 mg/mL trehalose) and resuspending the shipped powder using different tube types and resuspension temperatures indicated no clear trend (data not shown). This indicates that there was no evidence that temperature-mediated phase change during resuspension or tube adsorption were causes of phage inactivation.

The average titer reduction for F1, 2.1 ± 0.5 log(pfu/mL), was significantly less ($p < 0.05$) than for F2, 2.9 ± 0.2 log(pfu/mL). A possible reason for the greater titer reduction for F2 than for F1 is that F2 has more leucine at the surface than F1, and the leucine does not provide adequate glass stabilization as it was determined to be primarily crystalline using Raman spectroscopy (data not shown). Therefore, in Section 2.4.7, attempts to use amorphous shell formers to stabilize the phages at the surfaces of the dried microparticles were undertaken.

2.4.7 Effect of Amorphous Shell Former and Room Temperature Stability Testing

The results of processing phage CP30A by spray drying with different shell formers and storing for 1 month at dry room temperature conditions are given in Table 2.5. The use of trileucine resulted in the least overall titer reduction after processing, shipping, and 1 month of room temperature storage, with a total of 0.6 ± 0.1 log(pfu/mL) titer reduction, which is within the criteria of 1 log(pfu/mL) titer reduction for an acceptable biological powder production process given by Hoe *et al.* [392]. The use of pullulan with trehalose outperformed the standard formulation of leucine with trehalose. The results for pullulan and trehalose were repeatable for different batches, with no significant difference in titer reduction observed ($p > 0.5$). The use of surfactant resulted in much worse stabilization than the use of trileucine, despite the same solids content and surface activity, and also resulted in very low yield. Formulations with trehalose or pullulan alone performed poorly, worse than the 'Neat' lysate. The use of pullulan alone outperformed trehalose alone, and a higher solids content of trehalose outperformed a lower solids content in terms of titer reduction and yield. According to calculations based on the theory

presented by Vehring [364], pullulan is expected to solidify earlier in the drying process than trehalose due to greater enrichment at the surface, associated with a higher Péclet number. Additionally, trehalose at a higher initial dissolved solids content is expected to solidify earlier than trehalose at a lower initial dissolved solids content. Earlier solidification may prevent as many phages from accumulating on the surface and hence result in better stabilization, as supported by these results.

Table 2.5: Processing and 1-month dry room temperature storage titer reductions, in $\log_{10}$(pfu/mL), of phage CP30A powders spray dried with different formulations. Notation: L = leucine; T = trehalose; LLL = trileucine; P = pullulan; S = Pluronic F-68 surfactant; –DB denotes testing of a different batch. "N.M." indicates not measured. The formulations were described in more detail in Section 2.3.8.

Formulation	**Process Titer Reduction Relative to 'Neat'**	**Process Titer Reduction Relative to Lysate Control**	**Process Titer Reduction Relative to Feed Control**	**1-month Titer Reduction Relative to Process Lysate Control**
4LLL 100T	N.M.	N.M.	N.M.	0.6 ± 0.1
20P 100T -DB	-1.2 ± 0.2	1.3 ± 0.1	1.1 ± 0.2	1.7 ± 0.1
20P 100T	-1.1 ± 0.1	1.4 ± 0.1	1.0 ± 0.1	1.7 ± 0.1
20L 100T	-0.6 ± 0.1	1.9 ± 0.1	1.7 ± 0.1	1.9 ± 0.1
20P	+0.2 ± 0.2	2.7 ± 0.1	2.4 ± 0.2	N.M.
4S 100T	+0.2 ± 0.2	2.7 ± 0.2	2.4 ± 0.2	N.M.
100T	+0.5 ± 0.1	3.0 ± 0.0	2.4 ± 0.1	3.9 ± 0.2
20T	+1.2 ± 0.1	3.7 ± 0.0	3.3 ± 0.0	N.M.

SEMs of the powders are given in Figure 2.9, and unlike the cases without centrifugation and dilution in Figure 2.7, the expected morphologies are observed for pullulan and trehalose formulation, as well as for trehalose alone (vehicle SEMs not shown). This difference is likely due to the decreased impurity concentrations allowing for these excipients to control the shell formation. The lack of impurities at the surface could also be the reason for the lower titer reduction observed in Table 2.5 than in Table 2.4 for trileucine and pullulan shell former cases. The leucine

and trehalose powder appeared more spherical than expected, perhaps due to inhibited crystallization by even trace impurity levels. Indeed, de-convoluted Raman spectroscopy performed on leucine and trehalose powder stored dry at room temperature for 4 months indicated the leucine was only partially (70-80%) crystalline, while the trehalose was amorphous, as expected. The trileucine, pullulan, pluronic, and trehalose in the other formulations retained their amorphous structure after 4 months of dry room temperature storage. This is expected, as these powders were designed to have years of physical stability at room temperature.

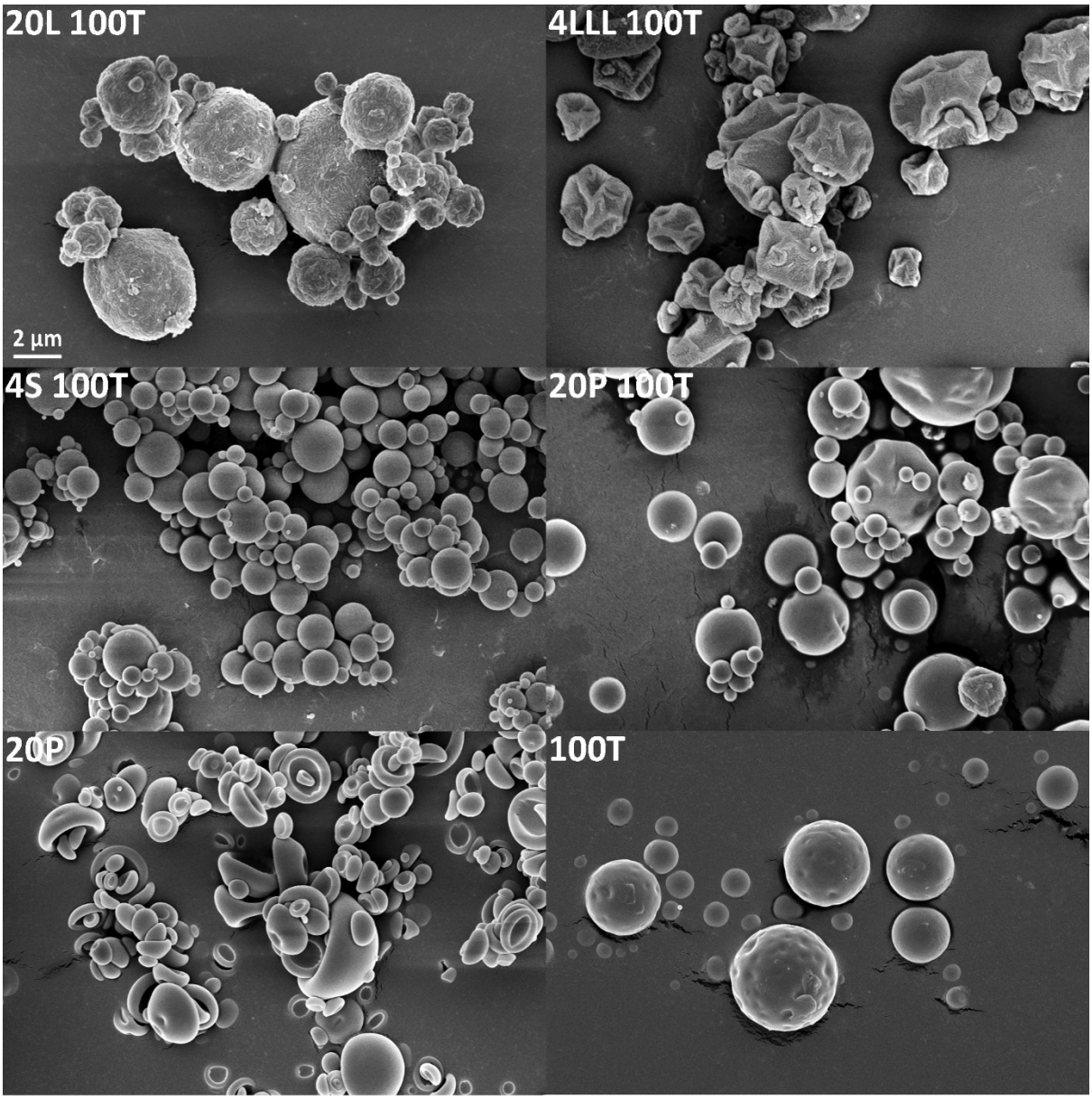

Figure 2.9: SEMs of the spray dried phage CP30A powders given in Table 2.5. 20T microparticles (not shown) were small (< 2 µm) and spherical. Images were taken of the powder after processing. The same scale bar applies to all images.

2.5 Discussion

The objective of this research was to develop a stable anti-*Campylobacter* phage powder with minimal titer reduction due to spray drying, shipping, and ambient temperature dry storage, and that can be used in chicken feed to decrease the levels of *Campylobacter* bacteria in the gut of chickens in Kenya. Processing losses of greater than 1 log(pfu/mL) would lead to more expensive

products which would be unsuitable for developing countries [392]. To the authors' knowledge, anti-*Campylobacter* phage have not been spray dried before. It became apparent early in the study that achieving a small titer reduction would be challenging for the anti-*Campylobacter* phages tested. Larger titer reductions were initially observed as compared to other phages in the literature that use similar formulation and spray drying process parameters. For example, Matinkhoo *et al.* [366] observed 0.4 ± 0.1 log(pfu/mL) titer reduction due to spray drying *Burkholderia* phage KS14 (*Myoviridae*) using a Büchi B-90 with 20% leucine and 80% trehalose formulation. The preparation method involved 0.45 μm filtration, centrifugation, and endotoxin removal. In the same study, 0.8 ± 0.1 log(pfu/mL) titer reduction was observed for *Burkholderia* phage KS4-M (*Myoviridae*) spray dried with a Büchi B-90 using the same formulation. Leung *et al.* [368] found ~1.3 log(pfu/mL) titer reduction for *Pseudomonas* phage PEV2 (*Podoviridae*) spray dried with a Büchi B-290 spray dryer using the same formulation, with a preparation method involving 1:100 dilution into formulation and pH adjustment to 7.5 using sodium hydroxide. A follow-up study found 0.7 ± 0.3 log(pfu/mL) titer reduction for phage PEV2 spray dried with the Büchi B-290 spray dryer with 30% leucine and 70% trehalose or 40% leucine and 60% trehalose formulation; 0.2 ± 0.1 log(pfu/mL) titer reduction was observed for *Pseudomonas* phage PEV40 (*Myoviridae*) using the same formulation and spray drying parameters [369].

To decrease the titer reduction due to spray drying for these anti-*Campylobacter* phages a large number of factors were tested. For the first time, to the author's knowledge, the effects of purification method (sterile filtration alone or a combination of sterile filtration and centrifugation), formulation method (neat or with excipients added directly to the lysate or with lysate diluted into excipient solution), spray dryer type (Büchi B-90 with a vibrating mesh atomizer or Büchi B-191 with a twin-fluid atomizer), and powder resuspension and plaque assay media (water or buffer) were tested for spray dried phage powders. Generally, better results were obtained using a combination of sterile filtration and centrifugation, the lysate diluted into excipient solution, the Büchi B-191 spray dryer with a twin-fluid atomizer, and water for powder resuspension and plaque assay. Additionally, parametric studies indicated that liquid shipping, vortexing, phage sedimentation in the liquid feed tube, choice of amplification media (buffer or water), cyclone collection, spray dryer inlet temperature (50°C or 70°C), certain plaque assay parameters (rehydration media, rehydration temperature, tube materials), and dry ambient temperature powder shipping were not major sources of titer reduction. Some differences in titer

reduction between anti-*Campylobacter* phage types (CP30A, CP20, and CP8) were demonstrated, a result supported by literature which indicates that phage titer reduction due to aerosolization is device- and phage strain-dependent [393-394]. By comparing the titer reduction of phage CP30A with the two tested spray dryers (subtracting the measured atomization titer reduction) to each other and to results of air drying in a Petri dish, it became evident that desiccation stress was the main cause of titer reduction. This was also supported indirectly by TEM which showed that desiccated phages had burst capsids that leaked DNA. In order to protect against desiccation stress and the corresponding phage inactivation, the use of amorphous glass stabilizers was tested. It was found that amorphous glass stabilizers did not perform well when the initial lysate was not centrifuged to remove impurities, or when dilution was not used to further lower impurity concentrations. Indeed, comparing the SEMs in Figures 2.7 to 2.9 demonstrates that the impurities affected the shell formation process and therefore likely concentrated on the surface, where the biologics are also likely to concentrate due to their large size and high Péclet number. The Péclet number is a dimensionless number used in particle engineering to characterize the ratio of surface recession rate due to droplet evaporation and diffusional rate of the solute to the interior of the droplet; a high Péclet number (> 1) indicates the solute will concentrate on the surface while a low Péclet number (< 1) indicates the solute will be relatively evenly distributed [364]. As a result, it was suspected that the phages would came into contact with the impurities at the surface (which could be detrimental), rather than with the glass stabilizers. Using TEM (images not shown), it was observed that the impurities are mainly bacterial debris that has passed through the 0.22 μm filter. This debris may contain a number of bacterial components including amino acids, lipids, and sugars, among others, that may not be suitable for glass stabilization at the surface. Hence, use of purification and dilution aided biological stability. Furthermore, it was found that increasing leucine concentration from a mass fraction of 0.25 to 0.40 resulted in greater inactivation of phage, likely because leucine was demonstrated to be primarily crystalline and thus would not offer glass stabilization. Indeed, there is no glass stabilization within a crystal, and phage may instead be broken apart or expelled (either to the interior or to the surface), as they will not fit in the crystal lattice. If phage are expelled to the surface they will not effectively bond with the crystals and may detach. Alternatively, phage may inhibit crystallization and crystal growth of leucine, as may impurities.

The purified and diluted phage CP30A formulation containing leucine and trehalose was shown to be stable during shipping at least three times one after the other between Canada and England (~20000 km total), even with a 37.7°C temperature excursion, a characteristic that may be crucial to its success in Kenya. In addition, the use of cold packs during shipment did not improve the titer of the powder relative to ambient temperature shipping. To our knowledge, this is the first shipping stability study that demonstrates that the cold chain is not necessary with proper formulation and dry packaging of phage powder.

The proposed particle formation mechanisms and their relationships to biologic stability are given in Figure 2.10 and are based on more detailed descriptions given elsewhere [353,364].[δ] The use of amorphous shell formers such as pullulan or trileucine with trehalose outperformed a crystalline leucine shell, and produced flowable powders. The use of pullulan or trehalose alone did not provide the same biological stabilization potential as did their combination.

[δ] A droplet emitted from the atomizer is assumed to initially be well-mixed in terms of the excipients being evenly distributed within the droplet, while the phages are assumed to be randomly distributed. "A": trileucine is surface-active and near saturation initially and forms an amorphous shell with small amounts of trehalose early, before all phage are present at the surface. The mainly trileucine shell folds since it is thin and the mainly trehalose interior has yet to solidify. The shell potentially maintains the same surface area upon folding and prevents phage from reaching the surface. "B": the crumpled appearance is controlled by the folded shell. The interior later solidifies into a glass through a progression from highly viscous solution to true density associated with further desiccation. "C": pullulan enriches at the surface due to high molecular mass and forms a viscous amorphous shell that may contain small amounts of trehalose; the shell contracts, causing phage to recede with the surface, and desiccates until the true density of the mixture is reached at the surface. "D": the surface is mainly pullulan, with some trehalose that prevented shell deformation. The interior is mainly trehalose with some pullulan. "E": nucleation at the surface results in small leucine crystals that eventually become close and large enough to form a shell. Trehalose and remaining leucine eventually solidify. "F": phage could be expelled from crystals, be damaged by inter-crystal forces, or inhibit crystallization. Small crystals are at the surface of the microparticles. The interior is primarily trehalose and may contain voids. "G": pullulan enriches near the surface and solidifies there. The thin shell is moderately rigid due to a high glass transition temperature and may easily deform and contract as it is not hindered by a trehalose interior. "H": there is no trehalose glass stabilizer or void space in the interior. "I": surfactant may form a film that recedes. "J": small cohesive spherical microparticle with phages near or on the surface where they are not adequately stabilized by the surfactant. "K": small cohesive solid spherical microparticle formed. There is a high chance that phages reside on the surface. "L": same as "K" except that a very small microparticle results and there is a very high chance that phages reside on surface. Void space is not shown in the schematic and may be possible in many cases. Note that there is a radial distribution of each excipient within the drying droplet rather than complete separation of excipients.

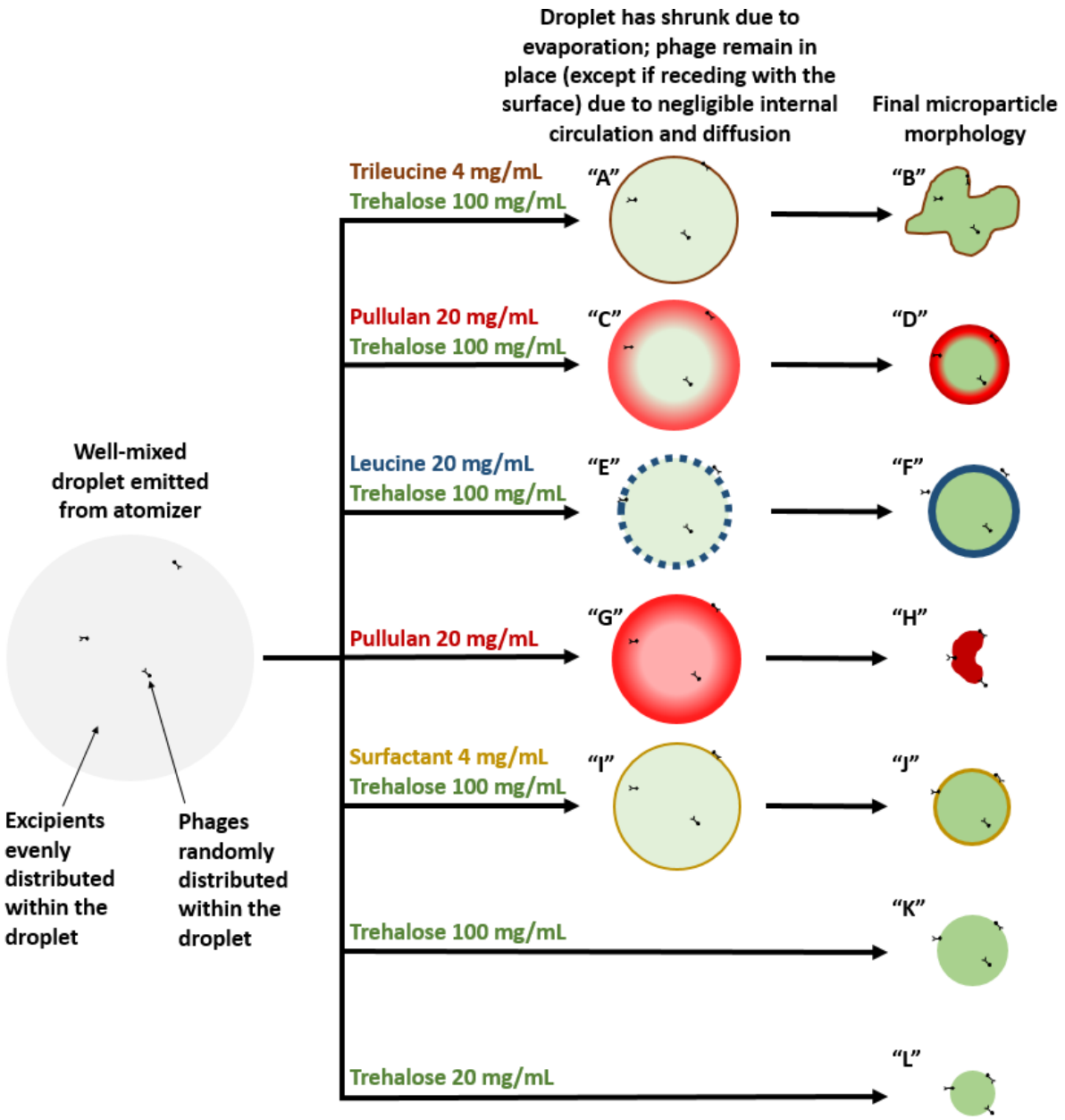

Figure 2.10: Schematic of the particle formation mechanisms for the different tested formulations in Table 2.5 and Figure 2.9 and their relationship to phage distribution and stabilization. More information regarding particle formation is given in the footnote on the previous page. Full resolution color image available online.

Trileucine has a high glass transition temperature, ~104°C, does not crystallize under typical spray drying conditions, has a low solubility in water (~6.8 mg/mL), and has a high surface activity, resulting in early precipitation during the evaporation of aqueous solution droplets [364,395]. The

high surface activity of trileucine may have resulted in an amorphous shell forming early in the drying process. To our knowledge, this is the first study in which phage have been spray dried with trileucine, and excellent biological stabilization was observed, with only 0.6 ± 0.1 log(pfu/mL) overall titer reduction due to liquid feed preparation, spray drying, tube transfer, ambient temperature shipping ~6600 km, 1 month of dry room temperature storage, and resuspension for plaque assay. It is expected that the early shell formation prevents phage from reaching the air interface, where irreversible loss of native phage protein structure could otherwise occur (see Chapter 1). Despite a similar surface activity, surfactant did not provide the level of stabilization that trileucine did perhaps due to poor biologic stabilization potential of the surfactant. The greater stabilization with trileucine as compared to pullulan may be related to the smaller molecular mass of trileucine, allowing the glass to more closely interact with the biologic, or to the surface activity, better preventing the phage from reaching the surface during drying.

Pullulan also showed excellent biologic stabilization potential, outperforming the standard shell forming excipient for spray drying phage, leucine. Pullulan has a high dry glass transition temperature, ~261°C [386], remains amorphous upon spray drying, and has a high molecular mass [396]. Pullulan will diffuse slowly and tend to enrich and increase the viscosity near the surface of the microparticles during drying, leading to early shell formation and potentially the prevention of phage from reaching the air interface and being exposed to desiccation stress. This excipient has demonstrated the ability to stabilize β-Galactosidase in lyophilized powder [386] and phages in films [387]. To our knowledge, pullulan has not been spray dried with biologics before. Pullulan is “generally recognized as safe” [397] and is used in industry as a film-forming agent [398]. Other polysaccharides may also be suitable for amorphous glass stabilization near the surface of spray dried microparticles. Whether the achieved powder titer is suitable for biocontrol applications is a subject of future work.

The proposed amorphous shell platform for stabilizing biologics developed in this work consists of a high glass transition temperature excipient that precipitates early in the spray drying process by either high initial dissolved solids content, high surface activity, or high molecular mass (associated with slow diffusion and hence high surface enrichment). The amorphous shell platform may be useful for a number of applications for stabilizing biologics in microparticles in the food and pharmaceutical industries.

2.6 Conclusions

Spray drying of phages requires a thorough exploration of the factors that may cause titer reduction. For spray drying anti-*Campylobacter* phages belonging to *Myoviridae*, twin-fluid atomizers are recommended over vibrating mesh atomizers and desiccation is expected to be a major cause of titer reduction. Based on data presented here, the use of a high glass transition temperature amorphous shell former that precipitates early in the drying process is recommended for glass stabilization of spray dried phage CP30A against the major inactivation factor, desiccation. Indeed, formulation using trileucine or pullulan as shell-forming excipients and trehalose as a bulking agent and glass stabilizer are promising alternatives to the standard leucine and trehalose formulation for the development of stable spray dried phage powders. With this approach, dry ambient temperature shipping and at least 1 month of dry room temperature storage of active anti-*Campylobacter* phage CP30A in a flowable powder was achieved. The proposed amorphous shell platform is expected to be useful for the stabilization of other biologics that tend to concentrate on the surface of spray dried microparticles and may have a plethora of applications in the food and pharmaceutical industries.

3 Amorphous Pullulan Trehalose Microparticle Platform for Respiratory Delivery

This chapter has been published in the journal paper "Carrigy NB, Ordoubadi M, Liu Y, Melhem O, Barona D, Wang H, Milburn L, Ruzycki CA, Finlay WH, Vehring R. 2019. Amorphous pullulan trehalose microparticle platform for respiratory delivery. International Journal of Pharmaceutics. 563:156-168." Additional material is given in Appendix B.

3.1 Abstract

Spray drying biologics and small-molecule drugs can increase their thermal stability relative to liquid dosage forms and allow for widespread distribution to developing countries without cold chain infrastructure. In this study, pullulan trehalose powder is spray dried for inhalation. The powder is characterized in terms of manufacturability, physical stability, device compatibility, and aerosol performance. The manufacturability is demonstrated by reasonable spray drying yield and powder flowability. The powder has relatively low cohesiveness and high compressibility without semi-elastic deformation. Short-term physical stability for ambient temperature dry storage and 40°C storage in commercial pressurized metered-dose inhaler propellants HFA 134a and HFA 227 is shown. A theoretical model predicts a high glass transition temperature near the surface of the microparticles where biologics are expected to reside. Emission from a commercial dry powder inhaler demonstrates high dispersibility, optimal size for inhalation, and adequate total lung dose, exceeding many commercial inhalation devices. The powder can be filled, stored, and actuated from a pressurized metered-dose inhaler without changes in particle morphology or solid phase. The pullulan trehalose platform thus appears promising for respiratory delivery.

Abbreviations: FPF = fine particle fraction; GSD = geometric standard deviation; HFA = hydrofluoroalkane; MMAD = mass median aerodynamic diameter; MOC = micro-orifice collector

3.2 Introduction

Biologics and small-molecule drugs are not always stable as a liquid dosage form at room temperature, and developing countries with endemic infectious diseases do not always have access to cold-chain infrastructure (see Chapter 1 [399]); therefore, methods to increase thermal stability are of interest. One such method is spray drying, which consists of atomizing a liquid formulation into droplets in a hot drying gas that evaporates the solvent, leaving the solute to form solid microparticles that are collected. In addition to increased thermal stability due to decreased water-

mediated degradation, solid dosage forms have less weight and volume due to solvent removal, which minimizes transportation costs and storage space requirements [400]. Additionally, dry powder delivery with inhalers removes the contamination risks and disposal issues associated with needles. As compared to lyophilization, spray drying is relatively low cost and a much faster process for producing dry powder [401-402]. Furthermore, particle size and properties are controlled in a single step in spray drying, making secondary milling unnecessary.

Biologics are gaining pharmaceutical market share relative to small molecules [403]. Biologics are used as prophylactic agents, e.g. vaccines, against infectious diseases, and as therapeutic agents against cancers, arthritis, diabetes, and other conditions [404]. Examples of biologics that have been stabilized by spray drying include monoclonal antibodies, recombinant human DNase, insulin, antigens, interleukin, bacteriophage, antimicrobial peptides, bacterial cell wall hydrolases, and various vaccines (see Chapter 1). The most commonly researched excipient combination for spray drying biologics is leucine and trehalose (see Chapter 1). The leucine is typically designed to be crystalline in order to increase surface roughness and thus aid dispersibility from dry powder inhalers, while trehalose solidifies to a glassy solid that protects the biologic against desiccation. However, leucine can crystallize under typical spray drying conditions and therefore be incapable of providing glass stabilization. Pullulan does not crystallize under typical spray drying conditions and therefore may be useful as an alternative excipient to leucine for stabilizing biologics. Previous work has demonstrated that pullulan and trehalose combinations stabilize β-Galactosidase in lyophilized powder [405], various proteins in air-dried and freeze-dried orodispersible films [406], and bacteriophages in air-dried films [407]. Further characterization and understanding of pullulan trehalose microparticles is therefore of interest.

Pullulan $(C_6H_5O_{10})_n$ is a linear exopolysaccharide produced by microorganisms that forms a slimy layer around the cell wall to protect against desiccation [408]. Pullulan is commonly used in industry as a film-forming agent [409] and is "generally recognized as safe" in the food industry [410-411], being non-toxic and non-carcinogenic [412]. Industrial production techniques are reviewed elsewhere [413]. Pullulan is a non-reducing sugar and is relatively impermeable to oxygen [412]. It has a high glass transition temperature [405], ~261°C. Teekamp *et al.* [405] showed that pullulan prevented trehalose from crystallizing at high humidity and temperature, thus improving physical stability.

Trehalose, $C_{12}H_{22}O_{11}$, is a non-reducing disaccharide also produced by microorganisms to protect against desiccation [414]. Trehalose is "generally recognized as safe" for use in foods [415]. It is a commonly used excipient for stabilizing biologics [416]. Trehalose has been suggested to be an excellent glass stabilizer because it has a high glass transition temperature, high hydration number, and small size (see Chapter 1).

The feasibility of pullulan trehalose powder as a formulation platform for inhalation products has not previously been assessed. In this paper, pullulan trehalose powder, produced either with a monodisperse droplet chain or a spray dryer, is characterized in terms of particle formation, morphology, glass stabilizing properties, manufacturability, powder packing properties, aerosol performance, and delivery device compatibility.

3.3 Materials and Methods

3.3.1 Monodisperse Droplet Chain

3.3.1.1 Experimental Procedure

Particle morphology was examined using a monodisperse droplet chain described elsewhere [417], to gain insight into the particle formation mechanism. Briefly, feed solutions of pullulan (Product no. J66961; Alfa Aesar, Tewksbury, MA, USA) and trehalose (Cat. No. BP2687; Fisher BioReagents, NH, USA) with a fixed total initial solute concentration of 1.875 mg/mL were formulated with the following excipient content combinations by percent mass of pullulan/trehalose: 0/100, 5/95, 10/90, 20/80, 40/60, 70/30, and 100/0. Heated gas at an initial temperature of 70°C entered a drying cylinder in a laminar flow at a rate of 5 L/min to evaporate the solvent and generate monodisperse dry microparticles. Individual droplets of the feed solutions were dispensed and injected into the cylinder at a frequency of 60 Hz using a piezoelectric droplet dispenser (MicroFab Technologies, Plano, TX, USA) with a 40 µm diameter micro-jet orifice. Images of the droplets were acquired immediately after the exit of the dispenser using a high-magnification camera with a collimated light source to determine the initial droplet diameters, according to a method described previously [417].

3.3.1.2 Normalized Volume Equivalent Diameter - Experiment

The volume equivalent diameter of the collected dry microparticles produced by the monodisperse droplet chain was determined experimentally for comparison to theoretical predictions from

particle formation models. The dried particles that exited the droplet chain cylinder were collected at ambient conditions using a collection stub. The particles on the stub were then imaged with a field emission scanning electron microscope (Zeiss Sigma FESEM, Oberkochen, Germany). The scanning electron microscope settings were a 3.00 kV accelerating voltage, 5000x magnification, 6-7 mm working distance, and use of an immersion lens (in-lens) detector. A gold coating of ~16 nm was applied prior to imaging with a sputter deposition system (Denton II; Denton Vacuum LLC, Moorestown, NJ, USA). The Feret diameter based on the longest dimension, which represents the hydrodynamic, or volume equivalent, diameter was determined using image analysis (ImageJ, National Institutes of Health, Bethesda, MD, USA). The volume equivalent diameter of the dry microparticles was normalized by the initial droplet diameter, as the initial droplet diameter varied slightly between experiments.

3.3.1.3 Normalized Volume Equivalent Diameter – Analytical Particle Formation Model

An analytical particle formation model was developed with the purpose of providing a method for quickly calculating volume equivalent diameter of the dry microparticles with reasonable accuracy, without the need for numerical methods. Previous amorphous particle formation models were limited to single-component systems [418-419]. In the following, the time at which multi-component amorphous systems reach the true density of the mixture at the surface of an evaporating micro-droplet and co-solidify is derived.

The total initial concentration of a mixture of dissolved solutes, $C_{0,\mathrm{mix}}$, commonly referred to as total solids content, is given by,

$$C_{0,\mathrm{mix}} = \sum_{\mathrm{i}} C_{0,\mathrm{i}} \tag{3.1}$$

where $C_{0,\mathrm{i}}$ is the initial solute concentration of solute i.

By mass conservation the total mean concentration of dissolved solutes in an evaporating droplet, $C_{\mathrm{m,mix}}$, is given by,

$$C_{\mathrm{m,mix}} = \frac{d_0^3}{d^3} C_{0,\mathrm{mix}} \tag{3.2}$$

where d is the instantaneous droplet diameter and d_0 is the initial droplet diameter.

The surface enrichment of solute i, E_{i}, is defined as [419],

$$E_{\mathrm{i}} = \frac{C_{\mathrm{s,i}}}{C_{\mathrm{m,i}}} \tag{3.3}$$

where $C_{\mathrm{s,i}}$ is the surface concentration of solute i and $C_{\mathrm{m,i}}$ is the mean concentration of solute i in the droplet.

The total concentration of a mixture of dissolved solutes at the surface of an evaporating droplet, $C_{\mathrm{s,mix}}$, neglecting interactions between the solutes, is given by,

$$C_{\mathrm{s,mix}} = \sum_{\mathrm{i}} C_{\mathrm{s,i}} = \sum_{\mathrm{i}} E_{\mathrm{i}} C_{\mathrm{m,i}} \tag{3.4}$$

The true density of a mixture of solids, $\rho_{\mathrm{T,mix}}$, is given by,

$$\rho_{\mathrm{T,mix}} = \frac{1}{\sum_{\mathrm{i}} \frac{Y_{\mathrm{i}}}{\rho_{\mathrm{T,i}}}} \tag{3.5}$$

where Y_{i} is the total mass fraction of solute i and $\rho_{\mathrm{T,i}}$ is the true density of solute i.

Similarly, at the surface the true density of a mixture of solids, $\rho_{\mathrm{T,mix,s}}$, is given by,

$$\rho_{\mathrm{T,mix,s}} = \frac{1}{\sum_{\mathrm{i}} \frac{Y_{\mathrm{i,s}}}{\rho_{\mathrm{T,i}}}} \tag{3.6}$$

where $Y_{\mathrm{i,s}}$ is the mass fraction of solute i at the surface, which is defined as,

$$Y_{\mathrm{i,s}} = \frac{C_{\mathrm{s,i}}}{C_{\mathrm{s,mix}}} \tag{3.7}$$

Substitution into the previous equation gives,

$$\rho_{\mathrm{T,mix,s}} = \frac{C_{\mathrm{s,mix}}}{\sum_{\mathrm{i}} \frac{C_{\mathrm{s,i}}}{\rho_{\mathrm{T,i}}}} \tag{3.8}$$

Solidification of solutes at the surface of an evaporating droplet is assumed to occur when the surface concentration of the mixture equals the true density of the mixture, i.e., when,

$$\rho_{\mathrm{T,mix,s}} = C_{\mathrm{s,mix}} \tag{3.9}$$

Therefore solidification at the surface occurs when,

$$\sum_{\mathrm{i}} \frac{C_{\mathrm{s,i}}}{\rho_{\mathrm{T,i}}} = 1 \tag{3.10}$$

By definition,

$$E_{\mathrm{i}} P_{\mathrm{i}} = \frac{C_{\mathrm{s,i}}}{C_{\mathrm{m,i}}} \frac{C_{\mathrm{0,i}}}{\rho_{\mathrm{T,i}}} \tag{3.11}$$

where P_{i} is a non-dimensional number equal to the ratio of the initial solute concentration of solute i and true density of solute i.

Therefore by substitution into the previous equation,

$$\sum_{\mathrm{i}} E_{\mathrm{i}} P_{\mathrm{i}} \frac{C_{\mathrm{m,i}}}{C_{\mathrm{0,i}}} = 1 \tag{3.12}$$

Noting that,

$$\frac{C_{\mathrm{m,i}}}{C_{\mathrm{0,i}}} = \frac{C_{\mathrm{m,mix}}}{C_{\mathrm{0,mix}}} \tag{3.13}$$

and making use of equation (3.2), the previous equation can be written,

$$\sum_{\mathrm{i}} E_{\mathrm{i}} P_{\mathrm{i}} = \frac{C_{\mathrm{0,mix}}}{C_{\mathrm{m,mix}}} = \left(\frac{d_{\mathrm{t,mix}}}{d_0}\right)^3 \tag{3.14}$$

where d_{t} is the diameter at the time for which co-solidification of a mixture occurs at the surface of a drying droplet, as this equation is only valid at that point in time due to previous assumptions.

The d^2 law is given by [418],

$$d^2 = d_0^2 - \kappa t \tag{3.15}$$

where d is the diameter at time t, and κ is the evaporation rate, which is assumed to be constant. The droplet lifetime, τ_{D}, is the time at which d in equation one equals zero, and is given by [418],

$$\tau_D = \frac{d_0^2}{\kappa} \tag{3.16}$$

where κ is the evaporation rate taken as 4.0×10^{-9} m^2/s [419].

Substituting into the previous equation gives,

$$\left(\frac{d}{d_0}\right)^2 = 1 - \frac{t}{\tau_D} \tag{3.17}$$

Raising both sides to the power of 3/2 gives,

$$\left(\frac{d}{d_0}\right)^3 = \left(1 - \frac{t}{\tau_D}\right)^{3/2} \tag{3.18}$$

Considering the time at which true density is reached at the surface and substituting into equation (3.14) gives,

$$\sum_i E_i P_i = \left(1 - \frac{t_{t,mix}}{\tau_D}\right)^{3/2} \tag{3.19}$$

where $t_{t,mix}$ is the time at which co-solidification occurs at the surface of a drying droplet for a mixture of dissolved solutes.

Raising both sides to the power of 2/3 and rearranging gives the time until amorphous co-solidification occurs on the surface of a droplet, $t_{t,mix}$,

$$t_{t,mix} = \tau_D \left[1 - \left(\sum_i E_i P_i\right)^{\frac{2}{3}}\right] \tag{3.20}$$

where τ_D is the droplet lifetime, E_i is the surface enrichment of component i, and P_i is a non-dimensional number relating the initial solute concentration of component i to its true density. This is similar to the single-component amorphous particle formation equation given by Vehring [418], but with a summation of the product of E_i and P_i for the individual solutes as the base number being raised to the power of 2/3.

The surface enrichment of component i is approximated by [419]

$$E_i = 1 + \frac{Pe_i}{5} + \frac{Pe_i^2}{100} - \frac{Pe_i^3}{4000} \tag{3.21}$$

where the Péclet number of component i is given by [419]

$$Pe_i = \frac{\kappa}{8D_i} \tag{3.22}$$

where D_i is the diffusion coefficient of solute i in the droplet solvent. The diffusion coefficient of trehalose in water was taken as 5.0×10^{-10} m^2/s [419]. The diffusion coefficient of pullulan in water was taken as 2.8×10^{-11} m^2/s, which corresponds to a molecular mass of 115 kDa [420].

The non-dimensional number P_i is defined as [418]

$$P_i = \frac{C_{0,i}}{\rho_{t,i}} \tag{3.23}$$

where $C_{0,i}$ is the initial solute concentration of component i and $\rho_{t,i}$ is the true density of component i. The true densities of trehalose and pullulan were assumed to be 1580 kg/m^3 [421] and 1850 kg/m^3 [422], respectively.

The d^2 law, which assumes a constant evaporation rate and hence constant temperature, was used to estimate the volume equivalent diameter at the time of co-solidification at the surface

$$d_v^2 = d_0^2 - \kappa t_{t,mix} \tag{3.24}$$

where the experimentally determined initial droplet diameter was used for calculation. The volume equivalent diameter of the dry microparticles were normalized by the initial droplet diameter as per Section 3.3.1.2.

3.3.1.4 Normalized Volume Equivalent Diameter - Numerical Particle Formation Model with Viscosity Correction

A numerical particle formation model similar to one described previously [423] was used to predict the volume equivalent diameter for comparison to the analytical model and experimental results. The model is based on a one-dimensional numerical solution to Fick's second law within a spherical droplet, including the effect of Stefan flow. Internal circulation was neglected. The concentration varied with radius as the dimensionless Péclet number, representing the ratio of evaporative surface recession to mass diffusivity, was on the order of 10 for pullulan. The droplet temperature was assumed to be spatially homogeneous as the dimensionless Lewis number, representing the ratio of thermal diffusivity to mass diffusivity, was on the order of 100. As Baldelli *et al.* [424] demonstrated, viscosity increases during drying due to increases in solute concentration as water solvent evaporates. This decreases the diffusion coefficient, increases the Péclet number, increases the surface enrichment, and leads to earlier solidification at the surface, and larger

predicted diameter. These effects were incorporated into the numerical model, with viscosity modelled as a function of solute concentration using trehalose viscosity values from the literature [425]. The volume equivalent diameter at the time solidification starts near the surface was an output of the model. The volume equivalent diameter of the dry particles were normalized by the experimentally measured initial droplet diameter as in Sections 3.3.1.2 and 3.3.1.3.

3.3.1.5 Radial Profiles of Local Mass Fractions and Dry Glass Transition Temperature

The radial profile of mass fractions and glass transition temperature is useful for predicting physical and biological stabilization potential at different locations within the microparticles. Using the output for the final radial composition of mass fractions in the microparticles from the multi-component numerical model with viscosity correction described in Section 3.3.1.4, the radial glass transition temperature profile was predicted using the Gordon-Taylor equation [426], modified to be a function of radius, according to

$$T_{\mathrm{g,dry}}(r) = \frac{\omega_{\mathrm{T}}(r) T_{\mathrm{g,T,dry}} + k\omega_{\mathrm{P}}(r) T_{\mathrm{g,P,dry}}}{\omega_{\mathrm{T}}(r) + k\omega_{\mathrm{P}}(r)} \tag{3.25}$$

where $T_{\mathrm{g,dry}}(r)$ is the dry glass transition temperature of well-mixed pullulan and trehalose which varies with radius r, $\omega_{\mathrm{T}}(r)$ and $\omega_{\mathrm{P}}(r)$ are the radial mass fractions of trehalose and pullulan, respectively, from the numerical model, $T_{\mathrm{g,T,dry}}$ and $T_{\mathrm{g,P,dry}}$ were assumed to be 394 K and 534 K, respectively, and k was assumed to be 0.4163 [405].

3.3.2 Spray Drying

3.3.2.1 Spray Drying Process Parameters

Relative to the droplet chain technique, spray drying has a much higher dry powder production rate, allowing for further characterization with techniques requiring large powder batches. The spray drying process was designed to yield inhalable amorphous powder that is physically stable at room temperature. A modified Büchi B-191 spray dryer (Büchi Labortechnik AG; Flawil, Switzerland), described previously (see Chapter 1), in combination with a twin-fluid atomizer, was used in this study. Process parameters chosen were an inlet temperature of 80°C, corresponding to an evaporation rate of 4.8×10^{-9} m^2/s [419], a drying gas flow rate of 540 L/min, a feed flow rate (spray rate) of 0.5 mL/min, and an atomizer air-to-liquid ratio of 14, which corresponds to an initial droplet mass median diameter of around 7 µm based on droplet size data for the twin-fluid atomizer

[427]. Feed solutions were formulated with a fixed total initial solute concentration of 50 mg/mL and the following excipient content combinations by percent mass of pullulan/trehalose: 0/100, 5/95, 10/90, 17/83, 20/80, 30/70, 40/60, and 100/0. The outlet temperature, outlet relative humidity, and powder moisture content were predicted to be 61°C, 0.8%, and 0.2%, respectively, using the process model described in Chapter 1.

3.3.2.2 Spray Dried Particle Morphology

Particle morphology was examined using scanning electron microscopy for spray dried particles with various excipient content combinations. The same scanning electron microscopy settings described in Section 3.3.1.2 were used. Additionally, a gallium beam in a helium ion microscope (Zeiss Orion NanoFab Helium Ion Microscope with Gallium Focused Ion Beam, Oberkochen, Germany) was used to cut 40% pullulan 60% trehalose microparticles and the internal structure was subsequently imaged using the same helium ion microscope.

3.3.2.3 Modulated Differential Scanning Calorimetry Measurements

The reversing heat flow was determined experimentally using modulated differential scanning calorimetry (Q1000, TA Instruments, New Castle, DE, USA) to elucidate if a radial distribution of glass transition temperature was present within the microparticles by comparison to theoretical models. The test conditions were equilibration at 25°C, isothermal hold for 5 minutes, and a ramp of 5°C/min up to 340°C with a modulation of ± 2°C/min. A dry nitrogen purge of 60 mL/min was used to keep the cell dry. The mass of powder was 2.2-2.6 mg for each measurement. The spray dried powder for these measurements contained either 100% pullulan at a solids content of 20 mg/mL, 100% trehalose at a solids content of 100 mg/mL, or 16.7% pullulan and 83.3% trehalose at a total solids content of 120 mg/mL. For these measurements the inlet temperature to the spray dryer was 70°C and the initial droplet diameter was predicted to be 9 μm.

The Fox equation [428] is a simple method for predicting the dry glass transition temperature of a mixture, $T_{\mathrm{g,dry}}$,

$$T_{\mathrm{g,dry}} = \frac{1}{\sum_{\mathrm{i}} \frac{Y_{\mathrm{i}}}{T_{\mathrm{g,i}}}} \tag{3.26}$$

where $T_{\mathrm{g,i}}$ represents the glass transition temperature of component i.

Another simple method for predicting the glass transition temperature is the Gordon-Taylor equation [426], previously given by equation (3.25), but with the use of constant mass fractions, corresponding to the initial solute mass fractions, rather than mass fractions at the end of the drying process that vary with radius within the microparticles. The same values for the constants were used as in Section 3.3.1.5. The results from these two simplified models were compared to predictions using equation (3.25), which uses local, radial mass fractions of pullulan and trehalose within the microparticles.

3.3.2.4 Modulated Compressed Bulk Density Measurements

Modulated compressed bulk density measurements were performed to determine the packing properties of the powder, using an apparatus described elsewhere [429]. Briefly, ~100 mg of the spray dried powder generated according to Section 3.3.2.1 was loaded into a cylindrical cavity and the force required to compress the powder to a specified volume was measured using a load cell located below the cavity. Displacement modulation was incorporated to differentiate between plastic (reversible) and semi-elastic (non-reversible) compression, the latter of which is recognized by the powder not returning to its initial volume on decompression. The relative humidity during the measurement was set to 0% using dry nitrogen purge. A transition pressure was defined as halfway between the last data point without semi-elastic deformation and the first data point with semi-elastic deformation, with typical compression increments of 40 μm. The compressed bulk density was reported at the transition pressure. Spray dried pullulan trehalose powders were tested in the range of 0-40% pullulan content.

3.3.2.5 Dry Powder Inhaler Aerosol Performance Measurements

To examine the aerosolization performance of the spray dried pullulan trehalose powder generated according to Section 3.3.2.1, emissions from a commercial low-resistance dry powder inhaler (Seebri® Breezhaler®, Novartis International AG; Basel, Switzerland) were measured downstream of an Alberta Idealized Throat (built in-house) using a Next Generation Impactor (Copley Scientific; Nottingham, UK). A custom mouthpiece adapter was rapid-prototyped with a PolyJet 3D printer (Objet Eden 350 V High Resolution 3D Printer, Stratsys, Ltd.; Eden Prarie, MN, USA) out of an acrylic compound (Objet VeroGray RGD850; Eden Prarie, MN, USA) and connected the dry powder inhaler to the Alberta Idealized Throat.

The powder was filled into dried size 3 hydroxypropyl methylcellulose capsules (Quali-V®-I; Qualicaps, Inc., Madrid, Spain) which are specifically designed for dry powder inhalers. These capsules are similar to the capsules used in the commercial Breezhaler® dry powder inhaler. The powder was manually filled into the capsules in a dry (< 0.1% relative humidity) environment, as verified by a hygrometer (MI70 Measurement Indicator with HMP77B humidity and temperature probe; Vaisala, Vantaa, Finland). The fill mass was 42 ± 9 mg per capsule. The filled capsules were kept dry prior to use. Three dry powder inhaler actuations and inhalations were performed, using three different powder-filled capsules, in order to capture sufficient mass on the impactor plates for accurate gravimetric measurement. The process was replicated twice for spray dried pullulan/trehalose with percent masses of 0/100, 10/90, and 40/60. To mitigate bounce, the plates of the Next Generation Impactor and the interior of the Alberta Idealized Throat were coated with silicone spray (Molykote™ 316 Silicone Release Spray, Dow Corning Corporation; Midland, MI, USA) and left to evaporate for 20 minutes. A blank run, with no capsule in the dry powder inhaler, verified that this time was sufficient for complete solvent evaporation, as the mean ± standard deviation of the mass change of the plates was 0.0 ± 0.1 mg.

Dry powder inhaler actuation was carried out according to the Breezhaler® pamphlet instructions. The capsule was pierced and inserted into the dry powder inhaler, and the dry powder inhaler then connected by the custom mouthpiece adapter to the throat and impactor. A critical flow controller (Critical Flow Controller Model TPK 2000, Copley Scientific Limited; Nottingham, UK) set a constant flow rate of 100 L/min through the system for 2.4 seconds, resulting in a 4 L inhalation volume, as recommended in the USP-601 monograph [430]. These are the conditions recommended if a 100 L/min flow rate results in a pressure drop of less than 4 kPa [430], which was the case as the pressure drop across the dry powder inhaler and throat was measured to be 3.4 kPa at 100 L/min using a differential pressure sensor (Model HSCDRRD160MDSA3, Honeywell; Morris Plains, NJ, USA). This is a reasonable value based on data in the literature [431-432]. The cut-off diameters of the impactor stages at this flow rate are 6.12 μm (stage 1), 3.42 μm (stage 2), 2.18 μm (stage 3), 1.31 μm (stage 4), 0.72 μm (stage 5), 0.40 μm (stage 6), 0.24 μm (stage 7), and 0.07 μm for the micro-orifice collector (MOC) [433].

The emitted dose was defined as the percent of the fill mass that was emitted from the dry powder inhaler, based on the weight of the dry powder inhaler before and after emission. The total lung

dose was defined as the percent of the emitted dose that is collected in the impactor [434], i.e., the dose collected downstream of the Alberta Idealized Throat. The fine particle fraction (FPF) was defined as the percent of the emitted dose that was collected on the impactor stages 2-MOC, i.e., with a size < 6.12 µm. The mass median aerodynamic diameter (MMAD) and geometric standard deviation (GSD) were determined by fitting the data to a cumulative distribution function,

$$y = \frac{1}{2}\left[1 + \text{erf}\left(\frac{\ln(x) - a}{b\sqrt{2}}\right)\right] \tag{3.27}$$

where $a = \ln(MMAD)$ and $b = \ln(GSD)$. The fit was performed using "cftool" in MATLAB (MathWorks, Inc., Natick, MA, USA). For each run the fit was performed with x as a column vector containing the upper size limits for stages 2-MOC (for example, the upper size limit is 6.12 µm for stage 2) and y as a column vector containing the corresponding cumulative mass data that ranged from 0-1. Note that the fit was performed using data from stages 2-MOC, since the pre-separator was not used and therefore no upper size limit was available for stage 1 [432].

3.3.2.6 Pressurized Metered-Dose Inhaler Physical Stability Measurements

The 40% pullulan 60% trehalose spray dried powder generated according to Section 3.3.2.1 was hand-filled with a crimper-filler (Lab Plant, Pamasol AG, Pfäffikon, Switzerland) into pressurized metered-dose inhaler canisters, either glass or aluminium, at concentrations of ~1 mg/mL in propellants hydrofluoroalkane (HFA) 134a or HFA 227. After sonication, actuation of 5-10 doses through a low-flow-rate single-nozzle impactor, described previously [435], allowed for collection of dry particles on a collection stub for scanning electron microscope imaging. The canisters were stored at room temperature or at 40°C in an incubator at ambient relative humidity for 42 days and then re-sampled using the same method for both scanning electron microscopy and solid phase analysis using a Raman spectroscopy instrument developed by Wang *et al.* [436]. Solid phase analysis was also performed for the spray dried powder kept in a dry box at ambient temperature for 42 days to verify the powder retained its amorphous solid phase without use of refrigeration or insertion into propellant.

3.3.3 Statistics

Student's t-tests were performed without assuming equal variance at a significance level of 0.05. Experimental results are generally presented as mean ± standard deviation of replicate measurements, with the number of replicates indicated in the text.

3.4 Results and Discussion

3.4.1 Monodisperse Droplet Chain

3.4.1.1 Microparticle Morphology

Scanning electron microscope images of the microparticles produced by the droplet chain are given in Figure 3.1. The produced microparticles were evidently monodisperse, despite folding. The folding occurs to a greater extent with increasing pullulan content in the formulation and results in more irregular, non-spherical, microparticles. This is explained by the particle engineering theory that with increasing pullulan concentration, the shell formation occurs earlier in the drying process due to higher Péclet numbers for pullulan. Subsequently, for higher pullulan contents, the shell folding begins earlier in the drying process, while the particle is relatively large and the shell thin. Further investigation would be required to fully understand the folding process. It is possible that the folded morphology for higher pullulan contents is also related to the high structural flexibility of pullulan [437]. Interparticle forces may also affect folding [438]. External voids are evident in each case. More rugose particles are typically advantageous for dispersibility.

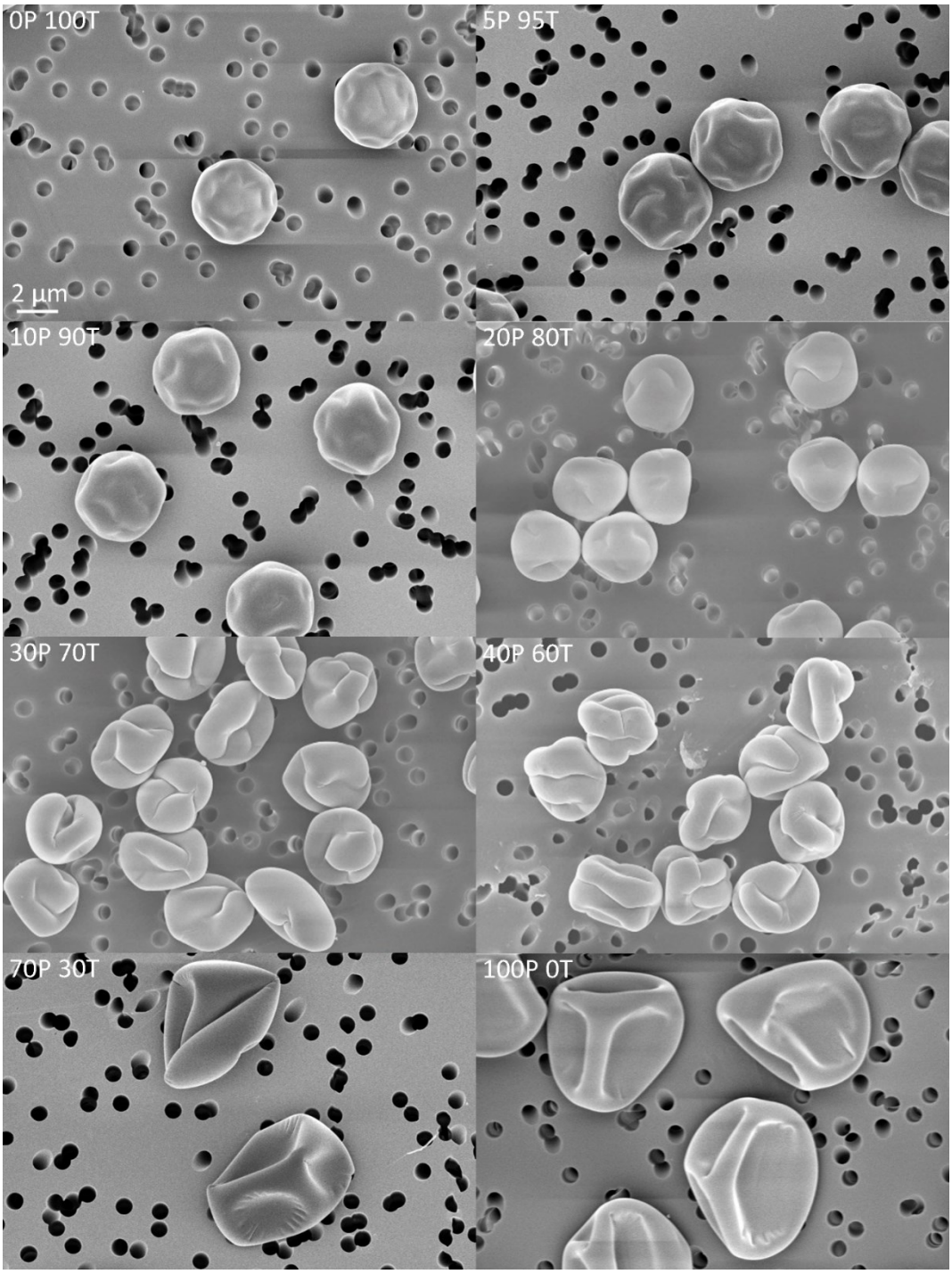

Figure 3.1: Scanning electron microscope images of particles produced using a monodisperse droplet chain technique. More folding is observed for particles with a higher mass fraction of pullulan. As an example of the legend, 30P 70T represents 30% pullulan 70% trehalose powder. The same scale bar applies to all images.

3.4.1.2 Normalized Volume Equivalent Diameter

For the droplet chain experiments, the Péclet numbers for pullulan and trehalose were 18 and 1.0, respectively. This corresponded to respective steady state surface enrichments of 6.3 and 1.2. The range of initial droplet diameters for all (n = 15) droplet chain experiments was 29-33 μm, with an overall mean ± standard deviation of 31 ± 1 μm.

Figure 3.2 shows the predicted normalized volume equivalent diameters from the two models and the experimental results for comparison. The experimental values and numerical predictions matched fairly closely; an exact match was not expected as the models do not account for the shell folding or particle contraction processes. The developed particle formation models may thus give reasonable but not exact predictions for other combinations of amorphous excipients that co-solidify. The analytical model tends to under-predict the diameter as it does not account for increased surface enrichment due to increased viscosity during drying. As expected, a larger normalized diameter is predicted for the numerical model which includes viscosity effects, as this leads to higher surface enrichment and earlier predicted co-solidification. Over-prediction of diameter was observed for the numerical model, perhaps related to particle contraction after shell formation that was not modelled. Both models predict increased diameter at higher pullulan contents, as true density at the surface is predicted to be reached earlier. This trend is verified by the experimental results.

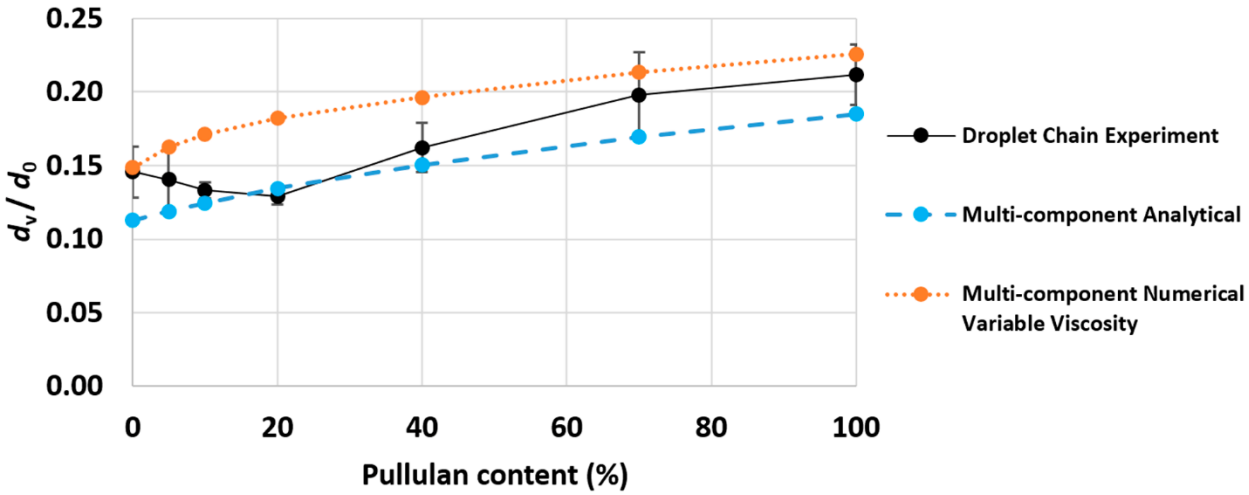

Figure 3.2: Experimental results and model predictions of volume equivalent diameter, d_v, normalized by initial droplet diameter, d_0, for different pullulan contents, demonstrating the reasonable accuracy of the particle formation models. Error bars represent standard deviation of two replicates, except for the 0% pullulan content case which represents three replicates. Colour version available online.

3.4.1.3 Radial Profiles of Local Mass Fractions and Dry Glass Transition Temperature

The numerical modelling results for the internal distributions of pullulan and trehalose mass fractions in the microparticles and the internal dry glass transition temperature radial profiles are given in Figure 3.3 and Figure 3.4, respectively. From Figure 3.3 it is apparent that pullulan concentrates on the surface of the microparticles even at a low overall mass fraction, and the mass fraction at the surface increases with increasing overall mass fraction of pullulan in the formulation. The high mass fraction of pullulan at the surface leads to an increase in the dry glass transition temperature near the surface, as shown in Figure 3.4. Since biologics are likely to reside near the surface due to their large size and low diffusion coefficient, use of pullulan is likely to increase the glass transition temperature in the vicinity of the biologic. The higher glass transition temperature near the surface may improve biologic stabilization and may also help prevent merging between particles during temporary temperature or relative humidity excursions, thus keeping the powder dispersible. In all cases, some trehalose is present at the surface, which may be necessary for biological stabilization, as small trehalose molecules may be necessary for efficient hydrogen bond replacement (see Chapter 1).

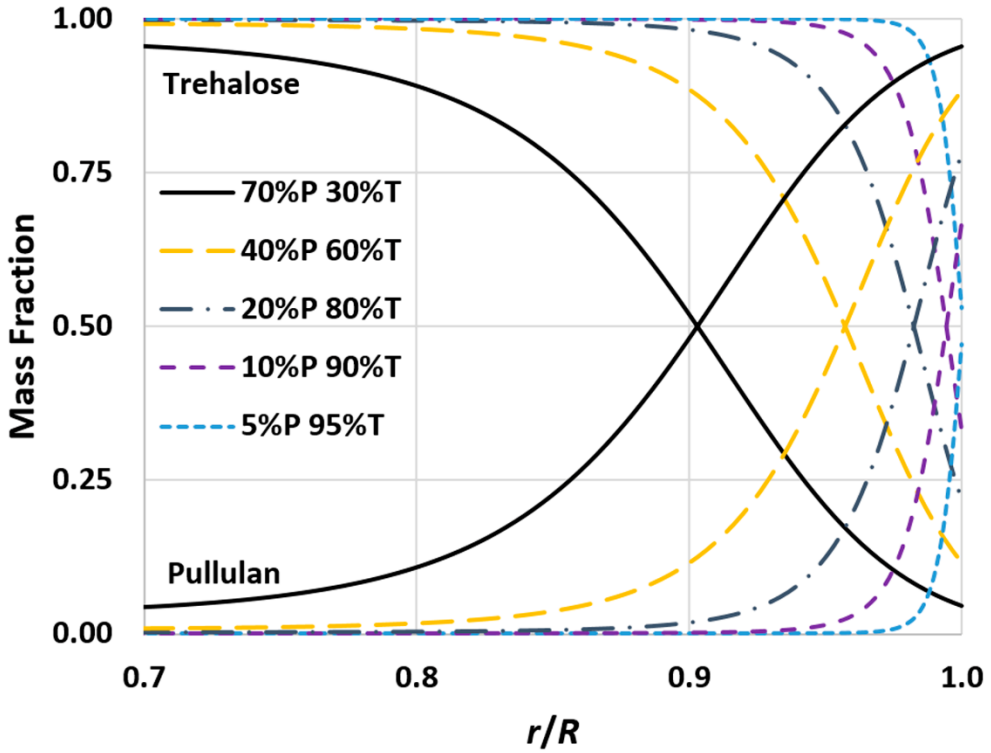

Figure 3.3: Internal radial distributions of mass fractions of pullulan and trehalose, demonstrating that pullulan tends to concentrate near the surface of the microparticles even at low initial mass fractions. The radial position within the microparticle, *r*, is normalized by the radius at the surface of the microparticle, *R*, on the x-axis. The legend depicts the total mass percentage of pullulan (P) and trehalose (T) in the powder. The values are approximately constant below an *r*/*R* ratio of 0.7. Colour version available online.

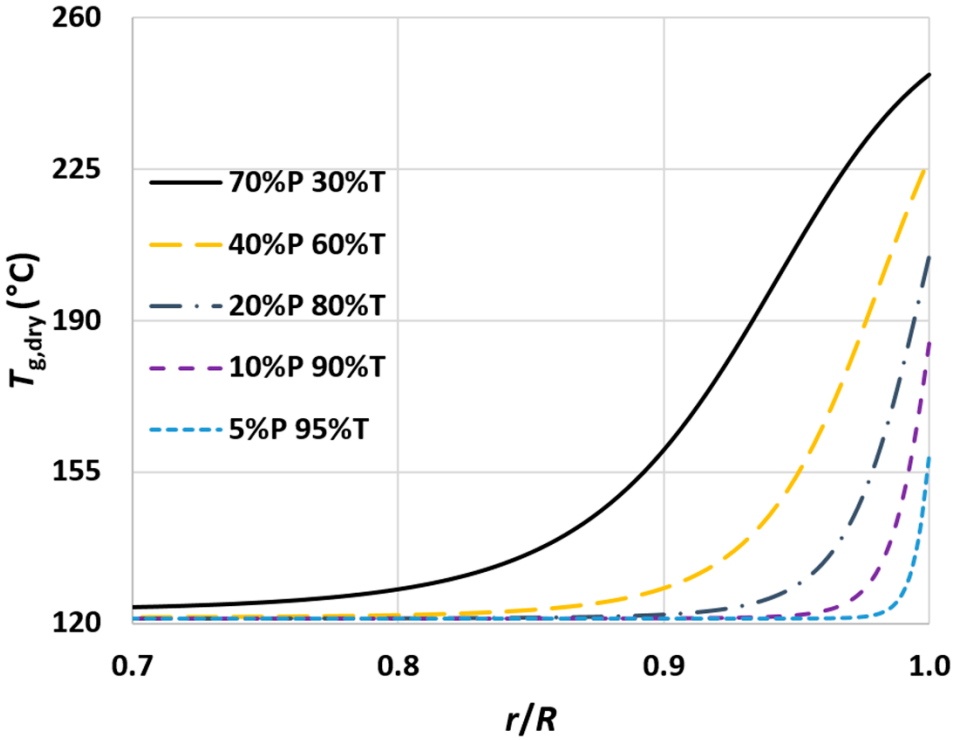

Figure 3.4: Internal radial distributions of local dry glass transition temperature, $T_{g,dry}$, calculated according to equation (3.25) using the mass fraction profiles in Figure 3.3. Biologics are expected to reside near the surface, where the glass transition temperature is higher, potentially leading to improved stability. The values are approximately constant below an *r*/*R* ratio of 0.7. Colour version available online.

3.4.2 Spray Drying

3.4.2.1 Spray Drying Process Model

For spray drying experiments, the droplet lifetime for a droplet emitted from the twin-fluid atomizer that is of the initial mass median diameter was 10.2 milliseconds. The corresponding Péclet numbers for pullulan and trehalose were 21 and 1.2, respectively. This corresponded to respective steady state surface enrichments of 7.3 and 1.3.

The outlet temperature for spray drying experiments matched the predictions from the process model within 2°C. The yield was 50-65% for each case, except for the 100% pullulan content case, for which 20-25% yield was obtained and stringy particles were present (images not shown), likely due to the high viscosity of pullulan preventing droplet breakup and causing drying of jets produced during the atomization process [408]. The yield, for the 0-40% pullulan content cases, is

reasonable for a laboratory-scale spray dryer, demonstrating suitable manufacturability. The yield is likely to increase for larger batch sizes or for scaled-up spray dryers.

3.4.2.2 Spray Dried Particle Morphology

Scanning electron microscope images of the particles produced by the spray dryer are given in Figure 3.5. As expected for production using a twin-fluid atomizer, the microparticles are polydisperse. The trend of increasing pullulan content causing an increase in folding is in agreement with droplet chain experiments.

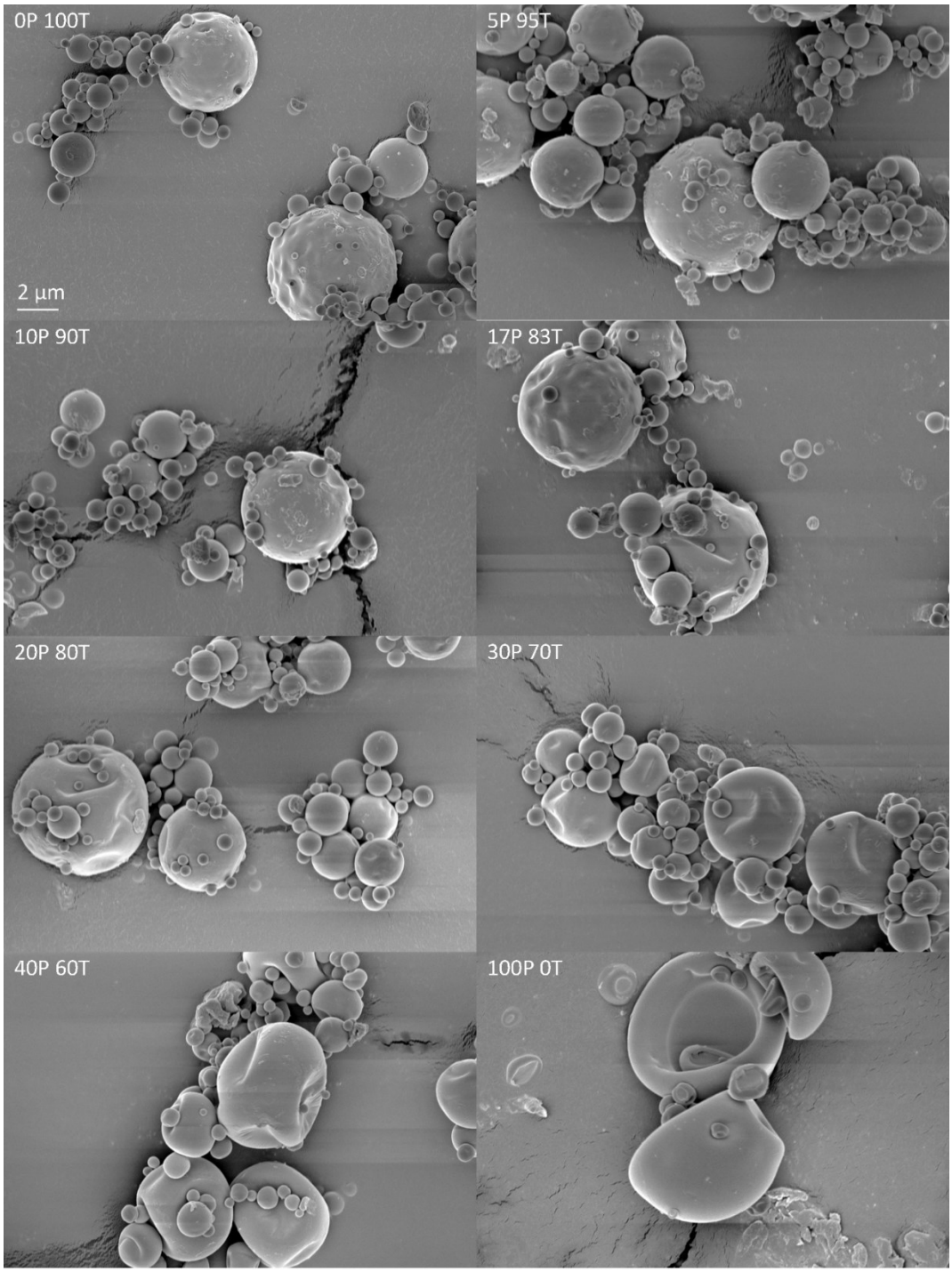

Figure 3.5: Scanning electron microscope images of freshly spray dried pullulan trehalose microparticles. More folding is observed for particles with a higher mass fraction of pullulan. The microparticles are not fused. The same imaging settings were used as in Figure 3.1. The same scale bar applies to all images.

Helium ion microscope images of spray dried 40% pullulan 60% trehalose particles are given in Figure 3.6. No internal void space was detected. The theoretical particle formation models predict that water is still present in the interior when solidification is initiated at the surface. Were water in the interior of the microparticle to simply evaporate and exit as vapour diffusion through a rigid shell, interior void space would be present. The lack of interior void space in the microparticles indicates that the particles continue to shrink after solidification at the surface occurs. In reality, there is a continuous transition from dilute aqueous solution to highly viscous liquid to amorphous 'solid', and shell deformation may be occurring throughout the process, which is not currently amenable to theoretical particle formation modelling.

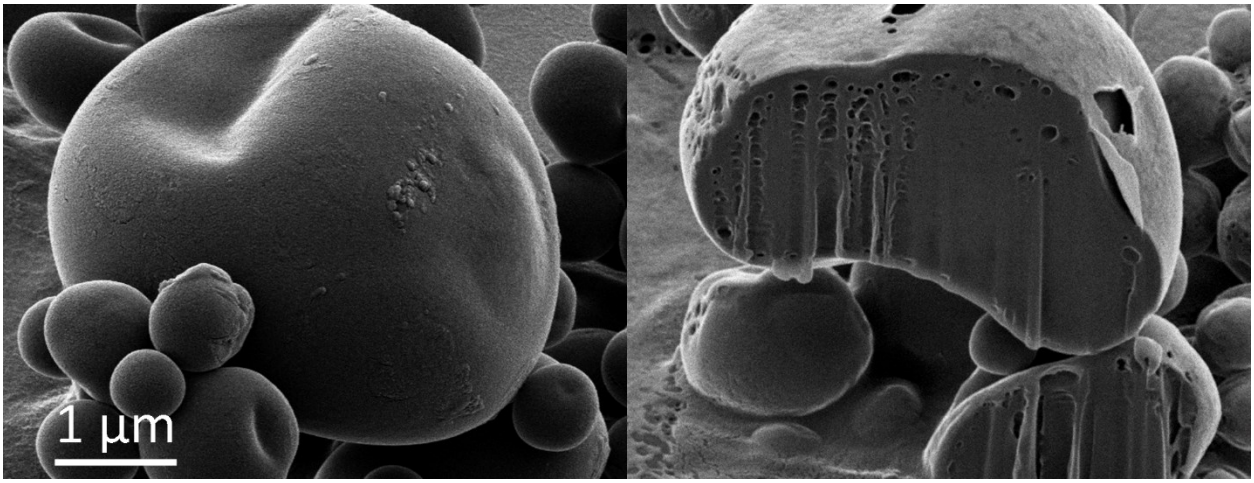

Figure 3.6: Helium ion microscope images of a 40% pullulan 60% trehalose microparticle before and after gallium ion beam milling. No internal void space was detected, suggesting that the particles continue to shrink after the shell is formed. The small holes visible in the cut particle on the right are artefacts of the cutting process. The peeled outer layer is the gold coating.

3.4.2.3 Modulated Differential Scanning Calorimetry Measurements

The results of modulated differential scanning calorimetry measurements on spray dried powders are given in Figure 3.7. The onset of glass transition for spray dried trehalose was near the glass transition temperature value of 121°C given by Teekamp *et al.* [405]. For spray dried pullulan, the onset of glass transition was ~255°C, slightly lower than the value of 261°C given by Teekamp *et al.* [405]. There was a glass transition at around 125°C for the spray dried pullulan trehalose powder, which is higher than the value measured for trehalose alone. This provides evidence that the pullulan addition increased the glass transition temperature relative to trehalose alone.

Additionally, for pullulan trehalose powder the glass transition extended over a larger range of temperatures than for trehalose powder. The fact that the glass transition temperature occurred over a larger range of temperatures is likely due to the fact that trehalose and pullulan form a mixture with radially changing composition ratio, which was previously predicted theoretically (see Figure 3.4). The onset of the glass transition at 125°C for the spray dried pullulan trehalose powder likely represents the interior ($r/R < 0.7$) of the particles while the extension at higher temperatures represents the higher glass transition occurring near the surface of the particles. By adding the reversing heat flow curves of pullulan and trehalose that were spray dried individually and subtracting away the reversing heat flow curve of pullulan and trehalose spray dried together, it is evident that the spray dried pullulan trehalose has less reversing heat flow at the lower temperature and more reversing heat flow at slightly higher temperature, providing further evidence for this explanation. Furthermore, in Figure 3.8, the predictions for the radial profile of glass transition temperature for this powder are given. The measured glass transition range in Figure 3.7 for pullulan trehalose particles is within the predicted range of 123°C at the interior to 164°C at the surface predicted by use of the numerical model and equation (3.25). The Fox and Gordon-Taylor equations over-predict the major component of the glass transition temperature, since they assume even mixing, i.e., constant radial profiles of mass fractions throughout the particles. In reality, the pullulan is only substantially increasing the glass transition temperature relative to trehalose near the surface, while the bulk of the powder is in the interior and is relatively unaffected and exhibits a lower glass transition temperature and earlier onset of glass transition.

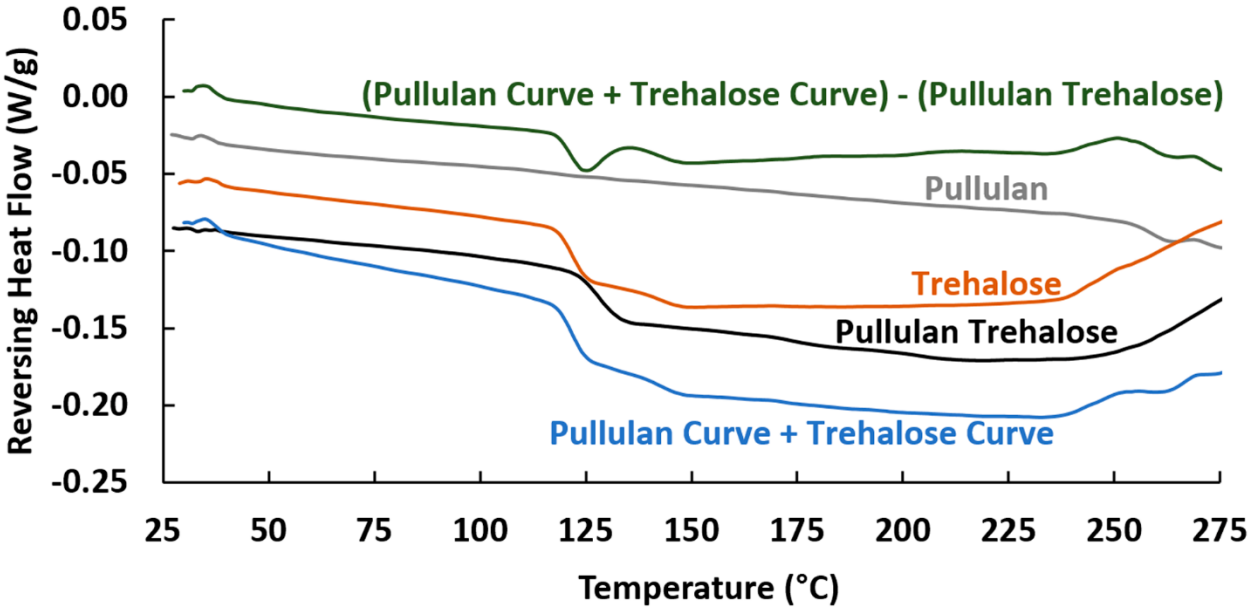

Figure 3.7: Modulated differential scanning calorimetry results of reversing heat flow. Spray dried pullulan trehalose powder has a higher glass transition temperature, extending over a larger range of temperatures, than trehalose alone. See the text for interpretation. "Pullulan" represents spray dried pullulan alone, "Trehalose" represents spray dried trehalose alone, "Pullulan Trehalose" represents spray dried pullulan trehalose formulation, "Pullulan Curve + Trehalose Curve" represents addition of "Pullulan" and "Trehalose" results, and "(Pullulan Curve + Trehalose Curve) - Pullulan Trehalose" represents subtraction of "Pullulan Trehalose" from "Pullulan Curve + Trehalose Curve". Colour version available online.

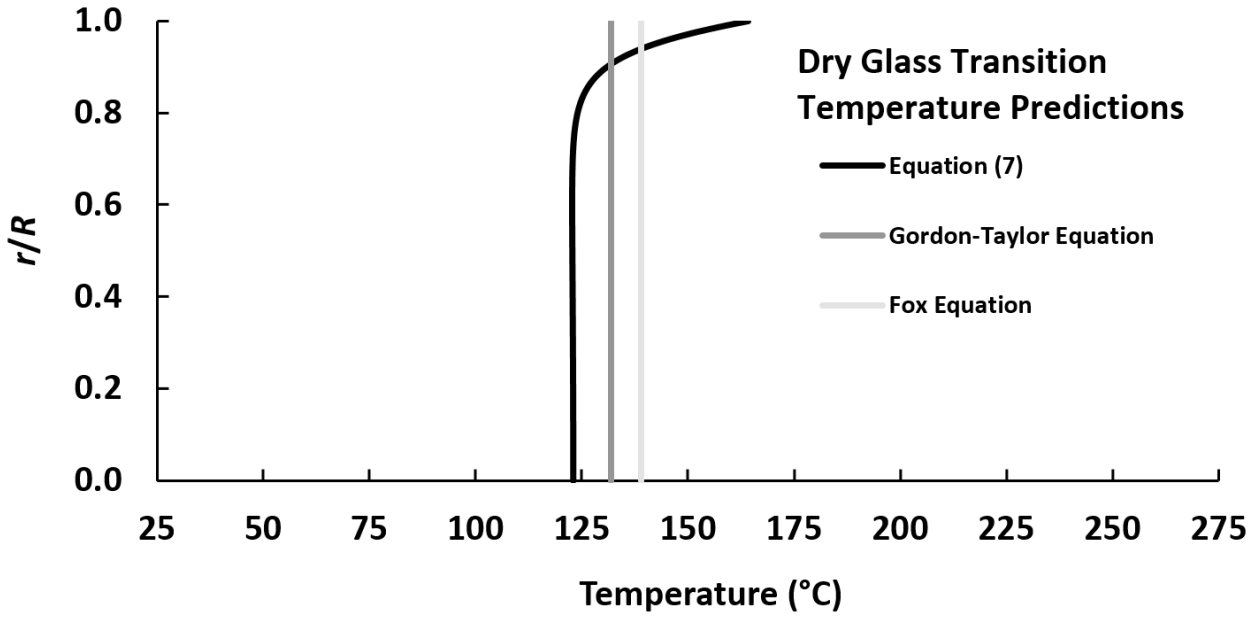

Figure 3.8: Radial glass transition temperature profile of 16.7% pullulan 83.3% trehalose powder predicted by use of the numerical model and equation (3.25) (ranging from 123°C at the interior to 164°C at the surface), as well as predictions made using the Gordon-Taylor equation (132°C) and the Fox equation (139°C), which do not vary with radius. The radial prediction is most representative of the experimental results given in Figure 3.7. Note that the x-axis is the same as in Figure 3.7 for comparison.

This is the first time, to the authors' knowledge, that a radial profile of glass transition temperature has been predicted and experimentally supported for dry particles. As the glass transition temperature is likely to be higher near the surface due to the higher surface enrichment of pullulan as compared to trehalose, and the biologics are likely to reside near the surface, it is possible that the biologic may be glass stabilized to withstand higher temperatures or moisture contents with pullulan addition. The further effect of moisture on glass transition temperature for pullulan trehalose powder has been studied elsewhere [405]. Fusing between particles may be decreased under higher temperature and humidity conditions by the increased glass transition temperature at the surface. The relatively high glass transition temperature of pullulan is an advantage compared to trileucine, another amorphous excipient that concentrates at the surface and forms folded particles. Trileucine has a lower glass transition temperature, ~104°C [439].

3.4.2.4 Modulated Compressed Bulk Density Measurements

The average compressed bulk density at the transition pressure was 410-470 kg/m^3 for all powders. At the transition pressure, 24-30% of the powder volume consisted of solid powder material, a reasonably high value relative to random close packing of spheres, indicating the powder is not extremely cohesive. The pullulan content, within the range of 0-40%, was not found to affect the compressed bulk density of the powders. The average transition pressure was in the range of 67-82 kPa for all powders. The powder was compressed by a factor of 1.7 ± 0.1 at this pressure, relative to the loose powder filled into the cavity. This is an important consideration for automated capsule or blister filling, e.g. when the biological dose per actuation needs to be optimized.

3.4.2.5 Dry Powder Inhaler Aerosol Performance Measurements

The mass collected on the different stages of the Next Generation Impactor are depicted in Figure 3.9. It is evident that similar aerosol performance occurred for all tested cases. The powder was easily filled into the capsules, demonstrating that the powder was flowable. For each powder the

average emitted dose was 93-94% of the packaged (capsule) dose, which is promising for dry powder inhaler applications.

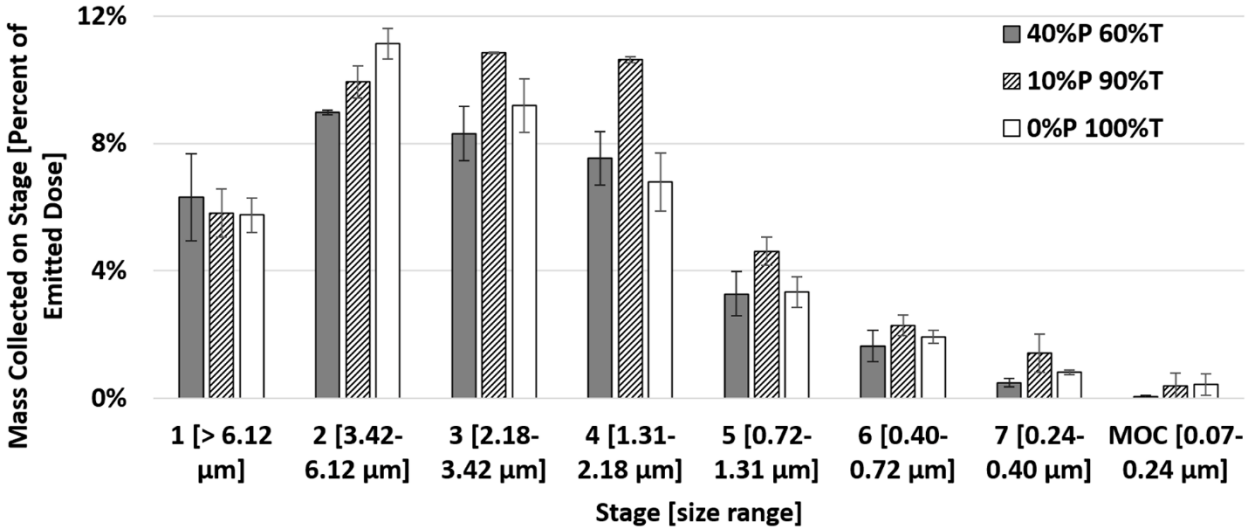

Figure 3.9: Mass collected past the Alberta Idealized Throat on each stage of the Next Generation Impactor for the different tested powders as a percent of the emitted dose from the Seebri® Breezhaler® dry powder inhaler. Similar trends are observed in the different cases. The error bars represent the standard deviations from two replicate measurements.

The aerosol performance results are summarized in Table 3.1. The total lung dose was not significantly different between any powder compositions ($p > 0.10$), although the FPF (< 6.12 µm) was significantly greater for the 10% pullulan 90% trehalose case than for the 0% pullulan 100% trehalose case ($p < 0.05$). The MMAD was not significantly different between any cases ($p > 0.05$).

Table 3.1: Aerosol performance of pullulan trehalose powder emitted from a Seebri® Breezhaler® dry powder inhaler through an Alberta Idealized Throat to a Next Generation Impactor.

Powder Composition	**Total Lung Dose (%)**	**FPF (%)**	**MMAD (μm)**
0% Pullulan 100% Trehalose	39.3 ± 1.6	33.6 ± 2.1	2.45 ± 0.03
10% Pullulan 90% Trehalose	45.9 ± 3.2	40.1 ± 2.4	2.16 ± 0.09
40% Pullulan 60% Trehalose	36.5 ± 1.4	30.2 ± 2.8	2.38 ± 0.09

Matinkhoo *et al.* [434] summarized the total lung dose of commercially available dry powder inhalers, which ranged from 5.5-40.5%, with a mean of 23%. In the present study, pullulan trehalose microparticles had a total lung dose of 37-46%, with a mean of 41%, indicating an improvement over commercial dry powder inhalers. Therefore, spray dried pullulan trehalose powder has suitable aerosol performance for an inhalation product. Nevertheless, improvements in aerosol performance could potentially be made with additions of a dispersibility-enhancing excipient, like leucine [434,440] or trileucine [439], although the effects of those excipients on glass stabilization and biological stability would need to be considered. From the analytical model described in Section 3.3.1.3 and the spray drying process model conditions in Section 3.3.2.1, a median particle size of 2.3-2.7 μm was predicted for these powders. The close match to the MMAD results in Table 3.1 supports the accuracy of the analytical model and the process model. The measured MMADs are suitable for deposition in all regions of the lung [441]. In each case, the GSD was ~1.9. A greater proportion of the total lung dose consisted of fine particles for increasing pullulan contents.

3.4.2.6 Pressurized Metered-Dose Inhaler Physical Stability Measurements

By visually examining settling of the spray dried pullulan trehalose powder within glass pressurized metered-dose inhaler canisters, it appeared that the powder maintains adequate suspension stability in either propellant after sonication for at least a few hours. The scanning

electron microscope images of the powder that was kept filled in the pressurized metered-dose inhaler canisters with commercial propellants HFA 134a and HFA 227 for 42 days at 40°C, and then actuated onto a stub, are shown in Figure 3.10. The scanning electron microscope images indicate a similar morphology and particle size to the images of the freshly spray dried 40% pullulan 60% trehalose powder given in Figure 3.5. In some images, not shown, there was evidence that some particles fused, which was perhaps related to moisture ingress into the canisters, as the seal is not perfect, and the canisters were not kept in a dry box. Further improvements could potentially be made to canister sealing or with the addition of additional excipients to prevent fusing, prior to measuring the emitted particle size. Nevertheless, Raman spectra, shown in Figure 3.11, demonstrated that all powders remained in a completely amorphous solid phase after being kept in suspension in the different propellants for 42 days at 40°C, and subsequent actuation. The microparticles also remained amorphous after 42 days storage in a dry box, without insertion into propellant, at ambient temperature conditions. The results indicate that spray dried pullulan trehalose microparticles have promising short-term physical stability in commercial propellants even at elevated temperatures and that actuation from a pressurized metered-dose inhaler does not damage them.

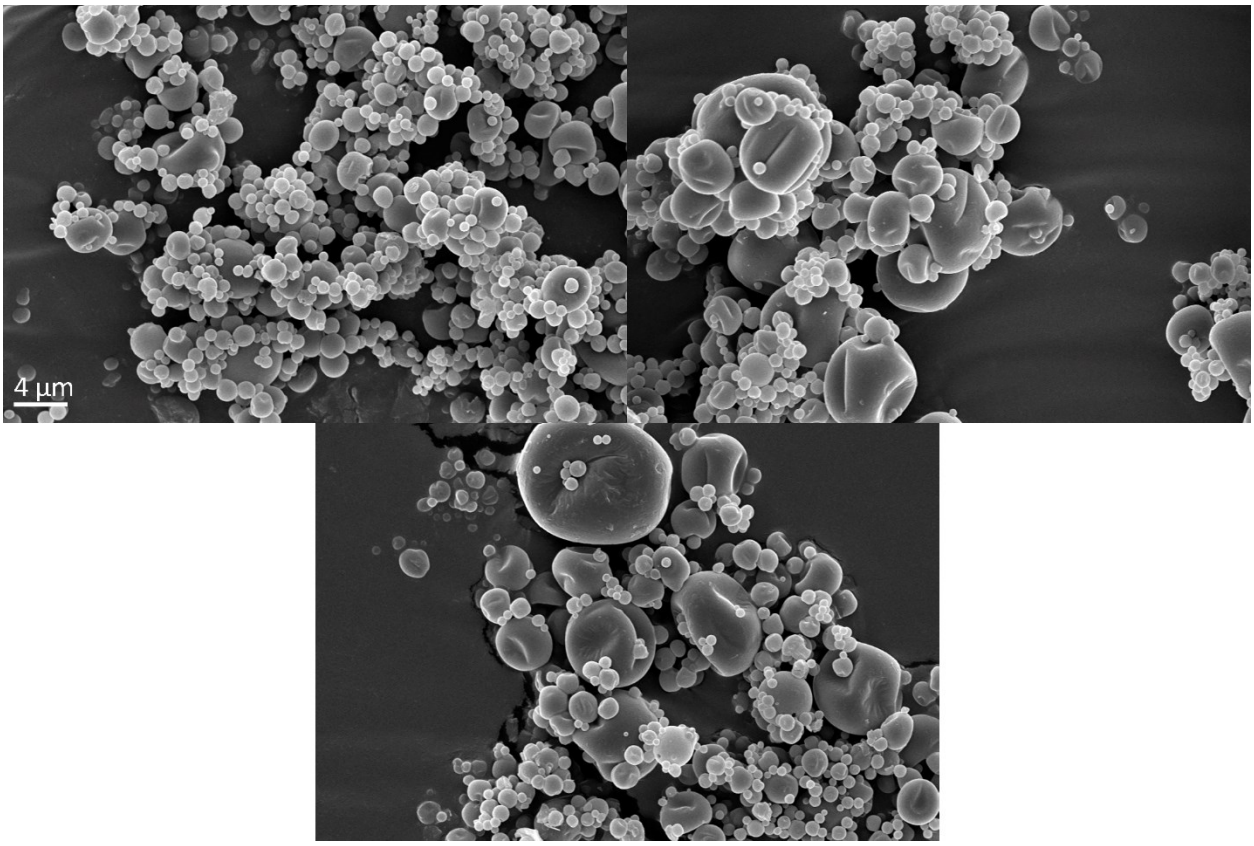

Figure 3.10: Scanning electron microscope images of spray dried 40% pullulan 60% trehalose microparticles after stability testing in different propellants and then actuation onto a stub via a low-flow-rate impactor. The particle morphology is similar to the freshly spray dried 40% pullulan 60% trehalose particles shown in Figure 3.5. Top-left: after storage and actuation from a glass canister filled with HFA 134a propellant kept at room temperature, ~22°C, for 42 days. Top-right: after storage and actuation from an aluminium canister filled with HFA 134a propellant kept at 40°C for 42 days. Bottom: after storage and actuation from a glass canister filled with HFA 227 propellant kept at 40°C for 42 days.

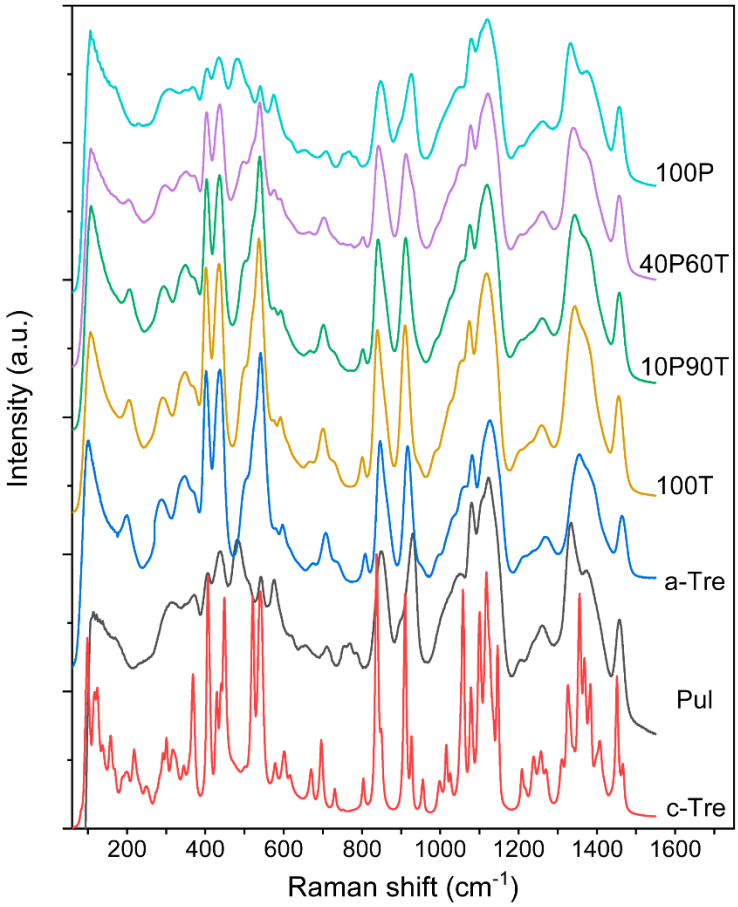

Figure 3.11: Raman spectra of pullulan trehalose microparticles and references, demonstrating the spray dried and stored microparticles remained in an amorphous solid phase for the different tested conditions. Legend: “c-Tre” is raw crystalline trehalose material, “Pul” is raw amorphous pullulan material, “a-Tre” is a spray dried trehalose reference from the literature [442], “100T” is spray dried 100% trehalose, “10P90T” is spray dried 10% pullulan 90% trehalose, “40P60T” is spray dried 40% pullulan 60% trehalose, “100P” is spray dried 100% pullulan. Prior to performing Raman spectroscopy, the spray dried powder was stored for 42 days in a dry box at ambient temperature. Storage for 42 days at ambient temperature or at 40°C in commercial propellants HFA 134a and HFA 227 resulted in the same spectra as the spray dried 40% pullulan 60% trehalose powder, indicating short-term elevated temperature storage in propellant did not affect solid phase. Colour version available online.

3.5 Conclusions

Spray dried pullulan trehalose microparticles are a promising non-reducing sugar-only, fully amorphous platform for respiratory delivery. The suitability is justified based on measurements

demonstrating acceptable manufacturability, physical stability, device compatibility, and aerosol performance.

Good manufacturability is demonstrated by a reasonable spray drying yield and the ability to easily fill the flowable powder into dry powder inhaler capsules. The manufacturability is robust, i.e., it varies little with the ratio of pullulan and trehalose in the formulation, despite increased pullulan content leading to more folded microparticles without internal void space. The powder is not too cohesive for use in inhalation devices. It can be compressed for automated filling without semi-elastic deformation. The efficient packing makes it a promising candidate for devices with small dosing volumes.

Short-term physical stability is evident as the powder maintains its amorphous phase during ambient temperature storage in a dry box and 40°C storage in pressurized metered-dose inhaler canisters containing commercial propellants HFA 134a and HFA 227. Actuation from a pressurized metered-dose inhaler does not affect the morphology or solid phase. The powder is theoretically predicted and experimentally supported to have a higher glass transition temperature near the surface, where biologics are expected to reside, than in the interior. The higher the mass fraction of pullulan in the formulation, the more pullulan surface enrichment that occurs, and the higher the glass transition temperature at the surface, potentially resulting in more protection against fusing for temporary temperature or humidity excursions. These findings indicate that this platform likely has outstanding environmental robustness and can withstand storage at elevated temperatures. Therefore, long-term stability and environmental robustness should be assessed in future studies. Cytotoxicity of pullulan trehalose powder in the lungs should also be assessed in future studies.

The platform appears to be compatible both with dry powder inhalers and pressurized metered-dose inhalers. It has suitable aerosol performance in a commercial dry powder inhaler, exceeding that of many available commercial products. The inhalable powder is in the correct size for deposition throughout the lungs. Accurate predictions of particle diameter can be made using the newly developed particle formation model for amorphous co-solidification from multi-component drying droplets, as demonstrated by a close match of diameter predictions to experimental measurements performed using a monodisperse droplet chain. Thus, the particle formation mechanism for this type of fully amorphous particle is well enough understood so that particle

formation, solid phase, and process models can be used to accelerate the development process. Further improvements to aerosol performance could potentially be made with incorporation of additional dispersibility-enhancing excipients, although it needs to be determined whether this reduces the stabilization potential of the platform.

4 Anti-Tuberculosis Bacteriophage D29 Delivery with a Vibrating Mesh Nebulizer, Jet Nebulizer, and Soft Mist Inhaler

This chapter has been published in the journal paper "Carrigy NB, Chang RY, Leung SSY, Harrison M, Petrova Z, Pope WH, Hatfull GF, Britton WJ, Chan H-K, Sauvageau D, Finlay WH, Vehring R. 2017. Anti-tuberculosis bacteriophage D29 delivery with a vibrating mesh nebulizer, jet nebulizer, and soft mist inhaler. Pharmaceutical Research. 34:2084-2096." Additional material is given in Appendix C.

4.1 Abstract

Purpose: To compare titer reduction and delivery rate of active anti-tuberculosis bacteriophage (phage) D29 with three inhalation devices.

Methods: Phage D29 lysate was amplified to a titer of 11.8 ± 0.3 $\log_{10}$(pfu/mL) and diluted 1:100 in isotonic saline. Filters captured the aerosolized saline D29 preparation emitted from three types of inhalation devices: 1) vibrating mesh nebulizer; 2) jet nebulizer; 3) soft mist inhaler. Full-plate plaque assays, performed in triplicate at multiple dilution levels with the surrogate host *Mycobacterium smegmatis*, were used to quantify phage titer.

Results: Respective titer reductions for the vibrating mesh nebulizer, jet nebulizer, and soft mist inhaler were 0.4 ± 0.1, 3.7 ± 0.1, and 0.6 ± 0.3 $\log_{10}$(pfu/mL). Active phage delivery rate was significantly greater ($p < 0.01$) for the vibrating mesh nebulizer ($3.3x10^8 \pm 0.8x10^8$ pfu/min) than for the jet nebulizer ($5.4x10^4 \pm 1.3x10^4$ pfu/min). The soft mist inhaler delivered $4.6x10^6 \pm 2.0x10^6$ pfu per 11.6 ± 1.6 µL ex-actuator dose.

Conclusions: Delivering active phage requires a prudent choice of inhalation device. The jet nebulizer was not a good choice for aerosolizing phage D29 under the tested conditions, due to substantial titer reduction likely occurring during droplet production. The vibrating mesh nebulizer is recommended for animal inhalation studies requiring large amounts of D29 aerosol, whereas the soft mist inhaler may be useful for self-administration of D29 aerosol.

4.2 Model Notation

$C_{d,p,i}$ = mass concentration of solute in the solvent droplets both exiting the mouthpiece and returning to the reservoir in the i^{th} nebulization cycle, assumed to be equal

$C_{e,p,i}$ = mass concentration of solute in the solvent droplets exiting the mouthpiece in the i^{th} nebulization cycle

$C_{n,p,i}$ = mass concentration of solute in the solvent exiting the nozzle in the i^{th} nebulization cycle

C_p = mass concentration of solute in the solvent

$C_{p,0}$ = mass concentration of solute in the solvent initially input to the reservoir

$C_{r,p,i}$ = mass concentration of solute in the solvent droplets returning to the reservoir in the i^{th} nebulization cycle

$Cu(f_{e,i})$ = fraction of the initial number of phage input to the jet nebulizer which have cumulatively exited the mouthpiece over i nebulization cycles

$Cu(i * X_i)$ = average number of nebulization cycles phage which exited the mouthpiece underwent

$f_{e,i}$ = fraction of the number of phage initially input to the reservoir, which exit the mouthpiece in the i^{th} nebulization cycle

i = nebulization cycle count

j = a summation index for i in $Cu(f_{e,i})$

k = a summation index for i in X_i

L = a summation index for i in $Cu(i * X_i)$

$\dot{m}_{e,s}$ = mass flow rate of solvent in droplets exiting the mouthpiece

$\dot{m}_{h,s}$ = mass flow rate of solvent exiting due to humidification of air supplied by the compressor

$\dot{m}_{n,s}$ = mass flow rate of solvent exiting the nozzle

$\dot{m}_p$ = mass flow rate of solute

$\dot{m}_{r,s}$ = mass flow rate of solvent returning to the reservoir

$\dot{m}_s$ = mass flow rate of solvent

m_{1p} = mass of a single phage

N = total number of nebulization cycles to complete aerosolization

$n_{e,p,i}$ = number of phage, either active or inactive, exiting the mouthpiece in the i^{th} nebulization cycle

$n_{p,0}$ = number of phage initially input to the reservoir

ρ_s = mass density of the solvent

$Q_{e,s}$ = volumetric flow rate of solvent in droplets exiting the mouthpiece

$Q_{h,s}$ = volumetric flow rate of solvent exiting due to humidification of air supplied by the compressor

$Q_{n,s}$ = volumetric flow rate of solvent exiting the nozzle

$Q_{r,s}$ = volumetric flow rate of solvent returning to the reservoir

Q_s = volumetric flow rate of solvent

t_i = time to complete the i^{th} nebulization cycle

$V_{e,s,i}$ = volume of solvent in droplets exiting the mouthpiece in the i^{th} nebulization cycle

V_F = volume of solvent initially input to the reservoir, termed fill volume

$V_{h,s,i}$ = equivalent liquid volume of solvent exiting the device due to humidification of air supplied by the compressor in the i^{th} nebulization cycle

$V_{n,s,i}$ = volume of solvent exiting the nozzle in the i^{th} nebulization cycle

$V_{r,s,i}$ = volume of solvent returning to the reservoir in the i^{th} nebulization cycle

X_i = fraction of the cumulative number of phage which have exited the mouthpiece after aerosolization is complete, which exited the mouthpiece in the i^{th} nebulization cycle

4.3 Introduction

Increasing incidence of bacterial resistance to antibiotics is a threat to global health [443]. For example, multidrug-resistant tuberculosis (MDR-TB), defined as resistant to the first-line antibiotics isoniazid and rifampicin, was observed in 3.3% of new TB cases globally in 2014 and 2015 [444]. Extensively drug-resistant TB (XDR-TB), which is resistant to the most effective second-line anti-TB antibiotics, occurred in 9.5% of MDR-TB cases [444]. Totally drug-resistant TB has also been reported [445], although it is classified as XDR-TB by the World Health Organization [446]. Exacerbating antibiotic resistance is the slow commercialization of new antimicrobials [443].

Bacteriophage (phage) therapy may be useful as an alternative or adjunct to antibiotics [447-449]. Phage are bacterial viruses that typically infect a narrow-spectrum of bacteria within a single genus [450-451], thus only minimally harming flora during phage therapy [451]. Additionally, antibiotic-resistance does not translate into phage-resistance [451]. Phage also have low inherent toxicity, and in some cases, have the potential to cause biofilm degradation [451].

Phage have co-evolved with bacteria and are the most numerous biologic entities on Earth [452]. New phage strains able to infect new pathogenic bacteria can be found relatively rapidly [451]. While not all phage are useful for therapeutic purposes, stable, lytic phage that effectively kill their host bacteria are routinely selected with the aid of genome sequencing and analysis [450]. A lytic phage binds to its target bacterium and injects its genetic material through the cell wall, initiating the biosynthesis of new phage within the bacterium [452]. These progeny phage, which can be produced on the order of one hundred per bacterium [453], escape by lysing the cell wall (which kills the bacterium) and go on to infect and replicate within neighbouring bacteria until all accessible and susceptible host bacteria are lysed [452].

Respiratory delivery of phage is an active topic in research and development [453-454], with phage-containing dosage forms for nebulizers and dry powder inhalers, and even some exploratory versions for pressurized metered dose inhalers, tested *in vitro* [455-459]. Phage are generally regarded as safe, exhibiting few if any side effects [454]. In Georgia and Russia, oral phage cocktails are even available to the public without prescription [447]. However, the development of commercial phage products for human therapy in Western medicine has been hindered by a

relative lack of private investment due in part to uncertainty over timelines necessary for obtaining regulatory approval [460-461].

Humans have been treated clinically using pulmonary phage delivery in parts of Eastern Europe, with efficacy reports being generally positive [447,462]. Excellent reviews of aerosol phage therapy have also been published [450,453,462]. However, human pulmonary delivery studies coming out of Eastern Europe do not conform to the standards required by regulatory authorities in the United States. Before more comprehensive studies in humans can be performed, animal studies to demonstrate safety and efficacy are a logical first step. To this end, Semler *et al.* [463] recently delivered phage from the family *Myoviridae* to mice using a nose-only inhalation device to treat antibiotic-resistant lung infections. This study showed that efficacy of phage delivered by inhalation was superior to that of phage delivered to control mice intraperitoneally, with a greater decrease in bacterial count and evidence of phage replication in the lungs [463]. In the Semler *et al.* [463] study, the success of phage therapy relied upon the delivery of enough active phage to start infection of the bacteria. The ratio of active phage to target bacteria is termed multiplicity of infection (MOI) and was a critical formulation design factor.

To ensure a high MOI in pulmonary phage delivery, titer reduction due to aerosolization should be minimized. Ensuring minimal titer reduction also decreases production costs and the chances of negative side effects associated with formulation excipients. For delivery to the lungs, undesirable titer reductions in the systemic system are circumvented when inhaled aerosol delivery is used instead of injection. Indeed, Liu *et al.* [464] found a higher concentration of active phage D29 in the lungs using inhaled aerosol delivery than using injection. However, stresses acting on phage in some inhalation devices can cause substantial titer reduction. A further discussion of factors that can contribute to phage titer reduction is given elsewhere [452-453]; these include temperature, shear, and osmotic shock.

This study examines how effectively a vibrating mesh nebulizer, a jet nebulizer, and a soft mist inhaler deliver active phage. To the authors' knowledge, the soft mist inhaler, which has the advantages of portability and electricity-free operation, has never before been tested with phage. Nebulizers, unlike metered-dose inhalers and dry powder inhalers, have the advantage of being able to deliver filtered phage lysate without further processing. Moreover, nebulizers can deliver

large amounts of aerosol continuously, including to those unable to coordinate the breathing maneuver required for inhalers, and can be more easily coupled to animal exposure devices. Nebulizers can also deliver resuspended phage powder should the need arise. Jet nebulizers and vibrating mesh nebulizers have previously been tested with phage [456, 465-466]; however, as far as the authors are aware, titer reduction and active phage delivery rate with these devices has never before been directly tested with phage D29. This lytic phage (Figure 4.1) is of particular interest as it can effectively kill a range of mycobacteria, including *Mycobacterium tuberculosis* [467]. Indeed, phage D29 is commonly used for TB diagnosis and drug-susceptibility testing [450]. It is of the *Caudovirales* order, having an icosahedral capsid (~55 nm 'wide') containing double-stranded deoxyribonucleic acid and a tail [450]. Its characteristic of a long (~130 nm), flexible and non-contractile tail places it in the *Siphoviridae* morphological family [450].

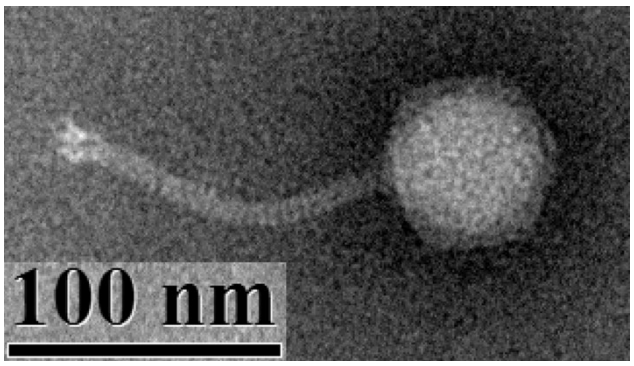

Figure 4.1: Transmission electron micrograph (TEM) (80 kV operation, Model: Morgagni 268; Philips – FEI, Hillsboro, Oregon, USA; with Gatan Orius CCD Camera and Gatan DigitalMicrograph™ Software Version 1.81.78) of phage D29. To generate the sample for imaging, a drop of lysate was placed on a TEM grid (300 mesh Copper grids with Formvar/Carbon Support Film; Prod # 01753-F; Ted Pella Inc., Redding, CA, USA), stained with 2% phosphotungstic acid for 30 seconds, and then removed using filter paper.

4.4 Materials and Methods

4.4.1 Phage D29 Bioprocessing and Shipping

High titer phage D29 lysate was generated and titered using well-established protocols [468]. Briefly, D29 from a laboratory stock was amplified on the host *Mycobacterium smegmatis* strain mc^2155 using solid media. A plate with confluent plaques was flooded with phage buffer, incubated overnight at 4°C, harvested and filtered through a 0.22 μm filter. The lysate was further

concentrated by centrifugation at $2.06x10^5$ m/s^2 [21,000 x g] for 90 minutes at 4°C, and pellet resuspension in phage buffer (10 mM $MgSO_4$, 1 mM $CaCl_2$, 10 mM Tris(hydroxymethul)aminomethane 7.5, and 68.5 mM NaCl). After amplification, ~2 mL of lysate was shipped from the University of Alberta, Canada, to the University of Sydney, Australia to perform the experiments. The phage lysate was wrapped in cold packs in an insulated Styrofoam container and sent using 2-day express shipping. The temperature during shipment was monitored and recorded (TempTale 4 USB MultiAlarm; Sensitech Canada; Markham, ON, Canada) and found to increase from 5°C to 20°C within the Styrofoam container over the two-day period, with a mean temperature of 11°C. No titer reduction was observed under these shipping conditions. Separate measurements of crude D29 lysate indicated no titer reduction after six weeks and ~2 log_{10}(pfu/mL) titer reduction after 10 months of storage at 4°C.

4.4.2 Plaque Assay

Plaque assays used the surrogate *M. smegmatis* mc^2155. The full-plate titer method, detailed elsewhere [468], was used, as the plaques were too large for spot assay. The plaque assays were performed in triplicate at multiple dilution levels. Negative control measurements were performed to confirm the absence of phage contamination in the stock materials. More details regarding the plaque assay protocol are given in Appendix A.

4.4.3 Dilution Stability

The amplified phage lysate was diluted 1:100 in isotonic saline (9 mg/mL sodium chloride (Sigma S5886, Lot#078K01272; Sigma Aldrich; St. Louis, MO, USA) in MilliQ water) within a 15 mL Falcon tube, and plaque assays were performed at time points of 0, 1.5, and 18 hours to compare the titer prior to and after dilution. This dilution lowers the concentration of components in the lysate that may not be suitable for inhalation at high concentrations, such as Tris pH 7.5. An additional diluted lysate sample was micropipetted onto a filter and left at room temperature for 50 minutes to verify whether some titer reduction could be due to phage binding to the filter during an experiment. All measurements were made at room temperature.

4.4.4 Aerosolization Titer Reduction

The three clinically-relevant inhalation devices tested were 1) Aerogen Solo vibrating mesh nebulizer (Model No. 06675745, Lot 60201509300103, Ref AG-AS3350-US; Aerogen Ltd., Dangan, Galway, Ireland) with Pro-X Controller (S/N AP-1510412, Ref AG-PX-1050-IN;

Aerogen Ltd., Dangan, Galway, Ireland); 2) Pari LC Sprint jet nebulizer (Part # 023F35-C; Pari Respiratory Equipment, Inc.; Midlothian, VA, USA) with Pari Boy SX Compressor (S/N: 2W14J03112; Type 085; Pari GmbH, Starnberg, Germany); 3) Respimat soft mist inhaler (Lot 401445B; Boehringer Ingelheim (Canada) Ltd., Burlington, ON, Canada).

For each run, a known volume from the stock of amplified phage lysate was diluted 1:100 in isotonic saline to create a saline phage D29 preparation, which was then pipetted into the inhalation device reservoir. Fill volumes were 6 mL for the vibrating mesh nebulizer, 8 mL for the jet nebulizer, and 4 mL for the soft mist inhaler. A filter (Suregard Bacterial/Viral Respiratory Filter; BIRD Healthcare, Port Melbourne, VIC, Australia) was connected to the aerosol outlet of the tested device. The aerosolized droplets were captured on the filter, without the use of breathing simulation.

For the vibrating mesh nebulizer, enough liquid was collected on the filter that it could be drawn directly for plaque assay to determine the output titer. The recovered liquid from the filter was vortexed to ensure uniformity prior to assay.

For the soft mist inhaler, a custom adapter made with a PolyJet 3D printer (Objet Eden 350V High Resolution 3D Printer; Stratsys, Ltd.; Eden Prairie, MN, USA) from an acrylic compound (Objet VeroGray RGD850; Stratsys, Ltd.; Eden Prairie, MN, USA) connected the filter to the mouthpiece. The small dose of liquid emitted from the soft mist inhaler meant that 10 actuations onto the filter and resuspension in phage buffer were necessary to draw liquid for plaque assay. The ex-actuator dose from the soft mist inhaler was measured by weighing the inhaler with a microbalance before and after 10 actuations. The dilution ratio occurring from phage buffer resuspension was determined using the gravimetrically measured ex-actuator dose of 11.6 ± 1.6 μL per actuation, which is within error of the expected 11.05 μL per actuation [469], and the known volume (10 mL) of phage buffer added to the filter in increments of 1 mL with a micropipette. The extra dilution was accounted for in output titer calculation. Additionally, the drug solution is normally stored in a cartridge that consists of an aluminium cylinder containing a double-walled polypropylene collapsible bag which contracts as the solution is withdrawn [470-471]; in the present study, the polypropylene bag was used without the aluminium cylinder to allow for refilling of the phage solution.

Experiments with a titer reduction detection limit of ~3 $\log_{10}$(pfu/mL) for the jet nebulizer produced no plates with ≥ 5 plaques. Further measurements with the jet nebulizer utilizing a titer reduction detection limit of ~4 $\log_{10}$(pfu/mL) were performed with aerosol collected on separate filters after 7 minutes, the subsequent 11 minutes, and the subsequent 24 minutes of nebulization. For these experiments, dilution of the liquid recovered on the filter was also performed with 10 mL of phage buffer. The filter mass was measured with a microbalance before and after nebulization to determine the dilution ratio and delivered volume.

Titer reduction was quantified as the difference in the base 10 logarithm of plaque-forming units per millilitre ($\log_{10}$(pfu/mL)) between the saline phage preparation input to the inhalation device and the aerosol collected on the filter after exiting the inhalation device. Percent deactivation due to aerosolization was calculated as [1 – (output titer per millilitre collected on the filter / input titer per millilitre of saline phage preparation input to the inhalation device)] · 100%.

4.4.5 Nebulization Cycle Count

For the jet nebulizer, only a fraction of the liquid exiting the nozzle in the form of primary droplets continues on to exit the mouthpiece, since much of the liquid from the droplets impacting the baffles and inner walls of the device return to the reservoir for renebulization. To quantify this fraction, the flow rates of liquid forming primary droplets and exiting the mouthpiece were determined separately as shown in Figure 4.2. The measurement of the flow rate exiting the nozzle was determined using tryptophan (L-Tryptophan; Cat #93659; Sigma Aldrich; St. Louis, MO, USA) in isotonic saline as a tracer, with the collecting filter assayed using UV spectrophotometry (8452A Diode Array Spectrophotometer; Hewlett-Packard, Mississauga, ON, Canada). The ambient air temperature and humidity for these measurements were approximately 23°C and 20% relative humidity.

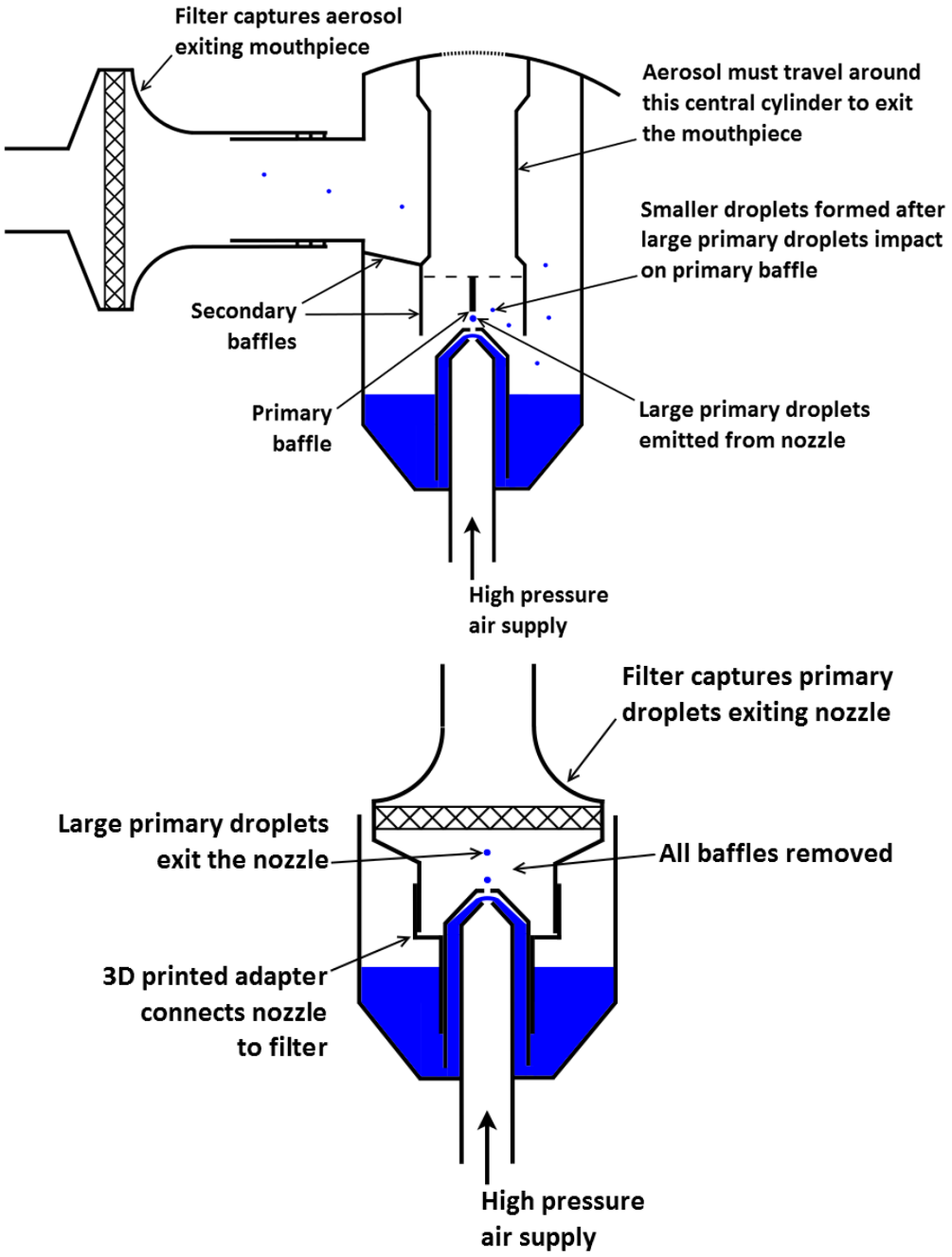

Figure 4.2: Schematic of filter measurements used to determine the flow rate of droplets exiting (top) the mouthpiece, using the unmodified jet nebulizer and (bottom) the nozzle in the form of primary droplets, using a jet nebulizer with all baffles removed. A fraction of the liquid volume from the droplets which impact the baffles and inner walls of the device is returned to the reservoir for renebulization. The experimental results for flow rate in each case were used as input to the mathematical model given in the Appendix to predict the number of nebulizations phage underwent prior to exiting the mouthpiece. Not to scale.

A mathematical model was developed to determine the average number of nebulization cycles undergone by the phage, i.e. the average number of times phage exited the nozzle and impacted the primary baffle prior to exiting the mouthpiece of the jet nebulizer. This impaction count may be an indicator of the cumulative stress the phage encounter before exiting the mouthpiece.

The solvent, water in this study, can follow three paths after exiting the nozzle: 1) humidify the air supplied by the compressor and exit the nebulizer as vapor; 2) exit the mouthpiece as aerosol droplets; 3) impact the interior of the device and return (drip back) to the reservoir. By assuming no mixing between the reservoir fluid and returning fluid in the same nebulization cycle, conservation of mass for the solvent gives

$$\dot{m}_{n,s} = \dot{m}_{h,s} + \dot{m}_{e,s} + \dot{m}_{r,s} \tag{4.1}$$

where $\dot{m}_{n,s}$ is the mass flow rate of the solvent exiting the nozzle, $\dot{m}_{h,s}$ is the mass flow rate of solvent which will exit the device via humidification of the air supplied by the compressor, $\dot{m}_{e,s}$ is the mass flow rate of solvent which will exit the mouthpiece of the device as aerosol droplets, and $\dot{m}_{r,s}$ is the mass flow rate of solvent which will return to the reservoir to exit the nozzle in the next nebulization cycle.

The solvent mass flow rate is related to volumetric flow rate by

$$\dot{m}_s = \rho_s \times Q_s \tag{4.2}$$

For water, ρ_s can be considered constant during jet nebulization. Equation (4.1) can thus be rewritten in terms of flow rates:

$$Q_{n,s} = Q_{h,s} + Q_{e,s} + Q_{r,s} \tag{4.3}$$

The flow rate exiting the nozzle, $Q_{n,s}$, was determined experimentally using tryptophan tracer assay, to be 17.64 mL/min. The flow rate exiting the mouthpiece of the device, $Q_{e,s}$, was determined to be 0.12 mL/min from the mass captured on the filter during phage experiments. The flow rate lost to humidification, $Q_{h,s}$, was calculated as the difference in flow rate determined based on mass loss from the nebulizer and mass captured on the outlet filter during phage experiments, and found to be 0.06 mL/min. This matched the theoretical amount of water required

to fully humidify the air supplied by the compressor. The flow rate returning to the reservoir, $Q_{r,s}$, was thus calculated using Equation (4.3), to be 17.46 mL/min.

It is assumed that solute does not exit the inhaler via humidification losses. Mass conservation for the solute (phage) is then given by

$$\dot{m}_{n,p} = \dot{m}_{e,p} + \dot{m}_{r,p} \tag{4.4}$$

The solute concentration in the solvent, C_p, is related to the mass flow rate by

$$\dot{m}_p = C_p \times Q_s \tag{4.5}$$

Assuming the solute remains in the droplets and reservoir fluid, Equation (4.4) and (4.5) can be combined to give

$$C_{n,p,i} \times Q_{n,s} = C_{e,p,i} \times Q_{e,s} + C_{r,p,i} \times Q_{r,s} \tag{4.6}$$

It is assumed that the humidification of the air supplied by the compressor occurs by evaporation of the droplets exiting the nozzle, which have a high air-liquid surface area to volume ratio, rather than from the liquid in the reservoir. The humidification due to evaporation of the primary and secondary droplets increases the solute concentration in the droplets. Assume that the increase in concentration in the droplets that exit the mouthpiece and that return to the reservoir is equal. Then, we can define the droplet concentration, $C_{d,p}$, as

$$C_{d,p,i} \equiv C_{e,p,i} = C_{r,p,i} \tag{4.7}$$

With each nebulization cycle, i, the concentration of the solute in the reservoir will increase. The concentration of solute in the reservoir in a specific cycle, i, is the same as the concentration of solute in the droplets in the previous cycle, $i-1$, as we have assumed no mixing between the reservoir fluid and returning fluid in the same cycle:

$$C_{n,p,i} = C_{r,p,i-1} = C_{d,p,i-1} \tag{4.8}$$

Define

$$C_{n,p,1} = C_{p,0} \tag{4.9}$$

where $C_{p,0}$ is the input mass concentration of solute in solvent. Here, $C_{n,p,1}$ represents the concentration of solute in solvent exiting the nozzle during the first nebulization cycle, when $i = 1$.

By combining Equations (4.6) and (4.7), and assuming that the respective volumetric flow rates are independent of nebulization cycle,

$$C_{n,p,i} \times Q_{n,s} = C_{d,p,i} \times (Q_{e,s} + Q_{r,s}) \tag{4.10}$$

Combining Equations (4.8) and (4.10)

$$C_{d,p,i-1} \times Q_{n,s} = C_{d,p,i} \times (Q_{e,s} + Q_{r,s}) \tag{4.11}$$

and rearranging Equation (4.11) gives

$$\frac{C_{d,p,i}}{C_{d,p,i-1}} = \frac{Q_{n,s}}{(Q_{e,s} + Q_{r,s})} \tag{4.12}$$

The value of $\frac{Q_{n,s}}{(Q_{e,s}+Q_{r,s})}$ is a constant, equal to 1.0034 in the present study. This value quantifies the increase in concentration of solute in the droplets emitted from the nozzle with each nebulization cycle, due to loss of solvent associated with humidification of the air supplied by the compressor.

When $i = 1$, using Equations (4.8), (4.9), and (4.11), one finds that

$$C_{d,p,1} = \frac{Q_{n,s}}{(Q_{e,s} + Q_{r,s})} C_{p,0} \tag{4.13}$$

For $i = 2$, Equation (4.12) gives

$$C_{d,p,2} = \frac{Q_{n,s}}{(Q_{e,s}+Q_{r,s})} C_{d,p,1} \tag{4.14}$$

Combining Equations (4.13) and (4.14), one finds that

$$C_{d,p,2} = \left(\frac{Q_{n,s}}{Q_{e,s} + Q_{r,s}}\right)^2 C_{p,0} \tag{4.15}$$

One can continue to show that in general

$$C_{d,p,i} = \left(\frac{Q_{n,s}}{Q_{e,s} + Q_{r,s}}\right)^{i} C_{p,0} \tag{4.16}$$

This equation demonstrates how the solute concentration in the droplets of a specific nebulization cycle, i, is related to the initial solute concentration in the reservoir.

In order to estimate the number of phage exiting the mouthpiece in a specific nebulization cycle, volumes are evaluated for each nebulization cycle. The volume returned to the nebulizer, $V_{r,s}$, in a specific cycle is equal to the volume exiting the nozzle, $V_{n,s}$, in the following cycle:

$$V_{n,s,i} = V_{r,s,i-1} \tag{4.17}$$

Equation (4.17) is valid for $i = 2 \rightarrow N$. For $i = 1$, the volume exiting the nozzle is assumed to be equal to the fill volume, V_F:

$$V_{n,s,1} = V_F \tag{4.18}$$

The time for a nebulization cycle to complete, t_i, is specified by

$$t_i = \frac{V_{n,s,i}}{Q_{n,s}} \tag{4.19}$$

The following volumes can then be obtained using t_i and the known flow rates:

$$V_{h,s,i} = Q_{h,s} \times t_i \tag{4.20}$$

$$V_{e,s,i} = Q_{e,s} \times t_i \tag{4.21}$$

$$V_{r,s,i} = Q_{r,s} \times t_i \tag{4.22}$$

where $V_{h,s,i}$ is the equivalent liquid volume exiting the device due to humification in a specific nebulization cycle, $V_{e,s,i}$ is the volume exiting the mouthpiece of the device as droplets in a specific nebulization cycle, and $V_{r,s,i}$ is the volume returned to the reservoir in a specific nebulization cycle.

The number of phage, either active or inactive, exiting the mouthpiece in a specific nebulization cycle, $n_{e,p,i}$, can be found according to

$$n_{e,p,i} = \frac{C_{d,p,i} \times V_{e,s,i}}{m_{1p}} \tag{4.23}$$

where m_{1p} is the mass of a single phage.

Similarly, the number of phage initially in the reservoir is

$$n_{p,0} = \frac{C_{p,0} \times V_F}{m_{1p}} \tag{4.24}$$

The fraction of the number of phage initially input to the reservoir that has exited the mouthpiece in a specific nebulization cycle, $f_{e,i}$, can therefore be found using Equations (4.16), (4.23), and (4.24), as

$$f_{e,i} = \frac{n_{e,p,i}}{n_{p,0}} = \left(\frac{Q_{n,s}}{Q_{e,s} + Q_{r,s}}\right)^i \times \frac{V_{e,s,i}}{V_F} \tag{4.25}$$

The fraction of the number of phage initially input to the reservoir that have cumulatively exited the mouthpiece of the device over i nebulization cycles, $Cu(f_{e,i})$, is given by

$$Cu(f_{e,i}) = \sum_{j=1}^{j=i} f_{e,j} \tag{4.26}$$

where j is a summation index. To solve Equation (4.26), for example, when $i = 3$,

$$\begin{aligned} Cu(f_{e,3}) = \sum_{j=1}^{j=3} f_{e,j} &= f_{e,1} + f_{e,2} + f_{e,3} \\ &= \left(\frac{Q_{n,s}}{Q_{e,s} + Q_{r,s}}\right)^1 \times \frac{V_{e,s,1}}{V_F} + \left(\frac{Q_{n,s}}{Q_{e,s} + Q_{r,s}}\right)^2 \times \frac{V_{e,s,2}}{V_F} \\ &\quad + \left(\frac{Q_{n,s}}{Q_{e,s} + Q_{r,s}}\right)^3 \times \frac{V_{e,s,3}}{V_F} \end{aligned} \tag{4.27}$$

A curve of was generated for the solution to Equation (4.26) for every i from $i = 1$ to $i = N$, where N represents the number of nebulization cycles when $V_{r,s,i}$ is equal to the residual volume of the

nebulizer after aerosolization is complete, which was experimentally determined to be 0.5 mL during phage measurements in this study. The fraction was converted to a percentage for the plot.

The average number of nebulization cycles phage that exited the mouthpiece underwent. To determine this value, one must consider that some phage are left in the residual volume of the nebulizer after aerosolization is complete.

The fraction of the cumulative number of phage that have exited the mouthpiece after N nebulization cycles, that exited the mouthpiece in the specific nebulization cycle i, is termed X_i, and is given by:

$$X_i = \frac{n_{e,p,i}}{\sum_{k=1}^{k=N} n_{e,p,k}} = \frac{n_{e,p,i}}{n_{e,p,1} + n_{e,p,2} + \cdots + n_{e,p,N}} \tag{4.28}$$

where k is a summation index.

It can be shown that the average number of nebulization cycles phage underwent prior to exiting the mouthpiece of the jet nebulizer, $Cu(i * X_i)$, is given by

$$Cu(i \times X_i) = \sum_{L=1}^{L=N} (L \times X_L) = (1 \times X_1) + (2 \times X_2) + \cdots + (N \times X_N) \tag{4.29}$$

where L is a summation index.

Other parameters such as total nebulization time and total volumes lost to humidification and exiting the mouthpiece can also be obtained using summations from 1 to N. Further outputs of the mathematical modelling are detailed in Appendix C.

4.4.6 Active Phage Delivery Rate

The number of active phage delivered per minute is of interest for inhalation studies with nebulizers, since long exposure times may not be practical and phage clearance may be relatively quick. Time-averaged aerosol production rate was determined for the vibrating mesh nebulizer using the time required to deplete the entire fill volume, as the residual volume was negligible. For the jet nebulizer, humidification of the air supplied by the compressor results in loss of solvent mass, and the residual volume was 0.5 mL; thus, the aerosol production rate was determined using both the mass captured on a filter during aerosolization titer reduction experiments and the time

over which the nebulization occurred. The active phage delivery rate for each nebulizer was calculated using the output titer and the measured aerosol production rates.

For the soft mist inhaler, the number of active phage delivered per actuation is a more relevant delivery parameter than the number of active phage delivered per minute. The number of active phage delivered per actuation from the soft mist inhaler was calculated using the gravimetrically measured emitted dose of aerosol and the measured output titer.

4.4.7 Statistics

Results are presented as mean ± standard deviation using results where plates had ≥ 5 plaques per plate. The number of plates used to calculate mean and standard deviation ranged from 2-8. Statistical comparisons utilized the Student's t-test without assuming equal variance, at a significance level of 0.05.

4.5 Results

4.5.1 Dilution Stability

The stability of phage D29 diluted in isotonic saline was measured (Table 4.1) for well over the maximum expected timeframe of an aerosolization experiment (50 minutes) to determine whether the dilution step would cause unexpected titer reduction during experimentation. Titer immediately after 1:100 dilution was 9.9 ± 0.1 $\log_{10}$(pfu/mL), which was not significantly different ($p > 0.1$) from the expected 9.8 ± 0.3 $\log_{10}$(pfu/mL), indicating the dilution itself did not lead to unexpected titer reduction in a Falcon tube. Furthermore, the titer of the saline phage preparation was not significantly different from the expected value ($p > 0.1$) after 18 hours at room temperature. There was also no indication of phage binding to the filter ($p > 0.1$). These results indicated that the test method itself was not a cause of significant titer reduction.

Table 4.1: Stability of phage D29 lysate at various time points after 1:100 dilution in isotonic saline in a 15mL Falcon tube, and after dilution and 50 minutes storage in a filter. All measurements were at room temperature. For no time point was titer after dilution significantly different from the expected 9.8 ± 0.3 $\log_{10}$(pfu/mL) ($p > 0.1$).

Test	**Time [min]**	**Titer [($\log_{10}$(pfu/mL)]**
Pre-Dilution	-	11.8 ± 0.3
1:100 Dilution - Tube	0	9.9 ± 0.1
	90	10.0 ± 0.4
	1080	9.6 ± 0.2
1:100 Dilution - Filter	50	9.4 ± 0.6

Plaque assays on the diluted saline phage preparation kept in a Falcon tube were also performed after each aerosolization experiment (termed input titer). In each case, an input titer > 9 $\log_{10}$(pfu/mL) was observed, further verifying the stability of D29 after dilution in isotonic saline at room temperature.

4.5.2 Aerosolization Titer Reduction

The input titers for the vibrating mesh nebulizer, jet nebulizer, and soft mist inhaler were respectively $2.3\text{x}10^9 \pm 0.4\text{x}10^9$, $2.4\text{x}10^9 \pm 0.3\text{x}10^9$, and $1.4\text{x}10^9 \pm 0.5\text{x}10^9$ pfu/mL, which were not significantly different from each other ($p > 0.1$). The respective output titers were $9.0\text{x}10^8 \pm 2.0\text{x}10^8$, $4.4\text{x}10^5 \pm 1.1\text{x}10^5$, and $4.0\text{x}10^8 \pm 1.6\text{x}10^8$ pfu/mL. The percent deactivation due to aerosolization was thus 60 ± 11 %, 99.981 ± 0.005 %, and 72 ± 14 % for the respective inhalation devices. Figure 4.3 illustrates the titer reduction, calculated as the $\log_{10}$ of input titer per mL minus the $\log_{10}$ of output titer per mL, for each inhalation device.

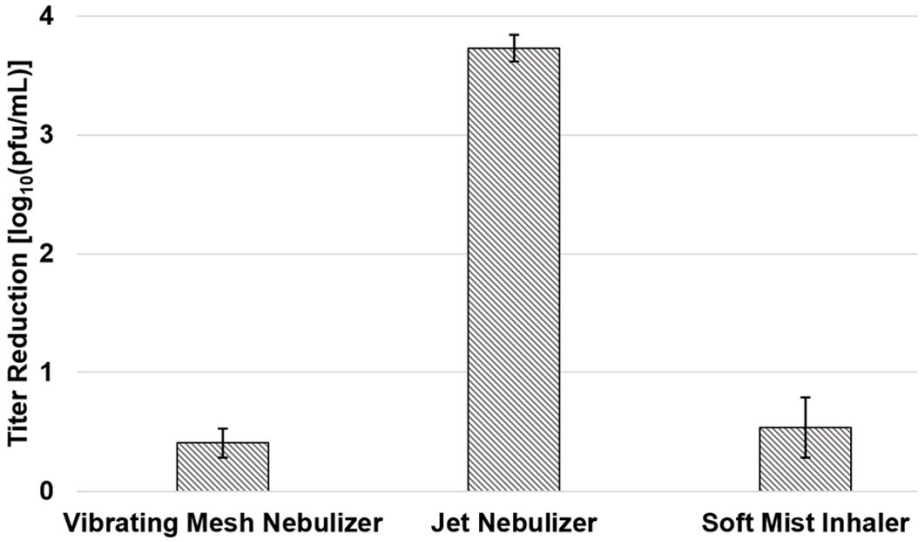

Figure 4.3: Titer reduction of phage D29 due to aerosolization with each inhalation device.

Titer reduction due to aerosolization was ~0.5 $\log_{10}$(pfu/mL) for both the vibrating mesh nebulizer and the soft mist inhaler. There was no significant difference in titer reduction between these two devices ($p > 0.1$). Titer reduction was significantly greater for the jet nebulizer than for either the soft mist inhaler or the vibrating mesh nebulizer ($p < 0.0005$).

4.5.3 Nebulization Cycle Count

The jet nebulizer is designed so that droplets which impact and spread on the baffles and nebulizer walls, being unable to return to the airflow, are returned (drip back) to the reservoir for renebulization [472]. The flow rate of droplets exiting the mouthpiece of the jet nebulizer was 0.122 ± 0.003 mL/min, while the flow rate of primary droplets exiting the nozzle was 17.6 ± 8.1 mL/min. These values were used in the mathematical model provided in the Appendix to calculate the cumulative percentage of phage (both active and inactive) that exited the mouthpiece of the jet nebulizer after each nebulization cycle, relative to the initial number of phage in the reservoir. The result is given in Figure 4.4, along with the average number of times phage (regardless of being active or inactive) were nebulized, i.e. exited the nozzle and impacted the primary baffle, prior to exiting the mouthpiece of the jet nebulizer. The results indicate that phage were exposed to the stresses of liquid breakup with a high-speed nozzle and impaction on the primary baffle an average of 96 times before exiting the mouthpiece. The predicted maximum number of nebulizations was 269, for the last phage exiting the mouthpiece and those remaining in the residual volume.

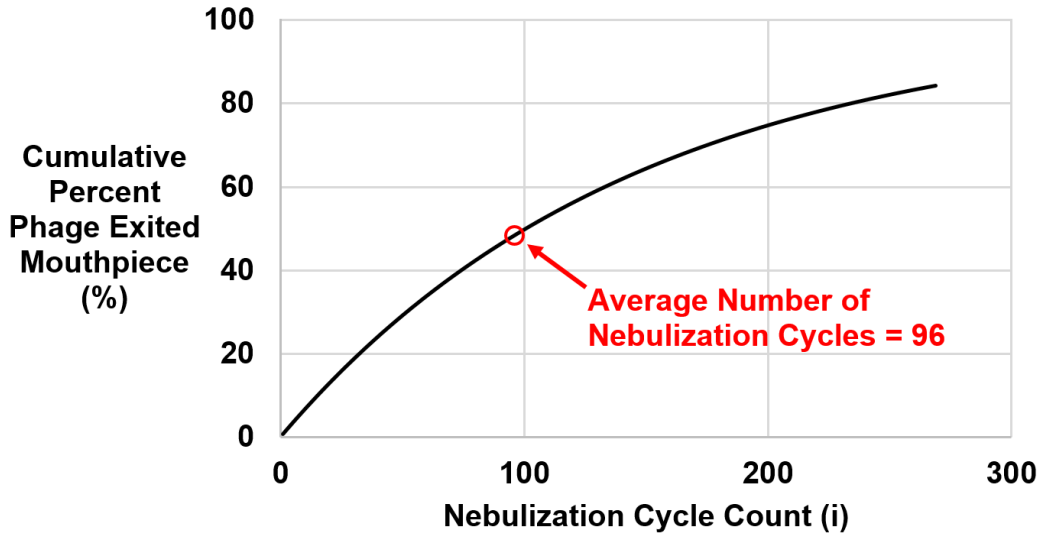

Figure 4.4: Cumulative percent of initial number of phage in the reservoir that has exited the mouthpiece of the jet nebulizer, regardless of being active or inactive, for each nebulization cycle count, which is noted as i in the Appendix. Due to the residual volume, not all phage exited the mouthpiece. The average number of nebulization cycles the phage which exited the mouthpiece underwent is also indicated.

4.5.4 Active Phage Delivery Rate

Table 4.2 indicates the aerosol production rate and the number of active phage delivered per minute by the vibrating mesh nebulizer and by the jet nebulizer, as well as the number of active phage delivered per actuation by the soft mist inhaler.

Table 4.2: Aerosol production rate and active phage delivery rate for each inhalation device. The loaded dose was $1.36x10^{10} \pm 0.21x10^{10}$ pfu for the vibrating mesh nebulizer and $1.89x10^{10} \pm 0.25x10^{10}$ pfu for the jet nebulizer. Delivered dose was $5.40x10^{9} \pm 1.20x10^{9}$ pfu for the vibrating mesh nebulizer and $2.21x10^{6} \pm 0.55x10^{6}$ pfu for the jet nebulizer. Delivered dose as a percent of loaded dose was 39.7 ± 10.8 % for the vibrating mesh nebulizer and 0.0117 ± 0.0033 % for the jet nebulizer. Nebulization times were 17 min for the vibrating mesh nebulizer and 42 min for the jet nebulizer.

Inhalation Device Type	**Aerosol Production Rate**	**Active Phage Delivery Rate**
Vibrating mesh nebulizer	0.364 ± 0.025 mL/min	$3.3x10^{8} \pm 0.8x10^{8}$ pfu/min
Jet nebulizer	0.122 ± 0.003 mL/min	$5.4x10^{4} \pm 1.3x10^{4}$ pfu/min
Soft mist inhaler	11.6 ± 1.6 µL/actuation	$4.6x10^{6} \pm 2.0x10^{6}$ pfu/actuation

Calculation shows the vibrating mesh nebulizer delivered active phage D29 ~6000 times faster than the jet nebulizer, which was statistically significant ($p < 0.01$). The more rapid active phage delivery rate is due mainly to the large titer reduction associated with the jet nebulizer, rather than to the difference in aerosol production rate. Calculation also shows that a single 11.6 µL ex-actuator dose from the soft mist inhaler, which lasts approximately 1.2 seconds [471], could deliver about as many active phage D29 as 1.5 hours of delivery with the jet nebulizer, which would require about 15 mL of the same formulation.

4.6 Discussion

Less than 1 $\log_{10}$(pfu/mL) titer reduction has been regarded in the literature as acceptable for nebulizing phage [453]. By this criterion, saline phage D29 preparation had an acceptable titer reduction when aerosolized with the vibrating mesh nebulizer, which uses the droplet production mechanism shown in Figure 4.5. Briefly, this device operates by the converse piezoelectric effect, wherein an applied voltage causes a fluctuating change in volume of a piezoceramic ring element. This element is connected via a metal washer to a 5 mm diameter aperture plate, perforated with 1000 precision-formed holes, vibrating it at ~128 kHz [473]. The vibration consists of ~1 µm vertical displacement of the aperture plate, which extrudes formulation through the ~3 µm orifices

in a micropump action [473] in what was found to be a relatively gentle process for phage D29. The quick delivery of large numbers of active phage with this device may make it particularly useful for animal studies as a high MOI may be achievable; additionally, it can be adapted to operate continuously with a syringe pump to potentially allow for hours of treatment with a high active phage delivery rate. Further methods to decrease titer reduction due to aerosolization using surfactants or other excipients have been proposed [455]; however, these excipients can complicate toxicology testing.

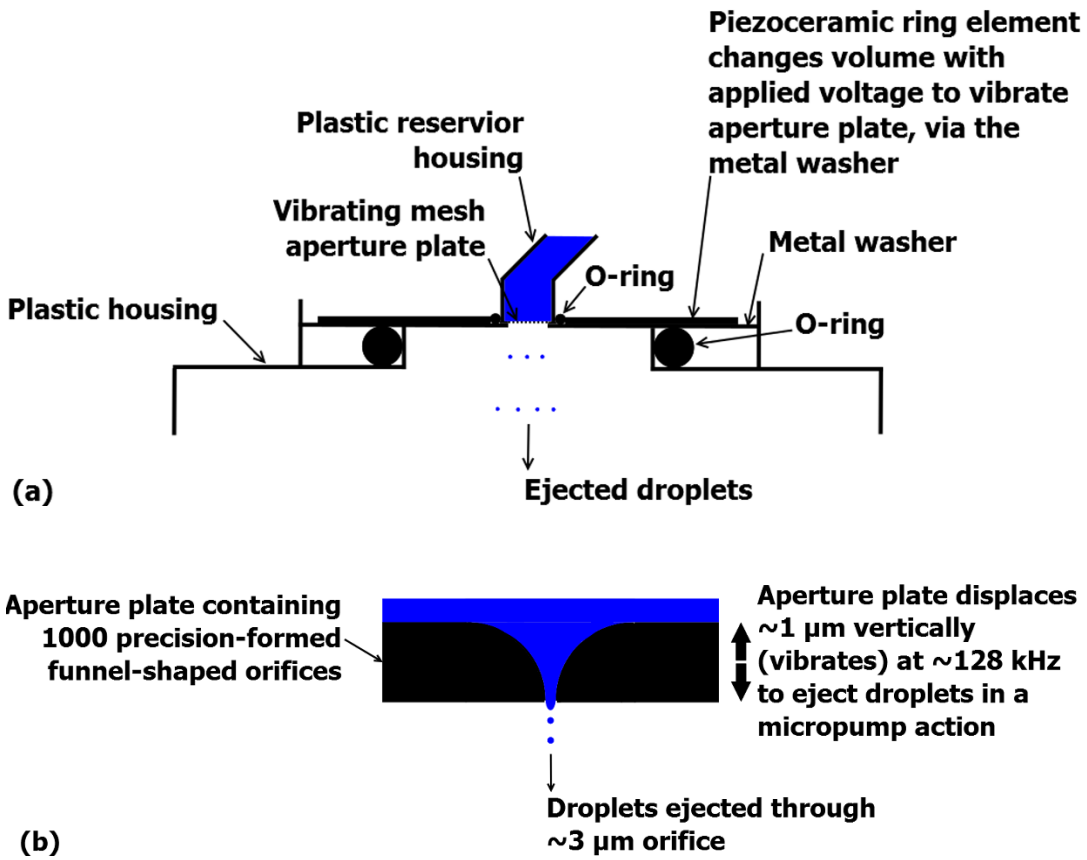

Figure 4.5: Vibrating mesh nebulizer droplet production mechanism: (a) the structure surrounding the aperture plate (b) close-up of a funnel-shaped orifice in the aperture plate illustrating the micropump action, which ejects droplets. This droplet production mechanism was found to be relatively undamaging to phage D29. Not to scale.

Saline phage D29 preparation also had acceptable titer reduction when aerosolized with the soft mist inhaler. Relevant components of this device are shown in Figure 4.6. Briefly, when the base of this device is turned 180 degrees, a helical cam gear compresses a spring and lowers the capillary

tube (which contains a one-way valve allowing liquid to travel only towards the nozzle) relative to the dosing chamber [471], drawing a pre-defined amount of liquid into the dosing chamber. When the dose-release button is pressed the spring releases, causing the capillary tube and one-way valve to move towards the nozzle outlet, thereby developing enough pressure downstream of the one-way valve to force the liquid through the pre-filter structure and nozzle outlet, where it collides in two small jets at an optimized angle to form a slowly moving aerosol [471]. The stresses acting on the phage in this device include pressure and shear. Hoe *et al*. [455] observed less than 1 $\log_{10}$ titer reduction after actuation of phage using a pressurized metered-dose inhaler, indicating their phage could survive relatively high levels of pressure and shear stress. This is in accord with the present study, where pressure and shear during soft mist inhaler actuation were relatively unharmful to phage D29. Were the soft mist inhaler used without dilution, two orders of magnitude more active phage could potentially be delivered per actuation (~5 x 10^8 pfu per actuation). In addition, this device is compact and lightweight, features that may make it an attractive option for self-administration of phage aerosol.

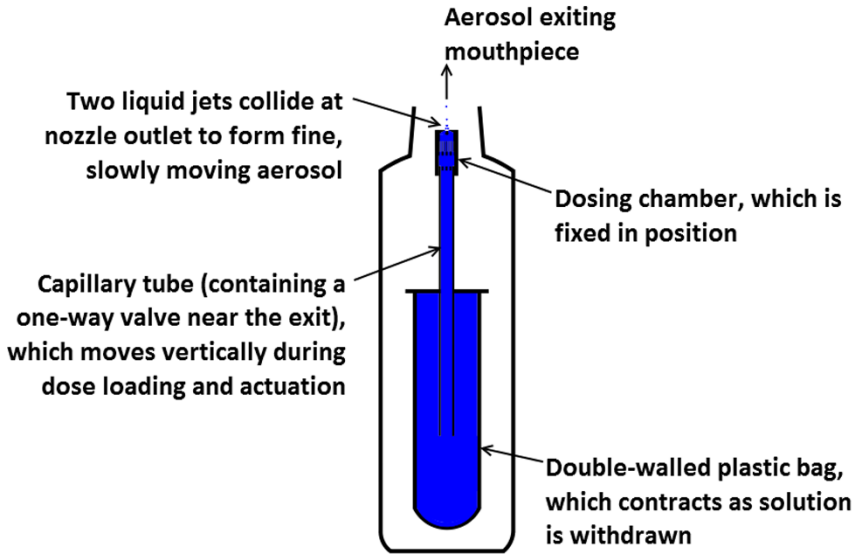

Figure 4.6: Schematic of the soft mist inhaler. Shear and pressurization can occur throughout the device but these were relatively undamaging to phage D29. Not to scale.

In contrast to the other two inhalation devices, an unacceptably large titer reduction of ~3.7 $\log_{10}$(pfu/mL) occurred with the jet nebulizer. The mechanics of this device are described by Finlay [472]; see Figure 4.2 for a diagram. Briefly, a pressurized air supply flows over a short section of liquid drawn up through a liquid feed tube by the low pressure at the orifice, through which gas

accelerates. Downstream of the orifice the air jet travels at a higher relative velocity than the forming sheath of liquid formulation, which is subjected to the nonlinear development of unstable waves caused by the discontinuity of viscosity at the air-liquid interface. Primary droplets are produced by disintegration of the liquid sheath at the resonant wave crests, or other mechanisms. These larger primary droplets, which exit the nozzle, are then thought to break up into smaller droplets through impaction on the primary baffle, rather than through aerodynamic forces. These smaller droplets attain a velocity away from the primary baffle and head towards the mouthpiece. Some droplets further impact on secondary baffles or nebulizer walls and are returned to the reservoir for renebulization. Calculations using the results of tracer assay measurement show that in each cycle approximately 99% of the aerosol was renebulized, with an equivalent of the entire 8 mL fill volume being recirculated approximately every 30 seconds. These values agree with literature for the Collison triple-head jet nebulizer, for which 99.92% of aerosol exiting the nozzle was renebulized, with an equivalent of the entire 20 mL fill volume being recirculated every 6 seconds [474].

In the present study, the first 10.5% of phage D29 in the reservoir that exited the mouthpiece of the jet nebulizer had undergone only 1-17 nebulization cycles but already had greater than 3 $\log_{10}$(pfu/mL) titer reduction. Thus, even relatively few nebulizations were damaging to most phage D29 within the preparation. It was suspected that large hydrodynamic stresses occurring during the baffle impaction primary droplet breakup process were responsible for the deactivation of liposomes and large molecules undergoing jet nebulization [472,475]. These stresses could also be the cause of phage titer reduction in this study. A low recovery rate has also been noted by Liu *et al.* [476] for D29 delivered with a Collison jet nebulizer.

Comparing the titer reduction resulting from aerosolization in this study and in the literature indicates that it is device-dependent and phage strain-dependent. For example, Golshahi *et al.* [456] observed that *Myoviridae* phage KS4-M readily survived aerosolization with a jet nebulizer (Pari LC Star) and a vibrating mesh nebulizer (Pari eFlow), while Sahota *et al.* [466] found recovery of relatively fewer viable phage on an impactor for *Myoviridae* phage PELP20 using the Omron vibrating mesh nebulizer (~2 $\log_{10}$(pfu) reduction) than they did using the AeroEclipse jet nebulizer (~1 $\log_{10}$(pfu) reduction). These findings contrast with the present results, where the vibrating mesh nebulizer was less harmful to *Siphoviridae* phage D29 than the jet nebulizer. Sahota

et al. [466] also noted lower titer recovery for *Myoviridae* phage PELI40 than for phage PELP20 with the jet nebulizer. Thus, given the present limited amount of data available in the literature, experimentally testing specific phage strains with specific inhalation devices is still necessary to determine the titer reduction due to aerosolization that will result, with ad-hoc predictions not advisable for new phage strains.

One direction that can be taken is to predict stress levels within prospective inhalation devices using a combination of experimental work, analytical modelling, and computational fluid dynamics [477]. The expected titer reduction could then be estimated from a titer reduction – stress level relationship generated from experiments designed to measure titer reduction after exposure of phage to controlled stress levels. The devices could then be redesigned to minimize the stresses causing deactivation. However, testing different types of inhalation devices with a specific phage strain intended for a cocktail is still desirable in the development of inhalation device – phage cocktail combinations. Phage strains that may be useful in the development of an anti-TB phage cocktail are discussed elsewhere [450].

The respirable active phage delivery rate for the present inhalation devices can be calculated as the product of fine particle fraction, active phage delivery rate, and, for the nebulizers, the fraction of a breathing cycle spent inhaling. Using a fine particle fraction of 56% for the vibrating mesh and jet nebulizers [478-479] and 69% for the soft mist inhaler [480], the active phage delivery rates given in Table 4.2, and a fraction of the breathing cycle spent inhaling relevant for an adult male, 43.5% [472], the respirable active phage delivery rate was calculated to be 8.0×10^7 pfu/min for the vibrating mesh nebulizer, 1.3×10^4 pfu/min for the jet nebulizer, and 3.2×10^6 pfu/actuation for the soft mist inhaler. The total respirable dose of active phage was 1.3×10^9 pfu for the vibrating mesh nebulizer and 5.4×10^5 pfu for the jet nebulizer. Some additional losses of phage due to extrathoracic deposition of fine particles can be expected to occur [472, 481].

The respirable dose of phage required to treat TB infection is not yet established. While Semler *et al.* [463] noted that successful treatment of antibiotic-resistant *Burkholderia cepacia complex* in mice required an MOI greater than 10 for treatment success, this bacteria group behaves differently in the lungs than TB, and therefore this MOI value is not expected to be directly relevant to D29. After entering the alveoli, TB bacteria are quickly engulfed by macrophages into phagosomes, where they may slow phagolysosome formation and survive the acidic phagolysosome

compartments which do form [482]. Xiong *et al.* [483] showed that the titer of D29 is higher after uptake in TB-infected macrophages than after uptake in uninfected macrophages, indicating that intracellular D29 replication may occur. Much titer reduction, however, occurred prior to D29 infecting TB, attributed to the acidic macrophage environment [483]. Basra [484] studied the stability of D29 at different temperatures and pH. Approximately 2 $\log_{10}$(pfu/mL) titer reduction was observed at pH 5 after 1 hour [484], which supports the hypothesis that the acidic environment in the macrophage can decrease the phage titer, although other digestive mechanisms occurring in the macrophage could also have led to the titer reduction. To counter this titer reduction and increase the chances that active phage infects TB within the macrophages, Xiong *et al.* [483] suggested repeated phage administration regimes. Other alternatives may involve encapsulation of phage and buffer in liposomes, which release these contents in the macrophage, or dry powder encapsulation of phage and buffer nanoparticles.

Prophylactic administration of D29 has also been proposed [450]. Were D29 to line the alveoli just prior to TB infection, it would have the opportunity to infect TB before macrophage uptake. The D29 progeny released upon lysis of the TB in the alveoli would offer further protection against additional TB entering the alveoli soon after. Alternatively, therapeutic treatment of TB after granuloma formation would likely require additional vectors.

For infections generating biofilms, phage therapy may require additional interventions. Darch *et al.* [485] showed that the use of a two-phage cocktail, which lysed planktonic *Pseudomonas aeruginosa* culture, did not remove all biofilm aggregates in synthetic sputum. On the other hand, some lytic phage can naturally penetrate biofilms by expressing depolymerases, which can also be applied exogenously [486-487]. Screening for host susceptibility and depolymerase effectiveness using a bank of phage may be required [487-488]. Phage can also be engineered to release biofilm-degrading substances upon cell lysis [488]. Additionally, D-amino acids can degrade certain biofilms [489] and have been spray dried in phage formulations with acceptable processing titer reduction [455].

Animal studies to demonstrate the feasibility of treating specific lung infections using phage should be performed prior to aerosol phage therapy in humans. When designing animal studies, it is important to consider differences in extrathoracic deposition with particle size between animals and humans; for example, much smaller particles are required to bypass the extrathoracic region

and reach the lungs of mice than of humans [481,490]. An additional factor to consider when determining the dose to nebulize is the loss of active phage due to aerosol deposition within the delivery interface. For example, aerosol deposition within a nose-only inhalation device has been shown to be substantial [490], and deposition occurs within the chamber and upon the exterior of animals in a whole-body aerosol exposure system. The use of a delivery interface optimized for use with a vibrating mesh nebulizer could result in a higher titer being inhaled by the animal than were a jet nebulizer used, thus improving the chance of successful treatment outcomes.

4.7 Conclusions

Pulmonary delivery of phage formulations at high titers requires a prudent choice of inhalation device. Based on data presented here, the vibrating mesh nebulizer is the recommended choice for delivering anti-TB phage D29 in animal studies, as there was a high active phage delivery rate with only a small reduction in titer due to aerosolization. In contrast, the jet nebulizer does not appear to be a good choice for D29 phage therapy because of substantial titer reduction, likely caused by stress associated with droplet production and renebulization processes. The soft mist inhaler can deliver phage D29 at high titers quickly and conveniently and, being pocket-sized, may prove useful for self-administered phage therapy applications. Titer reduction is inhalation device- and phage strain-dependent; thus, the survival of individual phage strains within a cocktail should be tested with different delivery devices while developing phage cocktail – inhalation device combinations.

5 Prophylaxis of *Mycobacterium tuberculosis* H37Rv Infection in a Preclinical Mouse Model via Inhalation of Nebulized Bacteriophage D29

This chapter has been submitted as a journal paper "Carrigy NB, Larsen SE, Reese V, Pecor T, Harrison M, Kuehl PJ, Hatfull GF, Sauvageau D, Finlay WH, Coler RN, Vehring R. Prophylaxis of Mycobacterium tuberculosis H37Rv infection in a preclinical mouse model via inhalation of nebulized bacteriophage D29. Antimicrobial Agents and Chemotherapy. Submitted April 26, 2019." Additional material is given in Appendix D.

5.1 Abstract

Globally, more people die annually from tuberculosis than from any other single infectious agent. Unfortunately, there is no commercially-available vaccine that is sufficiently effective at preventing the contraction of pulmonary tuberculosis in adults. In this study, pre-exposure prophylactic pulmonary delivery of active aerosolized anti-tuberculosis bacteriophage D29 was evaluated as an option for protection against *Mycobacterium tuberculosis* infection. An average bacteriophage concentration of approximately 1 PFU/alveolus was achieved in the lungs of mice using a nose-only inhalation device optimized using a dose simulation technique and adapted for use with a vibrating mesh nebulizer. Within 30 minutes of bacteriophage delivery, the mice received either a low dose (~50-100 CFU), or an ultra-low dose (~5-10 CFU), of *M. tuberculosis* H37Rv aerosol to the lungs. A prophylactic effect was observed with bacteriophage aerosol pre-treatment significantly decreasing *M. tuberculosis* burden in mouse lungs 24 hours and 3 weeks post-challenge ($p < 0.05$). These novel results indicate that a sufficient dose of nebulized mycobacteriophage aerosol to the lungs may be a valuable intervention to provide extra protection to health care professionals and other individuals at risk of exposure to tuberculosis.

5.2 Introduction

The World Health Organization (WHO) has identified intracellular bacterium *Mycobacterium tuberculosis* (*Mtb*) as the leading infectious killer globally for a fourth consecutive year [491]. Aside from being a significant co-morbidity in human immunodeficiency virus (HIV)-positive individuals, in both 2016 and 2017 tuberculosis (TB) was the cause of death for 1.3 million HIV-negative individuals [491]. Not only do low-income countries continue to suffer from endemic

TB, but so do some populations in developed countries such as Indigenous peoples in Nunavut, Canada [492].

The global community is increasingly concerned about the increase of drug-resistant *Mtb* strains. The WHO estimated that, in 2017, roughly 0.5 million *Mtb* infected individuals developed rifampicin resistance and over 80% of those cases were considered multidrug-resistant [491]. As global treatment success for drug-resistant *Mtb* cases remains dismally low - at roughly 55% -, alternative interventions that block transmission and subsequent new infections are urgently needed [491]. Vaccines against *Mtb* are an active area of research [491,493-496], and indeed much of the global community receives bacille Calmette–Guérin (BCG) vaccination against TB as youth. BCG and other vaccine candidates can induce limited prophylactic protection through adolescence [497]; however, BCG provides limited-to-no prophylactic effect if given to adults, does not prevent reactivation of latent tuberculosis, and does not prevent *Mtb* transmission [498-499]. Indeed, there is no vaccine that effectively prevents contraction of TB in adults [491]. The lengthy, complex, multidrug treatment regimens available to target active TB often result in poor side-effects for patients. This limits compliance and perpetuates the development of drug resistance.

Epidemiologic vulnerability correlates of TB disease include inhaled dose, which largely correlates with proximity to an active case or intensity of exposure over time. This is evidenced in highly-exposed health care workers who have a 2-4 fold higher infection risk compared to medical students with low exposure [500]. Indeed, many studies document the increased risk to health care workers [501-502] and additional interventions for this high-risk population are needed. Bacteriophage (phage) delivery may be leveraged as an adjunct to current preventative strategies, which include personal protective equipment, administrative and environmental controls [503-504], for health care professionals who are regularly exposed to infectious active cases of TB.

Phages are diverse viruses that have co-evolved with bacteria and represent the most common biologic on earth [505]. Phage strains are host- and receptor-restricted and therefore only capable of infecting a narrow-spectrum of bacteria, which notably results in minimal harm to host microbiomes such as gut flora [506]. Furthermore, antibiotic-resistance does not influence bacterial susceptibility to phage lysis [506], making phages an attractive tool against drug-resistance. Phages that kill their target host bacteria via cell lysis (lytic phage) are commonly identified through genome sequencing [507]. The lytic cycle comprises injection of DNA into the

cell, phage replication, and lysis of the cell wall to release the progeny. Lytic phage therapy is considered safe and regularly utilized clinically in Eastern Europe, where some phage cocktails are available without prescription [508]. Indeed, studies have repeatedly demonstrated that phages are not inherently harmful to humans [509].

Phage therapy is a viable option for compassionate use in the United States, with a recent study demonstrating successful treatment of a patient with disseminated multidrug-resistant *Acinetobacter baumannii* infection [510]. In the United Kingdom, a cystic fibrosis patient with disseminated *Mycobacterium abscessus* recently showed objective clinical improvement with intravenous three-phage cocktail treatment [511]. Clinical studies investigating pulmonary phage delivery generally report positive efficacy as well [508,512]. Accordingly, advanced research of aerosol phage therapy has become prevalent, including *in vitro* studies evaluating phage delivery with nebulizers, dry powder inhalers, and pressurized metered-dose inhalers [513-521]. As more than 80% of TB cases originate from *Mtb* infections in the lungs, aerosol delivery of phage may be an ideal mechanism for enabling activity at the primary site of *Mtb* infection [522]. Note that phage aerosol delivery without the use of additional vectors is unlikely to have efficacy against *Mtb* already harboured within a granuloma; even phage infection of *Mtb* within a macrophage, the primary target cell of *Mtb*, has low efficiency [523]. However, prophylactic delivery of phages to the alveoli may allow the phage to infect the mycobacteria before macrophage uptake [507,517,524]. Since the lungs contain millions of alveoli, a high dose of active phage is likely required for prophylaxis. Of particular interest for prophylactic protection against TB is *Siphoviradae* mycobacteriophage D29 (Figure 5.1), which can effectively infect and lyse a range of mycobacteria, including *Mtb* [525].

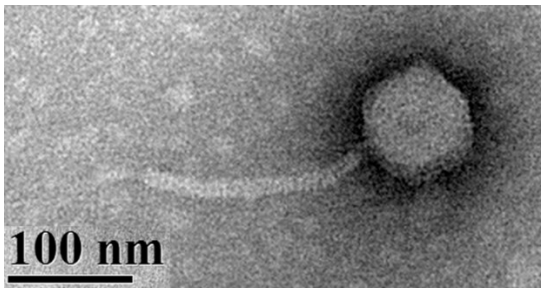

Figure 5.1: Transmission electron micrograph of phage D29. The icosahedral capsid contains double-stranded DNA. The tail is flexible and does not contract during infection. The method for imaging is described in Chapter 4.

Before testing the efficacy of phage D29 aerosol in humans, animal studies are of interest. Laboratory mice, commonly used for studying drug efficacy, have the advantages of low cost, short growth time, and small size, allowing for many mice to be tested simultaneously [526]. Different methods for delivering aerosol to mice include a nose-only inhalation device (NOID), whole-body exposure system, nose-drip, and intranasal or intratracheal instillation. Use of a NOID is the most common exposure method for rodents as it allows for a uniform distribution of aerosol in the lungs via the nasal inhalation route, which is applicable to rodents as they are obligate nasal breathers [527-529]. Whole-body exposure systems require larger doses as they are inefficient and cause aerosol deposition on the body of the mouse [526,528,530]. Nose-drip methods do not simulate natural aerosol inhalation and have variable inhaled droplet size. Instillation leads to non-uniform, patchy deposition, primarily near the site of instillation, and little or no alveolar deposition [527]. Furthermore, inhalation methods are preferable to injection as the aerosol is delivered directly to the site of infection, the lungs, and hence is available there at higher concentrations [531]. Semler et al. [532] demonstrated that phage aerosol delivery by inhalation with a NOID was superior to intraperitoneal delivery, as evidenced by a greater reduction in bacterial burden and phage replication in the lungs.

Effective phage delivery to the lungs requires a prudent choice of aerosol delivery device to avoid phage inactivation (see Chapter 4). Factors that may inactivate phage are thoroughly described elsewhere, and include shear stress, osmotic shock, and thermal stress, among others [533-534]. In Chapter 4, it was demonstrated that use of a vibrating mesh nebulizer afforded less phage D29 inactivation and a greater active phage D29 aerosol delivery rate than use of a jet nebulizer]. However, traditional NOID designs use jet nebulizers and have very low delivery efficiency. An adequate delivery method that allows retention of lytic capacity and ability to deliver high titers of phage are current hurdles to testing prophylactic delivery of phages to the lungs of mice. In this study, a NOID was modified for use with a vibrating mesh nebulizer to deliver high doses of active phage D29 to the lungs of mice.

In order to advance phage D29 as a candidate therapy for TB, we leveraged our well-established mouse model of low dose aerosol challenge of *Mtb.* We hypothesized that sufficient prophylactic pulmonary delivery of phage D29 would reduce *Mtb* bacterial burden 24 hours post-challenge. In order to evaluate our hypothesis, delivery parameters maximizing the inhaled dose in a repeatable

fashion were experimentally simulated and subsequently used throughout the challenge studies. Measurements were then performed to quantify the number of phage reaching the lungs of mice and their clearance kinetics. Finally, phage D29 aerosol was delivered to mice prior to *Mtb* aerosol to evaluate prophylactic protection afforded by this treatment.

5.3 Materials and Methods

5.3.1 Mice

The mice used in this study were female C57BL/6 mice 4-6 weeks of age, weighing 14-16 grams, purchased from Charles River Laboratories (Wilmington, MA, USA). Mice were housed at the Infectious Disease Research Institute (IDRI) biosafety level 3 animal facility under pathogen-free conditions and were handled in accordance with the specific guidelines of IDRI's Institutional Animal Care and Use Committee. The reported minute ventilation rate for CD-1 mice, similar to the C57BL/6 strain used here, was 1.46 mL/gram of body weight [535]. For an average mass of 15 grams, this corresponds to an average minute ventilation of ~22 mL/min per mouse, and this value was used for calculations for nose-only aerosol delivery.

5.3.2 Phage D29 Amplification, Shipping, and Plaque Assay

Phage D29 was prepared to a titer of 1.6×10^{12} PFU/mL via replication with *M. smegmatis* strain mc^2155 using solid media, sterile filtration, centrifugation, and pellet resuspension in buffer, as described elsewhere [https://phagesdb.org/workflow/, 517]. The amplified phage lysate was shipped to IDRI (Seattle, WA, USA) from the University of Alberta (Edmonton, AB, Canada) using cold packs and a Styrofoam container. This shipment did not result in titer reduction of the lysate. The titer of phage D29 was measured using full-plate plaque assay, as described elsewhere [https://phagesdb.org/workflow/, 517].

5.3.3 Lung Homogenization

It was necessary to homogenize the lungs of the mice to generate a representative liquid sample to assay and to determine the number of active phage and bacterial burden in the lungs. To verify the phage remained active after the high-shear homogenization process, a 20-µL sample of phage lysate was spiked in lung tissue within 2 mL of buffer, in a 15-mL Eppendorf tube, homogenized (Omni Prep Multi-Sample Homogenizer, Omni International; Kennesaw, GA, USA) for 1 minute,

and centrifuged for 2 minutes at 1800 rpm. The titer after homogenization was compared to the titer before homogenization to determine if the homogenization process inactivated the phages.

5.3.4 Nose-Only Inhalation Device – Device Design and Dose Simulation vs. In Vivo Experiment

A schematic of the developed NOID, a modified version of the device described by Nadithe et al. [526], set up for dose simulation experiments, is shown in Figure 5.2. Nadithe et al. [526] reported that their NOID design had substantial losses of aerosol. Only 0.108 ± 0.027% of the dose input to the jet nebulizer reached the mice, and only 8.19 ± 3.56% of that amount reached the lungs of the mice. This corresponded to 0.0087 ± 0.0021% (870 ppm) of the input dose reaching the lungs of all 12 mice combined. Much of this loss was attributed to the compressor of the jet nebulizer delivering 4.5 L/min of air flow into the system, resulting in a substantial amount of aerosol convecting by the noses of the mice and exiting the back of the device unused. This is because the combined total minute volume for 12 mice is only 0.264 L/min, and hence about 4.2 L/min of air flow, or 93% of aerosol available at the nosepieces, bypassed the mice. Therefore, in our modified design the minimum air flow rate into the system that could safely be used without developing a hypoxic environment [528], i.e. 0.5 L/min, was used. The negative pressure induced by a vacuum pump (Model UN726FTP, KNF Neuberger, Inc.; Trenton, NJ, USA) past the exit of the device caused the air flow into the NOID. The pressure difference between the front plenum, back plenum, and atmosphere was measured with manometers to rule out leaks in the system. A rotameter (Catalogue No. 5079K63; McMaster-Carr, Elmhurst, Il, USA), calibrated with a thermal mass flow meter (TSI 4043; TSI Incorporated, Shoreview, MN, USA), was used to measure the air flow rate into the NOID, which was controlled with valves past the exit filter and in the rotameter. An inlet air filter (Respirgard II 303; Vital Signs Incorporated, Englewood, CO, USA) prevented foreign virus or bacterial contamination from the air flow into the device.

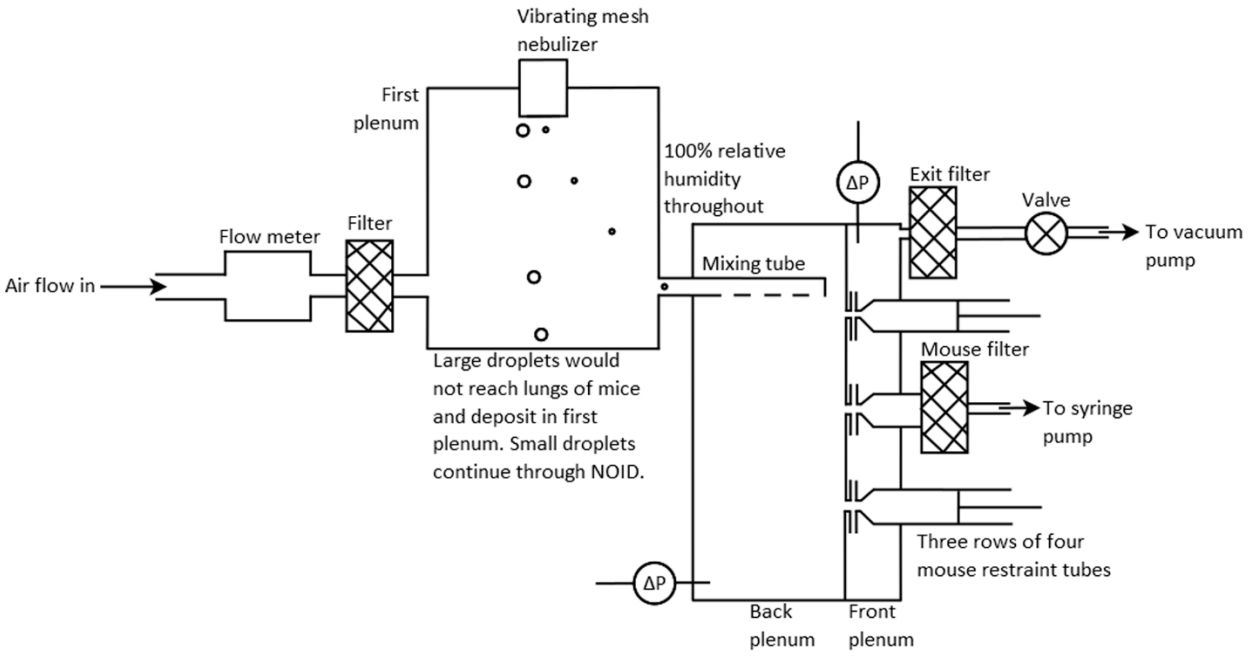

Figure 5.2: Schematic of a modified NOID adapted for use with a vibrating mesh nebulizer.

The NOID was modified to incorporate a vibrating mesh nebulizer (Aerogen Solo with Pro-X Controller; Aerogen Ltd., Dangan, Galway, Ireland) to produce the aerosol. The aerosol entered the first plenum, which was developed as preliminary experiments demonstrated that use of the commercial wye connector for the vibrating mesh nebulizer resulted in a large extent of aerosol recirculation, droplet coalescence, and deposition losses. This is because the small-volume wye connector was designed for use of > 3 L/min air flow rate whereas a lower air flow rate, 0.5 L/min, was used in this study.

The operation of the vibrating mesh nebulizer has been described in Chapter 4. The mesh consists of ~1000 orifices, each with a diameter of ~3 μm. The generated aerosol has been measured at the exit of a T-piece by laser diffraction to have a volume median diameter of ~5.5 μm and geometric standard deviation of ~1.8 [536]. The vibrating mesh nebulizer has a liquid droplet production rate of about 0.36 mL/min (Chapter 4), and hence with the chosen air flow in of 500 mL/min, liquid entered the system at a concentration of 720 g/m^3. Considering that room temperature air can hold ~17.3 g/m^3, the nebulizer produces approximately 42 times the amount of liquid required to fully saturate the air flow in, assuming it is initially dry. Hence, at a maximum, only about 2% of the mass of the droplets, corresponding to about 1% of the diameter assuming sphericity, is required to fully saturate the NOID. Therefore, the droplets essentially maintained their size after

atomization as they transited through the device, neglecting any coalescence. However, mice require small droplets for deposition in the lungs [526,537]. In the present NOID system, the large droplets were filtered out by the first plenum and the smaller droplets produced by the nebulizer, recalling that the geometric standard deviation is ~2, followed the air flow streamlines, due to a lower Stokes number, into the ~12-mm diameter mixing tube. This mixing tube ensured a uniform aerosol concentration entered near the top of the back plenum. Mice inhale through nosepieces attached to mouse restraint tubes, which used an airtight plunger to hold the mice in place with their noses at the noseports. The mice inhaled the aerosol from the back plenum through the noseports, and the excess air flow and exhaled air from the mice entered the front plenum and subsequently were filtered and exited the device.

Before proceeding to *in vivo* experiments, the dose was simulated to verify a biologically-relevant amount of aerosol would reach the lungs of mice. For dose simulation experiments a mouse restraint tube was replaced with a filter and attached to the nosepiece by an adapter, rapid-prototyped out of an acrylic compound (Objet VeroGray RGD850; Eden Prarie, MN, USA) using a PolyJet 3D printer (Objet Eden 350 V High Resolution 3D Printer, Stratsys, Ltd.; Eden Prarie, MN, USA). This filter was termed a mouse filter due to its surrogate mouse function and location within the set-up and was attached to a syringe pump (PHD ULTRA Syringe Pump with Push/Pull Mechanism; Model no. 70-3008; Harvard Apparatus, Hollison MA, USA). The syringe pump initiated a constant flow rate of 22 mL/min through the mouse filter, which is equivalent to the average minute volume for a mouse, as described previously. Only one port was evaluated because previous data with the unmodified NOID demonstrated a reasonably even distribution of aerosol between noseports [526]. Due to the > 10 mL filter dead volume, the steady flow equivalent of tidal flow was used, and the effect of exhalation on lung deposition was neglected. L-Tryptophan (Cat #93659; Sigma Aldrich, St. Louis, MO, USA) tracer in isotonic saline was atomized and captured on the mouse filter, as well as at various points within the NOID (nebulizer reservoir, first plenum, mixing tube, back plenum, nosepiece and adapter, exit filter) to determine where deposition occurred. The tracer concentration was assayed using ultraviolet-visible (UV-Vis) spectrophotometry (8452A Diode Array Spectrophotometer; Hewlett-Packard, Mississauga, ON, Canada). The deposition was quantified for two different versions, where different widths of the developed first plenum were tested: 32 mm and 95 mm. The length of the first plenum was kept fixed at 152 mm and the depth was kept fixed at 211 mm, as this was approximately the distance

at which bulk aerosol flow emitted from the nebulizer stopped after horizontal spray. Three replicate dose simulation experiments were performed for each of the two first plenum widths. As the interior volume of the NOID was ~4 L, the air flow through the system was allowed to continue for ~8 minutes after nebulization was complete to allow time for the aerosol to transit through the system.

A model was developed to predict the average number of active phage per alveolus reaching the lungs of one mouse in the NOID, $T_{\mathrm{m/A}}$, from the tryptophan experiments and literature data, and is given by,

$$T_{\mathrm{m/A}} = \frac{T_0 \cdot f_{\mathrm{n}} \cdot f_{\mathrm{i}} \cdot f_{\mathrm{m}} \cdot f_{\mathrm{l}}}{A_{\mathrm{m}}} \tag{5.1}$$

where T_0 is the initial titer of the lysate input into the vibrating mesh nebulizer in PFU, f_{n} is the fraction of the phage not inactivated by the nebulizer measured in Chapter 4 to be 0.319, f_{i} is the fraction of the breathing cycle spent inhaling approximated as 0.5, f_{m} is the fraction of the aerosol emitted from the nebulizer that is inhaled by a single mouse from tryptophan tracer dose simulation experiments, f_{l} is the fraction of aerosol that is inhaled by a mouse that reaches its lungs taken as 0.08 [526], and A_{m} is the number of alveoli per mouse taken as 4×10^7 [538].

For comparison to dose simulation, phage D29 was delivered to anesthetized mice and the lungs removed and homogenized within 5 mL of buffer. The number of active phage in the homogenate was determined by plaque assay. Three mice were taken down at each of 0, 30, and 90 minutes after phage exposure to obtain a preliminary measure of lung clearance.

5.3.5 Host Susceptibility

Prior to performing *in vivo* experiments it was confirmed that *Mtb* H37Rv is susceptible to phage D29 lysis. A 5 log dilution of phage D29 lysate was added to a sample of *Mtb* H37Rv and subsequently plated on agar plates. The CFU after incubating plates at 37°C and 5% CO_2 for 21 days was evaluated. Plates with or without D29 application were compared.

5.3.6 In Vivo Prophylactic Protection

The mice were acclimatized to remain calm in the restraint tubes of the NOID as per previous methods [537], therefore retaining a normal breathing pattern to maximize peripheral lung

deposition. Within 30 minutes of receiving phage D29 aerosol with the NOID, mice were challenged with *Mtb* H37Rv aerosol using a previously described Wisconsin-Madison aerosol chamber [496,539], calibrated to deliver ~50-100 bacteria (low dose) or ~5-10 bacteria (ultra-low dose). After *Mtb* aerosol inhalation and euthanization, the lung tissue was isolated and homogenized in 5 mL of PBS + Tween-80 (Sigma-Aldrich, St. Louis, Missouri, USA) buffer and the entire lung homogenate sample was plated on Middlebrook 7H10 agar plates and subsequently incubated at 37°C and 5% CO_2 for 3 weeks before colonies were counted. The bacterial burden of *Mtb* was evaluated 24 hours (n=2 experiments) and 21 days (n=1 experiment) post-challenge for the low dose model and at 24 hours (n=1 experiment) for the ultra-low dose model. The ultra-low dose bacterial challenge is expected to better reflect human infection conditions where relatively few bacteria are able to establish a pulmonary infection in the host. The NOID and Wisconsin-Madison aerosol chamber were disinfected with ethanol between all experiments.

5.3.7 Statistics

Significance was evaluated using Student's t-tests assuming equal variance at a significance level of 0.05. Two-sided t-tests were used to determine if results were significantly different, and one-sided t-tests were used to determine whether a result was significantly greater than or less than another result. Experimental results are generally represented as mean ± standard deviation.

5.4 Results

5.4.1 Lung Homogenization Does Not Reduce Phage Activity

Naïve mouse lungs were collected and spiked with an established titer of phage D29 and subsequently homogenized to determine if this process, used routinely to evaluate *Mtb* CFU *ex vivo*, would result in any loss of phage activity. The phage D29 titer after lung homogenization was 12.08 ± 0.03 log(PFU/mL) compared to the control titer before homogenization of 12.12 ± 0.04 log(PFU/mL), with no significant difference ($p > 0.5$; n=3 each). These data indicate that the lung homogenization did not cause phage D29 inactivation, nor did any innate tissue factor influence phage activity or the properties of the plaque assay used to quantify phage in a sample. This demonstrated the viability of this approach for quantifying pulmonary phage delivery.

5.4.2 Nose-Only Inhalation Device - Dose Simulation Matches In Vivo Experiment

Tryptophan tracer deposition at different locations within two different versions of the NOID quantified by assay of rinsate are presented in Table 5.1, as is the predicted dose to the lungs of a mouse, $T_{\mathrm{m/A}}$, calculated using equation (5.1). As shown, use of the smaller width of the first plenum achieved the target dose, with a $T_{\mathrm{m/A}}$ of 1.0 ± 0.1 PFU/alveolus, corresponding to a predicted dose of phage D29 to the lungs of mice of 7.6 ± 0.1 log(PFU/mouse). Hence, this NOID configuration was chosen for *in vivo* experiments.

Table 5.1: Tryptophan tracer deposition within two different versions of the NOID as a simulation of phage D29 delivery.

First plenum width (mm)	**Nebulizer reservoir (%)**	**First plenum (%)**	**Mixing tube (%)**	**Back plenum (%)**	**Nosepiece & adapter (%)**	**Mouse filter (%)**	**Exit filter (%)**	**Unacc ounted (%)**	**Predicted dose to a mouse $T_{\mathrm{m/A}}$ (PFU/alveolus)**
95	1.0 ± 0.8	61.2 ± 7.5	1.9	5.1 ± 1.2	0.062 ± 0.008	0.013 ± 0.005	1.07 ± 0.05	30 ± 6	0.4 ± 0.2
32	1.2 ± 0.6	60.3 ± 0.4	3.2	6.3 ± 0.6	0.073 ± 0.004	0.033 ± 0.004	1.50 ± 0.023	27 ± 3	1.0 ± 0.1

Results are presented as avg ± SD from 3 replicate experiments, except for the mixing tube which was measured once. The components are labeled in Figure 5.2.

It is important to note that the ratio of flow rate entering the exit filter (478 mL/min) to the flow rate entering the mouse filter and nosepiece with adapter (22 mL/min) was 22, whereas the ratio of dose on the exit filter (1.50%) to dose on the surrogate mouse filter and nosepiece with adapter (0.11%) was 14. If a uniform aerosol concentration were present the ratios would be equal. The latter ratio was lower, as expected, due to aerosol deposition in the front plenum.

A fraction of 0.044 = (22 mL/min) / (500 mL/min) of the total dose reaching all 12 noseports deposited on the single tested mouse filter and nosepiece with adapter, on which a dose of 0.11% was measured. Relative to the use of the unmodified NOID presented by Nadithe et al. [526], the amount of tryptophan reaching the mouse filter was improved by a factor of 1.8. Considering that approximately 6,000 times more active phage D29 were delivered per unit time with the vibrating mesh nebulizer than with the jet nebulizer (see Chapter 4), an improvement by a factor of approximately 11,000 was achieved over the unmodified NOID that used a jet nebulizer, in terms of the predicted number of active phage D29 reaching the lungs of the mice per unit time. The

small standard deviation indicated that the dosing was repeatable and consistent, and provided confidence in this modified NOID setup.

We next optimized phage D29 aerosol delivery to mice in the modified NOID setup with parameters described above. As phage D29 was amplified in *Mycobacterium smegmatis*, the resulting lysate input to the nebulizer clogged the mesh and hence had to be diluted 1:1 in isotonic saline prior to delivery. This dilution decreased the total stock volume such that 3 mL of 11.8 ± 0.1 log(PFU/mL) phage D29 lysate was delivered, rather than 6 mL of 12.2 ± 0.1 log(PFU/mL) which was assumed during dose simulation. For these conditions, the predicted dose in the lungs of mice was 6.9 ± 0.1 log(PFU/mouse), which is within the range of doses measured *in vivo* in the lungs of mice after phage D29 aerosol delivery, shown in Table 5.2. This indicates that the method of dose simulation and the model given by equation (5.1) were accurate for predicting *in vivo* phage dose to the lungs of mice. This also demonstrates the accuracy and reliability of the dose simulation and the NOID setup in general.

Table 5.2: Phage D29 dose in the lungs of mice post-NOID delivery.

Time between exposure and euthanization (min)	**Phage D29 dose in mouse lungs in log(PFU/mouse)***
0	6.6 ± 0.3
30	7.3 ± 0.1
90	7.0 ± 0.4

*avg ± SD of n=3 mice per time point

Along with total immediate delivery, potential pulmonary clearance of phage D29 was evaluated 30 and 90 minutes post-delivery, and no significant difference was observed ($p > 0.05$). Hence, phage D29 was not quickly cleared from the lungs of mice, providing confidence to proceed with *Mtb* exposure.

5.4.3 Mtb H37Rv is Susceptible to Phage D29

Before commencing bacterial aerosol challenge studies we confirmed prior data [540] indicating that *Mtb* strain H37Rv, a common laboratory strain, was susceptible to phage D29 lysate *in vitro*. A control plate (no phage added) contained 38 CFU, whereas 2 replicates with D29 addition resulted in 1 CFU and 2 CFU. Therefore, H37Rv lysis via phage D29 was 92-95% effective. The

lysis may have not been 100% effective due to phage not coming into contact with every bacterium during plating, or potentially due to phage resistance. The high lysis effectiveness provided confidence to proceed with *Mtb* exposure.

5.4.4 Inhaled Phage D29 Provides In Vivo Prophylactic Protection against TB

In order to evaluate the potential application of phage D29 aerosol as a prophylactic tool against *Mtb* infection we next quantified bacterial burden (CFU) of *Mtb* H37Rv in mouse lungs 24 hours post-infection, with or without phage D29 pre-treatment less than 30 minutes prior to *Mtb* exposure. An average of 7.7 ± 0.3 log(PFU/mouse) of phage D29 was delivered to the lungs in replicate 2, which correspond to ~1 PFU/alveolus on average, indicating the target dose of phage D29 was achieved. A significant reduction ($p < 0.05$) of bacterial burden in the lungs at 24 hours post-challenge was observed (Figure 5.3). These data suggest that with a target dose of 1 PFU/alveolus, a significant level of prophylactic protection against inhaled *Mtb* aerosol is indeed possible.

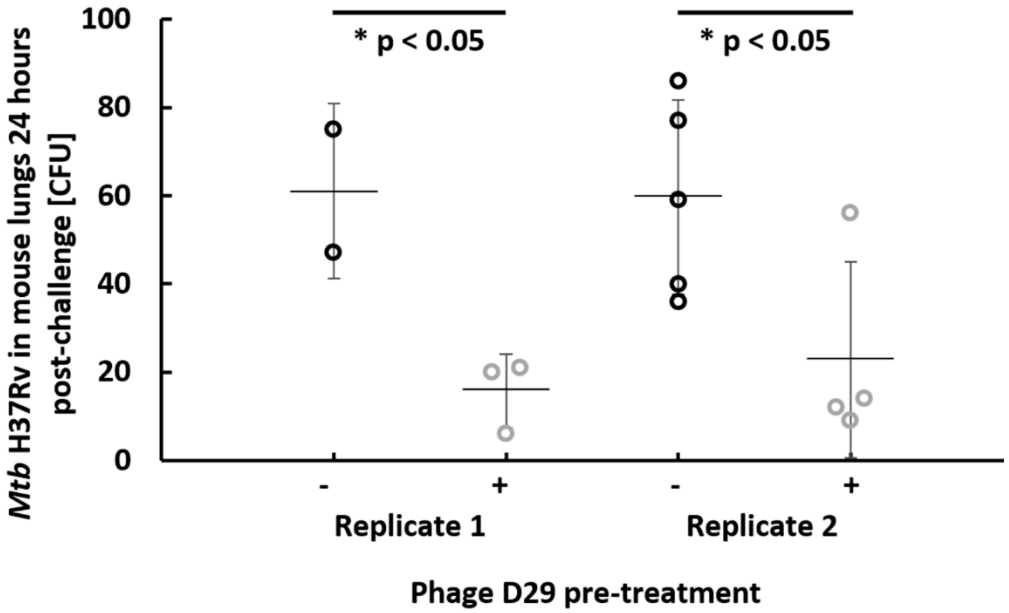

Figure 5.3: Pre-treatment with phage D29 aerosol delivered by nose-only inhalation significantly reduces pulmonary bacterial burden 24 hours post-challenge with low dose *Mtb* H37Rv. On the x-axis, "-" indicates no phage D29 pre-treatment and "+" indicates with phage D29 pre-treatment. Each circle represents a single mouse and error bars span the standard deviation around the mean indicated by the horizontal line.

A separate cohort of mice from replicate 1 were followed out to 3 weeks post-challenge to determine if effects of prophylactic phage application would persist over time. Bacterial burden was measured in the lungs and the spleen 3 weeks post-challenge (Figure 5.4). Interestingly, at 3 weeks phage D29 pre-treated mice sustained a significantly lower bacterial burden than mice that did not receive phage pre-treatment in the lungs ($p < 0.05$), although bacterial burden was not significantly different in the spleen ($p > 0.1$). The bacterial burden at 3 weeks was of a high magnitude.

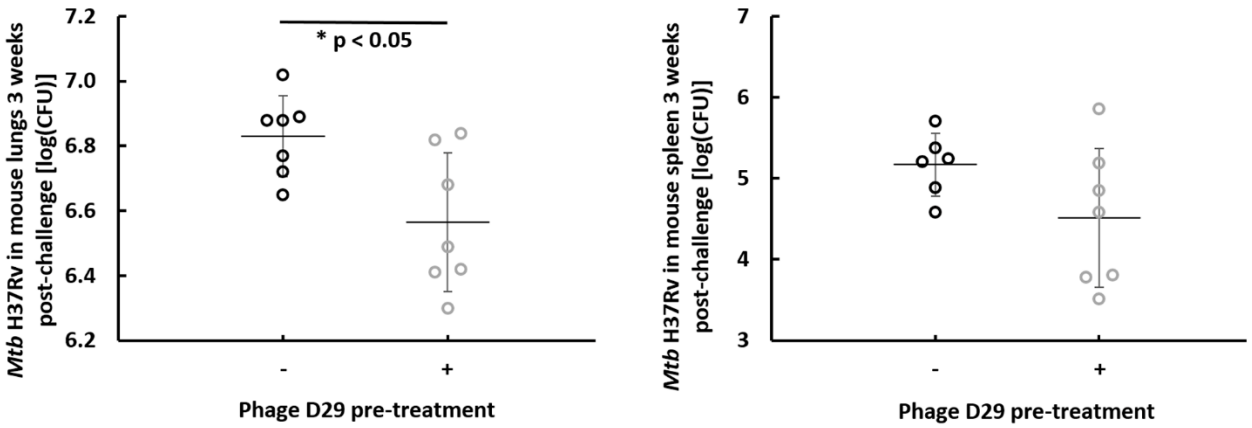

Figure 5.4: Log of bacterial burden 3 weeks post-challenge in the lungs (left) and spleen (right), without and with phage D29 pre-treatment. On the x-axis, "-" indicates no phage D29 pre-treatment and "+" indicates with phage D29 pre-treatment. Each circle represents a single mouse and error bars span the standard deviation around the mean indicated by the horizontal line.

In order to more closely simulate *Mtb* infections in humans we next optimized and utilized an ultra-low dose aerosol challenge of H37Rv calibrated to deliver 5-10 CFU of bacteria. An average of 7.4 ± 0.1 log(PFU/mouse) of phage D29 was delivered to the lungs. At 24 hours post-challenge, a significant reduction ($p < 0.05$) of *Mtb* in the lungs was observed in the group that received phage D29 aerosol pre-treatment, relative to the group that did not (Figure 5.5), providing important further evidence of prophylactic efficacy.

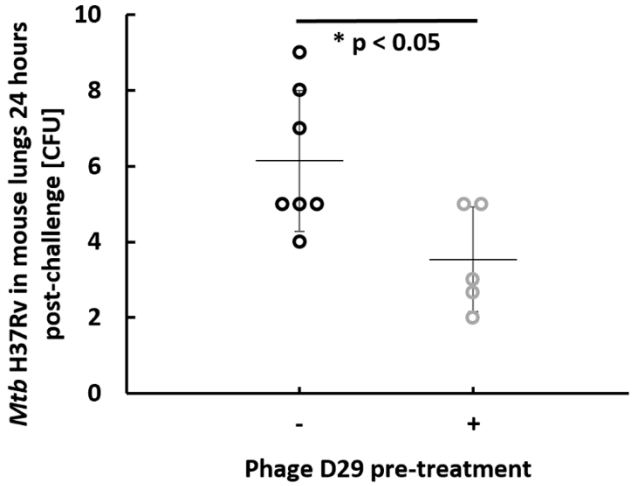

Figure 5.5: Pre-treatment with phage D29 aerosol delivered by nose-only inhalation significantly reduces pulmonary bacterial burden 24 hours post-challenge with ultra-low dose *Mtb* H37Rv. On the x-axis, "-" indicates no phage D29 pre-treatment and "+" indicates with phage D29 pre-treatment. Each circle represents a single mouse and error bars span the standard deviation around the mean indicated by the horizontal line.

5.5 Discussion

The results of this study demonstrate that inhalation of phage D29 aerosol prior to challenge with *Mtb* aerosol can significantly decrease the pulmonary bacterial burden in mice 24 hours and 3 weeks post-infection. These data suggest that inhaled mycobacteriophage aerosol resulted in *Mtb* lysis in the lungs prior to macrophage uptake and granuloma formation. This proof-of-principle study may have implications for the development of prophylactic aerosol treatments for health care professionals exposed to patients with active TB and reduction in *Mtb* transmission rates in this setting. This is important because many health care professionals are relatively unwilling to work in areas of hospitals with high-risk of tuberculosis transmission [541]. Additionally, more protection could potentially be offered to individuals in areas in which TB is endemic, or to other individuals at high-risk, such as household contacts and visiting family members at hospitals. This treatment is intended to complement normal precautions, which includes use of administrative controls, environmental controls, and personal respiratory protection [503-504].

The authors are only aware of one other study regarding prophylactic inhalation of phages prior to inhalation of bacteria [542], and that study demonstrated 4-day prophylaxis against multi-drug-

resistant (MDR) *Pseudomonas aeruginosa* in mice, but used intranasal instillation rather than an aerosol delivery device. Instillation results in localized deposition and is not as representative of natural inhalation to the different regions of the lungs as nose-only inhalation [527,543]. Therefore, we believe this work, the first study demonstrating prophylactic protection with phage using nose-only inhalation of aerosol represents a significant advancement in this area of research. Additionally, to the authors' knowledge, a much higher titer of phage was delivered to the lungs of mice by nose-only inhalation in this study than in any previous study. Relative to the use of a jet nebulizer in a previous NOID design [526], approximately 11,000 times more active phage D29 could be delivered to the lungs of mice, and with repeatable results, indicating a major improvement of dosing to mice was achieved with this novel approach. Furthermore, Liu et al. [531] only delivered 10^2–10^3 PFU of phage D29 to the lungs of mice using a Collison jet nebulizer with a NOID, which is orders of magnitude lower than in this study, in which > 10^7 PFU was delivered to the lungs of mice. This improvement allowed, for the first time, an average dose of ~1 PFU/alveolus to be achieved. It is important to consider that some alveoli are poorly perfused, and hence > 1 PFU per accessible alveolus may have been achieved on average. Another factor to consider is that phage progeny released after *Mtb* lysis would offer further protection in their vicinity, but are unlikely to be transferred to nearby alveoli, as they are non-motile. As *Mtb* is also non-motile, it is unlikely to move between alveoli and come into contact with phage in that manner.

The prophylactic delivery of an average of 1 PFU/alveolus allowed for a significant reduction of *Mtb* levels in the lungs, demonstrating a prophylactic effect. Whether such a decrease in TB levels is sufficient to decrease mortality rates is not known. While it is difficult to deliver more than 1 PFU/alveolus on average to a mouse using a NOID, such levels may be necessary to achieve complete bacterial eradication. Poisson statistics can be used to estimate the probability of a specific random occurrence during an interval of interest knowing the average number of occurrences in that interval [544]. Using this method, the probability, P, that an alveolus will contain a certain number of phage, x, can be predicted knowing the average number of PFU/alveolus, λ, according to

$$P = \frac{e^{-\lambda} \cdot \lambda^{x}}{x!} \tag{5.2}$$

Using the values $\lambda = 1$ and $x = 0$ gives $P = 0.37$. This indicates that if on average 1 PFU/alveolus is delivered to the lungs, the probability that an alveolus does not contain a phage is still 37%. Hence, the chance that a bacterium encounters at least one phage in an alveolus is only about 63%. In prophylactic phage administration experiments (see Figure 5.3) the average reduction in bacterial burden was from approximately 60 CFU to approximately 20 CFU, or about 67%. This is in close agreement with the prediction of 63% reduction in bacterial burden that assumes that all bacteria that deposit in an alveolus in the presence of at least one phage are inactivated.

To achieve at least one phage in 99% of the alveoli of a mouse, the average number of phage per alveolus would need to be $\lambda = 4.6$. For 99.9% coverage, it is $\lambda = 6.9$. A potential indicator of the dose required for complete prophylaxis is when the probability that an alveolus contains no phage becomes less than the inverse of the number of alveoli in the lungs, which for a mouse occurs with $\lambda > 17.5$.

Achieving a high dose of active phage in human lungs is not as difficult as in mice because deposition losses in the NOID would not be present and humans do not require equally small droplets for efficient lung deposition. Human lungs contain ~4.8×10^8 alveoli [545], ~10 times the number that mouse lungs have. An average number of phage per alveolus of approximately 20 may be required for complete prophylaxis in a human according to the above indicator. In Chapter 4 it was suggested that in humans, a respirable dose of active phage D29 of ~1.3×10^9 PFU could be achieved with delivery of 6 mL of diluted lysate using a vibrating mesh nebulizer. This corresponds to a dose to human lungs of ~2.7 PFU/alveolus on average, or 93% alveolar coverage. In that study, the phage D29 lysate was diluted 1:100 in isotonic saline prior to aerosolization as without dilution the lysate purification level was not sufficient to prevent mesh clogging. Potentially, without dilution, i.e. with better purification techniques, orders of magnitude higher titers may reach the lungs, on the order of 10^2 PFU/alveolus on average. This could be sufficient for complete prophylaxis according to the above described Poisson statistics argument. Additionally, with daily prophylactic doses, the likelihood that a specific alveolus receives a sufficient number of phages to eradicate intruding bacteria increases. As it may take days for granulomas to form [546], it is possible that phages delivered soon after *Mtb* exposure may still offer protection, but this depends on macrophage uptake dynamics [523], and awaits further exploration.

The development of regulatory-approved, commercial phage formulations for inhalation will likely require the use of cocktails containing various phages that target different receptors to ensure the *Mtb* does not become phage-resistant [507]. The development of anti-TB cocktails is an active area of research [507]. Phage D29 and others that may be included in a therapeutic cocktail would be applicable for prevention of drug-sensitive or drug-resistant strains of *Mtb*. Further development of phage cocktail therapy will require efficacy testing against clinical and drug-resistant *Mtb* strains and, importantly, measuring potential phage-induced host immune responses. It should be determined whether daily prophylactic doses of phage cocktails lead to an immune response that inactivates the phages, or to the development of bacteria which are resistant to all of the phages in the cocktail, although it is important to note that phages are capable of mutating to overcome bacterial resistance and new phages targeting different receptors can be isolated relatively rapidly.

Furthermore, in the development of phage cocktails it is of interest to demonstrate that each phage survives the nebulization process and efficiently reaches the lungs. Experimental dose simulation of phage delivery to mice using a tryptophan tracer, simulated breathing, and filter aerosol capture with a NOID, resulted in accurate prediction of phage dose reaching the lungs of mice *in vivo*. Hence, assuming the same droplet size distribution, it is possible that one could simply measure the phage activity retention from the nebulizer by aerosolization to a filter as described in Chapter 4, and predict the *in vivo* dose reaching the lungs of mice in the present NOID setup using the modelling approach (see equation (5.1)) and aerosol delivery efficiency results (Table 5.1) presented in this study. This would allow the lung dose of different phages in a cocktail to be predicted prior to *in vivo* experiments, saving time and resources, and expediting the development process.

5.6 Conclusions

In summary, inhalation of anti-TB mycobacteriophage D29 aerosol is a promising and novel approach to provide prophylactic protection against primary infection of inhaled *Mtb* aerosol. Significant reduction in bacterial burden was achieved with prophylactic delivery of an average dose of active phage D29 of ~1 PFU/alveolus to the lungs. Complete prophylaxis may be achievable with larger or repeated doses of active phages. The number of active phages reaching the alveoli can be predicted prior to animal studies with a NOID by aerosolizing a tracer, simulating breathing through a filter, assay of the recovered aerosol on the filter, and applying the

developed mathematical modeling approach. The development of a high titer phage cocktail against TB is recommended over monophage therapy. The cocktail may provide extra protection to health care professionals regularly exposed to patients with active TB and to individuals in areas with high rates of TB transmission. Additionally, countries with a high burden of TB and MDR-TB are often involved in military engagement with resulting additional risk of exposure. Given that the risk of *Mtb* transmission is higher in congregate settings, a single individual with TB disease exerts an immediate and disruptive impact upon patients' lives, military operations, and daily functioning at military and civil treatment facilities. Delivery of high doses of active phages to human lungs for prophylactic purposes appears achievable and proceeding to human clinical trials is of interest.

6 Conclusions

6.1 Summary

In this thesis experimental work and theoretical developments led to improvements in the way liquid and solid bacteriophage dosage forms are manufactured and delivered for respiratory delivery and food applications.

In Chapter 2 stable solid dosage forms of anti-*Campylobacter* bacteriophages for use in chicken feed were developed by spray drying, with the end goal developing a manufacturing method that could be applied to phages of Kenyan origin to decrease incidences of food poisoning in Kenya. Out of many tested factors that may have led to phage inactivation, the most important was desiccation stress. Reduction of this stress was achieved by the application of particle engineering theory to the design of fully amorphous particles containing a high glass transition temperature excipient at the surface. The developed formulations and drying methods resulted in better stabilization than the standard leucine and trehalose formulation. The powder was stable shipped and stored without use of refrigeration, which is crucial to its potential success in Kenya.

In Chapter 3, one of the best solid dosage form excipient combinations described in Chapter 2, pullulan and trehalose, was studied in more detail due to its many potential applications in the food and biopharmaceutical industries. A monodisperse droplet chain and a laboratory-scale spray dryer were used to develop microparticles containing different mass fractions of the excipients. A multi-component analytical particle formation model was developed to characterize the particle formation process and theoretical results closely matched monodisperse droplet chain experimental measurements. A radial glass transition temperature model was developed, and its applicability was supported by modulated differential scanning calorimetry measurements of spray dried powder. The powder was physically stable in commercial propellants inside pressurized metered-dose inhaler canisters under accelerated storage conditions and could be actuated without changes to morphology. The powder was effectively loaded into and dispersed from a dry powder inhaler in a size suitable for deposition throughout the lungs. These findings, along with the biological stability data in Chapter 2, led to the conclusion that pullulan and trehalose appears to be a suitable platform for respiratory delivery of biologics.

In Chapter 4 a jet nebulizer, a vibrating mesh nebulizer, and a soft mist inhaler were tested for delivering anti-tuberculosis phage D29. The most ineffective was the jet nebulizer, in which the phage was substantially inactivated during droplet production. A theoretical model demonstrated that in the jet nebulizer phage undergo many renebulization cycles prior to exiting the mouthpiece of the device. The soft mist inhaler was best for applications requiring quick self-administration of a reasonable dose of active phage D29. The best liquid dosage form for respiratory delivery of large amounts of anti-tuberculosis phage D29, as is required for animal studies, was use of the diluted lysate in the vibrating mesh nebulizer.

In Chapter 5 a nose-only inhalation device was adapted for use with a vibrating mesh nebulizer, rather than a jet nebulizer, for delivering large doses of phage D29 to the lungs of mice. The dose was predicted prior to *in vivo* studies by aerosolizing a tracer through the device and quantifying its deposition on a filter through which mouse inhalation was simulated. A higher dose of active phage was predicted to be achieved in the lungs of mice than in any previous study, and *in vivo* experimental results of delivery of active phage D29 to the lungs of mice was in remarkable agreement with dose simulation experiments. Subsequent challenge with *M. tuberculosis* H37Rv aerosol demonstrated that prophylactic respiratory delivery of phage D29 resulted in a protective effect against tuberculosis. The objectives outlined in Section 1.1 were thus achieved.

6.2 New Contributions to Knowledge

The following represent some of the new contributions to knowledge in this thesis.

- First study exploring the many factors which may inactivate phages during spray drying, and demonstration that for the tested *Myoviridae,* desiccation is the main inactivating stress
- First time it has been suggested that spray drying with an amorphous shell former results in better biological stability than spray drying with a crystallizing shell former
- First shipping stability study with spray dried phages demonstrating that biological stability is maintained with suitable packaging
- First time pullulan and trehalose have been proposed for spray drying biologics and first aerosol performance and physical stability characterization with those excipients
- First characterization of radial glass transition temperature within dry particles
- First multi-component particle formation model for use with evaporating microdroplets containing multiple excipients that co-solidify to an amorphous phase at the surface

- New method for quantifying liquid recirculation and for predicting the number of baffle impactions occurring in jet nebulizers
- New method for delivering phages to the lungs of mice, by coupling a vibrating mesh nebulizer with a nose-only inhalation device; demonstration that this results in larger amounts of phage in the lungs of mice than in any previous study
- An experimental method and theoretical model for simulating dosing with the nose-only inhalation device that accurately predicted results of *in vivo* experiments
- First *in vivo* study using phages to target tuberculosis in the lungs
- First study demonstrating inhaled phage aerosol generated with a vibrating mesh nebulizer provides prophylactic protection against a respiratory disease

6.3 Recommendations for Future Work

Further optimization of mass fractions for pullulan and trehalose formulation, as well as trileucine and trehalose formulation, could be performed with anti-*Campylobacte*r phages. Testing these formulations with phages of Kenyan origin rather than of United Kingdom origin is worth consideration. The results suggest that the use of more advanced purification techniques would allow for a higher titer power to be achieved, as dilution would not be necessary. Testing the maximum inlet temperature that the phages remain active with would be useful for spray drying scale-up as higher temperatures allow not only for larger batch sizes per unit time, but also for earlier shell formation and potentially less exposure to the drying gas and associated desiccation stress. Anti-*Campylobacter* phage CP30A powder is currently under long-term stability and further biological stability measurements are to be performed. Different moisture contents during storage could be explored in a future study. Further combinations of the tested excipients, and other excipients such as divalent cations (see Appendix C), salts to adjust osmolarity and modify desiccation stress, phosphate buffers, and arginine could be tested [56].

Aerosolization of spray dried pullulan and trehalose microparticles from a dry powder inhaler resulted in a total lung deposition and a fine particle fraction on par with commercial inhalation devices; however, further improvements could be made with addition of excipients that remain amorphous, such as trileucine [170], to further improve the aerosol performance.

In Chapter 2 it was found that desiccation is the main inactivating stress for anti-*Campylobacter* phages. In Chapter 4 stresses that occur during droplet production and renebulization caused

inactivation of anti-tuberculosis phage D29 with the jet nebulizer. During droplet production and renebulization in a jet nebulizer, the droplets undergo evaporation and hence the phages are exposed to desiccation stress at the surface of the shrinking droplets. This desiccation stress is repeated in each renebulization cycle. Further work could be done to determine the relative importance of desiccation and hydrodynamic shear stress on phage inactivation in jet nebulizers. Additionally, whether certain monomer surfactants or other excipients can decrease phage inactivation in jet nebulizers is a potential subject of future research.

The use of an anti-tuberculosis phage cocktail, containing many phages targeting different *M. tuberculosis* receptors, is necessary to decrease the effects of bacterial resistance to phages. Future research should demonstrate that other anti-tuberculosis phages, such as phage DS6A and phage BPs [112], are capable of being aerosolized without substantial titer reduction.

Further improvements could be made to the nose-only inhalation device design and these are discussed in Appendix D. As compared to mice, guinea pigs produce granuloma more like those of humans. Guinea pigs could be tested with anti-tuberculosis phages with further modifications to the nose-only inhalation device. As guinea pigs have larger airways, higher doses in the lungs could be achieved. Better lysate purification techniques would improve the ability to deliver large doses without the need for dilution.

The development and testing of dry powder phage products in animals is a topic of interest. Further work could be done to minimize the titer reduction of spray dried phage D29 (some results are shown in Appendix A) and to modify the nose-only inhalation device to deliver the powder to animals. Testing the retention of phage activity after dry powder inhaler or pressurized metered-dose inhaler emission is also a potential area of future reserach.

Many phage products and tested excipients are on the market for food applications. However, phages and certain tested excipients are not currently approved by regulatory agencies for delivery to the respiratory tract; therefore, testing safety and efficacy in the human lungs in well-designed clinical trials is an area of interest.

References

[1] La Mont CA. 1865. Improvement in preserving eggs. Patent US51263A.

[2] Peroy, S.R. 1872. Improvement in drying and concentrating liquid substances by atomizing. Patent US125406A.

[3] Desai, K.G.H., Park, H.J. 2005. Recent developments in microencapsulation of food ingredients. *Drying Technol* 23:1361-1394.

[4] Anandharamakrishnan, C., Padma Ishwarya, S. 2015. *Spray drying techniques for food ingredient encapsulation*. Chichester: John Wiley & Sons, Inc.

[5] Schuck, P., Jeantet, R., Bhandari, B. *et al*. 2016. Recent advances in spray drying relevant to the dairy industry: a comprehensive critical review. *Drying Technol* 34:1773-1790.

[6] Masters, K. 1994. Scale-up of spray dryers. *Drying Technol* 12:235-257.

[7] Gharsallaoui, A., Roudaut, G., Chambin, O., Voilley, A., Saurel, R. 2007. Applications of spray-drying in microencapsulation of food ingredients: an overview. *Food Res Int* 40:1107-1121.

[8] Ré, M.I. 1998. Microencapsulation by spray drying. *Drying Technol* 16:1195-1236.

[9] Shishir, M.R.I., Chen, W. 2017. Trends of spray drying: a critical review on drying of fruit and vegetable juices. *Trends Food Sci Technol* 65:49-67.

[10] Verma, A., Singh, S.V. 2015. Spray drying of fruit and vegetable juices-a review. *Crit Rev Food Sci Nutr* 55:701-719.

[11] Masters, K. 1972. *Spray drying: an introduction to principles, operational practice and applications.* London: Leonard Hill Books.

[12] Behboudi-Jobbehdar, S., Soukoulis, C., Yonekura, L., Fisk, I. 2013. Optimization of spray-drying process conditions for the production of maximally viable microencapsulated *L. acidophilus* NCIMB 701748. *Drying Technol* 31:1274-1283.

[13] Dianawati, D., Mishra, V., Shah, N.P. 2016. Survival of microencapsulated probiotic bacteria after processing and during storage: a review. *Crit Rev Food Sci Nutr* 56:1685-1716.

[14] Huang, S., Vignolles, M.L., Chen, X.D. *et al*. 2017. Spray drying of probiotics and other food-grade bacteria: a review. *Trends Food Sci Technol* 63:1-17.

[15] Broeckx, G., Vandenheuvel, D., Claes, I.J.J., Lebeer, S., Kiekens, F. 2016. Drying techniques of probiotic bacteria as an important step towards the development of novel pharmabiotics. *Int J Pharm* 505:303-313.

[16] Perdana, J., Bereschenko, L., Fox, M.B. *et al*. 2013. Dehydration and thermal inactivation of *Lactobacillus plantarum* WCFS1: comparing single droplet during drying to spray and freeze drying. *Food Res Int* 54:1351-1359.

[17] Perdana, J., Fox, M.B., Siwei, C., Boom, R.M., Schutyser, M.A.I. 2014. Interactions between formulation and spray drying conditions related to survival of *Lactobacillus plantarum* WCFS1. *Food Res Int* 56:9-17.

[18] Ghandi, A., Powell, I.B., Broome, M., Adhikari, B. 2013. Survival, fermentation activity and storage stability of spray dried *Lactococcus lactis* produced via different atomization regimes. *J Food Eng* 115:83-90.

[19] Murugesan, R., Orsat, V. 2012. Spray drying for the production of nutraceutical ingredients – a review. *Food Bioprocess Tech* 5:3-14

[20] Carneiro, H.C.F., Tonon, R.V., Grosso, C.R.F., Hubinger, M.D. 2013. Encapsulation efficiency and oxidative stability of flaxseed oil microencapsulated by spray drying using different combinations of wall materials. *J Food Eng* 115:443-451.

[21] Broadhead, J., Edmond Rouan, S.K., Rhodes, C.T. 1992. The spray drying of pharmaceuticals. *Drug Dev Ind Pharm* 18:1169-1206.

[22] Wisniewski, R. 2015. Spray drying technology review. Conference paper at the 45th International Conference on Environmental Systems, Bellevue.

[23] Jones, H.W., Wisniewski, R., Flynn, M. 2014. Space and industrial brine drying technologies. Conference paper at the 44th International Conference on Environmental Systems, Tuscon.

[24] Vehring, R. 2008. Pharmaceutical particle engineering via spray drying. *Pharm Res* 25:999-1022.

[25] Schwartzbach, H. 2011. Achieving aseptic drying with spray drying technologies. *Pharmaceutical Technology Europe* 23, no.9 (September): 90-92. http://www.pharmtech.com/achieving-aseptic-drying-spray-drying-technologies.

[26] Siew, A. 2016. Exploring the use of aseptic spray drying in the manufacture of biopharmaceutical injectables. *Pharmaceutical Technology* 40, no.7 (July): 24-27. http://www.pharmtech.com/exploring-use-aseptic-spray-drying-manufacture-biopharmaceutical-injectables.

[27] Quinn, Jr., J.J. 1965. The economics of spray drying. *Ind Eng Chem* 57:35-37.

[28] Holsinger, V.H., McAloon, A.J., Onwulata, C.I., Smith, P.W. 2000. A cost analysis of encapsulated spray-dried milk fat. *J Dairy Sci* 83:2361-2365.

[29] Pharmaceutical Technology Editors. 2010. The possibilities and challenges of spray drying. *Pharmaceutical Technology Europe* 22, no. 5 (May): 22-24. http://www.pharmtech.com/possibilities-and-challenges-spray-drying.

[30] Roser, B. 1991. Trehalose, a new approach to premium dried foods. *Trends Food Sci Technol* 2:166-169.

[31] Hoe, S., Boraey, M.A., Ivey, J.W., Finlay, W.H., Vehring, R. 2014. Manufacturing and device options for the delivery of biotherapeutics. *J Aerosol Med Pulm Drug Deliv* 27:315-328.

[32] Ledet, G.A., Graves, R.A., Bostanian, L.A., Mandal, T.K. 2015. Spray-drying of biopharmaceuticals. In *Lyophilized biologics and vaccines: modality-based approaches*, ed. D. Varshney, M. Singh, 273-297. New York: Springer Science+Business Media.

[33] Walters, R.H., Bhatnagar, B., Tchessalov, S., Izutsu, K.I., Tsumoto, K., Ohtake, S. 2014. Next generation drying technologies for pharmaceutical applications. *J Pharm Sci* 103:2673-2695.

[34] Kanojia, G., Willems, G.J., Frijlink, H.W., Kersten, G.F.A., Soema, P.C., Amorij, J.P. 2016. A design of experiment approach to predict product and process parameters for a spray dried influenza vaccine. *Int J Pharm* 511:1098-1111.

[35] Saluja, V., Amorij, J.P., Kapteyn, J.C., de Boer, A.H., Frijlink, H.W., Hinrichs, W.L.J. 2010. A comparison between spray drying and spray freeze drying to produce an influenza subunit vaccine powder for inhalation. *J Control Release* 144:127-133.

[36] Weers, J.G., Tarara, T.E., Clark, A.R. 2007. Design of fine particles for pulmonary drug delivery. *Expert Opin Drug Deliv* 4:297-313.

[37] Afkhami, S., LeClair, D.A., Haddadi, S. *et al*. 2017. Spray dried human and chimpanzee adenoviral-vectored vaccines are thermally stable and immunogenic *in vivo*. *Vaccine* 35:2916-2924.

[38] Gikanga, B., Turok, R., Hui, A., Bowen, M., Stauch, O.B., Maa, Y.F. 2015. Manufacturing of high-concentration monoclonal antibody formulations via spray drying-the road to manufacturing scale. *PDA J Pharm Sci Technol* 69:59-73.

[39] Chen, D., Kapre, S., Goel, A. *et al*. 2010. Thermostable formulations of a hepatitis B vaccine and a meningitis A polysaccharide conjugate vaccine produced by a spray drying method. *Vaccine* 28:5093-5099.

[40] Sou, T., Meeusen, E.N., de Veer, M., Morton, D.A.V., Kaminskas, L.M., McIntosh, M.P. 2011. New developments in dry powder pulmonary vaccine delivery. *Trends Biotechnol* 29:191-198.

[41] Tlaxca, J.L., Ellis, S., Remmele Jr., R.L. 2015. Live attenuated and inactivated viral vaccine formulation and nasal delivery: potential and challenges. *Adv Drug Deliv Rev* 93:56-78.

[42] World Health Organization. 2005. Monitoring vaccine wastage at country level: guideline for programme managers. http://apps.who.int/iris/handle/10665/68463 (accessed March 12, 2018).

[43] Huang, J., Garmise, R.J., Crowder, T.M. *et al*. 2004. A novel dry powder influenza vaccine and intranasal delivery technology: induction of systemic and mucosal immune responses in rats. *Vaccine* 23:794-801.

[44] LiCalsi, C., Christensen, T., Bennett, J.V., Phillips, E., Witham, C. 1999. Dry powder inhalation as a potential delivery method for vaccines. *Vaccine* 17:1796-1803.

[45] Lu, D., Hickey, A.J. 2007. Pulmonary vaccine delivery. *Expert Rev Vaccines* 6:213-226.

[46] Wang, S.H., Thompson, A.L., Hickey, A.J., Staats, H.F. 2012. Dry powder vaccines for mucosal administration: critical factors in manufacture and delivery. In *Mucosal vaccines: modern concepts, strategies, and challenges*, ed. P.A. Kozlowski, 121-156. Berlin: Springer-Verlag.

[47] Ohtake, S., Lechuga-Ballesteros, D., Truong-Le, V., Patzer, E.J. 2015. Strategies for heat-stable vaccines. In *Vaccine development and manufacturing*, ed. E.P. Wang, R. Ellis, N.S. Pujar, 287-318. Hoboken: John Wiley & Sons, Inc.

[48] Amorij, J.P., Huckriede, A., Wilschut, J., Frijlink, H.W., Hinrichs, W.L.J. 2008. Development of stable influenza vaccine powder formulations: challenges and possibilities. *Pharm Res* 25:1256-1273.

[49] Zhu, C., Shoji, Y., McCray, S. *et al*. 2014. Stabilization of HAC1 influenza vaccine by spray drying: formulation development and process scale-up. *Pharm Res* 31:3006-3018.

[50] Laube, B.L. 2005. The expanding role of aerosols in systemic drug delivery, gene therapy, and vaccination. *Respir Care* 50:1161-1176.

[51] Lovalenti, P.M., Anderl, J., Yee, L. *et al*. 2016. Stabilization of live attenuated influenza vaccines by freeze drying, spray drying, and foam drying. *Pharm Res* 33:1144-1160.

[52] Sou, T., Morton, D.A.V., Williamson, M., Meeusen, E.N., Kaminskas, L.M., McIntosh, M.P. 2015. Spray-dried influenza antigen with trehalose and leucine produces an aerosolizable powder

vaccine formulation that induces strong systemic and mucosal immunity after pulmonary administration. *J Aerosol Med Pulm Drug Deliv* 28:361-371.

[53] Smith, D.J., Bot, S., Dellamary, L., Bot, A. 2003. Evaluation of novel aerosol formulations designed for mucosal vaccination against influenza virus. *Vaccine* 21:2805-2812.

[54] Amorij, J.P., Saluja, V., Petersen, A.H., Hinrichs, W.L.J., Huckriede, A., Frijlink, H.W. 2007. Pulmonary delivery of an inulin-stabilized influenza subunit vaccine prepared by spray-freeze drying induces systemic, mucosal humoral as well as cell-mediated responses in BALB/c mice. *Vaccine* 25:8707-8717.

[55] Kunda, N.K., Alfagih, I.M., Miyaji, E.N. *et al*. 2015. Pulmonary dry powder vaccine of pneumococcal antigen loaded nanoparticles. *Int J Pharm* 495:903-912.

[56] Ohtake, S., Martin, R.A., Yee, L. *et al*. 2010. Heat-stable measles vaccine produced by spray drying. *Vaccine* 28:1275-1284.

[57] Corbanie, E.A., Remon, J.P., van Reeth, K., Landman, W.J.M., van Eck, J.H.H., Vervaet, C. 2007. Spray drying of an attenuated live Newcastle disease vaccine virus intended for respiratory mass vaccination of poultry. *Vaccine* 25:8306-8317.

[58] Huyge, K., van Reeth, K., de Beer, T. *et al*. 2012. Suitability of differently formulated dry powder Newcastle disease vaccines for mass vaccination of poultry. *Eur J Pharm Biopharm* 80:649-656.

[59] Kunda, N.K., Wafula, D., Tram, M., Wu, T.H., Muttil, P. 2016. A stable live bacterial vaccine. *Eur J Pharm Biopharm* 103:109-117.

[60] Muttil, P., Prego, C., Garcia-Contreras, L. *et al*. 2010. Immunization of guinea pigs with novel hepatitis B antigen as nanoparticle aggregate powders administered by the pulmonary route. *AAPS J* 12:330-337.

[61] Garcia Contreras, L., Awashthi, S., Hanif, S.N.M., Hickey, A.J. 2012. Inhaled vaccines for the prevention of tuberculosis. *J Mycobac Dis* S1:002.

[62] Tyne, A.S., Chan, J.G.Y., Shanahan, E.R. *et al*. 2013. TLR2-targeted secreted proteins from *Mycobacterium tuberculosis* are protective as powdered pulmonary vaccines. *Vaccine* 31:4322-4329.

[63] Lu, D., Garcia-Contreras, L., Muttil, P. *et al*. 2010. Pulmonary immunization using antigen 85-B polymeric microparticles to boost tuberculosis immunity. *AAPS J* 12:338-347.

[64] Lu, D., Garcia-Contreras, L., Xu, D. *et al*. 2010. Poly (lactide-co-glycolide) microspheres in respirable sizes enhance an *in vitro* T cell response to recombinant *Mycobacterium tuberculosis* antigen 85B. *Pharm Res* 24:1834-1843.

[65] Jin, T.H., Tsao, E., Goudsmit, J., Dheenadhayalan, V., Sadoff, J. 2010. Stabilizing formulations for inhalable powders of an adenovirus 35-vectored tuberculosis (TB) vaccine (AERAS-402). *Vaccine* 28:4369-4375.

[66] Garcia-Contreras, L., Wong, Y.L., Muttil, P. *et al*. 2008. Immunization by bacterial aerosol. *Proc Natl Acad Sci USA* 105:4656-4660.

[67] Wong, Y.L., Sampson, S., Germishuizen, W.A. *et al*. 2007. Drying a tuberculosis vaccine without freezing. *Proc Natl Acad Sci USA* 104:2591-2595.

[68] Bennett, J.V., de Castro, J.F., Valdespino-Gomez, J.L. *et al*. 2002. Aerosolized measles and measles-rubella vaccines induce better antibody booster responses than injected vaccines: randomized trials in Mexican schoolchildren. *Bull World Health Organ* 80:806-812.

[69] de Castro, J.F., Bennett, J.V., Gallardo Rincon, H., Alvarez y Munoz, M.T., Partida Sanchez, L.A.E., Santos, J.I. 2005. Evaluation of immunogenicity and side effects of triple viral vaccine (MMR) in adults, given by two routes: subcutaneous and respiratory (aerosol). *Vaccine* 23:1079-1084.

[70] Dilraj, A., Cutts, F.T., de Castro, J.F. *et al*. 2000. Response to different measles vaccine strains given by aerosol and subcutaneous routes to schoolchildren: a randomised trial. *Lancet* 355:798-803.

[71] Dilraj, A., Sukhoo, R., Cutts, F.T., Bennett, J.V. 2007. Aerosol and subcutaneous measles vaccine: measles antibody responses 6 years after re-vaccination. *Vaccine* 25:4170-4174.

[72] Patton, J.S., Platz, R.M. 1992. (D) Routes of delivery: case studies: (2) Pulmonary delivery of peptides and proteins for systemic action. *Adv Drug Deliv Rev* 8:179-196.

[73] Wolff, R.K. 1998. Safety of inhaled proteins for therapeutic use. *J Aerosol Med Pulm Drug Deliv* 11:197-219.

[74] Hyde, S.C., Pringle, I.A., Abdullah, S. *et al.* 2008. CpG-free plasmids confer reduced inflammation and sustained pulmonary gene expressions. *Nat Biotechnol* 26:549-551.

[75] Ruiz, F.E., Clancy, J.P., Perricone, M.A. *et al*. 2001. A clinical inflammation syndrome attributable to aerosolized lipid-DNA administration in cystic fibrosis. *Hum Gene Ther* 12:751-761.

[76] Heinemann, L. 2008. The failure of Exubera: are we beating a dead horse? *J Diabetes Sci Technol* 2:518-529.

[77] Chow, A.H.L., Tong, H.H.Y., Chattopadhyay, P., Shekunov, B.Y. 2007. Particle engineering for pulmonary drug delivery. *Pharm Res* 24:411-437.

[78] Peyre, M., Audran, R., Estevez, F. *et al*. 2004. Childhood and malaria vaccines combined in biodegradable microspheres produce immunity with synergistic interactions. *J Control Release* 99:345-355.

[79] Boehm, G., Peyre, M., Sesardic, D. *et al*. 2002. On technological and immunological benefits of multivalent single-injection microsphere vaccines. *Pharm Res* 19:1330-1336.

[80] McAdams, D., Chen, D., Kristensen, D. 2012. Spray drying and vaccine stabilization. *Expert Rev Vaccines* 11:1211-1219.

[81] Evaluate Ltd. 2017. EvaluatePharma® World Preview 2017, Outlook to 2022. http://www.evaluategroup.com/public/Reports/EvaluatePharma-World-Preview-2017.aspx (accessed March 9, 2018).

[82] Walsh, G. 2014. Biopharmaceutical benchmarks 2014. *Nat Biotechnol* 32:992-1000.

[83] Sane, S.U., Wong, R., Hsu, C.C. 2004. Raman spectroscopic characterization of drying-induced structural changes in a therapeutic antibody: correlating structural changes with long-term stability. *J Pharm Sci* 93:1005-1018.

[84] Costantino, H.R., Andya, J.D., Nguyen, P.H. *et al*. 1998. Effect of mannitol crystallization on the stability and aerosol performance of a spray-dried pharmaceutical protein, recombinant humanized anti-IgE monoclonal antibody. *J Pharm Sci* 87:1406-1411.

[85] Schüle, S., Schulz-Fademrecht, T., Garidel, P., Bechtold-Peters, K., Frieß, W. 2008. Stabilization of IgG1 in spray-dried powders for inhalation. *Eur J Pharm Biopharm* 69:793-807.

[86] Bowen, M., Turok, R., Maa, Y.F. 2013. Spray drying of monoclonal antibodies: investigating powder-based biologic drug substance bulk storage. *Drying Technol* 31:1441-1450.

[87] Abdul-Fattah, A.M., Truong-Le, V., Yee, L. *et al*. 2007. Drying-induced variations in physico-chemical properties of amorphous pharmaceuticals and their impact on stability (I): stability of a monoclonal antibody. *J Pharm Sci* 96:1983-2008.

[88] Mohanty, R.R., Das, S. 2017. Inhaled insulin – current direction of insulin research. *J Clin Diagn Res* 11:OE01-OE02.

[89] White, S., Bennett, D.B., Cheu, S. *et al*. 2005. EXUBERA®: pharmaceutical development of a novel product for pulmonary delivery of insulin. *Diabetes Technol Ther* 7:896-906.

[90] Miller, D.P., Tan, T., Nakamura, J., Malcolmson, R.J., Tarara, T.E., Weers, J.G. 2017. Physical characterization of Tobramycin Inhalation Powder: II. state diagram of an amorphous engineered particle formulation. *Mol Pharm* 14:1950-1960.

[91] Vehring, R., Lechuga-Ballesteros, D., Joshi, V., Noga, B., Dwivedi, S.K. 2012. Cosuspensions of microcrystals and engineered microparticles for uniform and efficient delivery of respiratory therapeutics from pressurized metered dose inhalers. *Langmuir* 28:15015-15023.

[92] Doty, A., Schroeder, J., Vang, K. *et al*. 2018. Drug delivery from an innovative LAMA/LABA co-suspension delivery technology fixed-dose combination MDI: evidence of consistency, robustness, and reliability. *AAPS PharmSciTech* 19:837-844.

[93] Maltesen, M.J., Bjerregaard, S., Hovgaard, L., Havelund, S., van de Weert, M. 2008. Quality by design – spray drying of insulin intended for inhalation. *Eur J Pharm Biopharm* 70:828-838.

[94] Sadrzadeh, N., Miller, D.P., Lechuga-Ballesteros, D., Harper, N.J., Stevenson, C.L., Bennett, D.B. 2010. Solid-state stability of spray-dried insulin powder for inhalation: chemical kinetics and structural relaxation modeling of Exubera above and below the glass transition temperature. *J Pharm Sci* 99:3698-3710.

[95] Ståhl, K., Claesson, M., Lilliehorn, P., Lindén, H., Bäckström, K. 2002. The effect of process variables on the degradation and physical properties of spray dried insulin intended for inhalation. *Int J Pharm* 233:227-237.

[96] Geller, D.E., Weers, J., Heuerding, S. 2011. Development of an inhaled dry-powder formulation of Tobramycin using PulmoSphere™ technology. *J Aerosol Med Pulm Drug Deliv* 24:175-182.

[97] Dobry, D.E., Settell, D.M., Baumann, J.M., Ray, R.J., Graham, L.J., Beyerinck, R.A. 2009. A model-based methodology for spray-drying process development. *J Pharm Innov* 4:133-142.

[98] Baghel, S., Cathcart, H., O'Reilly, N.J. 2016. Polymeric amorphous solid dispersions: a review of amorphization, crystallization, stabilization, solid-state characterization, and aqueous solubilization of Biopharmaceutical Classification System Class II drugs. *J Pharm Sci* 105:2527-2544.

[99] Paudel, A., Worku, Z.A., Meeus, J., Guns, S., van den Mooter, G. 2013. Manufacturing of solid dispersions of poorly water soluble drugs by spray drying: formulation and process considerations. *Int J Pharm* 453:253-284.

[100] Singh, A., van den Mooter, G. 2016. Spray drying formulation of amorphous solid dispersions. *Adv Drug Deliv Rev* 100:27-50.

[101] Vasconcelos, T., Marques, S., das Neves, J., Sarmento, B. 2016. Amorphous solid dispersions: rational selection of a manufacturing process. *Adv Drug Deliv Rev* 100:85-101.

[102] Kaye, R.S., Purewal, T.S., Oya Alpar, H. 2009. Simultaneously manufactured nano-in-micro (SIMANIM) particles for dry-powder modified-release delivery of antibodies. *J Pharm Sci* 98:4055-4068.

[103] Lee, H.K., Park, J.H., Kwon, K.C. 1997. Double-walled microparticles for single shot vaccine. *J Control Release* 44:283-293.

[104] Thomas, T.T., Kohane, D.S., Wang, A., Langer, R. 2004. Microparticulate formulations for the controlled release of interleukin-2. *J Pharm Sci* 93:1100-1109.

[105] Ungaro, F., d'Angelo, I., Miro, A., La Rotonda, M.I., Quaglia, F. 2012. Engineered PLGA nano- and micro-carriers for pulmonary delivery: challenges and promises. *J Pharm Pharmacol* 64:1217-1235.

[106] Kutter, E., Sulakvelidze, A. 2005. *Bacteriophages: biology and applications*. Boca Raton: CRC Press.

[107] Huff, W.E., Huff, G.R., Rath, N.C., Balog, J.M., Donoghue, A.M. 2002. Prevention of *Escherichia coli* infection in broiler chickens with a bacteriophage aerosol spray. *Poult Sci* 81:1486-1491.

[108] Abedon, S.T. 2015. Phage therapy of pulmonary infections. *Bacteriophage* 5:e1020260.

[109] Abedon, S.T., Kuhl, S.J., Blasdel, B.G., Kutter, E.M. 2011. Phage treatment of human infections. *Bacteriophage* 1:66-85.

[110] Chan, B.K., Abedon, S.T., Loc-Carrillo, C. 2013. Phage cocktails and the future of phage therapy. *Future Microbiol* 8:769-783.

[111] Haq, I.U., Chaudhry, W.N., Akhtar, M.N., Andleeb, S., Qadri, I. 2012. Bacteriophages and their implications on future biotechnology: a review. *Virol J* 9:9.

[112] Hatfull, G.F., Vehring R. 2016. Respirable bacteriophage aerosols for the prevention and treatment of tuberculosis. In *Drug delivery systems for tuberculosis prevention and treatment*, ed. A.J. Hickey, A. Misra, P.B. Fourie, 277-292. Chichester: John Wiley & Sons, Ltd.

[113] Kutter, E., de Vos, D., Gvasalia, G. *et al*. 2010. Phage therapy in clinical practice: treatment of human infections. *Curr Pharm Biotechnol* 11:69-86.

[114] Loc-Carrillo, C., Abedon, S.T. 2011. Pros and cons of phage therapy. *Bacteriophage* 1:111-114.

[115] Merabishvili, M., Pirnay, J.P., Verbeken, G. *et al*. 2009. Quality-controlled small-scale production of a well-defined bacteriophage cocktail for use in human clinical trials. *PLoS ONE* 4:e4944.

[116] Międzybrodzki, R., Borysowski, J., Weber-Dąbrowska, B. *et al*. 2012. Chapter 3 – clinical aspects of phage therapy. *Adv Virus Res* 83:73-121.

[117] Parracho, H.M.R.T., Burrowes, B.H., Enright, M.C., McConville, M.L., Harper, D.R. 2012. The role of regulated clinical trials in the development of bacteriophage therapeutics. *J Mol Genet Med* 6:279-286.

[118] Semler, D.D., Goudie, A.D., Finlay, W.H., Dennis, J.J. 2014. Aerosol phage therapy efficacy in *Burkholderia cepacia* complex respiratory infections. *Antimicrob Agents Chemother* 58:4005-4013.

[119] Ślopek, S., Weber-Dąbrowska, B., Dąbrowski, M., Kucharewicz-Krukowska, K. 1987. Results of bacteriophage treatment of suppurative bacterial infections in the years 1981-1986. *Arch Immunol Ther Exp (Warsz)* 35:569-583

[120] Malik, D.J., Sokolov, I.J., Vinner, G.K. *et al*. 2017. Formulation, stabilisation and encapsulation of bacteriophage for phage therapy. *Adv Colloid Interface Sci* 249:100-133.

[121] Hoe, S., Semler, D.D., Goudie, A.D. *et al*. 2013. Respirable bacteriophages for the treatment of bacterial lung infections. *J Aerosol Med Pulm Drug Deliv* 26:317-335.

[122] Parisien, A., Allain, B., Zhang, J., Mandeville, R., Lan, C.Q. 2008. Novel alternatives to antbiotics: bacteriophages, bacterial cell wall hydrolases, and antimicrobial peptides. *J Appl Microbiol* 104:1-13.

[123] Kwok, P.C.L., Grabarek, A., Chow, M.Y.T. *et al*. 2015. Inhalable spray-dried formulation of D-LAK antimicrobial peptides targeting tuberculosis. *Int J Pharm* 491:367-374.

[124] Chang, R.Y.K., Chen, K., Wang, J. *et al*. 2018. Proof-of-principle study in a murine lung infection model of antipseudomonal activity of phage PEV20 in a dry-powder formulation. *Antimicrob Agents Chemother* 62:e01714-17.

[125] Sulakvelidze, A., Alavidze, Z., Glenn Morris, Jr., J., 2001. Bacteriophage therapy. *Antimicrob Agents Chemother* 45:649-659.

[126] Leung, S.S.Y., Parumasivam, T., Nguyen, A. *et al*. 2018. Effect of storage temperature on the stability of spray dried bacteriophage powders. *Eur J Pharm Biopharm* 127:213-222.

[127] Leung, S.S.Y., Parumasivam, T., Gao, F.G. *et al*. 2016. Production of inhalation phage powders using spray freeze drying and spray drying techniques for treatment of respiratory infections. *Pharm Res* 33:1486-1496.

[128] Leung, S.S.Y., Parumasivam, T., Gao, F.G. *et al*. 2017. Effect of storage conditions on the stability of spray dried, inhalable bacteriophage powders. *Int J Pharm* 521:141-149.

[129] Matinkhoo, S., Lynch, K.H., Dennis, J.J., Finlay, W.H., Vehring, R. 2011. Spray-dried respirable powders containing bacteriophages for the treatment of pulmonary infections. *J Pharm Sci* 100:5197-5205.

[130] Liu, H.F., Ma, J., Winter, C., Bayer, R. 2010. Recovery and purification process development for monoclonal antibody production. *mAbs* 2:480-499.

[131] Kelley, B. 2007. Very large scale monoclonal antibody purification: the case for conventional unit operations. *Biotechnol Prog* 23:995-1008.

[132] Gottschalk, U. 2017. *Process scale purification of antibodies, 2nd edition.* Hoboken: John Wiley & Sons, Inc.

[133] Gagnon, P. 2012. Technology trends in antibody purification. *J Chromatogr A* 1221:57-70.

[134] Azevedo, A.M., Rosa, P.A.J., Filipa Ferreira, I., Raquel Aires-Barros, M. 2009. Chromatography-free recovery of biopharmaceuticals through aqueous two-phase processing. *Trends Biotechnol* 27:240-247.

[135] Janson, J.C. 2011. *Protein purification: principles, high resolution methods, and applications, 3rd edition.* Hoboken: John Wiley & Sons, Inc.

[136] GE Healthcare. 2010. Strategies for protein purification: handbook. https://www.gelifesciences.com/en/bs/solutions/protein-research/knowledge-center/protein-handbooks (accessed June 21, 2017).

[137] Grzenia, D.L., Carlson, J.O., Ranil Wickramasinghe, S. 2008. Tangential flow filtration for virus purification. *J Membr Sci* 321:373-380.

[138] van Reis, R., Brake, J.M., Charkoudian, J., Burns, D.B., Zydney, A.L. 1999. High-performance tangential flow filtration using charged membranes. *J Membr Sci* 159:133-142.

[139] Withington, R. 2001. Regulatory issues for phage-based clinical products. *J Chem Technol Biotechnol* 76:673-676.

[140] European Medicines Agency. 2017. ICH guideline Q8 (R2) on pharmaceutical development. http://www.ema.europa.eu/docs/en_GB/document_library/Scientific_guideline/2009/09/WC500002872.pdf (accessed April 20, 2018).

[141] Hoe, S., Ivey, J.W., Boraey, M.A. *et al*. 2014. Use of a fundamental approach to spray-drying formulation design to facilitate the development of multi-component dry powder aerosols for respiratory drug delivery. *Pharm Res* 31:449-465.

[142] Chaul, L.T., Conceição, E.C., Bara, M.T.F., Paula, J.R., Couto, R.O. 2017. Engineering spray-dried rosemary extracts with improved physicomechanical properties: a design of experiments issue. *Rev Bras Farmacogn* 27:236-244.

[143] Faghihi, H., Najafabadi, A.R., Vatanara, A. 2017. Optimization and characterization of spray-dried IgG formulations: a design of experiments approach. *DARU J Pharm Sci* 25:22.

[144] Prinn, K.B., Costantino, H.R., Tracy, M. 2002. Statistical modeling of protein spray drying at the lab scale. *AAPS PharmSciTech* 3:E4.

[145] Saboo, S., Tumban, E., Peabody, J. *et al*. 2016. Optimized formulation of a thermostable spray-dried virus-like particle vaccine against human papillomavirus. *Mol Pharm* 13:1646-1655.

[146] de Jesus, S.S., Filho, R.M. 2014. Drying of α-amylase by spray drying and freeze-drying – a comparative study. *Braz J Chem Eng* 31:625-631.

[147] Branston, S., Stanley, E., Ward, J., Keshavarz-Moore, E. 2011. Study of robustness of filamentous bacteriophages for industrial applications. *Biotechnol Bioeng* 108:1468-1472.

[148] Maa, Y.F., Hsu, C.C. 1997. Protein denaturation by combined effect of shear and air-liquid interface. *Biotechnol Bioeng* 54:503-512.

[149] Levy, M.S., Collins, I.J., Yim, S.S. *et al*. 1999. Effect of shear on plasmid DNA in solution. *Bioprocess Biosyst Eng* 20:7-13.

[150] Beckard, I.B., Asimakis, P., Bertolini, J., Dunstan, D.E. 2011. The effect of shear flow on protein structure and function. *Biopolymers* 95:733-745.

[151] Biddlecombe, J.G., Craig, A.V., Zhang, H. *et al*. 2007. Determining antibody stability: creation of solid-liquid interfacial effects within a high shear environment. *Biotechnol Prog* 23:1218-1222.

[152] Cordova, A., Deserno, M., Gelbart, W.M., Ben-Shaul, A. 2003. Osmotic shock and the strength of viral capsids. *Biophys J* 85:70-74.

[153] Jończyk, E., Kłak, M., Międzybrodzki, R., Górski, A. 2011. The influence of external factors on bacteriophages-review. *Folia Microbiol (Praha)* 56:191-200.

[154] Drees, K.P., Abbaszadegan, M., Maier, R.M. 2003. Comparative electrochemical inactivation of bacteria and bacteriophage. *Water Res* 37:2291-2300.

[155] Nanjiao, Y., Rong, F., Juan, Z. Yong, Y. 2013. Inactivation of *Escherichia coli* phage by pulsed electric field treatment. *J Chem Pharm Res* 5:210-214.

[156] Plowright, W., Herniman, K.A.J., Rampton, C.S. 1971. Studies on rinderpest culture vaccine. IV. The stability of the reconstituted product. *Res Vet Sci* 12:40-46.

[157] Greene, G.I., Babel, F.J. 1948. Effect of ultraviolet irradiation on bacteriophage active against *Streptococcus lactis*. *J Dairy Sci* 31:509-515.

[158] Iriarte, F.B., Balogh, B., Momol, M.T., Smith, L.M., Wilson, M., Jones, J.B. 2007. Factors affecting survival of bacteriophage on tomato leaf surfaces. *Appl Environ Microbiol* 73:1704-1711.

[159] Iwasawa, Y., Ishihara, K. 1967. Resistance of *Staphylococcus aureus* to desiccation, heat and ultraviolet rays in relation to phage pattern. *Jpn J Microbiol* 11:305-309.

[160] Müller-Merbach, M., Rauscher, T., Hinrichs, J. 2005. Inactivation of bacteriophages by thermal and high-pressure treatment. *Int Dairy J* 15:777-784.

[161] Cambell-Renton, M.L. 1941. Experiments on drying and on freezing bacteriophage. *J Pathol* 53:371-384.

[162] Arribas, M., Kubota, K., Cabanillas, L., Lázaro, E. 2014. Adaptation to fluctuating temperatures in an RNA virus is driven by the most stringent selective pressure. *PLoS ONE* 9:e100940.

[163] Maassab, H.F., DeBorde, D.C. 1985. Development and characterization of cold-adapted viruses for use as live virus vaccines. *Vaccine* 3:355-369.

[164] Satpathy, G.R., Török, Z., Bali, R. *et al*. 2004. Loading red blood cells with trehalose: a steps towards biostabilization. *Cryobiology* 49:123-136.

[165] Santivarangkna, C., Higl, B., Foerst, P. 2008. Protection mechanisms of sugars during different stages of preparation process of dried lactic acid starter cultures. *Food Microbiol* 25:429-441.

[166] Ohtake, S., Wang, Y.J. 2011. Trehalose: current use and future applications. *J Pharm Sci* 100:2020-2053.

[167] Chang, R.Y., Wong, J., Mathai, A. *et al*. 2017. Production of highly stable spray dried phage formulations for the treatment of *Pseudomonas aeruginosa* lung infection. *Eur J Pharm Biopharm* 121:1-13.

[168] Feng, A.L., Boraey, M.A., Gwin, M.A., Finlay, P.R., Kuehl, P.J., Vehring, R. 2011. Mechanistic models facilitate efficient development of leucine containing microparticles for pulmonary drug delivery. *Int J Pharm* 409:156-163.

[169] Gliński, J., Chavepeyer, G., Platten, J.K. 2000. Surface properties of aqueous solutions of L-leucine. *Biophys Chem* 84:99-103.

[170] Lechuga-Ballesteros, D., Charan, C., Stults, C.L.M. *et al*. 2008. Trileucine improves aerosol performance and stability of spray-dried powders for inhalation. *J Pharm Sci* 97:287-302.

[171] Vehring, R., Foss, W.R., Lechuga-Ballesteros, D. 2007. Particle formation in spray drying. *J Aerosol Sci* 38:728-746.

[172] Chew, N.Y.K., Chan, H.K. 2001. Use of solid corrugated particles to enhance powder aerosol performance. *Pharm Res* 18:1570-1577.

[173] Ivey, J.W., Bhambri, P., Church, T.K., Lewis, D.A., Vehring, R. 2018. Experimental investigations of particle formation from propellant and solvent droplets using a monodisperse spray dryer. *Aerosol Sci Technol.* 52:702-716.

[174] Boraey, M.A., Hoe, S., Sharif, H., Miller, D.P., Lechuga-Ballesteros, D., Vehring, R. 2013. Improvement of the dispersibility of spray-dried budesonide powders using leucine in an ethanol-water cosolvent system. *Powder Technol* 236:171-178.

[175] Ji, S., Thulstrup, P.W., Mu, H. *et al*. 2016. Effect of ethanol as a co-solvent on the aerosol performance and stability of spray-dried lysozyme. *Int J Pharm* 513:175-182.

[176] Ibrahim, B.M., Jun, S.W., Lee, M.Y., Kang, S.H., Yeo, Y. 2010. Development of inhalable dry powder formulation of basic fibroblast growth factor. *Int J Pharm* 385:66-72.

[177] Manning, M.C., Chou, D.K., Murphy, B.M., Payne, R.W., Katayama, D.S. 2010. Stability of protein pharmaceuticals: an update. *Pharm Res* 27:544-575.

[178] Goebel-Stengel, M., Stengel, A., Taché, Y., Reeve Jr., J.R. 2011. The importance of using the optimal plastic and glassware in studies involving peptides. *Anal Biochem* 414:38-46.

[179] Hlady, V., Buijs, J. 1996. Protein adsorption on solid surfaces. *Curr Opin Biotechnol* 7:72-77.

[180] Höger, K., Mathes, J., Frieß, W. 2015. IgG1 adsorption to siliconized glass vials-influence of pH, ionic strength, and nonionic surfactants. *J Pharm Sci* 104:34-43.

[181] Mathes, J.M. 2010. Protein adsorption to vial surfaces – quantification, structural and mechanistic studies. PhD Diss., Ludwig-Maximilians-Universität München.

[182] Nakanishi, K., Sakiyama, T., Imamura, K. 2001. On the adsorption of proteins on solid surfaces, a common but very complicated phenomenon. *J Biosci Bioeng* 91:233-244.

[183] Rabe, M., Verdes, D., Seeger, S. 2011. Understanding protein adsorption at solid surfaces. *Adv Colloid Interface Sci* 162:87-106.

[184] MacRitchie, F. 1978. Proteins at interfaces. *Adv Protein Chem* 32:283-326.

[185] Abdul-Fattah, A.M., Kalonia, D.S., Pikal, M.J. 2007. The challenge of drying method selection for protein pharmaceuticals: product quality implications. *J Pharm Sci* 96:1886-1916.

[186] Lefebvre, A.H., McDonell, V.G. 2017. *Atomization and sprays, 2nd edition*. Boca Raton: CRC Press.

[187] Ashgriz, N. 2011. *Handbook of atomization and sprays: theory and applications*. New York: Springer Science+Business Media, LLC.

[188] Snyder, H.E., Lechuga-Ballesteros, D. 2008. Spray drying: theory and pharmaceutical applications. In *Pharmaceutical dosage forms – tablets: unit operations and mechanical properties, 3rd edition*, ed. L.L. Augsburger, S.W. Hoag, 227-260. Boca Raton: CRC Press.

[189] Cal, K., Sollohub, K. 2010. Spray drying technique. I: hardware and process parameters. *J Pharm Sci* 99:575-586.

[190] Thybo, P., Hovgaard, L., Andersen, S.K., Sæderup Lindeløv, J. 2008. Droplet size measurements for spray dryer scale-up. *Pharm Dev Technol* 13:93-104.

[191] Liu, W., Chen, X.D., Selomulya, C. 2015. On the spray drying of uniform functional microparticles. *Particuology* 22:1-12.

[192] Ameri, M., Maa, Y.F. 2006. Spray drying of biopharmaceuticals: stability and process considerations. *Drying Technol* 24:763-768.

[193] Vandenheuvel, D., Singh, A., Vandersteegen, K., Klumpp, J., Lavigne, R., van den Mooter, G. 2013. Feasibility of spray drying bacteriophages into respirable powders to combat pulmonary bacterial infections. *Eur J Pharm Biopharm* 84:578-582.

[194] Carrigy, N.B., Liang, L., Wang, H. *et al*. 2018. Mechanistic modeling expedites the development of spray dried biologics. Conference paper at the 21st International Drying Symposium 2018, Valencia.

[195] Abdul-Fattah, A.M., Truong, V.L. 2010. Drying process methods for biopharmaceutical products: an overview. In *Formulation and process development strategies for manufacturing biopharmaceuticals*, ed. F. Jameel, S. Hershenson, 705-738. Hoboken: John Wiley & Sons, Inc.

[196] Millqvist-Fureby, A., Malmsten, M., Bergenståhl, B. 1999. Spray-drying of trypsin – surface characterisation and activity preservation. *Int J Pharm* 188:243-253.

[197] Maa, Y.F., Prestrelski, S.J. 2000. Biopharmaceutical powders: particle formation and formulation considerations. *Curr Pharm Biotechnol* 1:283-302.

[198] Lee, G. 2002. Spray-drying of proteins. In *Rational design of stable protein formulations: theory and practice,* ed. J.F. Carpenter, M.C. Manning, 135-158. New York: Kluwer Academic/Plenum Publishers.

[199] Adler, M., Lee, G. 1999. Stability and surface activity of lactate dehydrogenase in spray-dried trehalose. *J Pharm Sci* 88:199-208.

[200] Adler, M., Unger, M., Lee, G. 2000. Surface composition of spray-dried particles of bovine serum albumin/trehalose/surfactant. *Pharm Res* 17:863-870.

[201] Mumenthaler, M., Hsu, C.C., Pearlman, R. 1994. Feasibility study on spray-drying protein pharmaceuticals: recombinant human growth hormone and tissue-type plasminogen activator. *Pharm Res* 11:12-20.

[202] Abdul-Fattah, A.M., Lechuga-Ballesteros, D., Kalonia, D.S., Pikal, M.J. 2008. The impact of drying method and formulation on the physical properties and stability of methionyl human growth hormone in the amorphous solid state. *J Pharm Sci* 97:163-184.

[203] Kawakami, K., Sumitani, C., Toshihashi, Y., Yonemochi, E., Terada, K. 2010. Investigation of the dynamic process during spray-drying to improve aerodynamic performance of inhalation particles. *Int J Pharm* 390:250-259.

[204] Nuzzo, M., Millqvist-Fureby, A., Sloth, J., Bergenstahl, B. 2015. Surface composition and morphology of particles dried individually and by spray drying. *Drying Technol* 33:757-767.

[205] Maa, Y.F., Costantino, H.R., Nguyen, P.A., Hsu, C.C. 1997. The effect of operating and formulation variables on the morphology of spray-dried protein particles. *Pharm Dev Technol* 2:213-223.

[206] Jaskulski, M., Wawrzyniak, P., Zbiciński, I. 2015. CFD model of particle agglomeration in spray drying. *Drying Technol* 33:1971-1980.

[207] Finlay, W.H. 2001. *The mechanics of inhaled pharmaceutical aerosol: an introduction*. London: Academic Press.

[208] Baldelli, A., Power, R.M., Miles, R.E.H., Reid, J.P., Vehring, R. 2016. Effect of crystallization kinetics on the properties of spray dried microparticles. *Aerosol Sci Technol* 50:693-704.

[209] Leong, K.H. 1987. Morphological control of particles generated from the evaporation of solution droplets: theoretical considerations. *J Aerosol Sci* 18:511-524.

[210] Boraey, M.A., Vehring, R. 2014. Diffusion controlled formation of microparticles. *J Aerosol Sci* 67:131-143.

[211] He, G., Bhamidi, V., Tan, R.B.H., Kenis, P.J.A., Zukoski, C.F. 2006. Determination of critical supersaturation from microdroplet evaporation experiments. *Cryst Growth Des* 6:1175-1180.

[212] Baldelli, A., Vehring, R. 2016. Control of the radial distribution of chemical components in spray-dried crystalline microparticles. *Aerosol Sci Technol* 50:1130-1142.

[213] Lin, R., Woo, M.W., Wu, Z. *et al*. 2017. Spray drying of mixed amino acids: the effect of crystallization inhibition and humidity treatment on the particle formation. *Chem Eng Sci* 167:161-171.

[214] Baldelli, A., Vehring, R. 2016. Analysis of cohesion forces between monodisperse microparticles with rough surfaces. *Coll Surf A* 506:179-189.

[215] Sou, T., Forbes, R., Gray, J. *et al*. 2016. Designing a multi-component spray-dried formulation platform for pulmonary delivery of biopharmaceuticals: the use of polyol, disaccharide, polysaccharide and synthetic polymer to modify solid-state properties for glass stabilization. *Powder Technol* 287:248-255.

[216] Yu, L., Mishra, D.S., Rigsbee, D.R. 1998. Determination of the glass properties of D-mannitol using sorbitol as an impurity. *J Pharm Sci* 87:774-777.

[217] Bergfors, T.M. 2001. *Protein crystallization: techniques, strategies, and tips: a laboratory manual.* La Jolla: International University Line.

[218] Roos, Y.H., Drusch, S. 2016. *Phase transition in foods, 2nd edition.* Kidlington: Academic Press.

[219] Hinds, W.C. 1999. *Aerosol technology: properties, behavior, and measurement of airborne particles, 2nd edition.* New York: John Wiley & Sons, Inc.

[220] Lintingre, E., Lequeux, F., Talini, L., Tsapis, N. 2016. Control of particle morphology in the spray drying of colloidal suspensions. *Soft Matter* 12:7435-7444.

[221] Biswas, P., Sen, D., Mazumder, S., Basak, C.B., Doshi, P. 2016. Temperature mediated morphological transition during drying of spray colloidal droplets. *Langmuir* 32:2464-2473.

[222] Boulogne, F., Giorgiutti-Dauphiné, F., Pauchard, L. 2013. The buckling and invagination process during consolidation of colloidal droplets. *Soft Matter* 9:750-757.

[223] Pathak, B., Basu, S. 2015. Phenomenology and control of buckling dynamics in multicomponent colloidal droplets. *J Appl Phys* 117:244901.

[224] Sadek, C., Pauchard, L., Schuck, P. *et al*. 2015. Mechanical properties of milk protein skin layers after drying: understanding the mechanisms of particle formation from whey protein isolate and native phosphocaseinate. *Food Hydrocoll* 48:8-16.

[225] Sen, D., Mazumder, S., Melo, J.S., Khan, A., Bhattyacharya, S., D'Souza, S.F. 2009. Evaporation driven self-assembly of a colloidal dispersion using spray drying: volume fraction dependent morphological transition. *Langmuir* 25:6690-6695.

[226] Sen, D., Melo, J.S., Bahadur, J. *et al*. 2010. Buckling-driven morphological transformation of droplets of a mixed colloidal suspension during evaporation-induced self-assembly by spray drying. *Eur Phys J E* 31:393-402.

[227] Tsapis, N., Dufresne, E.R., Sinha, S.S. *et al*. 2005. Onset of buckling in drying droplets of colloidal suspensions. *Phys Rev Lett* 94:018302.

[228] Bahadur, J., Sen, D., Mazumder, S., Bhattacharya, S., Frielinghaus, H., Goerigk, G. 2011. Origin of buckling phenomenon during drying of micrometer-sized colloidal droplets. *Langmuir* 27:8404-8414.

[229] Carlson, R.L., Sendelbeck, R.L., Hoff, N.J. 1967. Experimental studies of the buckling of complete spherical shells. *Exp Mech* 7:281-288.

[230] Sloth, J., Jørgensen, K., Bach, P., Jensen, A.D., Kiil, S., Dam-Johansen, K. 2009. Drying of suspensions for pharma and bio products: drying kinetics and morphology. *Ind Eng Chem Res* 48:3657-3664.

[231] Nandiyanto, A.B.D., Okuyama, K. 2011. Progress in developing spray-drying methods for the production of controlled morphology particles: from the nanometer to submicrometer size ranges. *Adv Powder Technol* 22:1-19.

[232] Weers, J., Tarara, T. 2014. The PulmoSphere™ platform for pulmonary drug delivery. *Ther Deliv* 5:277-295.

[233] Haig, C.W., Hursthouse, A., McIlwain, S., Skyes, D. 2014. The effect of particle agglomeration and attrition on the separation efficiency of a Stairmand cyclone. *Powder Technol* 258:110-124.

[234] Fletcher, D.F., Guo, B., Harvie, D.J.E., Langrish, T.A.G., Nijdam, J.J., Williams, J. 2006. What is important in the simulation of spray dryer performance and how do current CFD models performs? *Appl Math Model* 30:1281-1292.

[235] Keshani, S., Ramli Wan Daud, W., Nourouzi, M.M., Namvar, F., Ghasemi, M. 2015. Spray drying: an overview on wall deposition, process and modeling. *J Food Eng* 146:152-162.

[236] Langrish, T.A.G. 2007. New engineered particles from spray dryers: research needs in spray drying. *Drying Technol* 25:981-993.

[237] Lechuga-Ballesteros, D., Bakri, A., Miller, D.P. 2003. Microcalorimetric measurement of the interactions between water vapor and amorphous pharmaceutical solids. *Pharm Res* 20:308-318.

[238] Wong, J., Ricci, M., Chan, H.K. 2016. Spray drying strategies to stop tuberculosis. In *Drug delivery systems for tuberculosis prevention and treatment*, ed. A.J. Hickey, A. Misra, P.B. Fourie, 161-196. Chichester: John Wiley & Sons, Ltd.

[239] Shah, B., Kakumanu, V.K., Bansal, A.K. 2006. Analytical techniques for quantification of amorphous/crystalline phases in pharmaceutical solids. *J Pharm Sci* 95:1641-1665.

[240] Wang, H., Boraey, M.A., Williams, L., Lechuga-Ballesteros, D., Vehring, R. 2014. Low-frequency shift dispersive Raman spectroscopy for the analysis of respirable dosage forms. *Int J Pharm* 469:197-205.

[241] Vehring, R. 2005. Red-excitation dispersive Raman spectroscopy is a suitable technique for solid-state analysis of respirable pharmaceutical powders. *Appl Spectrosc* 59:286-292.

[242] Strachan, C.J., Rades, T., Gordon, K.C., Rantanen, J. 2007. Raman spectroscopy for quantitative analysis of pharmaceutical solids. *J Pharm Pharmacol* 59:179-192.
[243] Breen, E.D., Curley, J.G., Overcashier, D.E., Hsu, C.C., Shire, S.J. 2001. Effect of moisture on the stability of a lyophilized humanized monoclonal antibody formulation. *Pharm Res* 18:1345-1353.
[244] Mahlin, D., Bergström, C.A.S. 2013. Early drug development predictions of glass-forming ability and physical stability of drugs. *Eur J Pharm Sci* 49:323-332.
[245] Shur, J., Nevell, T.G., Ewen, R.J. *et al*. 2008. Cospray-dried unfractionated heparin with L-leucine as a dry powder inhaler mucolytic for cystic fibrosis therapy. *J Pharm Sci* 97:4857-4868.
[246] Li, L., Sun, S., Parumasivam, T. *et al*. 2016. L-leucine as an excipient against moisture on *in vitro* aerosolization performances of highly hygroscopic spray-dried powders. *Eur J Pharm Biopharm* 102:132-141.
[247] Fäldt, P., Bergenståhl, B., Carlsson, G. 1993. The surface coverage of fat on food powders analyzed by ESCA (electron spectroscopy for chemical analysis). *Food Struct* 12:225-234.
[248] Kim, E.H.J., Chen, X.D., Pearce, D. 2003. On the mechanisms of surface formation and the surface compositions of industrial milk powders. *Drying Technol* 21:265-278.
[249] Heng, D., Tang, P., Cairney, J.M. *et al*. 2007. Focused-ion-beam milling: a novel approach to probing the interior of particles used for inhalation aerosols. *Pharm Res* 24:1608-1617.
[250] Baldelli, A., Boraey, M.A., Nobes, D.S., Vehring, R. 2015. Analysis of the particle formation process of structured microparticles. *Mol Pharm* 12:2562-2573.
[251] Beker, M.J., Rapoport, A.I. 1987. Conservation of yeasts by dehydration. In *Advances in biochemical engineering/biotechnology*, ed. A. Fiechter, 127-171. Berlin: Springer-Verlag.
[252] Crowe, J.H., Hoekstra, F.A., Crowe, L.M. 1989. Membrane phase transitions are responsible for imbibitional damage in dry pollen. *Proc Natl Acad Sci USA* 86:520-523.
[253] Poirier, I., Maréchal, P.A., Richard, S., Gervais, P. 1999. *Saccharomyces cerevisiae* viability is strongly dependant on rehydration kinetics and the temperature of dried cells. *J Appl Microbiol* 86:87-92.
[254] Speck, M.L., Myers, R.P. 1946. The viability of dried skim-milk cultures of *Lactobacillus bulgaricus* as affected by the temperature of reconstitution. *J Bacteriol* 52:657-663.

[255] Wang, Y.C., Yu, R.C., Chou, C.C. 2004. Viability of lactic acid bacteria and bifidobacteria in fermented soymilk after drying, subsequent rehydration and storage. *Int J Food Microbiol* 93:209-217.

[256] Morgan, C.A., Herman, N., White, P.A., Vesey, G. 2006. Preservation of micro-organisms by drying; a review. *J Microbiol Methods* 66:183-193.

[257] Leach, R.H., Scott, W.J. 1959. The influence of rehydration on the viability of dried micro-organisms. *J Gen Microbiol* 21:295-307.

[258] Muller, J.A., Stanton, C., Sybesma, W., Fitzgerald, G.F., Ross, R.P. 2010. Reconstitution conditions for dried probiotic powders represent a critical step in determining cell viability. *J Appl Microbiol* 108:1369-1379.

[259] Hoekstra, F.A., Golovina, E.A., van Aelst, A.C., Hemminga, M.A. 1999. Imbibitional leakage from anhydrobiotes revisited. *Plant Cell Environ* 22:1121-1131.

[260] Ingvarsson, P.T., Yang, M., Nielsen, H.M., Rantanen, J., Foged, C. 2011. Stabilization of liposomes during drying. *Expert Opin Drug Deliv* 8:375-388.

[261] Crowe, L.M., Crowe, J.H., Rudolph, A., Womersley, C., Appel, L. 1985. Preservation of freeze-dried liposomes by trehalose. *Arch Biochem Biophys* 242:240-247.

[262] Marsh, D., Watts, A., Knowles, P.F. 1976. Evidence for phase boundary lipid. Permeability of Tempo-choline into dimyristoylphosphatidylcholine vesicles at the phase transition. *Biochemistry* 15:3570-3578.

[263] de Swart, R.L., LiCalsi, C., Quirk, A.V. *et al*. 2007. Measles vaccination of macaques by dry powder inhalation. *Vaccine* 25:1183-1190.

[264] Golshahi, L., Seed, K.D., Dennis, J.J., Finlay, W.H. 2008. Toward modern inhalational bacteriophage therapy: nebulization of bacteriophages of *Burkholderia cepacia* complex. *J Aerosol Med Pulm Drug Deliv* 21:351-359.

[265] Lentz, Y.K., Worden, L.R., Anchordoquy, T.J., Lengsfeld, C.S. 2005. Effet of jet nebulization on DNA: identifying the dominant degradation mechanism and mitigation methods. *J Aerosol Sci* 36:973-990.

[266] Cutts, F.T., Clements, C.J., Bennett, J.V. 1997. Alternative routes of measles immunization: a review. *Biologicals* 25:323-338.

[267] Roth, Y., Chapnik, J.S., Cole, P. 2003. Feasibility of aerosol vaccination in humans. *Ann Otol Rhinol Laryngol* 112:264-270.

[268] Sabin, A.B. 1983. Immunization against measles by aerosol. *Rev Infect Dis* 5:514-523.

[269] Jones, S.A., Martin, G.P., Brown, M.B. 2006. Stabilisation of deoxyribonuclease in hydrofluoroalkanes using miscible vinyl polymers. *J Control Release* 115:1-8.

[270] Liao, Y.H., Brown, M.B., Jones, S.A., Nazir, T., Martin, G.P. 2005. The effects of polyvinyl alcohol on the in vitro stability and delivery of spray-dried protein particles from surfactant-free HFA 134a-based pressurised metered dose inhalers. *Int J Pharm* 304:29-39.

[271] Carrigy, N.B., O'Reilly, C., Schmitt, J., Noga, M., Finlay, W.H. 2014. Effect of facial material softness and applied force on face mask dead volume, face mask seal, and inhaled corticosteroid delivery through an idealized infant replica. *J Aerosol Med Pulm Drug Deliv* 27:290-298.

[272] Dance Biopharm Inc. 2017. Dance Biopharm and Phillips-Medisize enter into joint development agreement for advanced inhaled insulin delivery. https://www.dancebiopharm.com/news-and-events/press-releases/detail/8/dance-biopharm-and-phillips-medisize-enter-into-joint (accessed April 20, 2018).

[273] Carrigy, N.B., Chang, R.Y., Leung, S.S.Y. *et al.* 2017. Anti-tuberculosis bacteriophage D29 delivery with a vibrating mesh nebulizer, jet nebulizer, and soft mist inhaler. *Pharm Res* 34:2084-2096.

[274] Arulmuthu, E.R., Williams, D.J., Baldascini, H., Versteeg, H.K., Hoare, M. 2007. Studies on aerosol delivery of plasmid DNA using a mesh nebulizer. *Biotechnol Bioeng* 98:939-955.

[275] Astudillo, A., Leung, S.S.Y., Kutter, E., Morales, S., Chan, H.K. 2018. Nebulization effects on structural stability of bacteriophage PEV 44. *Eur J Pharm Biopharm* 125:124-130.

[276] Carrigy, N.B., Ruzycki, C.A., Golshahi, L., Finlay, W.H. 2014. Pediatric *in vitro* and *in silico* models of deposition via oral and nasal inhalation. *J Aerosol Med Pulm Drug Deliv* 27:149-169.

[277] Carrigy, N.B., Martin, A.R., Finlay, W.H. 2015. Use of extrathoracic deposition models for patient-specific dose estimation during inhaler design. *Curr Pharm Des* 21:3984-3992.

[278] Finlay, W.H., Golshahi, L., Noga, M. 2012. New validated extrathoracic and pulmonary deposition models for infants and children. Conference paper at Respiratory Drug Delivery 2012, Tucson.

[279] Javaheri, E., Golshahi, L., Finlay, W.H. 2013. An idealized geometry that mimics average infant nasal airway deposition. *J Aerosol Sci* 55:137-148.

[280] Golshahi, L., Finlay, W.H. 2012. An idealized child throat that mimics average pediatric oropharyngeal deposition. *Aerosol Sci Technol* 46:i-iv.

[281] Ruzycki, C.A., Golshahi, L., Vehring, R., Finlay, W.H. 2014. Comparison of *in vitro* deposition of pharmaceutical aerosols in an idealized child throat with *in vivo* deposition in the upper respiratory tract of children. *Pharm Res* 31:1525-1535.

[282] Stapleton, K.W., Guentsch, E., Hoskinson, M.K., Finlay, W.H. 2000. On the suitability of κ-ε turbulence modeling for aerosol deposition in the mouth and throat: a comparison with experiment. *J Aerosol Sci* 31:739-749.

[283] Matida, E.A, Finlay, W.H., Lange, C.F., Grgic, B. 2004. Improved numerical simulation of aerosol deposition in an idealized mouth-throat. *J Aerosol Sci* 35:1-19.

[284] Copley Scientific. 2018. Alberta Idealised Throat (AIT). http://www.copleyscientific.com/home/inhaler-testing/aerodynamic-particle-size/improved-in-vitro-in-vivo-correlation-ivivc/alberta-idealised-throat-ait (accessed April 26, 2018).

[285] Depreter, F., Pilcer, G., Amighi, K. 2013. Inhaled proteins: challenges and perspectives. *Int J Pharm* 447:251-280.

[286] Xiong, X., Zhang, H.M., Wu, T.T. *et al*. 2014. Titer dynamic analysis of D29 within MTB-infected macrophages and effect on immune function of macrophages. *Exp Lung Res* 40:86-98.

[287] Lai, M.C., Topp, E.M. 1999. Solid-state chemical stability of proteins and peptides. *J Pharm Sci* 88:489-500.

[288] Lechuga-Ballesteros, D., Miller, D.P., Zhang, J. Residual water in amorphous solids: measurement and effects on stability. In *Amorphous food and pharmaceutical systems*, ed. H. Levine, 275-316. Cambridge: Royal Society of Chemistry Publishing.

[289] Zallen, R. 1983. *The physics of amorphous solids.* Weinheim: Wiley-VCH Verlag GmbH & Co. KGaA.

[290] Yu, L. 2001. Amorphous pharmaceutical solids: preparation, characterization and stabilization. *Adv Drug Deliv Rev* 48:27-42.

[291] Crowe, J.H., Carpenter, J.F., Crowe, L.M. 1998. The role of vitrification in anhydrobiosis. *Annu Rev Physiol* 60:73-103.

[292] Carpenter, J.F., Crowe, J.H. 1989. An infrared spectroscopic study of the interactions of carbohydrates with dried proteins. *Biochemistry* 28:3916-3922.

[293] Mensink, M.A., Frijlink, H.W., van der Voort Maarschalk, K., Hinrichs, W.L.J. 2017. How sugars protect proteins in the solid state and during drying (review): mechanisms of stabilization in relation to stress conditions. *Eur J Pharm Biopharm* 114:288-295.

[294] Arakawa, T., Prestrelski, S.J., Kenney, W.C., Carpenter, J.F. 2001. Factors affecting short-term and long-term stabilities of proteins. *Adv Drug Deliv Rev* 46:307-326.

[295] Vandenheuvel, D., Meeus, J., Lavigne, R., van den Mooter, G. 2014. Instability of bacteriophage in spray-dried trehalose powders is caused by crystallization of the matrix. *Int J Pharm* 472:202-205.

[296] Averett, D., Cicerone, M.T., Douglas, J.F., de Pablo, J.J. 2012. Fast relaxation and elasticity-related properties of trehalose-glycerol mixtures. *Soft Matter* 8:4936-4945.

[297] Weng, L., Elliott, G.D. 2015. Local minimum in fragility for trehalose/glycerol mixtures: implications for biopharmaceutical stabilization. *J Phys Chem B* 119:6820-6827.

[298] Laitinen, R., Löbmann, K., Strachan, C.J., Grohganz, H., Rades, T. 2013. Emerging trends in the stabilization of amorphous drugs. *Int J Pharm* 453:65-79.

[299] Cicerone, M.T., Soles, C.L. 2004. Fast dynamics and stabilization of proteins: binary glasses of trehalose and glycerol. *Biophys J* 86:3836-3845.

[300] Lechuga-Ballesteros, D., Miller, D.P. 2006. The hydration limit of amorphous solids and long-term stability. In *Water properties of food, pharmaceutical, and biological materials*, ed. M. del Pilar Buera, J. Welti-Chanes, P.J. Lillford, H.R. Corti, 303-308. Boca Raton: CRC Press.

[301] Chan, H.K., Clark, A.R., Feeley, J.C. *et al*. 2004. Physical stability of salmon calcitonin spray-dried powders for inhalation. *J Pharm Sci* 93:792-804.

[302] Miller, D.P., Lechuga-Ballesteros, D. 2006. Rapid assessment of the structural relaxation behavior of amorphous pharmaceutical solids: effect of residual water on molecular mobility. *Pharm Res* 23:2291-2305.

[303] Hancock, B.C., Shamblin, S.L., Zografi, G. 1995. Molecular mobility of amorphous pharmaceutical solids below their glass transition temperatures. *Pharm Res* 12:799-806.

[304] Andronis, V., Zografi, G. 1998. The molecular mobility of supercooled amorphous indomethacin as a function of temperature and relative humidity. *Pharm Res* 15:835-842.

[305] Yoshioka, M., Hancock, B.C., Zografi, G. 1994. Crystallization of indomethacin from the amorphous state below and above its glass transition temperature. *J Pharm Sci* 83:1700-1705.

[306] Verbeken, G., Pirnay, J.P., de Vos, D. *et al*. 2012. Optimizing the European regulatory framework for sustainable bacteriophage therapy in human medicine. *Arch Immunol Ther Exp (Warsz)* 60:161-172.

[307] World Health Organization. 2009. Stability testing of active pharmaceutical ingredients and finished pharmaceutical products. WHO Technical Report Series, No. 953, 2009 – Annex 2. http://apps.who.int/medicinedocs/en/d/Js19133en/ (accessed March 13, 2018).

[308] Mazzeo, A., Carpenter, P. 2009. Stability studies for biologics. In *Handbook of stability testing in pharmaceutical development: regulations, methodologies, and best practices*, ed. K. Huynh-Ba, 353-369. New York: Springer Science+Business Media, LLC.

[309] International Conference on Harmonisation. 1995. Stability testing of biotechnological/biological products: Q5C. http://www.ich.org/products/guidelines/quality/article/quality-guidelines.html (accessed April 20, 2018).

[310] Bajaj, S., Singla, D., Sakhuja, N. 2012. Stability testing of pharmaceutical products. *J Appl Pharm Sci* 02:129-138.

[311] U.S. Food & Drug Administration. 2003. Guidance for industry: Q1A(R2) stability testing of new drug substances and products. http://academy.gmp-compliance.org/guidemgr/files/Q1A(R2).PDF (accessed April 20, 2018).

[312] Kommanaboyina, B., Rhodes, C.T. 1999. Trends in stability testing, with emphasis on stability during distribution and storage. *Drug Dev Ind Pharm* 25:857-868.

[313] Allison, L.M.C., Mann, G.F., Perkins, F.T., Zuckerman, A.J. 1981. An accelerated stability test procedure for lyophilized measles vaccines. *J Biol Stand* 9:185-194.

[314] Greenspan, L. 1977. Humidity fixed points of binary saturated aqueous solutions. *J Res Natl Stand Sec A* 81A:89-96.

[315] Young, J.F. 1967. Humidity control in the laboratory using salt solutions–a review. *J Chem Technol Biotechnol*. 17:241-245.

[316] Weintraub, S. 2002. Demystifying silica gel. Proceedings of the Objects Specialty Group Session 30th Annual Meeting, Miami.

[317] Waterman, K.C., MacDonald, B.C. 2010. Package selection for moisture protection for solid, oral drug products. *J Pharm Sci* 99:4437-4452.

[318] Ivey, J.W., Vehring, R. 2010. The use of modeling in spray drying of emulsions and suspensions accelerates formulation and process development. *Comput Chem Eng* 34:1036-1040.
[319] Rumble, J.R. 2018. *CRC handbook of chemistry and physics, 98th edition*. Boca Raton: CRC Press.
[320] Teekamp, N., Tian, Y., Visser, J.C. *et al*. 2017. Addition of pullulan to trehalose glasses improves the stability of β-galactosidase at high moisture conditions. *Carbohydr Polym* 176:374-380.
[321] Iglesias, H.A., Chirife, J., Buera, M.P. 1997. Adsorption isotherm of amorphous trehalose. *J Sci Food Agric* 75:183-186.
[322] Fan, F., Roos, Y.H. 2016. Crystallization and structural relaxation times in structural strength analysis of amorphous sugar/whey protein systems. *Food Hydrocoll* 60:85-97.
[323] Roe, K.D., Labuza, T.P. 2005. Glass transition and crystallization of amorphous trehalose-sucrose mixtures. *Int J Food Prop* 8:559-574.
[324] Moynihan, C.T., Easteal, A.J., Wilder, J. Dependence of the glass transition temperature on heating and cooling rate. *J Phys Chem* 78:2673-2677.
[325] Gordon, M., Taylor, J.S. 1952. Ideal copolymers and the second-order transitions of synthetic rubbers. I. non-crystalline copolymers. *J Chem Technol Biotechnol* 2:493-500.
[326] Crowe, L.M., Reid, D.S., Crowe, J.H. 1996. Is trehalose special for preserving dry biomaterials? *Biophys J* 71:2087-2093.
[327] Chen, T., Fowler, A., Toner, M. 2000. Literature review: supplemented phase diagram of the trehalose-water binary mixture. *Cryobiology* 40:277-282.
[328] Gaspar, F., Vicente, J., Neves, F., Authelin, J.R. 2014. Spray drying: scale-up and manufacturing. In *Amorphous solid dispersions: theory and practice*, ed. N. Shah, H. Sandhu, D.S. Choi, H. Chokshi, A.W. Malick, 261-302. New York: Springer.
[329] Ananta, E., Volkert, M., Knorr, D. 2005. Cellular injuries and storage stability of spray-dried *Lactobacillus rhamnosus* GG. *Int Dairy J* 15:399-409.
[330] Kaakoush, N.O., Castaño-Rodríguez, N., Mitchell, H.M., and Man, S.M. (2015). Global epidemiology of *Campylobacter* infection. *Clin. Microbiol. Rev.* 28:687-720.
[331] Osano, O., and Arimi, S.M. (1999). Retail poultry and beef as sources of *Campylobacter jejuni. East Afr. Med. J.*. 76:141-143.

[332] Kittler, S., Fischer, S., Abdulmawjood, A., Glünder, G., and Klein, G. (2013). Effect of bacteriophage application on *Campylobacter jejuni* loads in commercial broiler flocks. *Appl. Env. Microbiol*. 79:7525-7533.

[333] Wagenaar, J.A., French, N.P., and Havelaar, A.H. (2013). Preventing Campylobacter at the source: why is it so difficult? *Clin. Infect. Dis.* 57:1600-1606.

[334] O'Reilly, C.E., Jaron, P., Ochieng, B., Nyaguara, A., Tate, J.E., Parsons, M.B. *et al*. (2012). Risk factors for death among children less than 5 years old hospitalized with diarrhea in rural western Kenya, 2005-2007: a cohert study. *PLoS Med.* 9:e1001256.

[335] World Health Organization, Food and Agricultural Organization of the United Nations & World Organisation for Animal Health. The Global View of Campylobacteriosis: Report of an Expert Consultation, Ultrecht, Netherlands, 9-11 July 2012. World Health Organization. Available at: http://www.who.int/iris/handle/10665/80751.

[336] Carron, M., Chang, Y.-M., Momanyi, K., Akoko, J., Kiiru, J., Bettridge, J., *et al*. (2018). *Campylobacter*, a zoonotic pathogen of global importance: prevalence and risk factors in the fast-evolving chicken meat system of Nairobi, Kenya. *PLoS Negl. Trop. Dis.* 12:e0006658.

[337] Loc Carrillo, C., Atterbury, R.J., El-Shibiny, A., Connerton, P.L., Dillon, E., Scott, A. *et al*. (2005). Bacteriophage therapy to reduce *Campylobacter jejuni* colonization of broiler chickens. *Appl. Env. Microbiol*. 71:6554-6563.

[338] Wagenaar, J.A., van Bergen, M.A.P., Mueller, M.A., Wassenaar, T.M., and Carlton, R.M. (2005). Phage therapy reduces *Campylobacter jejuni* colonization in broilers. *Vet. Microbiol.* 109:275-283.

[339] Firlieyanti, A.S., Connerton, P.L., and Connerton, I.F. (2016). Campylobacters and their bacteriophages from chicken liver: the prospect for phage biocontrol. *Int. J. Food Microbiol*. 237:121-127.

[340] Janež, N., Kokošin, A., Zaletel, E., Vranac, T., Kovač, J., Vučković, D. *et al.* (2014). Identification and characterization of new *Campylobacter* group III phages of animal origin. *FEMS Microbiol. Lett.* 359:64-71.

[341] Connerton, P.L., Timms, A.R., and Connerton, I.F. (2011). Campylobacter bacteriophages and bacteriophage therapy. *J. Appl. Microbiol*. 111:255-265.

[342] Kutter, E., and Sulakvelidze, A. (2005). *Bacteriophages: Biology and Applications*. Boca Raton: CRC Press.

[343] Kutter, E., de Vos, D., Gvasalia, G., Alavidze, Z., Gogokhia, L., Kuhl, S. *et al.* (2010). Phage therapy in clinical practice: treatment of human infections. *Curr. Pharm. Biotechnol.* 11:69-86.

[344] Loc-Carrillo, C., and Abedon, S.T. (2011). Pros and cons of phage therapy. *Bacteriophage* 1:111-114.

[345] Richards, P.J., Connerton, P.L. and Connerton, I.F. (2019). Phage biocontrol of *Campylobacter jejuni* in chickens does not produce collateral effects on the gut microbiota. *Front. Microbiol*. 10:476.

[346] Walters, R.H., Bhatnagar, B., Tchessalov, S., Izutsu, K.I., Tsumoto, K., and Ohtake, S. (2014). Next generation drying technologies for pharmaceutical applications. *J. Pharm. Sci.* 103:2673-2695.

[347] Afkhami, S., LeClair, D.A., Haddadi, S., Lai, R., Toniolo, S.P., Ertl, H.C. *et al*. (2017). Spray dried human and chimpanzee adenoviral-vectored vaccines are thermally stable and immunogenic *in vivo*. *Vaccine* 35:2916-2924.

[348] Weers, J.G., Tarara, T.E., and Clark, A.R. (2007). Design of fine particles for pulmonary drug delivery. *Expert Opin. Drug Deliv.* 4:297-313.

[349] Amorij, J.P., Huckriede, A., Wilschut, J., Frijlink, H.W., and Hinrichs, W.L.J. (2008). Development of stable influenza vaccine powder formulations: challenges and possibilities. *Pharm. Res.* 25:1256-1273.

[350] Chen, D., Kapre, S., Goel, A., Suresh, K., Beri, S., Hickling, J. *et al*. (2010). Thermostable formulations of a hepatitis B vaccine and a meningitis A polysaccharide conjugate vaccine produced by a spray drying method. *Vaccine* 28:5093-5099.

[351] Saluja, V., Amorij, J.P., Kapteyn, J.C., de Boer, A.H., Frijlink, H.W., and Hinrichs, W.L.J. (2010). A comparison between spray drying and spray freeze drying to produce an influenza subunit vaccine powder for inhalation. *J. Control. Release* 144:127-133.

[352] Kanojia, G., Willems, G.J., Frijlink, H.W., Kersten, G.F.A., Soema, P.C., and Amorij, J.P. (2016). A design of experiment approach to predict product and process parameters for a spray dried influenza vaccine. *Int. J. Pharm.* 511:1098-1111.

[353] Carrigy, N.B., and Vehring R. (2019). "Engineering Stable Spray Dried Biologic Powder for Inhalation," in *Pharmaceutical Inhalation Aerosol Technology, Third Edition*, ed. A.J. Hickey, S.R.P. da Rocha (Boca Raton, FL: CRC Press), Chapter 12.

[354] Quinn, Jr., J.J. (1965). The economics of spray drying. *Ind. Eng. Chem.* 57:35-37.

[355] Roser, B. (1991). Trehalose, a new approach to premium dried foods. *Trends Food Sci. Technol.* 2:166-169.

[356] Desai, K.G.H., and Park, H.J. (2005). Recent developments in microencapsulation of food ingredients. *Drying Technol.* 23:1361-1394.

[357] Holsinger, V.H., McAloon, A.J., Onwulata, C.I., and Smith, P.W. (2000). A cost analysis of encapsulated spray-dried milk fat. *J. Dairy Sci.* 83:2361-2365.

[358] Schwartzbach, H. (2011). Achieving aseptic drying with spray drying technologies. *Pharmaceutical Technology Europe* 23:90-92.

[359] Anandharamakrishnan, C., and Padma Ishwarya, S. (2015). *Spray drying techniques for food ingredient encapsulation*. Chichester: John Wiley & Sons, Ltd.

[360] Siew, A. (2016). Exploring the use of aseptic spray drying in the manufacture of biopharmaceutical injectables. *Pharmaceutical Technology* 40:24-27.

[361] Huang, S., Vignolles, M.-L., Chen, X.D., Le Loir, Y., Jan, G., Schuck, P. *et al*. (2017). Spray drying of probiotics and other food-grade bacteria: a review. *Trends Food Sci. Technol.* 63:1-17.

[362] Hoe, S., Boraey, M.A., Ivey, J.W., Finlay, W.H., and Vehring, R. (2014a). Manufacturing and device options for the delivery of biotherapeutics. *J. Aerosol Med. Pulm. Drug Deliv.* 27:315-328.

[363] Ledet, G.A., Graves, R.A., Bostanian, L.A., and Mandal, T.K. (2015). "Spray-drying of Biopharmaceuticals," in *Lyophilized Biologics and Vaccines: Modality-based Approaches*, ed. D. Varshney, and M. Singh (New York: Springer Science+Business Media), 273-297.

[364] Vehring, R. (2008). Pharmaceutical particle engineering via spray drying. *Pharm. Res.* 25:999-1022.

[365] Carlton, R.M. (1999). Phage therapy: past history and future prospects. *Arch. Immunol. Ther. Exp. (Warsz.)* 47:267-274.

[366] Matinkhoo, S., Lynch, K.H., Dennis, J.J., Finlay, W.H., and Vehring, R. (2011). Spray-dried respirable powders containing bacteriophages for the treatment of pulmonary infections. *J. Pharm. Sci.* 100:5197-5205.

[367] Leung, S.S.Y., Parumasivam, T., Gao, F.G., Carrigy, N.B., Vehring, R., Finlay, W.H. *et al*. (2016). Production of inhalation phage powders using spray freeze drying and spray drying techniques for treatment of respiratory infections. *Pharm. Res.* 33:1486-1496.

[368] Leung, S.S.Y., Parumasivam, T., Gao, F.G., Carter, E.A., Carrigy, N.B., Vehring, R. *et al*. (2017). Effect of storage conditions on the stability of spray dried, inhalable bacteriophage powders. *Int. J. Pharm.* 521:141-149.

[369] Leung, S.S.Y., Parumasivam, T., Nguyen, A., Gengenbach, T., Carter, E.A., Carrigy, N.B. *et al*. (2018). Effect of storage temperature on the stability of spray dried bacteriophage powders. *Eur. J. Pharm. Biopharm.* 127:213-222.

[370] Chang, R.Y., Wong, J., Mathai, A., Morales, S., Kutter, E., Britton, W. *et al*. (2017). Production of highly stable spray dried phage formulations for the treatment of *Pseudomonas aeruginosa* lung infection. *Eur. J. Pharm. Biopharm.* 121:1-13.

[371] Javed, M.A., Ackermann, M.-W., Azeredo, J., Carvalho, C.M., Connerton, I., Evoy, S. *et al*. (2014). A suggested classification for two groups of *Campylobacter* myoviruses. *Arch. Virol.* 159:181-190.

[372] Scott, A. E., Timms, A. R., Connerton, P. L., Carrillo, C. L., Radzum, K. A., and Connerton, I. F. (2007a). Genome dynamics of *Campylobacter jejuni* in response to bacteriophage predation. *PLoS Pathog*. 3:e119.

[373] Scott, A. E., Timms, A. R., Connerton, P. L., El-Shibiny, A., and Connerton, I. F. (2007b). Bacteriophage influence *Campylobacter jejuni* types populating broiler chickens. *Environ. Microbiol.* 9:2341–2353.

[374] Siringan, P., Connerton, P. L., Payne, R. J., and Connerton, I. F. (2011). Bacteriophage-mediated dispersal of *Campylobacter jejuni* biofilms. *Appl. Environ. Microbiol*. 77:3320–3326.

[375] Siringan, P., Connerton, P. L., Cummings, N. J., and Connerton, I. F. (2014). Alternative bacteriophage life cycles: the carrier state of *Campylobacter jejuni*. *Open Biol*. 4:130200.

[376] Brathwaite, K. J., Siringan, P., Connerton, P. L., and Connerton, I. F. (2015). Host adaption to the bacteriophage carrier state of *Campylobacter jejuni*. *Res. Microbiol*. 166:504–515.

[377] Carrigy, N.B., Chang, R.Y., Leung, S.S.Y., Harrison, M., Petrova, Z., Pope, W.H. *et al.* (2017). Anti-tuberculosis bacteriophage D29 delivery with a vibrating mesh nebulizer, jet nebulizer, and soft mist inhaler. *Pharm. Res.* 34:2084-2096.

[378] Cairns, B.J., Timms, A.R., Jansen, V.A.A., Connerton, I.F., and Payne, R.J.H. (2009). Quantitative models of *in vitro* bacteriophage-host dynamics and their application to phage therapy. *PLoS Pathog.* 5:e1000253.

[379] Wang, H., Boraey, M.A., Williams, L., Lechuga-Ballesteros, D., and Vehring, R. (2014). Low-frequency shift dispersive Raman spectroscopy for the analysis of respirable dosage forms. *Int. J. Pharm*. 469:197-205.

[380] Ahmadi, H., Radford, D., Kropinksi, A.M., Lim, L.T., and Balamurugan, S. (2017). Thermal-stability and reconstitution ability of *Listeria* phages P100 and A511. *Front. Microbiol.* 8:2375.

[381] Hoe, S., Ivey, J.W., Boraey, M.A., Shamsaddini-Shahrbabek, A., Javaheri, E., Matinkhoo, S. *et al.* (2014b). Use of a fundamental approach to spray-drying formulation design to facilitate the development of multi-component dry powder aerosols for respiratory drug delivery. *Pharm. Res.* 31:449-465.

[382] Boraey, M.A., and Vehring, R. (2014). Diffusion controlled formation of microparticles. *J. Aerosol Sci*. 67:131-143.

[383] Ghandi, A., Powell, I.B., Howes, T., Chen, X.D., and Adhikari, B. (2012). Effect of shear rate and oxygen stresses on the survival of *Lactococcus lactis* during the atomization and drying stages of spray drying: a laboratory and pilot scale study. *J. Food Eng.* 113:194-200.

[384] Masters, K. (1972). *Spray Drying: An Introduction to Principles, Operational Practice and Applications*. London: Leonard Hill.

[385] Vandenheuvel, D., Meeus, J., Lavigne, R., van den Mooter, G. 2014. Instability of bacteriophage in spray-dried trehalose powders is caused by crystallization of the matrix. *Int J Pharm* 472:202-205.

[386] Teekamp, N., Tian, Y., Visser, J.C., Olinga, P., Frijlink, H.W., Woerdenbag, H.J. *et al*. (2017). Addition of pullulan to trehalose glasses improves the stability of β-galactosidase at high moisture contents. *Carbohydr. Polym*. 176:374-380.

[387] Leung, V., Szewczyk, A., Chau, J., Hosseinidoust, Z., Groves, L., Hawsawi, H., Anany, H., Griffiths, H.W., Ali, M.M., Filipe, C.D.M., 2018. Long-term preservation of bacteriophage antimicrobials using sugar glasses. ACS Biomater. Sci. Eng. 4, 3802-2808.

[388] Cambell-Renton, M.L. (1941). Experiments on drying and on freezing bacteriophage. *J. Pathol.* 53:371-384.

[389] Ohtake, S., Martin, R.A., Yee, L., Chen, D., Kristensen, D.D., Lechuga-Ballesteros, D. *et al*. (2010). Heat-stable measles vaccine produced by spray drying. *Vaccine* 28:1275-1284.

[390] Tlaxca, J.L., Ellis, S., and Remmele Jr., R.L. (2015). Live attenuated and inactivated viral vaccine formulation and nasal delivery: potential and challenges. *Adv. Drug Deliv. Rev.* 93:56-78.

[391] Lovalenti, P.M., Anderl, J., Yee, L., Nguyen, V., Ghavami, B., Ohtake, S. *et al*. (2016). Stabilization of live attenuated influenza vaccines by freeze drying, spray drying, and foam drying. *Pharm. Res.* 33:1144-1160.

[392] Hoe, S., Semler, D.D., Goudie, A.D., Lynch, K.H., Matinkhoo, S., Finlay, W.H. *et al.* (2013). Respirable bacteriophages for the treatment of bacterial lung infections. *J. Aerosol. Med. Pulm. Drug Deliv.* 26:317-335.

[393] Sahota, J.S., Smith C.M., Radhakrishnan, P., Winstanley, C., Goderdzishvili, M., Chanishvili, N., et al. (2015). Bacteriophage delivery by nebulization and efficacy against phenotypically diverse pseudomonas aeruginosa from cystic fibrosis patients. *J. Aerosol Med. Pulm. Drug Deliv.* 28:353-360.

[394] Astudillo, A., Leung, S.S.Y., Kutter, E., Morales, S., and Chan, H.K. (2018). Nebulization effects on structural stability of bacteriophage PEV 44. *Eur. J. Pharm. Biopharm.* 125:124-130.

[395] Lechuga-Ballesteros, D., Charan, C., Stults, C.L.M., Stevenson, C.L., Miller, D.P., Vehring, R. *et al*. (2008). Trileucine improves aerosol performance and stability of spray-dried powders for inhalation. *J. Pharm. Sci.* 97:287-302.

[396] Singh, R.S., and Saini, G.K. (2012). "Biosynthesis of pullulan and its applications in food and pharmaceutical industry," in *Microorganisms in Sustainable Agriculture and Biotechnology*, T. Satyanarayana, B.N. Johri, and A. Prakash (Dordrecht: Springer Science+Business Media B.V.), 509-553.

[397] European Food Safety Authority. (2004). Opinion of the Scientific Panel on food additives, flavourings, processing aids and materials in contact with food (AFC) on request from the Commission related to Pullulan PI-20 for use as a new food additive. *EFSA Journal* 85:1-32.

[398] Leathers, T.D. (2003). Biotechnology production and applications of pullulan. *Appl. Microbiol. Biotechnol.* 62:468-473.

[399] Carrigy, N.B., Vehring, R., 2019. Engineering stable spray dried biologic powder for inhalation, in: Hickey, A.J., da Rocha, S.R.P. (Eds.), Pharmaceutical Inhalation Aerosol Technology, Third Edition. CRC Press, Boca Raton, pp. 291-326.

[400] Walters, R.H., Bhatnagar, B., Tchessalov, S., Izutsu, K.I., Tsumoto, K., Ohtake, S., 2014. Next generation drying technologies for pharmaceutical applications. J. Pharm. Sci. 103, 2673-2695. https://doi.org/10.1002/jps.23998.

[401] Schwartzbach, H., 2011. Achieving aseptic drying with spray drying technologies. Pharmaceutical Technology Europe 23, 90-92. http://www.pharmtech.com/achieving-aseptic-drying-spray-drying-technologies

[402] Siew, A., 2016. Exploring the use of aseptic spray drying in the manufacture of biopharmaceutical injectables. Pharmaceutical Technology 40, 24-27. http://www.pharmtech.com/exploring-use-aseptic-spray-drying-manufacture-biopharmaceutical-injectables.

[403] Evaluate Ltd., 2017. EvaluatePharma® World Preview 2017, Outlook to 2022. http://www.evaluategroup.com/public/Reports/EvaluatePharma-World-Preview-2017.aspx (accessed March 9, 2018).

[404] Walsh, G., 2014. Biopharmaceutical benchmarks 2014. Nat. Biotechnol. 32, 992-1000. https://doi.org/10.1038/nbt.3040.

[405] Teekamp, N., Tian, Y., Visser, J.C., Olinga, P., Frijlink, H.W., Woerdenbag, H.J., Hinrichs, W.L.J., 2017. Addition of pullulan to trehalose glasses improves the stability of β-galactosidase at high moisture conditions. Carbohydr. Polym. 176, 374-380. https://doi.org/10.1016/j.carbpol/2017.08.084.

[406] Tian, Y., Visser, C.J., Klever, J.S., Woerdenbag, H.J., Frijlink, H.W., Hinrichs, W.L.J., 2018. Orodispersible films based on blends of trehalose and pullulan for protein delivery. Eur. J. Pharm. Biopharm. 133, 104-111. https://doi.org/10.1016/j.ejpb.2018.09.016.

[407] Leung, V., Szewczyk, A., Chau, J., Hosseinidoust, Z., Groves, L., Hawsawi, H., Anany, H., Griffiths, H.W., Ali, M.M., Filipe, C.D.M., 2018. Long-term preservation of bacteriophage antimicrobials using sugar glasses. ACS Biomater. Sci. Eng. 4, 3802-2808. https://doi.org/10.1021/acsbiomaterials.7b00468.

[408] di Stefano, F., 2017. Pullulan as release enhancer for controlled release capsular device: performance assessment and preparation methods. M.Sc. Thesis. Department of Chemistry, Materials and Chemical Engineering, Politecnico di Milano, Milan, Italy.

[409] Leathers, T.D., 2003. Biotechnological production and applications of pullulan. Appl. Microbiol. Biotechnol. 62, 468-473. https://doi.org/10.1007/s00253-003-1386-4.

[410] European Food Safety Authority, 2004. Opinion of the Scientific Panel on food additives, flavourings, processing aids and materials in contact with food (AFC) on request from the Commission related to Pullulan PI-20 for use as a new food additive. EFSA J. 85, 1-32. https://doi.org/10.2903/j.efsa.2004.85.

[411] United States Food and Drug Administration, 2019a. GRAS Notices: GRN No. 99. https://www.accessdata.fda.gov/scripts/fdcc/index.cfm?set=GrASNotices&id=99&sort=GRN_No&order=DESC&startrow=1&type=advanced&search=%C2%A4%C2%A4pullulan%C2%A4 (accessed 26 March 2019).

[412] Rekha, M.R., Sharma, C.P., 2007. Pullulan as a promising biomaterial for biomedical applications: a perspective. Trends Biomater. Artif. Organs 20, 116-121.

[413] Sugumaran, K.R., Ponnusami, V., 2017. Review of production, downstream processing and characterization of microbial pullulan. Carbohydr. Polym. 173, 573-591. https://doi.org/10.1016/j.carbpol.2017.06.022.

[414] Crowe, J.H., Carpenter, J.F., Crowe, L.M., 1998. The role of vitrification in anhydrobiosis. Annu. Rev. Physiol. 60, 73-103. https://doi.org/10.1146/annurev.physiol.60.1.73.

[415] United States Food and Drug Administration, 2019b. GRAS Notices: GRN No. 45. https://www.accessdata.fda.gov/scripts/fdcc/index.cfm?set=GrASNotices&id=45 (accessed 26 March 2019).

[416] Ohtake, S., Wang, Y.J., 2011. Trehalose: current use and future applications. J. Pharm. Sci. 100, 2020-2053. https://doi.org/10.1002/jps.22458.

[417] Gomez, M., Ordoubadi, M., McAllister, R.A., Melhem, O., Barona, D., Gracin, S., Ajmera, A., Lechuga-Ballesteros, D., Finlay, W.H., Vehring, R., 2018. Monodisperse droplet chain technique to support development of co-solvent based inhalation products, in: Dalby, R.N., Byron, P.R., Hindle, M., Peart, J., Traini, D., Young, P.M., Farr, S.J., Suman, J.D., Watts, A. (Eds.), Respiratory Drug Delivery 2018, Vol. 2. Tuscon, pp. 563-568.

[418] Vehring, R., 2008. Pharmaceutical particle engineering via spray drying. Pharm. Res. 25, 999-1022. https://doi.org/10.1007/s11095-007-9475-1.

[419] Vehring, R., Foss, W.R., Lechuga-Ballesteros, D., 2007. Particle formation in spray drying. J. Aerosol Sci. 38, 728-746. https://doi.org/10.1016/j.aerosci.2007.04.005.

[420] Nishinari, K., Kohyama, K., Williams, P.A., Phillips, G.O., Burchard, W., Ogino, K., 1991. Solution properties of pullulan. Macromolecules 24, 5590-5593. https://doi.org/10.1021/ma00020a017.

[421] Grasmeijer, N., Frijlink, H.W., Hinrichs, W.L.J., 2016. Model to predict inhomogeneous protein-sugar distribution in powders prepared by spray drying. J. Aerosol Sci. 101, 22-33. https://doi.org/10.1016/j.jaerosci.2016.07.012.

[422] Sangon Biotech, 2018. Safety Data Sheets: Pullulan. https://www.sangon.com/productImage/SDS/A506209/A506209_EN_S.pdf (accessed January 18, 2019).

[423] Ordoubadi, M., Gregson, F., Finlay, W.H., Vehring, R., Reid, J.P., 2018. Interaction of evaporating multicomponent microdroplets with humid environments, in: Dalby, R.N., Byron, P.R., Hindle, M., Peart, J., Traini, D., Young, P.M., Farr, S.J., Suman, J.D., Watts, A. (Eds.), Respiratory Drug Delivery 2018, Vol. 2. Tuscon, pp. 569-572.

[424] Baldelli, A., Power, R.M., Miles, R.E.H., Reid, J.P., Vehring, R., 2016. Effect of crystallization kinetics on the properties of spray dried microparticles. Aerosol Sci. Technol. 50, 693-704. https://doi.org/10.1080/02786826.2016.1177163.

[425] Ekdavi-Sever, N., de Pablo, J.J., Feick, E., von Meerwall, E., 2003. Diffusion of sucrose and alpha, alpha-trehalose in aqueous solution. J. Phys. Chem. A. 107, 936-943. https://doi.org/10.1021/jp020187b.

[426] Gordon, M., Taylor, J.S., 1952. Ideal copolymers and the second-order transitions of synthetic rubbers. I. non-crystalline copolymers. J. Chem. Technol. Biotechnol. 2, 493-500. https://doi.org/10.1002/jctb.5010020901.

[427] Hoe, S., Ivey, J.W., Boraey, M.A., Shamsaddini-Shahrbabek, A., Javaheri, E., Matinkhoo, S., Finlay, W.H., Vehring, R., 2014. Use of a fundamental approach to spray-drying formulation design to facilitate the development of multi-component dry powder aerosols for respiratory drug delivery. Pharm. Res. 31, 449-465. https://doi.org/10.1007/s11095-013-1174-5.

[428] Fox, T.G., 1956. Influence of diluent and copolymer composition on the glass temperature of a polymer system. Bull. Am. Phys. Soc. 1, 123-128.

[429] Shahrbabak, A.S., 2013. Uniaxial compression of pharmaceutical powders. M.Sc. Thesis, Department of Mechanical Engineering, University of Alberta, Edmonton, Canada.

[430] United States Pharmacopeia, 2017. <601> Aerosols, nasal sprays, metered-dose inhalers, and dry powder inhalers.

[431] Krüger, P., Ehrlein, B., Zeir, M., Greguletz, R., 2014. Inspiratory flow resistance of marketed dry powder inhaler (DPI). Eur. Respir. J. 44, 4635.

[432] Ruzycki, C.A., Martin, A.R., Vehring, R., Finlay, W.H., 2018. An *in vitro* examination of the effects of altitude on dry powder inhaler performance. J. Aerosol Med. Pulm. Drug Deliv. 31, 221-236. https://doi.org/10.1089/jamp.2017.1417.

[433] Marple, V.A., Olson, B.A., Santhanakrishnan, K., Mitchell, J., Murray, S.C., Hudson-Curtis, B.L., 2003. Next generation pharmaceutical impactor (a new impactor for pharmaceutical inhaler testing). Part II: archival calibration. J. Aerosol Med. Pulm. Drug Deliv. 16, 301-324. https://doi.org/10.1089/089426803769017668.

[434] Matinkhoo, S., Lynch, K.H., Dennis, J.J., Finlay, W.H., Vehring, R., 2011. Spray-dried respirable powders containing bacteriophages for the treatment of pulmonary infections. J. Pharm. Sci. 100, 5197-5205. https://doi.org/10.1002/jps.22715.

[435] Wang, H., Bhambri, P., Ivey, J., Vehring, R., 2017. Design and pharmaceutical applications of a low-flow-rate single-nozzle impactor. Int. J. Pharm. 533, 14-25. https://doi.org/10.1016/j.ijpharm.2017.09.047.

[436] Wang, H., Boraey, M.A., Williams, L., Lechuga-Ballesteros, D., Vehring, R., 2014. Low-frequency shift dispersive Raman spectroscopy for the analysis of respirable dosage forms. Int. J. Pharm. 469, 197-205. https://doi.org/10.1016/j.ijpharm.2014.04.058.

[437] Kato, T., Okamoto, T., Tokuya, T., Takahashi, A., 1982. Solution properties and chain flexibility of pullulan in aqueous solution. Biopolymers. 21, 1623-1633. https://doi.org/10.1002/bip.360210812.

[438] Tsapis, N., Dufresne, E.R., Sinha, S.S., Riera, C.S., Hutchinson, J.W., Mahadevan, L. Weitz, D.A., 2005. Onset of buckling in drying droplets of colloidal suspensions. Phys. Rev. Lett. 94, 018302. https://doi.org/10.1103/PhysRevLett.94.018302.

[439] Lechuga-Ballesteros, D., Charan, C., Stults, C.L.M., Stevenson, C.L., Miller, D.P., Vehring, R., Tep, V., Kuo, M.C., 2008. Trileucine improves aerosol performance and stability of spray-dried powders for inhalation. J. Pharm. Sci. 97, 287-302. https://doi.org/10.1002/jps.21078.

[440] Feng, A.L., Boraey, M.A., Gwin, M.A., Finlay, P.R., Kuehl, P.J., Vehring, R., 2011. Mechanistic models facilitate efficient development of leucine containing microparticles for

pulmonary drug delivery. Int. J. Pharm. 409, 156-163. https://doi.org/10.1016/j.ijpharm.2011.02.049.

[441] Finlay, W.H., 2001. The mechanics of inhaled pharmaceutical aerosol: an introduction. Academic Press, London.

[442] Wang, H., Nobes, D.S., Vehring, R., 2019. Particle surface roughness improves colloidal stability of pressurized pharmaceutical suspensions. Pharm. Res. 36, 43. https://doi.org/10.1007/s11095-019-2572-0.

[443] Ventola CL. The antibiotic resistance crisis. Part 1: Causes and Threats. P&T. 2015;40(4):277-283.

[444] World Health Organization. Multidrug-resistant tuberculosis (MDR-TB): 2016 Update. 2016 [Accessed 2017 February 21]. Available from: http://www.who.int/tb/challenges/mdr/mdr_tb_factsheet.pdf.

[445] Udwadia ZF, Amale RA, Ajbani KK, Rodrigues C. Totally drug-resistant tuberculosis in India. Clin Infect Dis. 2012;54(4):579-581.

[446] World Health Organization. Drug-resistant TB: Totally drug-resistant TB FAQ. 2017 [Accessed 2017 February 21]. Available from: http://www.who.int/tb/areas-of-work/drug-resistant-tb/totally-drug-resistant-tb-faq/en/.

[447] Abedon ST, Kuhl SJ, Blasdel BG, Kutter EM. Phage treatment of human infections. Bacteriophage. 2011;1(2):66-85.

[448] Kutateladze M, Adamia R. Bacteriophages as potential new therapeutics to replace or supplement antibiotics. Trends Biotechnol. 2010;28(12):591-595.

[449] Verbeken G, Huys I, Pirnay J-P, Jennes S, Chanishvili N, Scheres J, Gorski A, de Vos D, Ceulemans C. Taking bacteriophage therapy seriously: a moral argument. BioMed Res Int. 2014: 621316.

[450] Hatfull GF, Vehring R. Respirable bacteriophage aerosols for the prevention and treatment of tuberculosis. In: Hickey AJ, Misra A, Fourie PB, editors. Drug delivery systems for tuberculosis prevention and treatment. Chichester, UK: John Wiley & Sons, Ltd.; 2016. pp. 277-292.

[451] Loc-Carrillo C, Abedon ST. Pros and cons of phage therapy. Bacteriophage. 2011;1(2):111-114.

[452] Kutter E, Sulakvelidze A. Bacteriophages: biology and applications. Boca Raton: CRC Press; 2005.

[453] Hoe S, Semler DD, Goudie AD, Lynch KH, Matinkhoo S, Finlay WH, Dennis JJ, Vehring R. Respirable bacteriophages for the treatment of bacterial lung infections. J Aerosol Med Pulm Drug Deliv. 2013;26(6):317-335.
[454] Kutter E, de Vos D, Gvasalia G, Alavidze Z, Gogokhia L, Kuhl S, Abedon ST. Phage therapy in clinical practice: treatment of human infections. Curr Pharm Biotechnol. 2010;11(1):69-86.
[455] Hoe S, Boraey MA, Ivey JW, Finlay WH, Vehring R. Manufacturing and device options for the delivery of biotherapeutics. J Aerosol Med Pulm Drug Deliv. 2014;27(5):315-328.
[456] Golshahi L, Seed KD, Dennis JJ, Finlay WH. Toward modern inhalational bacteriophage therapy: nebulization of bacteriophages of Burkholderia cepacia complex. J Aerosol Med Pulm Drug Deliv. 2008;21(4):351-360.
[457] Matinkhoo S, Lynch KH, Dennis JJ, Finlay WH, Vehring R. Spray-dried respirable powders containing bacteriophages for the treatment of pulmonary infections. J Pharm Sci. 2011;100(12):5197-5205.
[458] Leung SY, Parumasivam T, Gao FG, Carrigy NB, Vehring R, Finlay WH, Morales S, Britton WJ, Kutter E, Chan H-K. Production of inhalation phage powders using spray freeze drying and spray drying techniques for treatment of respiratory infections. Pharm Res. 2016;33(6):1486-1496.
[459] Golshahi L, Lynch KH, Dennis JJ, Finlay WH. In vitro lung delivery of bacteriophages KS4-M and ϕKZ using dry powder inhalers for treatment of Burkholderia cepacia complex and Pseudomonas aeruginosa infections in cystic fibrosis. J Appl Microbiol. 2011;110(1):106-117.
[460] Parracho HMRT, Burrowes BH, Enright MC, McConville ML, Harper DR. The role of regulated clinical trials in the development of bacteriophage therapeutics. J Mol Genet Med. 2012;6:279-286.
[461] Verbeken G, Pirnay J-P, de Vos D, Jennes S, Zizi M, Lavigne R, Casteels M, Huys I. Optimizing the European regulatory framework for sustainable bacteriophage therapy in human medicine. Arch Immunol Ther Exp (Warsz). 2012;60(3):161-172.
[462] Abedon ST. Phage therapy of pulmonary infections. Bacteriophage. 2015;5(1):1-13.
[463] Semler DD, Goudie AD, Finlay WH, Dennis JJ. Aerosol phage therapy efficacy in Burkholderia cepacia complex respiratory infections. Antimicrob Agents Chemother. 2014;58(7):4005-4013.

[464] Liu K-Y, Yang W-H, Dong X-K, Cong L-M, Li N, Li Y, Wen Z-B, Yin Z, Lan Z-J, Li W-P, Li J-S. Inhalation study of mycobacteriophage D29 aerosol for mice by endotracheal route and nose-only exposure. J Aerosol Med Pulm Drug Deliv. 2016;29(5):393-405.

[465] Cooper CJ, Denyer SP, Maillard J-Y. Stability and purity of a bacteriophage cocktail preparation for nebulizer delivery. *Letters in Applied Microbiology.* 2013;58(2):118-122.

[466] Sahota JS, Smith CM, Radhakrishnan P, Winstanley C, Goderdzishvili M, Chanishvili N, Kadioglu A, O'Callaghan C, Clokie MR. Bacteriophage Delivery by Nebulization and Efficacy Against Phenotypically Diverse Pseudomonas aeruginosa from Cystic Fibrosis Patients. J Aerosol Med Pulm Drug Deliv. 2015;28(5):353-360.

[467] Froman S, Will DW, Bogen E. Bacteriophage active against virulent mycobacterium tuberculosis I. isolation and activity. Am J Public Health Nations Health. 1954;44(10):1326-1333.

[468] phagesDB.org. Phage hunting procedure & protocols. 2016 December 2. Available from: phagesdb.org/workflow/.

[469] Engel M, Heinrichs S. Use of tiotropium salts in the treatment of moderate persistent asthma. 2015. Patent US 20150224090 A1.

[470] Dalby R, Spallek M, Voshaar T. A review of the development of Respimat Soft Mist Inhaler. Int J Pharm. 2004;283(1-2):1-9.

[471] Dalby R, Eicher J, Zierenberg B. Development of Respimat® Soft Mist™ Inhaler and its clinical utility in respiratory disorders. Med Devices (Auckl). 2011;4:145-155.

[472] Finlay WH. The mechanics of inhaled pharmaceutical aerosols: an introduction. San Diego: Academic Press; 2001.

[473] Fink JB. New technology offers new opportunities: continuous bronchodilator therapy during mechanical ventilation. [Accessed 2017 February 22]. Available from: https://www.aerogen.com/uploads/Publications/Continuous%20Bronchodilator%20Therapy%20During%20Mechanical%20Ventilation%20Jim%20Fink.pdf.

[474] May KR. The collison nebulizer: description, performance and application. J Aerosol Sci. 1973;4(3):235-243.

[475] Lentz YK, Worden LR, Anchordoquy TJ, Lengsfeld CS. Effect of jet nebulization on DNA: identifying the dominant degradation mechanism and mitigation methods. J Aerosol Sci. 2005;36(8):973-990.

[476] Liu K, Wen Z, Yang W, Wang J, Hu L, Dong X, Lu J, Li J. Impact of relative humidity and collection media on mycobacteriophage D29 aerosol. Appl Environ Microbiol. 2012;78(5):1466-1472.

[477] Arulmuthu ER, Williams DJ, Baldascini H, Versteeg HK, Hoare M. Studies on aerosol delivery of plasmid DNA using a mesh nebulizer. Biotechnol Bioeng. 2007;98(5):939-955.

[478] Sidler-Moix A-L, Di Paolo ER, Dolci U, Berger-Gryllaki M, Cotting J, Pannatier A. Physicochemical aspects and efficiency of albuterol nebulization: comparison of three aerosol types in an in vitro pediatric model. Respir Care. 2015;60(1):38-46.

[479] Fédération Antadir Commission Medico-Technique & Sociale. Fiche de synthese du dispositif: Pari Boy SX / Pari LC® Sprint SP. 2007 Sep [Accessed 2017 May 12]. Available from: http://www.antadir.com/uploads/product/95/pdf/synthese-pari-lc-sprint-v4-inter.pdf.

[480] Wachtel H, Ziegler J. Improved assessment of inhaler device performance using laser diffraction. Respiratory Drug Delivery VIII. 2002;2:379-381.

[481] Carrigy NB, Martin AR, Finlay WH. Use of extrathoracic deposition models for patient-specific dose estimation during inhaler design. Curr Pharm Des. 2015;21(27):3984-3992.

[482] Vandal OH, Nathan CF, Ehrt S. Acid resistance in Mycobacterium tuberculosis. J Bacteriol. 2009;191(15):4714-4721.

[483] Xiong X, Zhang HM, Wu TT, Xu L, Gan YL, Jiang LS, Zhang L, Guo SL. Titer dynamic analysis of D29 within MTB-infected macrophages and effect on immune function of macrophages. Exp Lung Res. 2014;40(2):86-98.

[484] Basra SK. The isolation and characterization of phages with lytic activity against Mycobacterium avium subspecies paratuberculosis, and their application using Bioluminescent assay in real-time Loop-mediated isothermal amplification assay for rapid detection. Master of Science Thesis. Department of Food Science, University of Guelph. 2013. Guelph, ON, Canada.

[485] Darch SE, Kragh KN, Abbott EA, Bjarnsholt T, Bull JJ, Whiteley M. Phage inhibiting pathogen dissemination by targeting bacterial migrants in a chronic infected model. mBio. 2017;8(2):e00240-17.

[486] Abedon ST. Bacteriophages and biofilms: ecology, phage therapy, plaques. New York: Nova Science Publishers, Inc.; 2011.

[487] Drulis-Kawa Z, Majkowska-Skrobek G, Maciejewska B, Delattre A-S, Lavigne R: Learning from bacteriophages – advantages and limitations of phage and phage-encoded protein applications. Curr Protein Pept Sci. 2012;13(8):699-722.
[488] Lu TK, Collins JJ. Dispersing biofilms with engineered enzymatic bacteriophage. PNAS. 2007;104(27):11197-11202.
[489] Kolodkin-Gal I, Romero D, Cao S, Clardy J, Kolter R, Losick R. D-amino acids trigger biofilm disassembly. Science. 2010;328(5978):627-629.
[490] Nadithe V, Rahamatalla M, Finlay WH, Mercer JR, Samuel J. Evaluation of nose-only aerosol inhalation chamber and comparison of experimental results with mathematical simulation of aerosol deposition in mouse lungs. J Pharm Sci. 2003;92(5):1066-1076.
[491] World Health Organization. 2018. Global tuberculosis report 2018. Available from: https://www.who.int/tb/publications/global_report/en/
[492] Orr P. 2013. Tuberculosis in Nunavut: looking back, moving forward. CMAJ 185:287-288.
[493] Contreras GL, Awashthi S, Hanif SNM, Hickey AJ. 2012. Inhaled vaccines for the prevention of tuberculosis. J Mycobac Dis S:1.
[494] Tyne AS, Chan JGY, Shanahan ER, Atmosukarto I, Chan H-K, Britton WJ, West NP. 2013. TLR2-targeted secreted proteins from Mycobacterium tuberculosis are protective as powdered pulmonary vaccines. Vaccine 31:4322-4329.
[495] Aerosol Vaccines for Tuberculosis Workshop Summary Group. 2015. Developing aerosol vaccines for Mycobacterium tuberculosis: workshop proceedings National Institute of Allergy and Infectious Diseases, Bethesda, Maryland, USA, April 9, 2014. Vaccine 33:3038-3046.
[496] Baldwin SL, Reese VA, Huang PD, Beebe EA, Podell BK, Reed SG, Coler RN. 2016. Protection and long-lived immunity induced by the ID93/GLA-SE vaccine candidate against a clinical *Mycobacterium tuberculosis* isolate. Clin Vaccine Immunol 53:137-147.
[497] Nemes H, Geldenhuys H, Rozot V, Rutkowski KT, Ratangee F, Bilek N, Mabwe S, Makhethe L, Erasmus M, Toefy A, Mulenga H, Hanekom WA, Self SG, Bekker L-G, Ryall R, Gurunathan S, DiazGranados CA, Andersen P, Kromann I, Evans T, Ellis RD, Landry B, Hokey DA, Hopkins R, Ginsberg AM, Scriba TJ, Hatherill M. 2018. Prevention of *M. tuberculosis* infection with H4:IC31 vaccine or BCG revaccination. N Engl J Med 379:138-149.
[498] Rodrigues LC, Mangtani P, Abubakar I. 2011. How does the level of BCG vaccine protection against tuberculosis fall over time? BMJ 343:d5974.

[499] Rowland R, McShane H. 2014. Current transmission prevention methods: vaccination, p 33-52. *In* Zellweger J-P (ed), Clinical insights: tuberculosis prevention. Future Medicine Ltd, London, UK.

[500] Toujani S, Cherif J, Mjid M, Hedhli A, Ouahchy Y, Beji M. 2017. Evaluation of tuberculin skin test positivity and early tuberculin conversion among medical intern trainees in Tunisia. Tanaffos 16:149-456.

[501] Joshi R, Reingold AL, Menzies D, Pai M. 2006. Tuberculosis among health-care workers in low- and middle-income countries: a systematic review. PLoS Med 3:e494.

[502] Uden L, Barber E, Ford N, Cooke GS. 2017. Risk of tuberculosis infection and disease for health care workers: an updated meta-analysis. Open Forum Infect Dis 4:ofx137.

[503] Fox GJ, Marks GB, Britton WJ. 2014. Current transmission prevention methods: reducing disease spread from infected individuals, p 53-76. *In* Zellweger J-P (ed), Clinical insights: tuberculosis prevention. Future Medicine Ltd, London, UK.

[504] Verkuijl S, Middelkoop K. 2016. Protecting our front-liners: occupational tuberculosis prevention through infection control strategies. Clin Infect Dis 62:S231-S237.

[505] Hatfull GF. 2015. Dark matter of the biosphere: the amazing world of bacteriophage diversity. J Virology 89:8107-8110.

[506] Loc-Carrillo C, Abedon ST. 2011. Pros and cons of phage therapy. Bacteriophage 1:111-114.

[507] Hatfull GF, Vehring R. 2016. Respirable bacteriophage aerosols for the prevention and treatment of tuberculosis, p 277-292. *In* Hickey AJ, Misra A, Fourie PB (ed), Drug delivery systems for tuberculosis prevention and treatment. John Wiley & Sons, Ltd, Chichester, UK.

[508] Abedon ST, Kuhl SJ, Blasdel BG, Kutter EM. 2011. Phage treatment of human infections. Bacteriophage 1:66-85.

[509] Gordillo Altamirano FL, Barr JJ. 2019. Phage therapy in the postantibiotic era. Clin Microbiol Rev 32:e00066-18.

[510] Schooley RT, Biswas B, Gill JJ, Hernandez-Morales A, Lancaster J, Lessor L, Barr JJ, Reed SL, Rohwer F, Benler S, Segall AM, Taplitz R, Smith DM, Kerr K, Kumaraswamy M, Nizet V, Lin L, McCauley MD, Strathdee SA, Benson CA, Pope RK, Leroux BM, Picel AC, Mateczun AJ, Cilwa KE, Regeimbal JM, Estrella LA, Wolfe DM, Henry MS, Quinones JV, Salka S, Bishop-Lilly KA, Young R, Hamilton T. 2017. Development and use of personalized bacteriophage-based

therapeutic cocktails to treat a patient with a disseminated resistant *Acinetobacter baumannii* infection. Antimicrob Agents Chemother 61:e00954-17.

[511] Dedrick RM, Guerrero-Bustamante CA, Garlena RA, Russell DA, Ford K, Harris K, Gilmour KC, Soothill J, Jacobs-Sera D, Schooley RT, Hatfull GF, Spencer H. Engineered bacteriophages for treatment of a patient with a disseminated drug resistant *Mycobacterium abscessus*. Nat Med. In-press.

[512] Abedon ST. 2015. Phage therapy of pulmonary infections. Bacteriophage 5:1-13.

[513] Golshahi L, Seed KD, Dennis JJ, Finlay WH. 2008. Toward modern inhalational bacteriophage therapy: nebulization of bacteriophages of *Burkholderia cepacia* complex. J Aerosol Med Pulm Drug Deliv 21:351-360.

[514] Golshahi L, Lynch KH, Dennis JJ, Finlay WH. 2011. *In vitro* lung delivery of bacteriophages KS4-M and ϕKZ using dry powder inhalers for treatment of *Burkholderia cepacia* complex and *Pseudomonas aeruginosa* infections in cystic fibrosis. J Appl Microbiol 110:106-117.

[515] Matinkhoo S, Lynch KH, Dennis JJ, Finlay WH, Vehring R. 2011. Spray-dried respirable powders containing bacteriophages for the treatment of pulmonary infections. J Pharm Sci 100:5197-5205.

[516] Hoe S, Boraey MA, Ivey JW, Finlay WH, Vehring R. 2014. Manufacturing and device options for the delivery of biotherapeutics. J Aerosol Med Pulm Drug Deliv 27:315-328.

[517] Carrigy NB, Chang RY, Leung SSY, Harrison M, Petrova Z, Pope WH, Hatfull GF, Britton WJ, Chan H-K, Sauvageau D, Finlay WH, Vehring R. 2017. Anti-tuberculosis bacteriophage D29 delivery with a vibrating mesh nebulizer, jet nebulizer, and soft mist inhaler. Pharm Res 34:2084-2096.

[518] Leung SY, Parumasivam T, Gao FG, Carrigy NB, Vehring R, Finlay WH, Morales S, Britton WJ, Kutter E, Chan H-K. 2016. Production of inhalation phage powders using spray freeze drying and spray drying techniques for treatment of respiratory infections. Pharm Res 33:1486-1496.

[519] Leung SSY, Parumasivam T, Gao FG, Carter EA, Carrigy NB, Vehring R, Finlay WH, Morales S, Britton WJ, Kutter E, Chan H-K. 2017. Effect of storage conditions on the stability of spray dried, inhalable bacteriophage powders. Int J Pharm 521:141-149.

[520] Leung SSY, Parumasivam T, Nguyen A, Gengenbach T, Carter EA, Carrigy NB, Wang H, Vehring R, Finlay WH, Morales S, Britton WJ, Kutter E, Chan H-K. 2018. Effect of storage

temperature on the stability of spray dried bacteriophage powders. Eur J Pharm Biopharm 127:213-222.

[521] Leung SSY, Carrigy NB, Vehring R, Finlay WH, Morales S, Carter EA, Britton WJ, Kutter E, Chan H-K. 2019. Jet nebulization of bacteriophage with different tail morphologies – structural effects. 664:322-326.

[522] Muttil P, Wang C, Hickey AJ. 2009. Inhaled drug delivery for tuberculosis therapy. Pharm Res 26:2401-2416.

[523] Xiong X, Zhang HM, Wu TT, Xu L, Gan YL, Jiang LS, Zhang L, Guo SL. 2014. Titer dynamic analysis of D29 within MTB-infected macrophages and effect on immune function of macrophages. Exp Lung Res 40:86-98.

[524] Hatfull GF. 2014. Mycobacteriophages: windows into tuberculosis. PLoS Pathog 10:e1003953.

[525] Froman S, Will DW, Bogen E. 1954. Bacteriophage active against virulent mycobacterium tuberculosis I. isolation and activity. Am J Public Health Nations Health 44:1326-1333.

[526] Nadithe V, Rahamatalla M, Finlay WH, Mercer JR, Samuel J. 2003. Evaluation of nose-only aerosol inhalation chamber and comparison of experimental results with mathematical simulation of aerosol deposition in mouse lungs. J Pharm Sci 92:1066-1076.

[527] Leong BKJ, Coombs JK, Sabaitis CP, Rop DA, Aaron CS. 1998. Quantitative morphometric analysis of pulmonary deposition of aerosol particles inhaled via intratracheal nebulization, intratracheal instillation or nose-only inhalation in rats. J Appl Toxicol. 18:149-160.

[528] Wolff, RK. 2015. Toxicology studies for inhaled and nasal delivery. Mol Pharm 12:2688-2696.

[529] Phillips JE. 2017. Inhaled efficacious dose translation from rodent to human: a retrospective analysis of clinical standards for respiratory diseases. Pharmacol Ther 178:141-147.

[530] Phalen RF. 1976. Inhalation exposure of animals. Environ Health Perspect 16:17-24.

[531] Liu K-Y, Yang W-H, Dong X-K, Cong L-M, Li N, Li Y, Wen Z-B, Yin Z, Lan Z-J, Li W-P, Li J-S. 2016. Inhalation study of mycobacteriophage D29 aerosol for mice by endotracheal route and nose-only exposure. J Aerosol Med Pulm Drug Deliv 29:393-405.

[532] Semler DD, Goudie AD, Finlay WH, Dennis JJ. 2014. Aerosol phage therapy efficacy in *Burkholderia cepacia* complex respiratory infections. Antimicrob Agents Chemother 58:4005-4013.

[533] Kutter E, Sulakvelidze A. 2005. Bacteriophages: biology and applications. CRC Press, Boca Raton, USA.
[534] Hoe S, Semler DD, Goudie AD, Lynch KH, Matinkhoo S, Finlay WH, Dennis JJ, Vehring R. 2013. Respirable bacteriophages for the treatment of bacterial lung infections. J Aerosol Med Pulm Drug Deliv 26:317-335.
[535] Fairchild GA. 1972. Measurement of respiratory volume for virus retention studies in mice. Appl Microbiol 24:812-818.
[536] Martin AR, Ang A, Katz IM, Häussermann S, Caillibotte G, Texereau J. 2011. An *in vitro* assessment of aerosol delivery through patient breathing circuits used with medical air or a helium-oxygen mixture. J Aerosol Med Pulm Drug Deliv 24:225-234.
[537] Kuehl PJ, Anderson TL, Candelaria G, Gershman B, Harlin K, Hersterman JY, Holmes T, Hoppin J, Lackas C, Norenberg JP, Yu H, McDonald JD. 2012. Regional particle size dependent deposition of inhaled aerosol in rats and mice. Inhal Toxicol 24:27-35.
[538] Soutiere SE, Tankersley CG, Mitzner W. 2004. Differences in alveolar size in inbred mouse strains. Respir Physiol Neurobiol 140:283-291.
[539] Larsen SE, Baldiwin SL, Orr MT, Reese VA, Pecor T, Granger B, Dubois Cauwelaert N, Podell BK, Coler RN. 2018. Enhanced anti-*Mycobacterium tuberculosis* immunity over time with combined drug and immunotherapy treatment. Vaccines (Basel) 6:30.
[540] Jacobs-Sera D, Marinelli LJ, Bowman C, Broussard GW, Guerrero Bustamante C, Boyle MM, Petrova ZO, Dedrick RM, Pope WH, SEA-PHAGES, Modlin RL, Hendrix RW, Hatfull GF. 2012. On the nature of mycobacteriophage diversity and host preference. Virology 434:187-201.
[541] Kanjee Z, Amico KR, Li F, Mbolekwa K, Moll AP, Friedland GH. 2012. Tuberculosis infection control in a high drug-resistance setting in rural South Africa: information, motivation, and behavioral skills. J Infect Public Health 5:67-81.
[542] Roach DR, Leung CY, Henry M, Morello E, Singh D, di Santo JP, Weitz JS, Debarbieux L. 2017. Synergy between the host immune system and bacteriophage is essential for successful phage therapy against an acute respiratory pathogen. Cell Host Microbe 22:38-47.
[543] Bowen LE, Rivers K, Trombley JE, Bohannon JK, Li SX, Boydston JA, Eichelberger MC. 2012. Development of a murine nose-only inhalation model of influenza: comparison of disease caused by instilled and inhaled A/PR/8/34. Front Cell Infect Microbiol 2:74.

[544] Wheeler AJ, Ganji AR. 2010. Introduction to engineering experimentation, 3rd edition. Pearson Higher Education, Upper Saddle River, NJ, USA.

[545] Ochs M, Nyengaard JR, Jung A, Knudsen L, Voigt M, Wahlers T, Richter J, Gundersen HJ. 2004. The number of alveoli in the human lung. Am J Respir Crit Care Med 169:120-124.

[546] Guirado E, Mbawuike U, Keiser TL, Arcos J, Azad AK, Wang S-H, Schlesinger LS. 2015. Characterization of host and microbial determinants in individuals with latent tuberculosis infection using a human granuloma model. mBio 6:e02537-14.

[547] Carrigy NB, Ly A, Harrison M, Sauvageau D, Martin A, Finlay WH, Vehring R. Comparison of spray drying and atmospheric spray freeze drying for the production of active anti-tuberculosis bacteriophage D29 dry powder for inhalation. In *Respiratory Drug Delivery Europe 2019.*

[548] Schmid KC. Spray drying of protein precipitates and evaluation of the nano spray dryer B-90. PhD Thesis. Faculty of Chemistry and Pharmacy, Ludwig Maximilian University of Munich. 2011. Munich, Germany.

[549] Lee SH, Heng D, Ng WK, Chan HK, Tan RB. Nano spray drying: a novel method for preparing protein nanoparticles for protein therapy. *International Journal of Pharmaceutics* 403:192-200.

[550] Matinkhoo S, Lynch KH, Dennis JJ, Finlay WH, Vehring R. Spray-dried respirable powders containing bacteriophages for the treatment of pulmonary infections. J Pharm Sci. 2011;100(12):5197-5205.

[551] Basra SK. The isolation and characterization of phages with lytic activity against Mycobacterium avium subspecies paratuberculosis, and their application using Bioluminescent assay in real-time Loop-mediated isothermal amplification assay for rapid detection. MSc Thesis. Department of Food Science, University of Guelph. 2013. Guelph, ON, Canada.

[552] Feng, A.L., Boraey, M.A., Gwin, M.A., Finlay, P.R., Kuehl, P.J., Vehring, R., 2011. Mechanistic models facilitate efficient development of leucine containing microparticles for pulmonary drug delivery. Int. J. Pharm. 409, 156-163. https://doi.org/10.1016/j.ijpharm.2011.02.049.

[553] Vehring, R., Foss, W.R., Lechuga-Ballesteros, D., 2007. Particle formation in spray drying. J. Aerosol Sci. 38, 728-746. https://doi.org/10.1016/j.aerosci.2007.04.005.

[554] Vehring, R., 2008. Pharmaceutical particle engineering via spray drying. Pharm. Res. 25, 999-1022. https://doi.org/10.1007/s11095-007-9475-1.

[555] phagesDB.org. Phage hunting procedure & protocols. 2016 December 2. Available from: phagesdb.org/workflow/.
[556] Roos WH, Ivanovska IL, Evilevitch A, Wuite GJ. Viral capsids: mechanical characteristics, genome packaging and delivery mechanisms. *Cell Mol Life Sci.* 2007;64:1484-1497.
[557] Evilevitch A, Lavelle L, Knobler CM, Raspaud E, Gelbart WM. Osmotic pressure inhibition of DNA ejection from phage. *PNAS.* 2003;100:9292-9295.
[558] Cordova A, Deserno M, Gelbart WM, Ben-Shaul-A. Osmotic shock and the strength of viral capsids. *Biophys J.* 2003;85:70-74.
[559] Finlay WH. The mechanics of inhaled pharmaceutical aerosols: an introduction. San Diego: Academic Press; 2001.
[560] Stone BR, Heimbuch BK, Wu CY, Wander JD. 2012. Design, construction and validation of a nose-only inhalation exposure system to measure infectivity of filtered bioaerosols in mice. J Appl Microbiol 113: 757-766.
[561] Oldham MJ, Phalen RF, Budiman T. 2009. Comparison of predicted and experimentally measured aerosol deposition efficiency in BALB/C mice in a new nose-only exposure system. Aerosol Science and Technology 43:970-977.
[562] Pauluhn J. 1994. Validation of an improved nose-only exposure system for rodents. J Appl Toxicol 14:55-62.
[563] Mainelis G, Seshadri S, Garbuzenko OB, Han T, Wang Z, Minko T. 2013. Characterization and application of a nose-only exposure chamber for inhalation delivery of liposomal drugs and nucleic acids to mice. J Aerosol Med Pulm Drug Deliv 26:345-354.
[564] Kuehl PJ, Anderson TL, Candelaria G, Gershman B, Harlin K, Hesterman JY, Holmes T, Hoppin J, Lackas C, Norenberg JP, Yu H, McDonald JD. 2012. Regional particle size dependent deposition of inhaled aerosol in rats and mice. Inhalation Toxicology 24:27-35.
[565] Tuttle RS, Sosna WA, Daniels DE, Hamilton SB, Lednicky JA. 2010. Design, assembly, and validation of a nose-only inhalation exposure system for studies of aerosolized viable influenza H5N1 virus in ferrets. *Virology* 7:135.
[566] Leong BKJ, Coombs JK, Sabaitis CP, Rop DA, Aaron CS. 1998. Quantitative morphometric analysis of pulmonary deposition of aerosol particles inhaled via intratracheal nebulization, intratracheal instillation or nose-only inhalation in rats. J Appl Toxicol 18:149-160.

[567] Raabe OG, Al-Bayati MA, Teague SV, Rasolt A. 1988. Regional deposition of inhaled monodisperse coarse and fine aerosol particles in small laboratory animals. Ann occup Hyg 32:53-63.

[568] Fennelly KP, Jones-López EC. 2015. Quantity and quality of inhaled dose predicts immunopathology in tuberculosis. Front Immunol 6:313.

[569] Kuehl PJ, Boyden T, Dobry DE, Doyle-Eisele M, Friesen DT, McDonald JD, Murri BG, Vodak DT, Lyon DK. 2016. Inhaled PYY(3-36) dry-powder formulation for appetite suppression. *Drug Dev Ind Pharm* 42:150-156.

[570] Ly A, Carrigy NB, Wang H, Harrison M, Sauvageau D, Martin AR, Vehring R, Finlay WH. Atmospheric spray freeze drying of sugar solution with phage D29. *Front Microbiol* 2019;10:488.

[571] Leung SSY, Parumasivam T, Gao FG, Carrigy NB, Vehring R, Finlay WH, Morales S, Britton WJ, Kutter E, Chan H-K. 2016. Production of inhalation phage powders using spray freeze drying and spray drying techniques for treatment of respiratory infections. *Pharm Res* 33:1486-1496.

Appendix A

Modeling heat loss from the Büchi B-191 spray dryer

In Chapter 1 the process model for the Büchi B-191 was introduced. Experiments were performed to determine the heat loss from the spray dryer for different operating conditions. Table A.1 shows the experimental conditions and results for testing heat loss as required for development of the process model. In each case the atomizing gas flow rate was 1.51×10^{-4} kg/s. The specific heat capacity of air was 1.005 kJ/(kg·K) and of water was 4.1813 kJ/(kg·K). The latent heat for water was 2257 kJ/kg. The room temperature was 21.1-22.1°C and the room relative humidity was 24.9-30.5%. The B-191 was located in a fume hood with a sash height of 30 cm. The cyclone pressure drop was ~1.3 kPa at ~450 L/min. The dryer was left to equilibrate for 10 minutes after the inlet temperature stabilized prior to recording the outlet temperature. The drying and atomizing gas were nitrogen.

Table A.1: Measurements performed to characterize heat loss with the Büchi B-191 spray dryer.

T_{in} (°C)	T_{out} (°C)	Q_f (mL/min)	Q_{dg} (L/min)	$\dot{Q}_{loss}$(kW)
50	33.2	2	453	0.078
50	36.7	1	460	0.085
50	40.3	0	467	0.091
70	47.2	2	496	0.152
70	50.7	1	503	0.157
70	54.2	0	503	0.160
80	54.5	2	510	0.186
80	57.8	1	510	0.190
80	61.3	0	510	0.192
70	43.5	2	340	0.106
70	47.7	1	340	0.115
70	51.7	0	340	0.125
70	44.7	1	227	0.078

The results are plotted in Figure A.1.

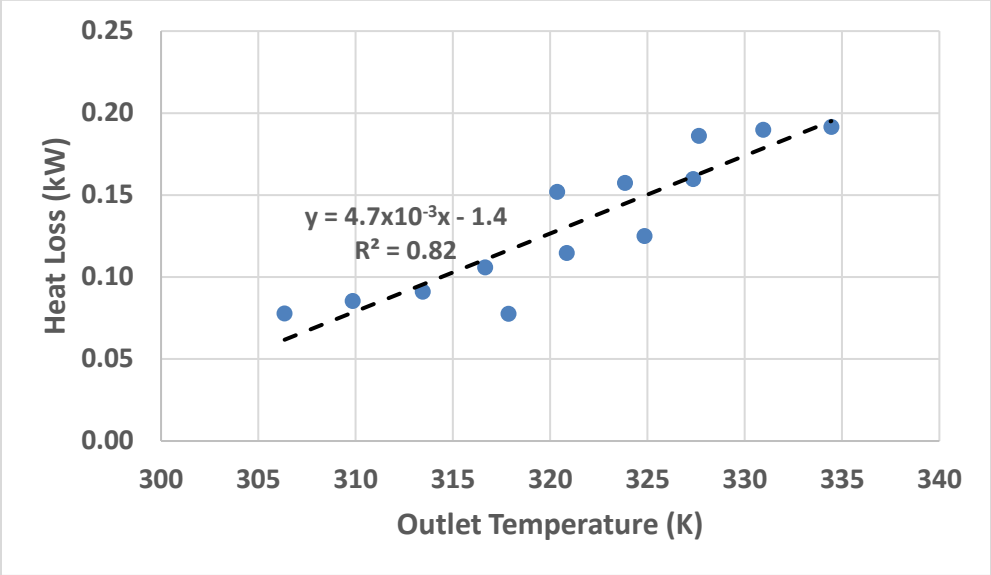

Figure A.1: Results of the heat loss process model fit for the Büchi B-191.

From the linear fit in Figure A.1, the constants required for estimating the outlet temperature using the process model are $\alpha = 0.0047$ kW/K and $\beta = -1.4$ kW. Note that 1 kW = 1 kJ/s.

Spray drying phage D29 with the Büchi B-191 spray dryer

Phage D29 was spray dried in 25% leucine and 75% trehalose with a total solids content of 30 mg/mL with the Büchi B-191 spray dryer with purification, 1:1000 dilution, and the other conditions the same as in Chapter 2. The resulting titer reduction was 2.6 ± 0.2 log(pfu/mL), which is similar to the anti-*Campylobacter* phages spray dried with this formulation.

Spray drying phage D29 using an inlet temperature of 60°C, drying gas flow rate of ~500 L/min, air-to-liquid ratio of 15, corresponding to an initial mass median diameter of 7 μm, and predicted outlet temperature of 46°C and outlet relative humidity of 1.5% was performed with different formulations [547]. Specifically, 140 μL of sterile-filtered lysate at a titer of 11.7 ± 0.1 log(pfu/mL) was diluted into 14 mL aqueous solution containing 5 mg/mL trileucine and 45 mg/mL trehalose, or 20 mg/mL pullulan and 40 mg/mL trehalose. The powder was resuspended to a concentration of ~10 mg/mL. The titer reduction was 1.2 ± 0.1 log(pfu/mL) for trileucine trehalose and 4.6 ± 0.1 log(pfu/mL) for pullulan trehalose, although a large impurity was apparent in the pullulan trehalose resuspension, potentially making the latter results invalid. A similar titer reduction was observed for the trileucine trehalose formulation as compared to atmospheric spray freeze drying [547]. An SEM of the trileucine trehalose powder containing phage D29 is shown in Figure A.2.

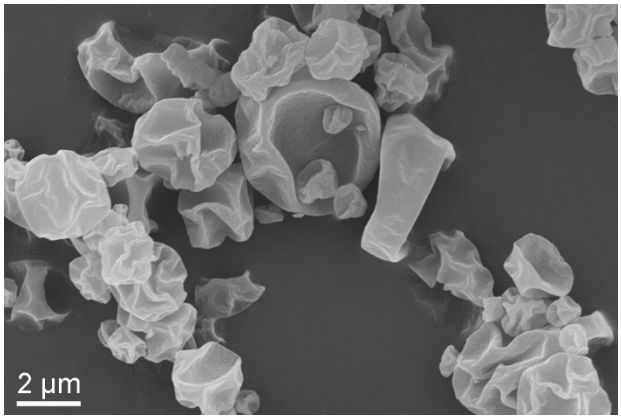

Figure A.2: SEM of trileucine trehalose powder containing phage D29 [547].

Büchi B-90 spray dryer modifications and process modelling

In Chapter 2, the reason the Aerogen Solo was used for droplet production rather than the stock Büchi B-90 atomizer was that the latter was malfunctioning, which I diagnosed to be due to a cracked piezoceramic element, which was expensive to replace. The Aerogen Solo was used outside of the drying chamber so that the liquid feed was not exposed to the high temperature in the drying chamber, which could inactivate biologics. Additionally, no peristaltic pump was required to feed the atomizer and hence there was no recirculation in the feed tubing, which has been shown to inactivate lactate dehydrogenase enzyme [548]. Further modifications include the addition of a pressure gauge and a vacuum pump for biohazard control in the enclosure, and the addition of a hygrometer past the outlet to measure the relative humidity, which is useful for estimating the moisture content in the powder.

A process model for the Büchi B-90 spray dryer was developed with the Aerogen Solo inside the spray dryer, and was later found to be reasonably accurate for when the Aerogen Solo was moved to outside the spray dryer. Measurements were performed with a drying gas flow rate of 100 L/min, feed flow rate of 0.45 mL/min, and chamber pressure of 6.4-6.6 kPa. The effect of the atomizing gas flow rate was neglected as it was small relative to the drying gas flow rate. The inlet temperatures were 55, 65, 75, and 85°C and the heat losses were 0.027, 0.035, 0.045, and 0.057 kW. The results are plotted in Figure A.3. The relative humidity values were 12.5%, 9.1%, 6.9%, and 5.7% for the respective cases. Note that the relative humidity is very sensitive to the spray rate of the Aerogen atomizer, which itself is sensitive to parameters of the formulation such as viscosity and surface activity. Therefore, it is desirable to perform runs with the specific formulation to be tested in order to determine the spray rate before using the process model. Also note that the outlet temperature is dependent on the collecting voltage used, as explained in Chapter 2, and was 13.7 kV for the heat loss experiments, which is the standard voltage used without modification of the spray dryer (this effect is further discussed later in this appendix).

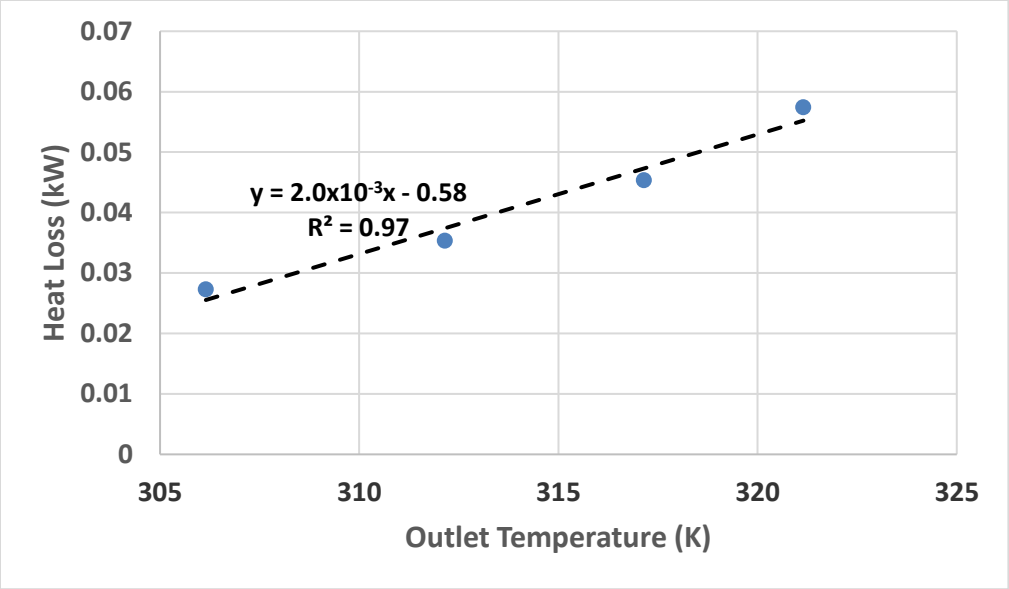

Figure A.3: Results of heat loss measurements for the modified Büchi B-90 spray dryer for use in process model development.

From the linear fit in Figure A.3, the constants required for estimating the outlet temperature with the process model are $\alpha = 0.0020$ kW/K and $\beta = -0.58$ kW.

In Figure A.4 the outlet temperature and outlet relative humidity are predicted for different inlet temperatures and drying gas flow rates for the modified Büchi B-90 spray dryer.

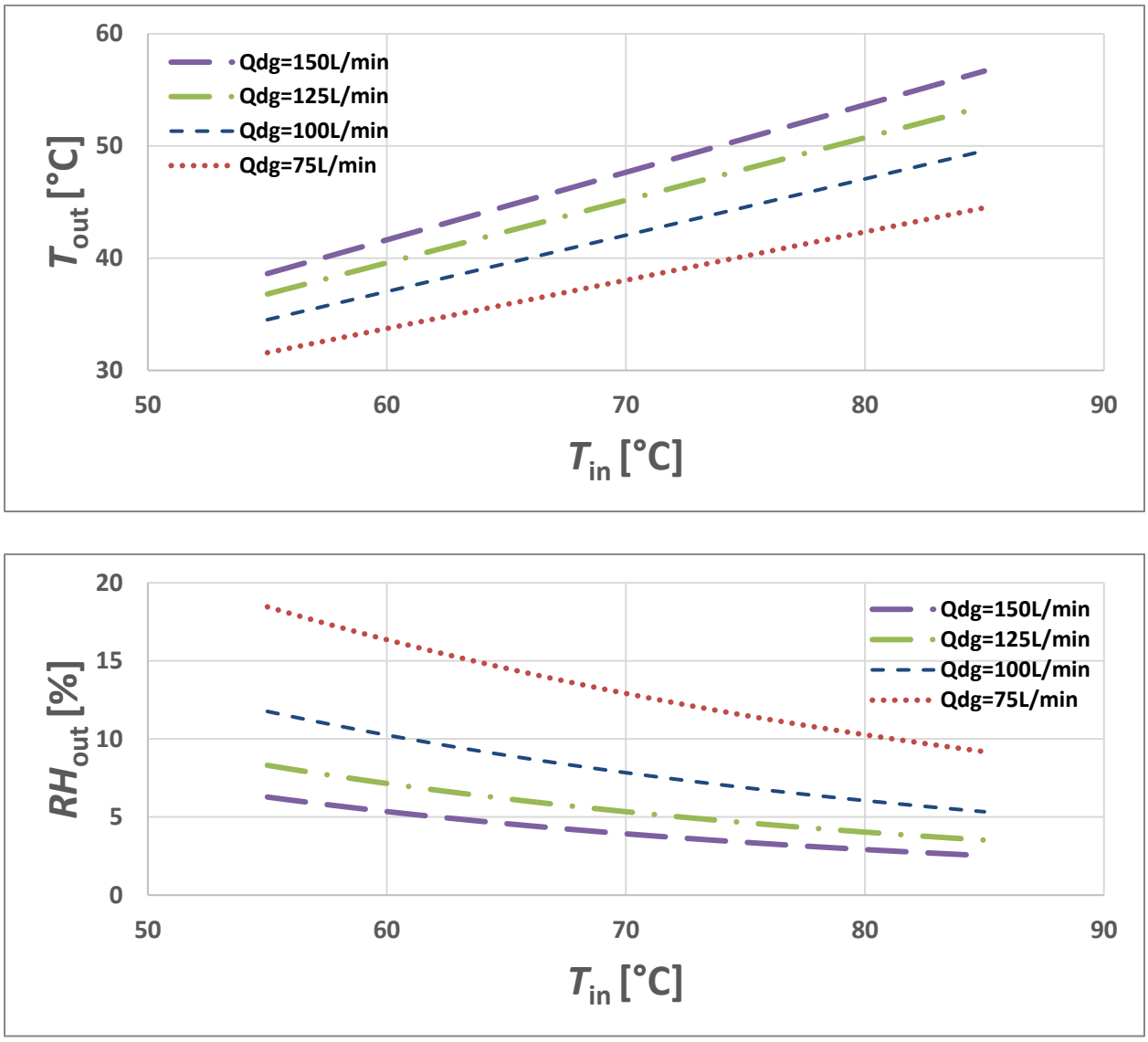

Figure A.4: Outlet temperature (top) and outlet relative humidity (bottom) process model predictions for the modified Büchi B-90 spray dryer for different inlet temperatures and drying gas flow rates. Note that the results are only valid for a spray rate of 0.45 mL/min and a collecting voltage of 13.7 kV. If instead the spray rate is 1 mL/min, the predicted relative humidity ranges from 6.4-52% for the cases presented.

The outlet temperature was measured to change with the collecting voltage as per Figure A.5. This effect has not been described in the literature, as the collecting voltage is normally not adjustable in the spray dryer. An external switch was added to turn on and off the collecting voltage as the

safety controls were malfunctioning; at this time a potentiometer was also added to adjust the voltage. The experiments were performed without atomization of any liquid, indicating that the effect was not caused by evaporative cooling. Additionally, the outlet temperature sensor of the Büchi B-90 was replaced with an analog temperature sensor, and the results were the same, indicating it was not some sort of electrical anomaly.

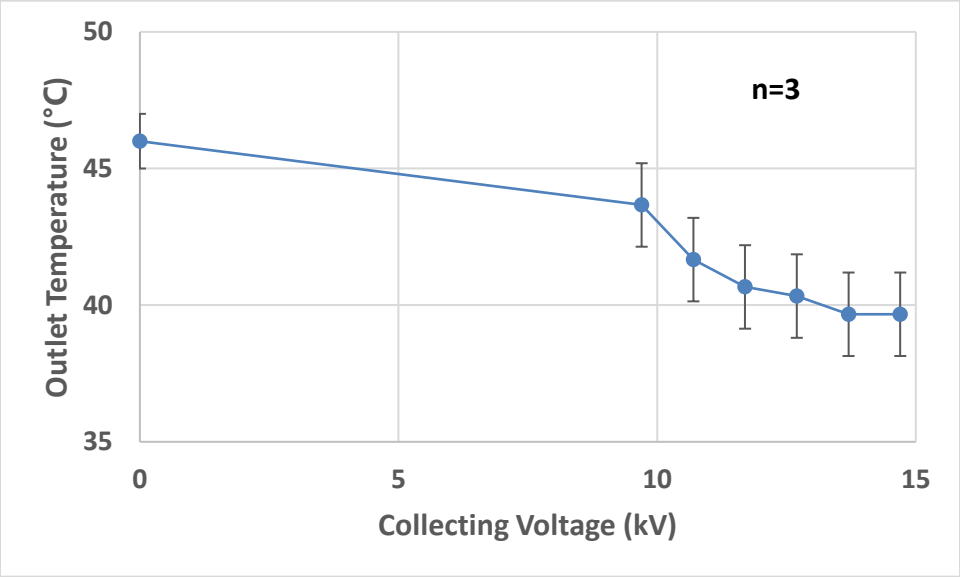

Figure A.5: Change in outlet temperature for different collecting voltages. The process conditions for these experiments were an inlet temperature of 70°C and drying gas flow rate of 100 L/min, with no spray and hence no evaporative cooling.

From Figure A.5 it is evident that increasing the collecting voltage increased the heat loss from the spray dryer. This was a slow process, whereby the outlet temperature decreased gradually over a period of 30-45 seconds, which indicated that potentially the heat loss was due to changes in the flow profile in the drying chamber. A schematic of the collecting electrode is given in Figure A.6.

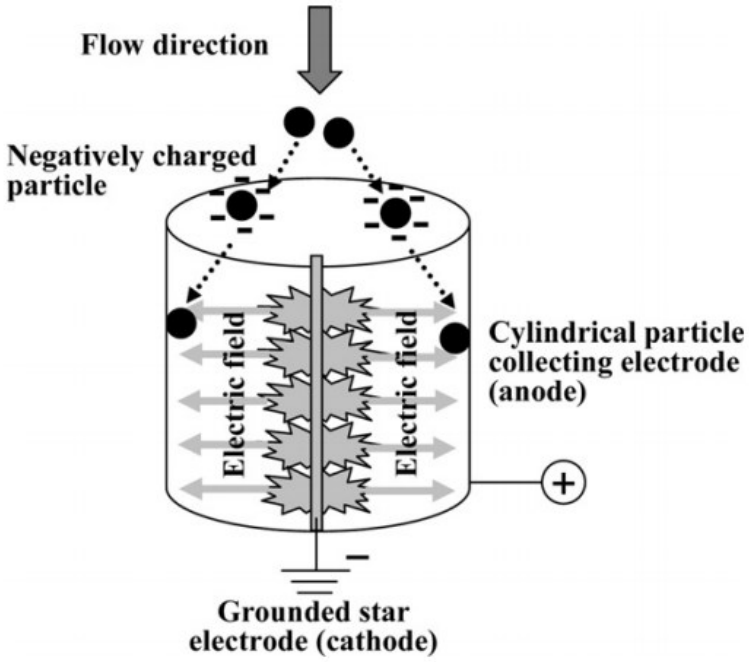

Figure A.6: Schematic of the collecting electrode in the Büchi B-90 [549].

Unlike a typical corona charger, it is the inner electrode that is grounded and the outer electrode that has a positive voltage. Near sharp tips, such as those in the star electrode, the electric field strength is strongest and ionization of the drying gas occurs. The ionization results in electrons forming near the sharp tips of the star electrode. These electrons collide with atoms to generate pairs of electrons and positive ions and collide with dry particles. The negatively-charged dry particles repel each other and travel towards the outer electrode. The observation that the heat loss increases with collecting voltage indicates that there may be bulk airflow induced by the voltage on the collecting electrode; in particular, increasing collecting voltage increases radial airflow towards the outer collecting electrode, causing the hot air initially near the center of the cylinder to come into contact with the cooler outer electrode, increasing heat loss.

Bulk airflow is induced by high voltage electrodes in devices such as solid-state fans and ion thrusters for spacecraft propulsion, which take advantage of the "ion wind" principle. Note that in my experiments, in addition to powder deposition on the collecting electrode, there was often much powder deposition on the star electrode, indicating a limitation of this collection method.

Spray drying phage D29 with the Büchi B-90

The formulations tested were TTB (3 mg/mL trileucine, 25.5 mg/mL trehalose, 1.5 mg/mL trisodium citrate) and LTC (6 mg/mL leucine, 23.4 mg/mL trehalose, 0.6 mg/mL casein sodium salt). The latter formulation is similar to the successful formulation used for spray dried phages in the study by Matinkhoo *et al.* [550]. TTB formulation with 1:100 phage D29 lysate diluted into it was spray dried with the B-90 spray dryer (with the Aerogen inside the spray dryer) using the settings: inlet temperature 75°C, drying gas flow rate 100 L/min, collecting voltage 13.7 kV, chamber pressure 6.5 kPa, with an outlet temperature 33-40°C, relative humidity 6.5-8.1%, and spray rate 0.27 mL/min. The collection efficiency was 40%. The powder was then moisture equilibrated in an environmental chamber (as described on the following pages), stored for 1 month at 30°C, and ambient temperature shipped to and from Sydney. The results for TTB are shown in Figure A.7.

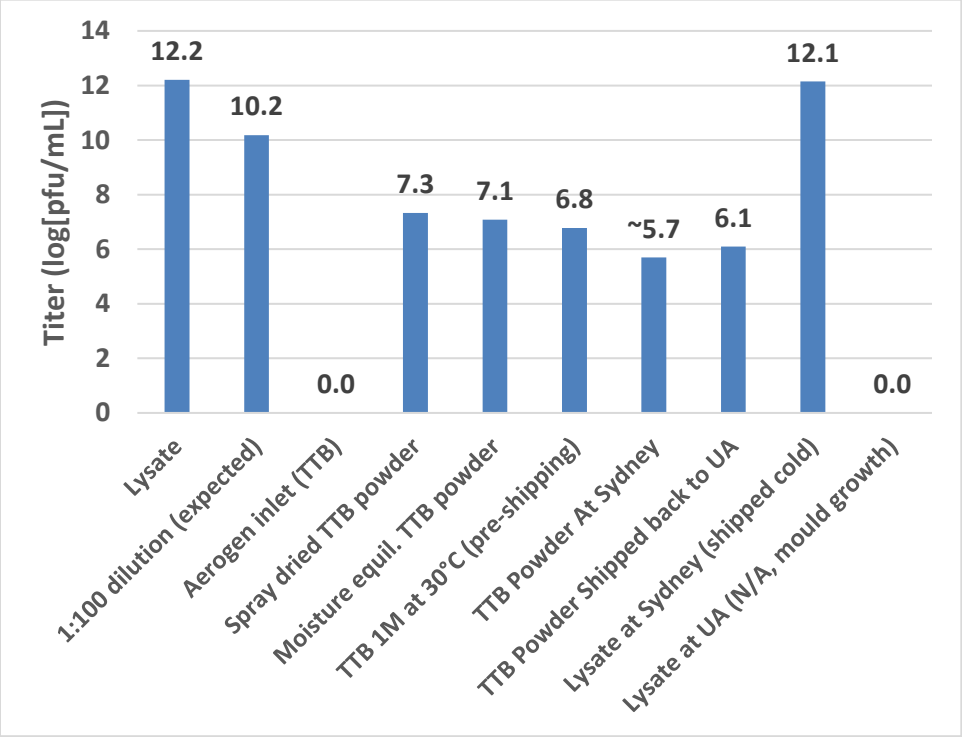

Figure A.7: Results of spray drying and shipping phage D29 in TTB formulation.

The titer reduction due to spray drying with the B-90 was 2.9 log(pfu/mL). In Appendix C the results of nebulizing phage D29 in TTB and LTC formulation are presented and only ~1.0 log(pfu/mL) and ~0.4 log(pfu/mL) resulted, indicating much of the inactivation is caused by other

factors. It was observed that the titer of phage D29 in TTB in the residual volume of the Aerogen atomizer was below the detection limit of 5.8 log(pfu/mL), and therefore it was suspected that the heat in the Aerogen reservoir caused by the hot drying gas flowing over it during the run inactivated the phage before it was atomized. The temperature of the liquid in the reservoir during the run was measured to be 53-62°C (with the reservoir found to be heating up at a rate of ~3.5°C/min). An ambient control measurement indicated that temperature only rose ~2°C in the reservoir due to vibrating mesh atomization, and therefore the effect was deduced to be caused by the hot drying gas. Literature indicates that phage D29 is not stable at 55°C [551], further confirming the hypothesis that the use of the Aerogen in the drying chamber is not suitable due to heating of the reservoir liquid. Additionally, D29 in LTC or in TTB with only 5% trileucine had a negligible titer in the reservoir at the end of a spray drying run. For this reason, the Aerogen was moved outside the spray dryer for the study in Chapter 2.

As the titer in the reservoir likely decreased over time, the powder generated early in the spray drying run likely had higher titer than the powder generated near the end of the run, resulting in a powder containing an average of 7.3 log(pfu/mL). The powder was moisture equilibrated for 3 days at 5% relative humidity and only 0.2 log(pfu/mL) titer reduction resulted due to this process. The moisture equilibration process involved placing all material in the Lunaire environmental chamber as shown in Figure A.8 and A.9.

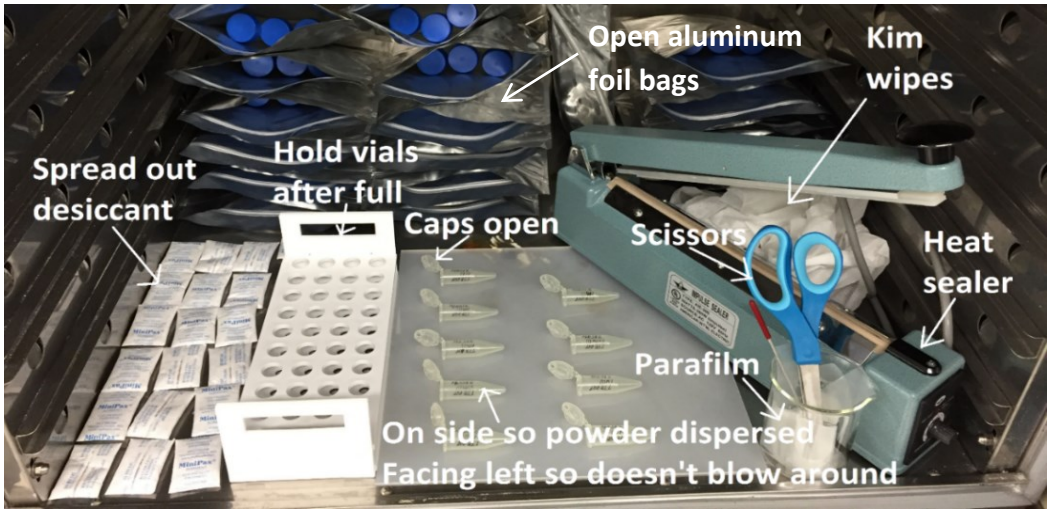

Figure A.8: Moisture equilibration method for powder generated from spray drying phage D29 in TTB formulation with the B-90. The powder was placed in the vials and a balance of a nitrogen purge and a feedback mechanism to atomize liquid into the chamber resulted in control of the relative humidity. The temperature was set to 30°C (the same temperature used for stability measurement) and the relative humidity to 5%.

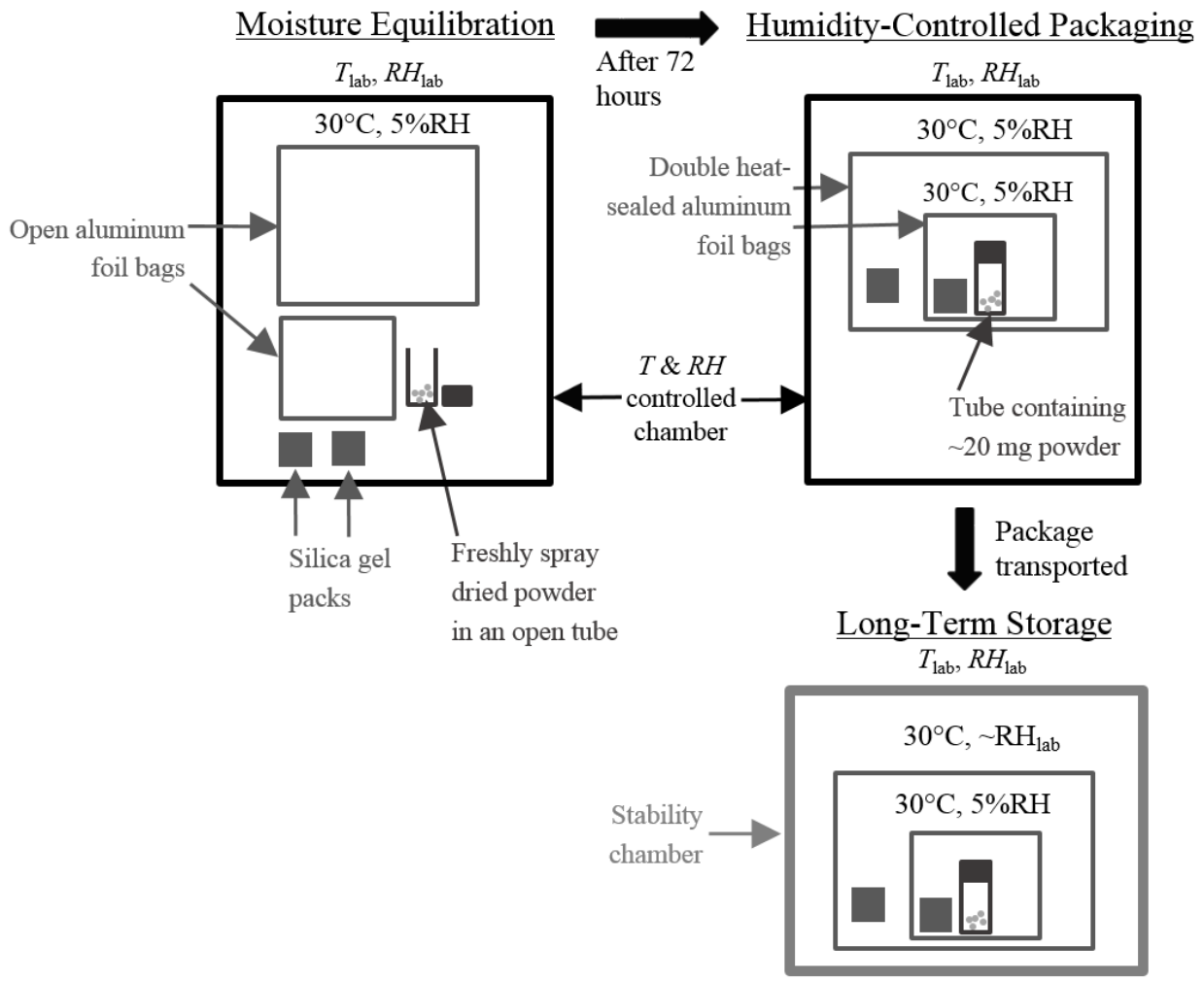

Figure A.9: Details of the packaging and storage method for spray dried phage D29.

After 1 month of storage at 30°C, the TTB D29 powder only lost an additional 0.3 log(pfu/mL) of titer. Upon ambient temperature shipment to the University of Sydney and back the titer dropped another 0.7 log(pfu/mL). In comparison, the liquid lysate shipped at ambient temperature to the University of Sydney and back contained mould growth and was not tittered (Figure A.10). Hence, dry powder shipment was successful whereas liquid shipment was not.

Figure A.10: Phage D29 lysate containing mould growth after ambient temperature shipment from Edmonton, Canada, to Sydney, Australia, and back.

An SEM of the phage D29 TTB powder is shown in Figure A.11, possibly showing a phage on the surface of the particle, as it is the right size and shape.

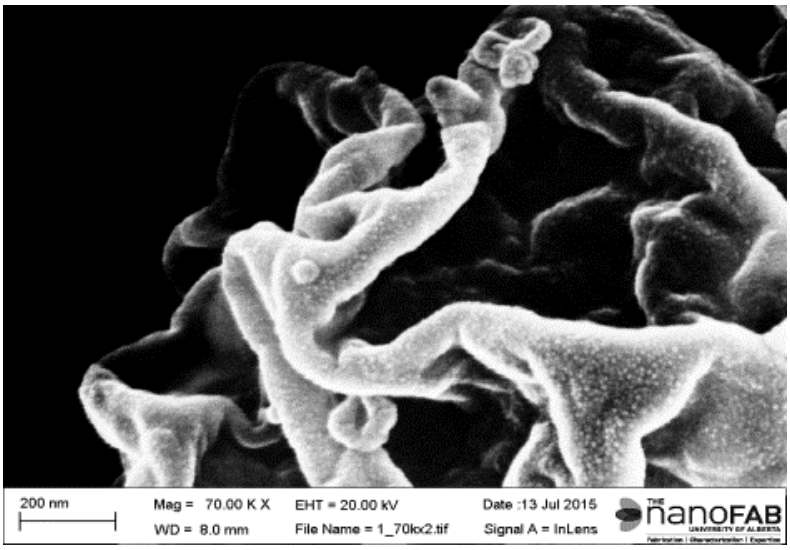

Figure A.11: SEM image of phage D29 TTB powder possibly showing a phage on the surface of the particle.

Purification of anti-*Campylobacter* phages

Without centrifugation it was observed that many bacteria that appeared alive were in the lysate. An example is shown in the TEM in Figure A.12.

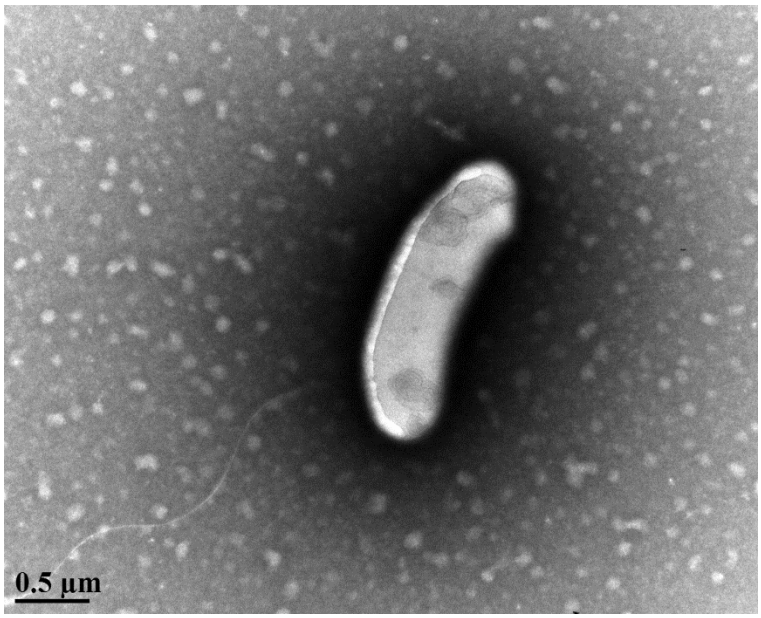

Figure A.12: A TEM of live bacteria in 0.22µm filtered CP30A lysate that has not been centrifuged. Approximately 1 bacterium was found per 100 phage, although not all bacteria appeared alive.

Temperature excursion during shipping phage CP30A experiments

An example of the temperature during shipment for CP30A experiments described in Chapter 2 is shown in Figure A.13.

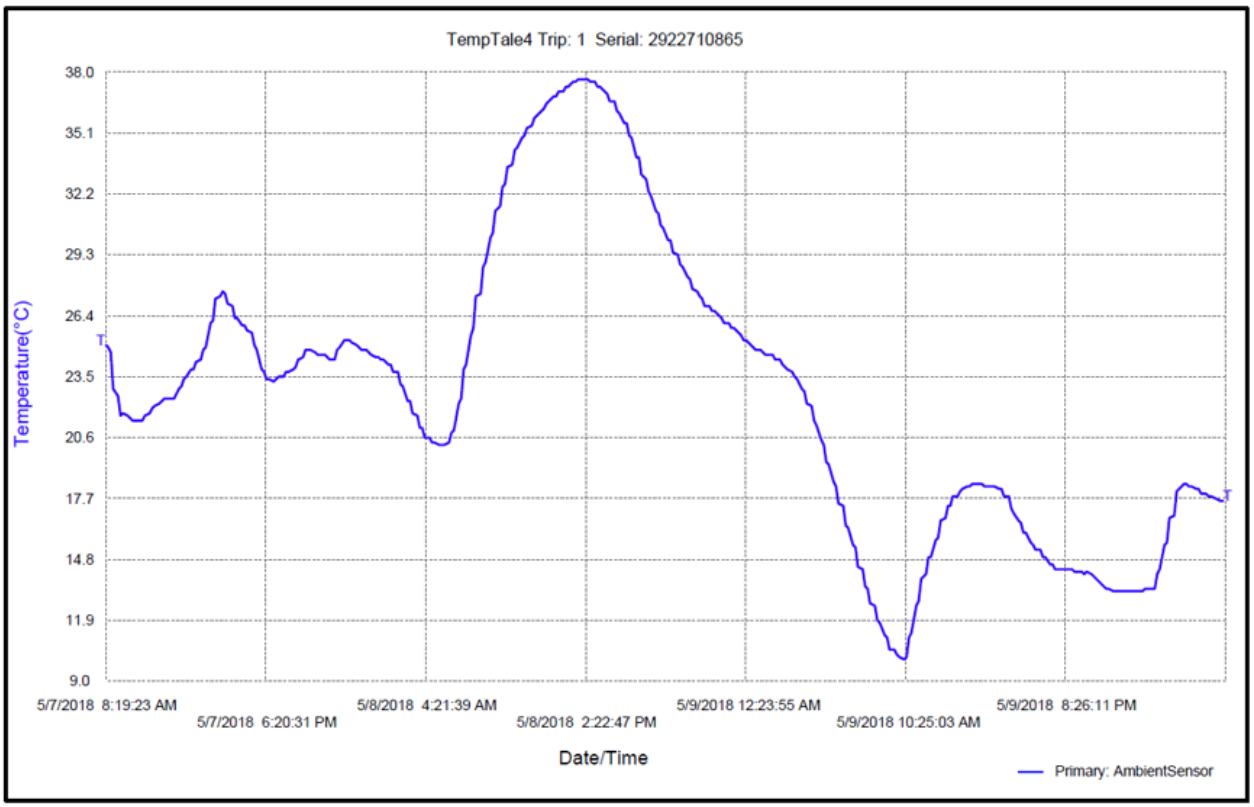

Figure A.13: Temperature of dry powder shipped under ambient conditions from Edmonton, Canada to Nottingham, UK. The maximum excursion for the LT phage CP30A powder shipped ambient was 37.7°C, as noted in Chapter 2. Despite this, minimal if any additional phage titer reduction was observed, which may be important to the success of the phage powder in Kenya.

Additional spray drying measurements with anti-*Campylobacter* phages

Further data regarding the testing of different powder resuspension methods, is given in Table A.2.

Table A.2: Titer reduction due to spray drying using different resuspension methods (path 12). Measurements were performed with purified and diluted phage CP20 with F1 and F2. LB = lowbind.

Formulation	**Temperature (°C)**	**Tube Type**	**Titer Reduction [(log_{10}(pfu/mL)] Relative to Lysate Control**	**Titer Reduction [(log_{10}(pfu/mL)] Relative to Feed Control**
F1	4	1.5 mL	2.5 ± 0.1	1.6 ± 0.2
		2.0 mL	1.6 ± 0.1	0.8 ± 0.2
		LB 2.0 mL	1.7 ± 0.1	0.8 ± 0.2
	37	1.5 mL	2.9 ± 0.1	2.0 ± 0.2
		2.0 mL	1.9 ± 0.1	1.0 ± 0.2
		LB 2.0 mL	1.9 ± 0.1	1.0 ± 0.2
F2	4	1.5 mL	2.8 ± 0.1	2.1 ± 0.3
		2.0 mL	3.2 ± 0.3	2.5 ± 0.4
		LB 2.0 mL	2.8 ± 0.1	2.0 ± 0.3
	37	1.5 mL	2.9 ± 0.2	2.2 ± 0.3
		2.0 mL	2.8 ± 0.1	2.0 ± 0.2
		LB 2.0 mL	3.0 ± 0.2	2.2 ± 0.3

The F1 powder from Table A.2 was examined using confocal Raman spectroscopy (inVia™ Qontor®; Renishaw, Wotton-under-Edge, UK) by company staff. This allowed for the interior composition to be mapped. The resulting images are shown in Figure A.14 and demonstrate that a core-shell structure is indeed formed in leucine trehalose powder.

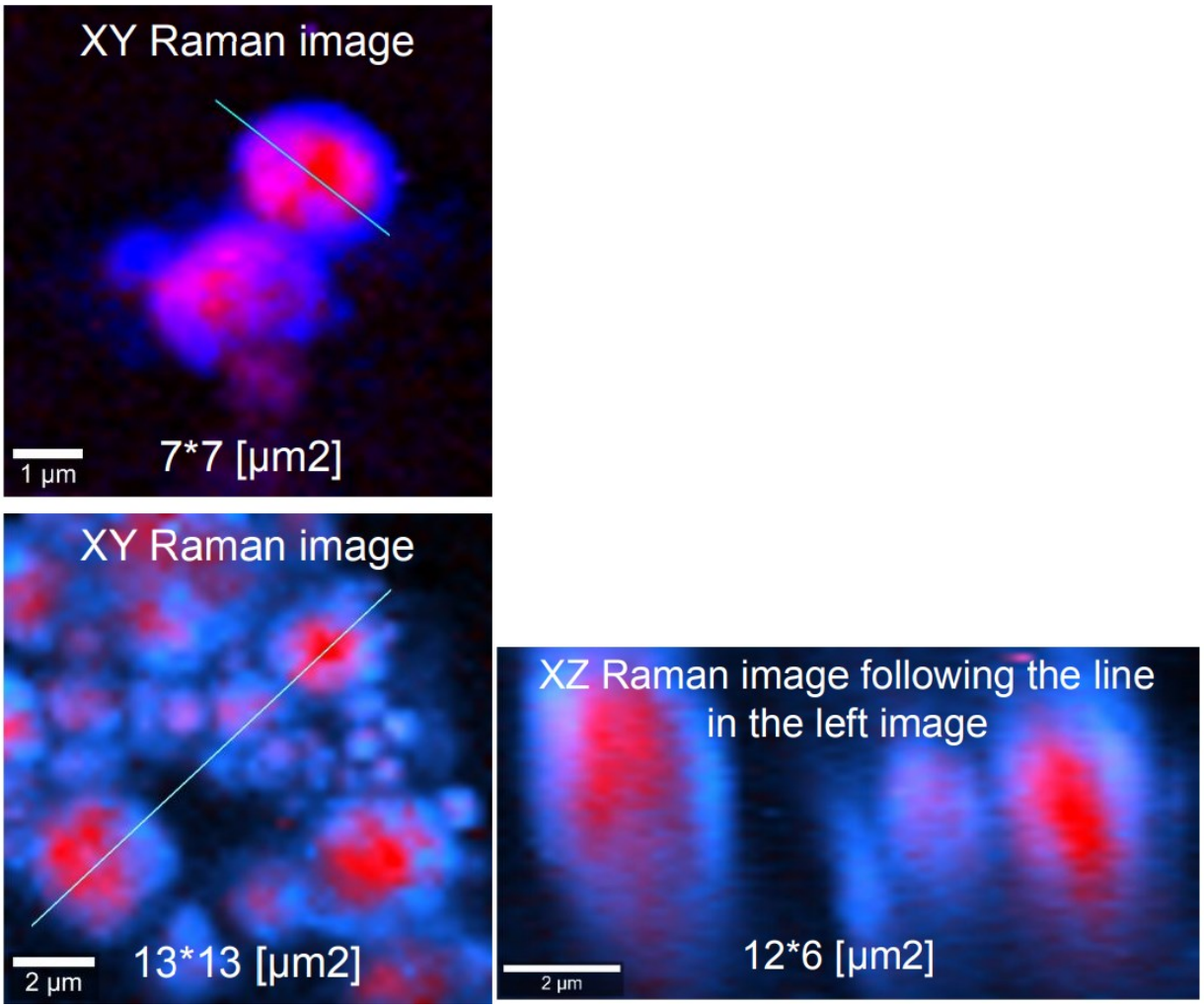

Figure A.14: Confocal Raman spectroscopy of formulation F1 containing phage CP20. Blue represents leucine and red represents trehalose.

Raman spectroscopy was also performed to determine the solid phase of the leucine and trehalose for F1 and F2 powder from Table A.2, as shown in Figure A.15. The results demonstrate that leucine is mostly, but not fully, crystalline and trehalose is fully amorphous for both 25% leucine, 75% trehalose, and 40% leucine, 60% trehalose. One would expect the leucine to be fully crystalline under the tested conditions based on data from Feng *et al.* [552]; hence, it appears that even though the lysate is purified and diluted before adding to the leucine and trehalose, something in the lysate is interfering with leucine crystallization. This is not unexpected, as even small amounts of impurities are capable of drastically affecting crystallization kinetics, as mentioned in Chapter 1. The predicted times available for crystallization were 11.5 milliseconds for F1 and 15.8 milliseconds for F2.

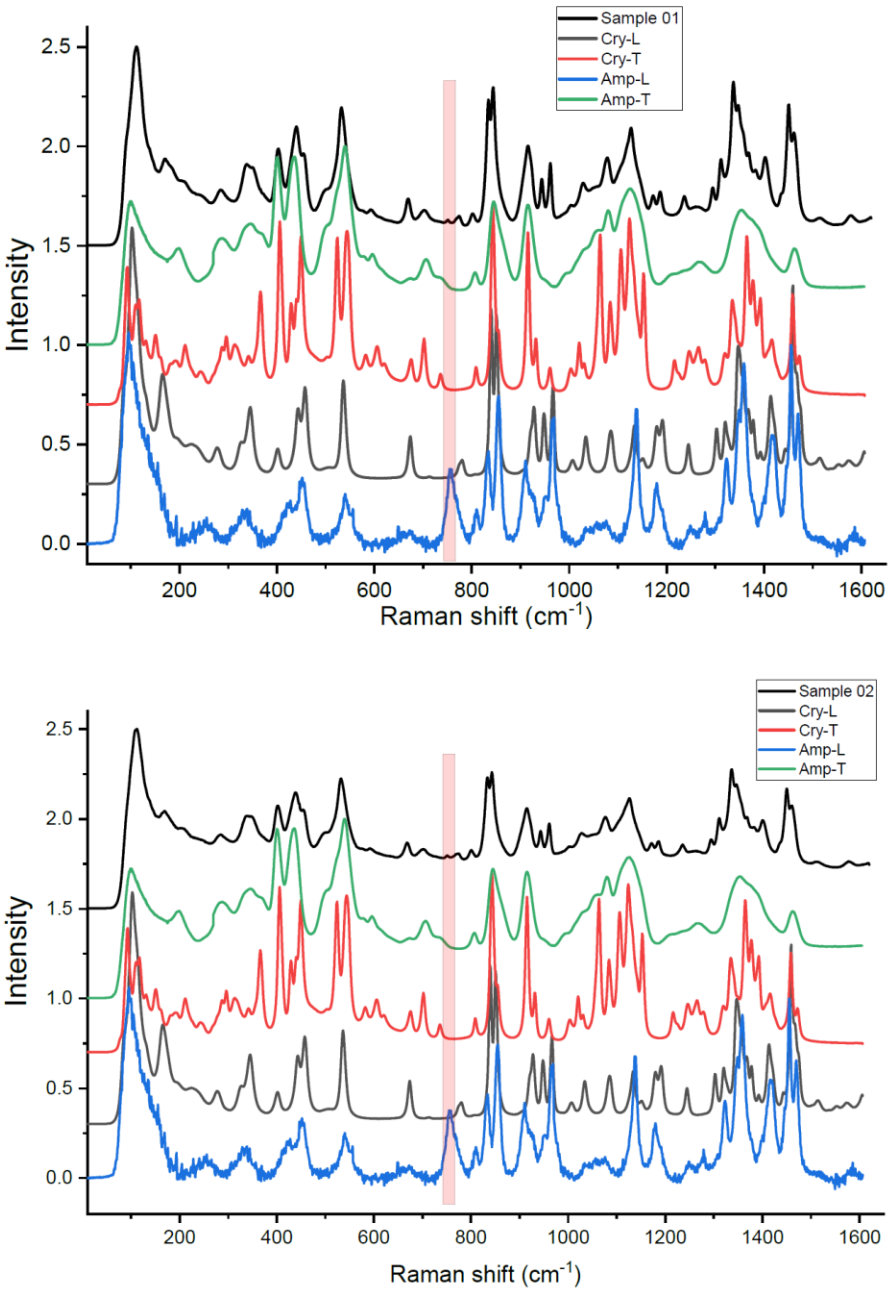

Figure A.15: Raman spectroscopy of 25% leucine 75% trehalose (top) and 40% leucine 60% trehalose (bottom), containing phage CP20, demonstrating partially crystalline leucine and fully amorphous trehalose.

SEM images were taken of powder F1 and F2 to determine the morphology of the powder that contains partially crystalline leucine (Figure A.16). The morphology is not similar to the leucine trehalose vehicle, discussed in Chapter 2, indicating the impurities affecting crystallization also affect the morphology of the spray dried powder.

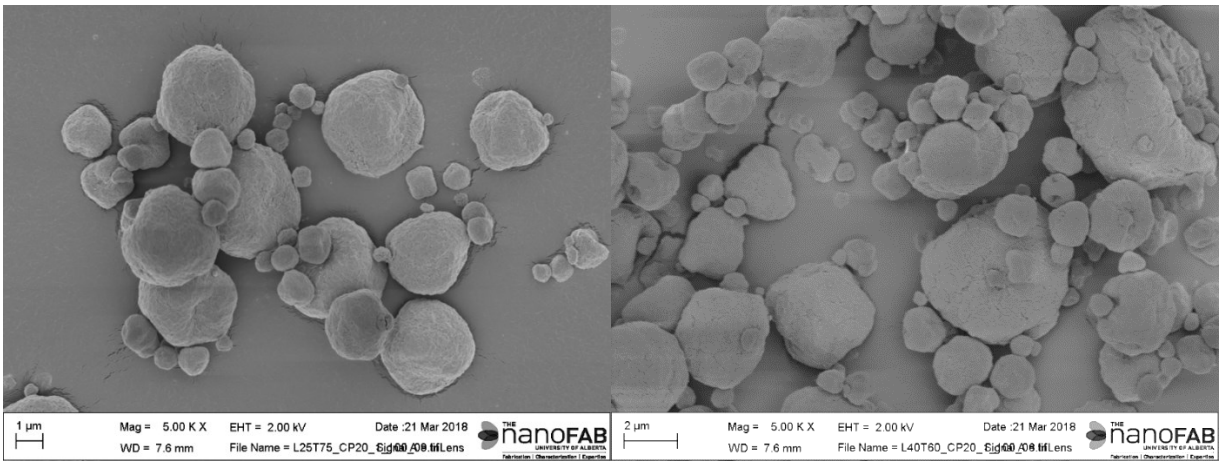

Figure A.16: SEM of 25% leucine 75% trehalose (left) and 40% leucine 60% trehalose (right), containing phage CP20.

Further measurements showed that use of a glass Bijou bottle for powder resuspension led to > 3 log(pfu/mL) titer reduction, indicating that glass is not a good material for resuspension. Previous experience in Prof. Ian Connerton's group at the University of Nottingham indicates that glass is not useful for working with phages due to binding to the wall materials, as was discussed in Chapter 1.

It was hypothesized that spray drying the same phage multiple times would produce spray drying-resistant phages. This was tested by repeatedly spray drying the same phages and resuspending to 30 mg/mL, and then isolating the phages, and repeatedly desiccating them to, ideally, develop a desiccation-resistant population. This was performed with phage CP30A using purified lysate and 1:100 dilution, with a total solids content of 30 mg/mL (7.5 mg/mL leucine, 22.5 mg/mL trehalose). The results are shown in Table A.3.

Table A.3: Titer reduction in log(pfu/mL) after repeatedly spray drying and resuspending the same population of phage CP30A. The number of spray dried powder resuspensions equals 1 case refers to phages that have been spray dried once.

Number of Spray Dried Powder Resuspensions	**Titer Reduction Relative to SD 'Neat'**	**Titer Reduction Relative to Lysate Control**	**Titer Reduction Relative to Feed Control**
1	-0.9	1.6	1.7
2	-0.5	3.6	2.1
3	-2.4	3.7	0.1

The first time the phage were spray dried there was 1.6 log(pfu/mL) titer reduction. The second time there was 2.0 log(pfu/mL) titer reduction. The third time there was 0.1 log(pfu/mL) titer reduction. Thus, it was thought that spray drying-resistant phages were isolated, and that this was perhaps related to inhomogeneity in the initial phage population. However, as shown in Figures A.17 and A.18, desiccating and rehydrating the apparently spray drying-resistant phages did not lead to small titer reduction due to desiccation and rehydration in a Petri dish, indicating they were in fact not desiccation-resistant.

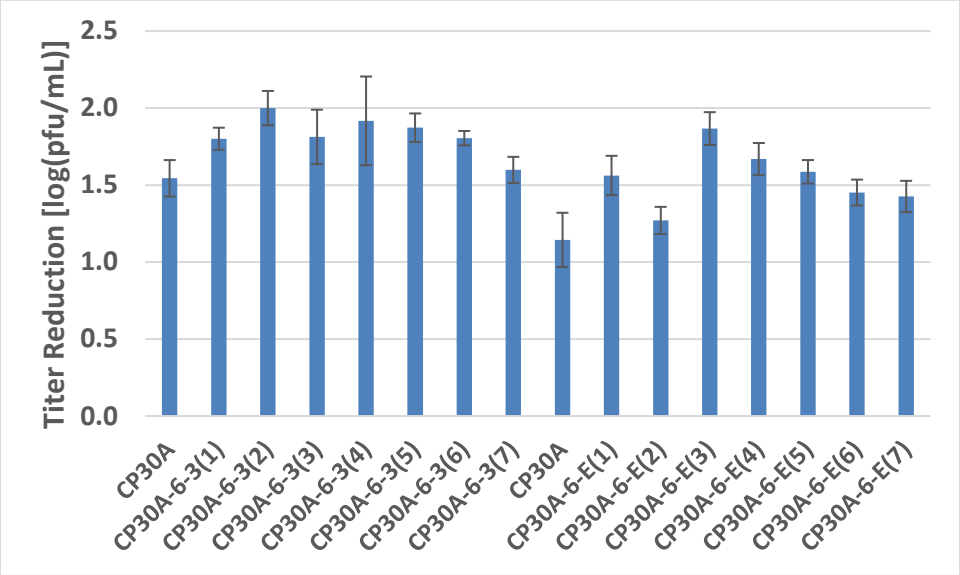

Figure A.17: Titer reduction due to desiccation of the apparently spray drying-resistant phages, for different samples plated from the same powder.

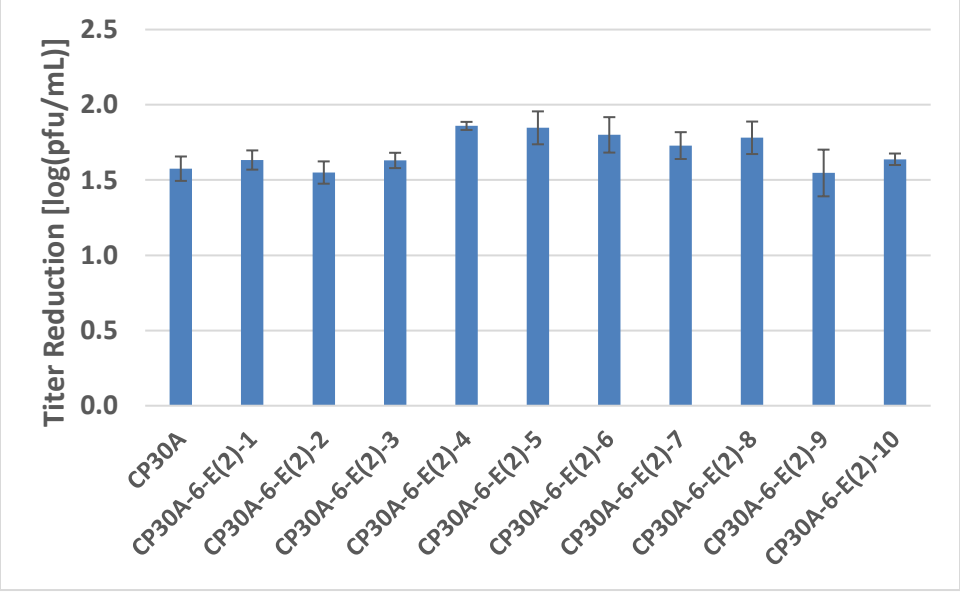

Figure A.18: Titer reduction due to desiccating a case with low titer reduction represented by CP30A-6-E(2) in Figure A.17.

Taking a sample from the case with the least titer reduction in a Petri dish did not lead to less titer reduction due to desiccation. Attempts to develop desiccation- or spray drying-resistant phages were abandoned. It is more likely that phages which were initially damaged (during amplification

and purification) were inactivated and phages that were initially undamaged survived. This may be the case for nebulized phage D29 in Chapter 4 as well. These results may indicate the importance of gentle purification.

It was hypothesized that the residual moisture content in the powder would affect the titer reduction. Different parameters were tested as per Table A.4. These measurements were performed with a total solids content of 120 mg/mL, phage CP30A, and purified, 1:100 diluted lysate. The formulation was 20 mg/mL leucine and 100 mg/mL trehalose, although additional measurements were performed with addition of 5 mg/mL citric acid-trisodium citrate buffer to adjust the pH to 5 or 6, to determine if a lower pH decreased titer reduction, and with the use of HPLC water (Fischer Scientific) rather than deionized water.

Table A.4: Spray drying parameters used to obtain different moisture contents in the powder. Parameters were predicted as per Chapter 1.

B-191 Parameters & Predicted Outputs	**0.7%H_2O Cases**	**2%H_20 Case**	**4%H_20 Case**
Inlet temperature - T_{in}	70°C	70°C	70°C
Drying gas flow rate - Q_{dg}	$4.2x10^2$ L/min	$3.5x10^2$ L/min	$3.5x10^2$ L/min
Atomizing gas flow rate - Q_{ag}	7.6 L/min	7.6 L/min	7.6 L/min
Liquid feed flow rate - Q_f	1.0 mL/min	2 mL/min	3.3 mL/min
Air-to-liquid ratio - *ALR*	9.1	4.5	2.8
Initial Droplet Diameter - d_0	9 μm	10 μm	11 μm
Outlet temperature - T_{out}	49°C	44°C	40°C
Outlet relative humidity - RH_{out}	3%	9%	18%
Water Mass Fraction in Powder - w_{out}	0.007	0.02	0.04
Wet Glass Transition Temperature - T_g	100°C	80°C	55°C

The results of the aforementioned spray drying experiments are shown in Table A.5.

Table A.5: Titer reduction in log(pfu/mL) of spray dried phage CP30A at different residual moisture contents, using different water solvent types, and different pH.

Test	Titer Reduction Relative to SD 'Neat'	Titer Reduction Relative to Lysate Control	Titer Reduction Relative to Feed Control
0.7% H2O	-0.6	1.9	1.7
0.7% H2O, HPLC water	-0.4	2.1	1.7
2% H2O	-0.8	1.7	1.7
4% H2O	+0.1	2.6	2.6
0.7% H2O, pH = 6	>+0.5	>3	N/A
0.7% H2O, pH = 5	>+0.5	>3	N/A

Some residual moisture (predicted to be 2%) may be beneficial relative to a predicted 0.7%, but there does not appear to be a large difference. Too much residual moisture (4%) appeared harmful. Use of the HPLC water did not help. The citric acid-trisodium citrate buffer inactivates the phages, regardless of the pH tested. It is not the pH of the buffer but rather the buffer components themselves that are inactivating the phage, as previous data in Chapter 2 indicated buffering to pH 7.2 was also detrimental to phage activity.

Note that further unsuccessful attempts were made to develop high titer anti-*Campylobacter* phage powder stable to shipping by atmospheric spray freeze drying, 3-4 log(pfu/mL) titer reduction, and freeze drying, indicating the large titer reduction for drying these phages is not peculiar to spray drying.

Appendix B

Further analysis of pullulan trehalose microparticle formation

As shown in Figure B.1, the initial droplet diameter was fairly constant between experiments averaging about 31 μm.

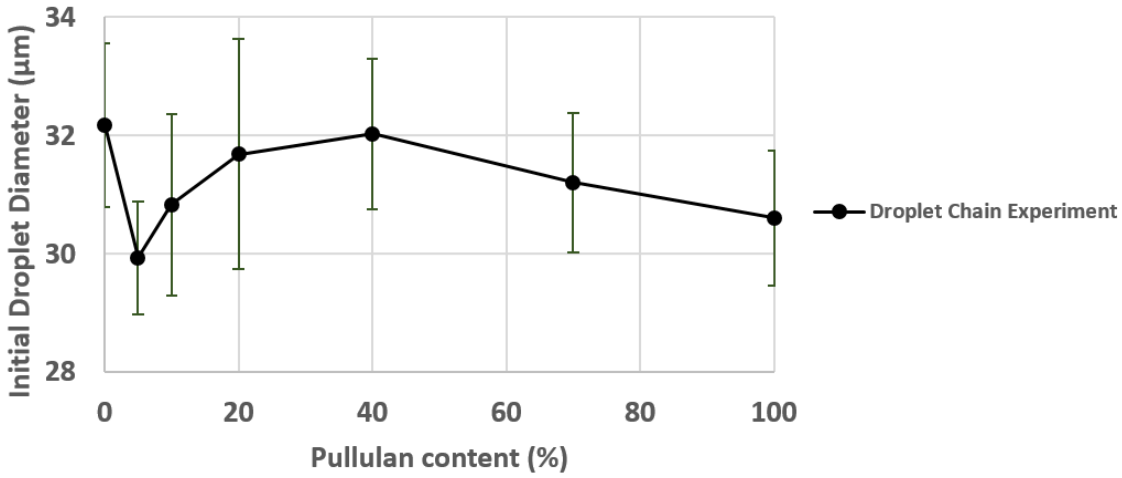

Figure B.1: Initial droplet diameter for different pullulan contents. N=2 except N=3 for the 0% pullulan case.

From the initial droplet diameter (d_0) and the volume equivalent diameter (d_v), the particle density (ρ_p) could be predicted according to [553]

$$\rho_p = \left(\frac{d_0}{d_v}\right)^3 \sum_i C_{0,i} \tag{B.1}$$

where $\sum_i C_{0,i}$ is the feed concentration (1.875 mg/mL) and d_v includes external voids. The predicted and measured particle density values are given in Figure B.2.

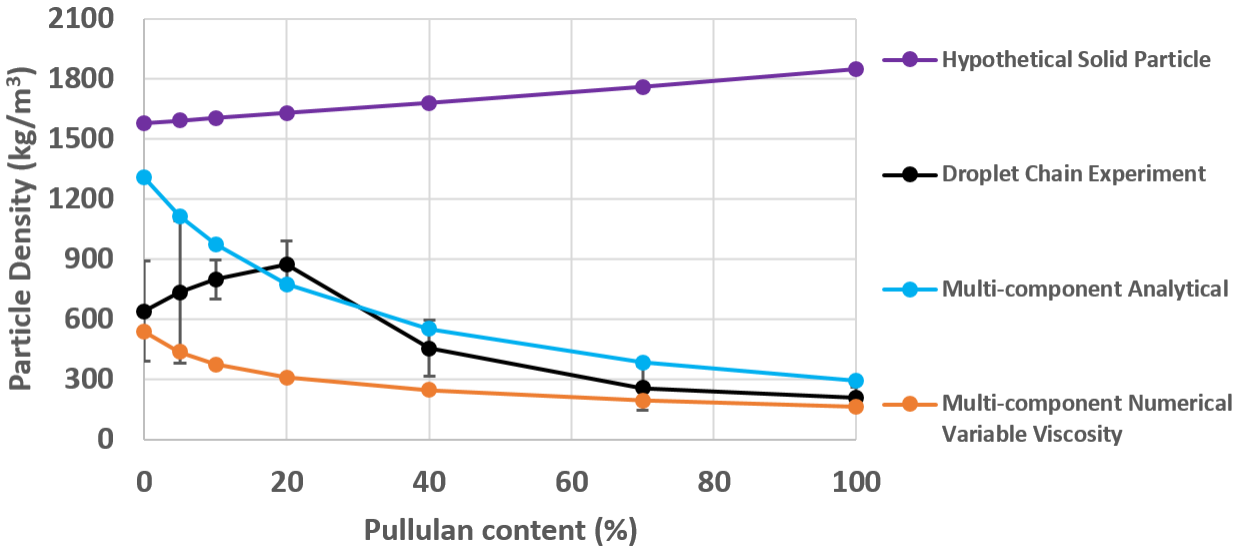

Figure B.2: Experimental results and numerical predictions of particle density for different pullulan contents. Colour available online.

Note that the particle density can also be defined as

$$\rho_p = \frac{m_p}{V_h} \tag{B.2}$$

where m_p is the mass of the particle which could be estimated from the initial droplet diameter and solute concentration and V_h is the hydrodynamic volume of the particle, which includes external voids, and can be defined as

$$V_h = \frac{\pi}{6} d_v^3 \tag{B.3}$$

If the hydrodynamic volume remains constant after shell folding, internal voids are transferred to external voids and the particle density remains constant after shell folding.

The particle density is useful for prediction of aerodynamic diameter, which can be calculated according to Equation (B.4) assuming spherical droplets and particles and neglecting slip correction. [554]

$$d_a = d_v \left(\frac{\rho_p}{\rho^*}\right)^{1/2} \tag{B.4}$$

The reference density ρ^* is equal to 1000 kg/m^3. The predicted and measured aerodynamic diameter values are given in Figure B.3. The results indicate that the powder is on the large side for an inhalable powder.

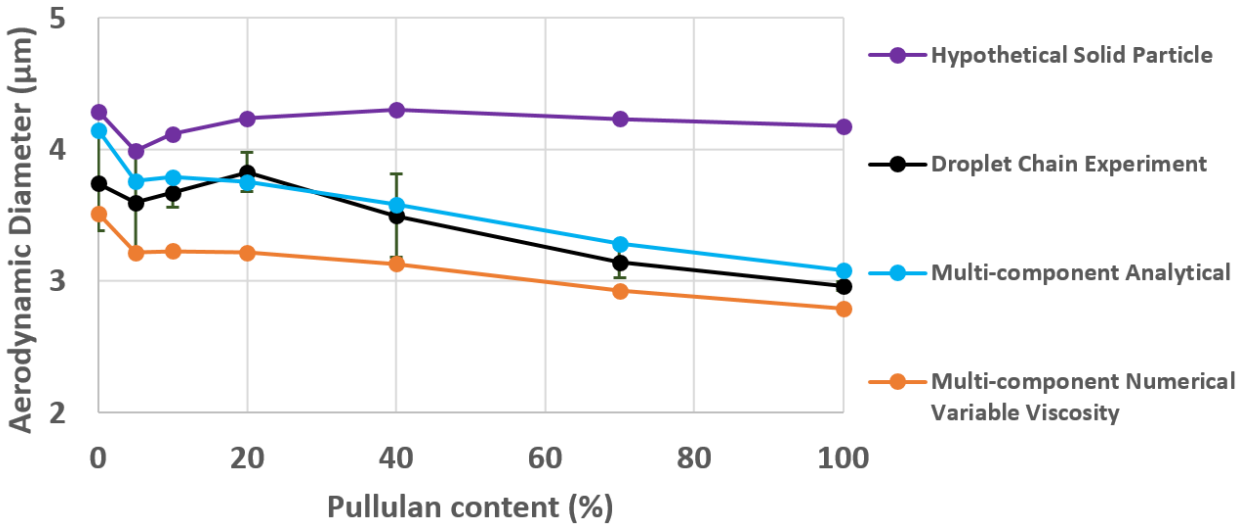

Figure B.3: Experimental results and numerical predictions of aerodynamic diameter for different pullulan contents. Colour available online.

The shrinkage ratio, here defined as the hydrodynamic volume of the particle as a fraction of the initial droplet volume, can be calculated according to

$$f_V = \frac{d_v^3}{d_0^3} \tag{B.5}$$

The shrinkage ratio is an important indicator of whether biologic material may reside on the surface of the microparticles. The predicted and measured shrinkage ratio values are given in Figure B.4.

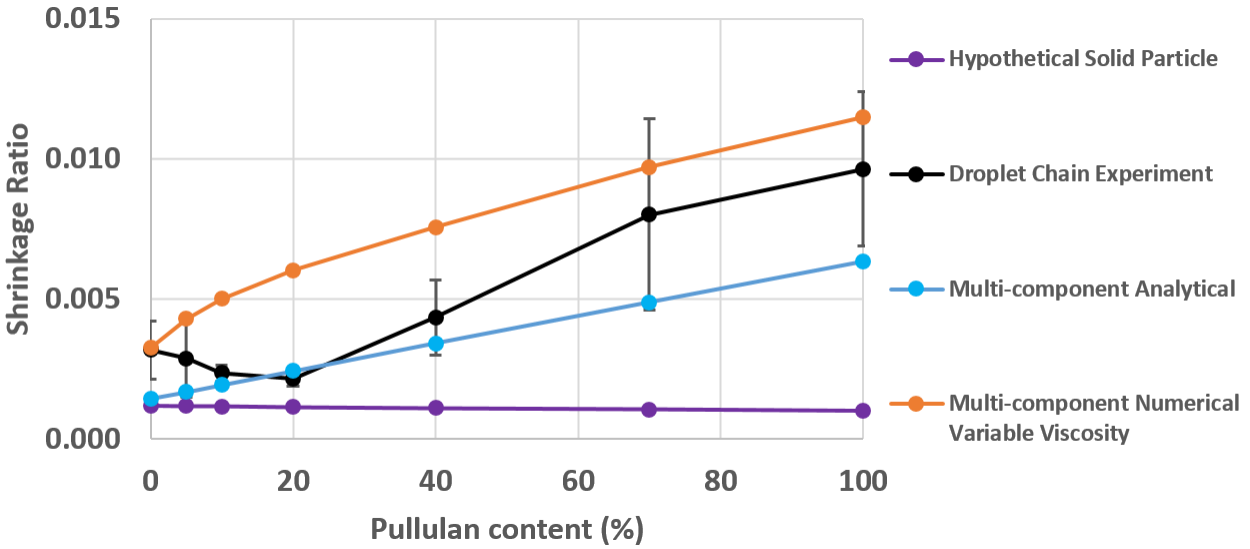

Figure B.4: Experimental results and numerical predictions of shrinkage ratio for different pullulan contents. Colour available online.

At high pullulan contents the shrinkage ratio increased, indicating the droplet shrunk less before precipitation occurred. Therefore, the biologic may have less chance of residing on the surface at the higher pullulan content, although at all contents there was much shrinkage. However, this ratio is much larger for spray drying where solids contents are higher and initial droplet diameters lower. The high initial viscosity may have an effect, however.

The total void space (external and internal) is calculated according to

$$\emptyset = \frac{d_v^3 - d_{v,solid}}{d_v^3} \tag{B.6}$$

where $d_{v,solid}$ is predicted according to

$$d_{v,solid} = d_0 \left(\sum_i \frac{Y_i}{\rho_{t,i}} \sum_i C_{0,i} \right)^{1/3} \tag{B.7}$$

where Y_i is the overall mass fraction of the component i and the other variables were defined previously. Note that this represents the void space at the time of shell formation and does not account for subsequent shrinkage. The predicted values are given in Figure B.5.

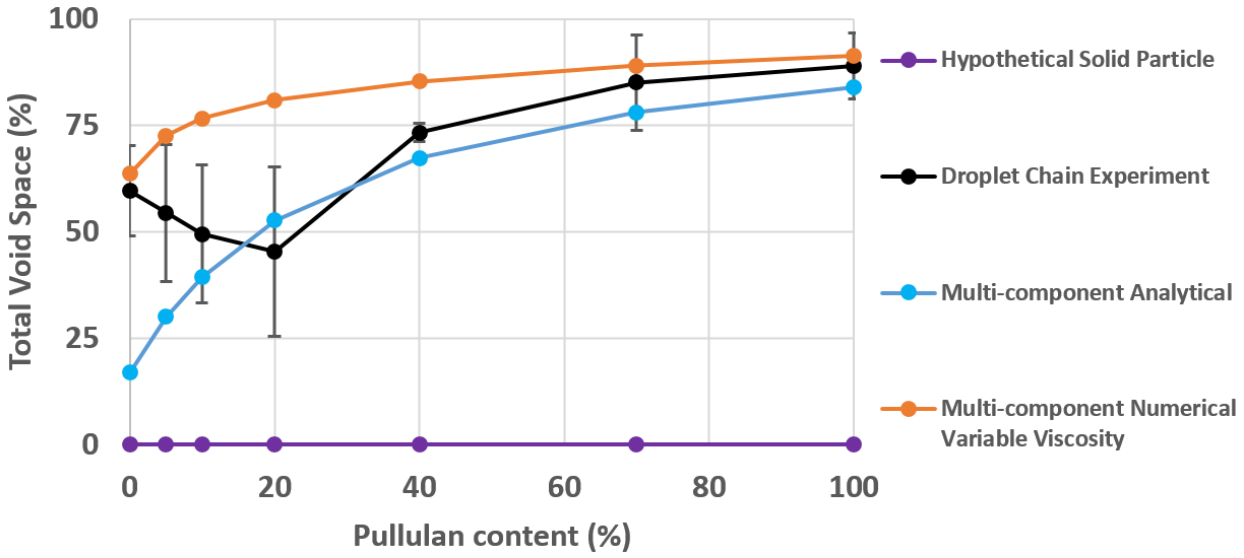

Figure B.5: Predictions of total void space at the time of initial shell formation for different pullulan contents. Colour available online.

Assuming that all solute precipitates into a rigid spherical shell with outer diameter d_v at time t_t, the internal diameter of the formed particle, d_i, which contains void space, is given by the following equation derived from a mass balance

$$d_i = \sqrt[3]{d_v^3 - \frac{d_0^3 \sum_i C_{0,i}}{\rho_{t,ave}}} \tag{B.8}$$

where $\rho_{t,ave}$ is the average true density of the shell which is the same as the average true density of all components and is thus given by

$$\rho_{t,ave} = \frac{1}{\sum_i \frac{Y_i}{\rho_{t,i}}} \tag{B.9}$$

where Y_i is the mass fraction of component i in the formulation.

The shell thickness, δ_s, can be estimated according to

$$\delta_s = \frac{d_v - d_i}{2} \tag{B.10}$$

Note that the internal diameter and shell thickness predictions assume no shrinkage after shell formation. The predicted values are given in Figure B.6.

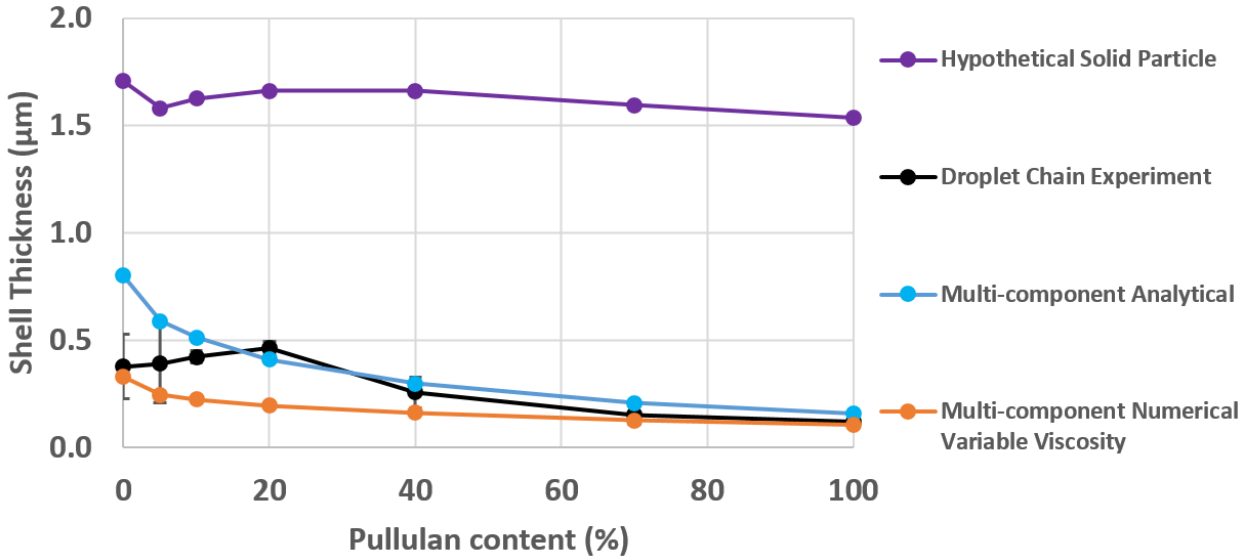

Figure B.6: Predictions of shell thickness at the time of initial shell formation for different pullulan contents. Colour available online.

By comparison to the SEM in Chapter 3, it is noted that there is a trend of smaller shell thickness leading to more wrinkled particles.

Appendix C

Phage D29 plaque assay protocol

The following protocol was developed in order to perform plaque assays with phage D29. It is similar to the method developed by Prof. Graham Hatfull's group at the University of Pittsburgh [555], but contains slight changes to speed up the process and more details regarding why things are done a certain way, which will be useful for a beginner. Note that this process may differ between different phages. Dr. Rachael Chang and Dr. Sharon Leung, then at the University of Sydney, and Melissa Harrison and Prof. Dominic Sauvageau at the University of Alberta, deserve much credit for helping to develop this procedure. An outline containing some of the basic steps are given in Figure C.1. More details are in the text that follows.

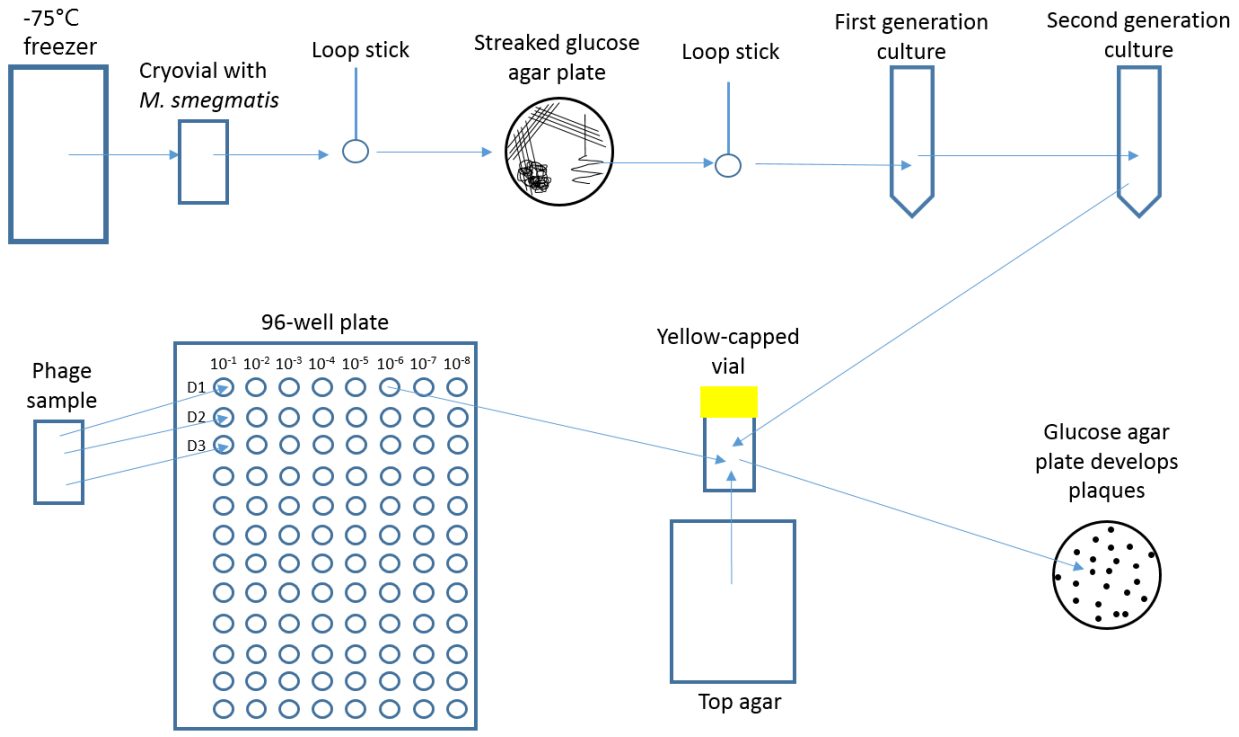

Figure C.1: Diagram showing the basic steps involved in performing a full plate plaque assay. The yellow-capped vial for a specific dilution contains 10 µL of phage diluted in buffer with $CaCl_2$, 500 µL of second generation bacterial culture, and 4.5 mL of top agar kept at 56°C.

1) **Preparation of glucose agar plates**

Combine the following ingredients in a glass flask or bottle. About 36 plates can be made per litre of material, requiring about 6 hours of time. Agar may dry out if more than 1 litre is made at a time.

- 7H10 agar (19.0 g/1 L media)
- 40% glycerol (12.5 mL/1 L media) (stored in fridge or cold room)
- 40% dextrose (4.95 mL/1 L media) (stored in fridge or cold room; to make dextrose solution, add 100mL of filtered water to a 250mL beaker and weigh out 40g dextrose. Put beaker solution on a hot plate at 50°C and add parafilm to top. When ready, start stir function and add dextrose slowly so that it doesn't clump. Leave to dissolve and then pour into 50mL Eppendorf tubes before use)
- ddH2O (990 mL/1 L media)

Mix the ingredients well by hand by inverting and shaking well, until the color is homogeneous. Then, loosen the cap and autoclave the solution. After autoclaving, cool the solution to 56°C using a water bath. Temporarily remove the solution from the water bath, place on a paper towel so it doesn't cool down as quickly, and quickly add the following ingredients in the order that they are listed.

- 0.1 M CaCl2 (10 mL/1 L media) (stored in fridge or cold room)
- Carbenicillin Solution (1 mL/1 L media) (stored in fridge or cold room; be quick and store with aluminum foil as the antibiotics are light sensitive)
- Cyclohecimide Solution (1 mL/1 L media) (“ ”)

The antibiotic Carbenicillin serves to remove bacteria other than *M. smegmatis,* while Cyclohecimide inhibits mold and yeast growth. *M. smegmatis* is resistant to these antibiotics. Mix the solution well by hand and put the bottle back in the water bath. Take many sterile Petri dishes, remove lids, and place in a fume hood. Remove the solution from the water bath. Use a serological pipette to distribute 20-25 mL of solution into each Petri dish. Be sure not to distribute the whole volume from the serological pipette so that bubbles don't form (if they do, remove them with the pipette). Make as many plates as possible with the solution available. Once the solution is dried in the Petri dishes, put the lids back on, and stack 12 plates together

one on top of the other. Use plastic cling wrap to wrap together each stack of 12 plates to keep the moisture within the plates. Store the plates upside down at 4°C and do not use for at least 24 hours. Place aluminum foil over the plates as the antibiotics are light-sensitive. The plates can be stored for 2 months if not dried out.

2) Preparation of working *M. smegmatis strain mc²155* cultures

Prepare the *M. smegmatis* for storage in the -70°C freezer using the following recipe.

- 0.47 g 7H9 powder
- 90 mL 50% (w/v) glycerol
- 10 mL ADC (see below)
- 50 µL of Tween®80

The solution should be 0.22 µm filtered. It can be stored up to 6 months at 4°C. Transfer a single colony to a 1 mL cryovial and store at -70°C.

The ADC (albumin-dextrose-catalase, so-called even without the catalase; a nutrition source) is prepared using the following recipe.

- 60 g dextrose
- 25.5 g NaCl
- 150 g Albumin
- 2850 ml ddH2O

First, a stir bar is placed in a beaker, then add, in this order, Albumin, NaCl, and ddH20. When the albumin comes into contact with water it becomes sticky and large chunks form that may not easily go into solution. A spatula can be used to smash these large chunks on the side walls of the beaker to more easily dissolve. Stir until the Albumin and NaCl are dissolved and then add dextrose while stirring. Filter sterilize but don't autoclave. Store for up to 6 months at 4°C. Do not autoclave as it is not stable at higher temperatures.

Take out a cryovial containing stock of *M. smegmatis* from the -70°C freezer. Streak the bacteria onto a glucose agar plate (see Step 1). Streaking consists of dipping a stick with a loop on the end into the cryovial, wiping the loop back and forth over a small portion of the

glucose agar plate, then making 3 streaks out from there with a new loop, and 3 more streaks out from there using another new loop, repeating, and then streaking once more using a squiggle process (see the streaked plate in Figure C.1).

After streaking, the parafilmed plate should be incubated for three days at 37°C, after which time several isolated colonies should have grown. If the plate is not parafilmed, check after two days. After the incubation period, 'pick' a colony from the squiggle to generate to higher numbers. Picking a single colony ensures that the bacteria population is homogeneous, and that the titer results have little variability and chance for contamination from other bacteria. After incubation, the streaks should be a light tan color with a waxy consistency. After picking a colony, the plates can be parafilmed and stored at 4°C for continued use. Generally, a streaked plate is useful for about 1 month, as the bacteria may adapt to life in the fridge and no longer grow the same, and the growth rate is important for phage infection. Additionally, if the plate dries up it will no longer be useful. It is a good idea to make multiple streaked plates at once, as success is not guaranteed.

3) Prepare first generation bacteria culture (7H9 WITH Tween®80)

Prepare 7H9 broth using the following recipe.

- 4.7 g 7H9 broth base
- 5 ml 40% glycerol
- 900 ml ddH2O

The above are combined in a beaker. Add a stir bar, place on a stir plate, and mix moderately until well-combined (about 5-10 minutes); mix by hand and then autoclave at 110°C for 15 minutes. Should be yellow-green after autoclaving.

The colony that has been picked from Step 2 using a loop (ensuring you use a 'generous portion' of bacteria) should be dipped into a 4 mL solution of first generation liquid culture in order to grow the bacteria to larger numbers. The recipe for the first generation liquid culture is as follows (add in order shown). This solution can be prepared in a sterile 50 mL Falcon tube and then aliquoted into sterile 15 mL Falcon tubes, each containing 4 mL of the solution.

- 45mL of 7H9 broth (from above)
- 5 mL of ADC (see Step 1)
- 0.5 mL of 0.1M $CaCl_2$
- 50 µL of 50 mg/mL Carbenicillin (light sensitive; take from cold room just prior to adding)
- 50 µL of 10 mg/mL Cycloheximide (light sensitive; take from cold room just prior to adding)
- 125 µL Tween®80

The solution contains growth media and Tween surfactant to prevent clumping of the bacteria. Label as 1st generation with the date. Invert a few times. Incubate at 37°C in a *shaking* incubator for 24 hours. 'Speed 11' was used, and different speeds may not work. The first generation liquid can be stored at 4°C away from light for use in multiple 2nd generation cultures. The 1st generation culture is typically fine to store for about 3 weeks. The amount of 1st generation needed is 400µL / 10mL · the amount of 2nd generation that is needed (see Step 4 regarding the amount of 2nd generation that is needed).

4) Prepare second generation bacteria culture (7H9 WITHOUT Tween®80).

Prepare the same solution (add in order shown) as in Step 3 but without Tween (see below).

- 45mL of 7H9 broth (see Step 3)
- 5 mL of ADC (see Step 3)
- 0.5 mL of 0.1M $CaCl_2$
- 50 µL of 50 mg/mL Carbenicillin (light sensitive; take from cold room just prior to adding)
- 50 µL of 10 mg/mL Cycloheximide (light sensitive; take from cold room just prior to adding)

Much more solution than this may be needed and multiple 50 mL Falcon tubes can be used. Aliquot 10 mL of the above solution to different 50 mL Falcon tubes. Use a cage to store the tubes upright.

Slowly vortex the 1st generation culture from Step 3 and ensure it is cloudy using an optical density instrument. To do this, put in a blank cuvette containing media only (no bacteria, no bubbles) and measure optical density, then put a cuvette in that contains 0.5 mL of 1st

generation culture and sample. An optical density > 1 worked, while 0.3 and 0.7 did not work, due to poor bacterial growth associated with an incubator shaking speed that was too fast.

To the 10 mL aliquots of 2nd generation solution above (in 50 mL Falcon tubes), add 400 µL of 1st generation culture. Incubate with shaking at 37°C and 'speed 11' (specific to the shaking incubator in the Mycobacteria Laboratory at the Centenary Institute in Sydney) for 24 hours. Note that the test tube must be 5 times the volume of the culture to be prepared. After removal, ensure there are no clumps and do not vortex the 2nd generation culture too many times. The 2nd generation culture can be used for a week.

The amount of 2nd generation culture needed is 0.5 mL · #plates (see Step 5 regarding the # of plates {the same as the number of 5 mL yellow-capped tubes} that are needed).

5) Dilution series and full plate titer plaque assay

Generate phage buffer with CaCl2 as follows.

- 10 ml 1 M Tris, pH 7.5 (cold room)
- 10 ml 1 M MgSO4
- 4 g NaCl
- 980 ml dd H2O

Combine the above in a beaker and stir moderately for ~5 minutes. Aliquot 100 mL into 10 bottles and autoclave. After autoclaving, add 1 mL of 0.1 M CaCl2 to each 100 mL of phage buffer using a micropipette and mix, storing at 4°C.

The day before doing plaque assay, label a 96-well microplate with 10^-1 => 10^-max and 5 mL yellow-capped tubes with e.g. -5 D1, -6 D2, etc. (only use tubes for the dilution levels that you are plating). Also, add 180 µL of phage buffer with $CaCl_2$ to each well of microplate. This is most easily done using a multi-channel micropipette using fluid from a Petri dish. Store the microplate at 4°C.

Make Middlebrook Top Agar (MBTA) using the following recipe.

- 4.7 g of 7H9 broth base
- 7.0 g NobleAgar (since BactoAgar expensive; could use any __agar)
- ddH2O up to 1L

Combine all the ingredients in a heat proof beaker and autoclave, then aliquot to 200 mL sterile bottles and store at 4°C for at most 1 month.

Make "Dilution" 7H9 as follows. The final concentration of the CaCl2 should be 2 mM.

- 100 ml 7H9 broth (see beginning of Step 3)
- 2 ml 0.1 M CaCl2

Securely close the bottle and invert several times to mix.

Make top agar using the following recipe.

- 50 ml MBTA (see above)
- 50 ml "Dilution" 7H9 (see above)

Each Petri dish requires ~5 mL of top agar, and hence ~2.5 mL each of MBTA and "Dilution" 7H9. The MTBA is semi-solid if stored in the fridge, so heat in a microwave (with cap undone as pressure could build up) until *completely* solidified and bubbles. This will take 1-2 minutes for 50 mL, and one should pause the microwave about every 30 seconds to shake the bottle. Remove the melted MTBA from the microwave and sterilely add an equal volume of "Dilution" 7H9. Cap and shake to mix. Before it solidifies, put it in a water bath at 56°C, or use it all quickly (place it on a paper towel so it doesn't cool down as quickly). If it does solidify, it can be re-heated in the microwave until it's completely liquid again. If the top agar is too hot, it could inactive the phage and bacteria, while if it is too cool, it will make chunky plates that are difficult to analyze and give poor results. Top agar (which should be white) and MTBA should be re-heated three times at most.

Ensure there is enough materials; #plates · 4.5 mL + margin = volume of top agar; ensure enough plates and that they are not dried out; #plates = #dilutions [3, i.e. 10^-5, -6, -7] · #tests · #replicates [3] + #controls [1 per replicate]

Vortex the 2nd generation culture and add 0.5mL to each labelled yellow-capped tube; one can leave it there while doing serial dilutions.

Label plates from the cold room on bottom edges in small writing according to yellow-capped tubes and place in fume hood.

Vortex the phage sample (e.g. resuspended spray dried phage powder) and, using micropipette, add 20 µL of it to first well of each dilution. Store phage sample at 4°C. With a new micropipette tip mix up and down 12 times (at 20 µL volume setting) and in circles and then transfer to next well, ensuring the liquid goes in the phage buffer with $CaCl_2$ in the well and not on the sides of the well (submerse the tip directly into the buffer). Change the tip for each well and repeat, using the plate cover to keep track of which well you used last.

Add 10 µL from wells of interest using a micropipette to the yellow-capped tubes that already contain 500 µL of 2nd generation culture. Keep the wells in the fridge after and redo if something messes up.

To plate, move the bottle with the top agar from the water bath to the fume hood, keeping paper towel underneath and ensure it doesn't cool down too much while plating. Use a serological pipette to add ~4.5 mL of top agar to the yellow-capped tubes (only 4-6 at a time, ensuring the tip does not touch the bacteria solution). If too much top agar is added it won't solidify correctly, causing it to separate when the plate is flipped, while if too little is added complete coverage on the plate won't occur. One at a time, invert the tube 5 times to mix and then quickly pour onto a glucose agar plate (see Step 1) and immediately but gently swirl (ensuring no bubbles form) to ensure even distribution of plaques over the plate. Repeat inversion, pouring, and swirling for other tubes. Cool the plates with the lids off (can stack lids from successive plates) until the agar has solidified (generally this take ~15 minutes), at which point it will turn clearer/whiter. Slowly flip the plates to ensure the solid doesn't separate.

Incubate the plates upside-down (to ensure no dripping of condensate onto the lawn) at 37°C, with a maximum of 4 plates stacked to ensure even heat distribution, for ~24 hours. Use plastic cling wrap if it is necessary to store for longer, noting that larger plaques will occur with longer incubation time and they may overlap each other making interpretation difficult. Leave the plates for longer if bacteria grew slowly (low optical density) or unexpectedly small plaques.

6) Count plaques

After the plates have incubated for 20-48 hours, many plaques should be visible. One may count the plaques directly and take a picture of each plate to analyze the plaque count and save it on a computer. A ten-fold decrease in the number of plaques per plate across each plated dilutions should be observed.

The titer is calculated according to the following equation.

$$Titer\left[\frac{pfu}{mL}\right] = DF \times \#plaques/plate \times \frac{1000\ \mu L/mL}{10\ \mu L/plate} \quad \text{(C.1)}$$

DF refers to dilution factor, for example, with 10^{-7} dilution, DF is 10^{7}. The number of plaques per plate is counted for the plate at that specific dilution level. A value of 10 µL/plate is included since 10 µL of the phage sample is added to the yellow-capped tubes and then the plate in Step 5.

7) Cleaning

Autoclave before disposing of plates and other materials. Do not use ethanol in the autoclave and ensure things entering the autoclave have indicating tape and are left slightly open. Before autoclaving, ensure water is covering the bottom element and water is in the crates at the bottom. Wipe down the fume hood and other contaminated surfaces with 80% ethanol. If available, further decontaminate surfaces using UV lights for ~20 minutes.

Further data generated with the jet nebulizer mathematical model

The mathematical model for renebulization in the jet nebulizer described in Chapter 4 was used for generating the following figures.

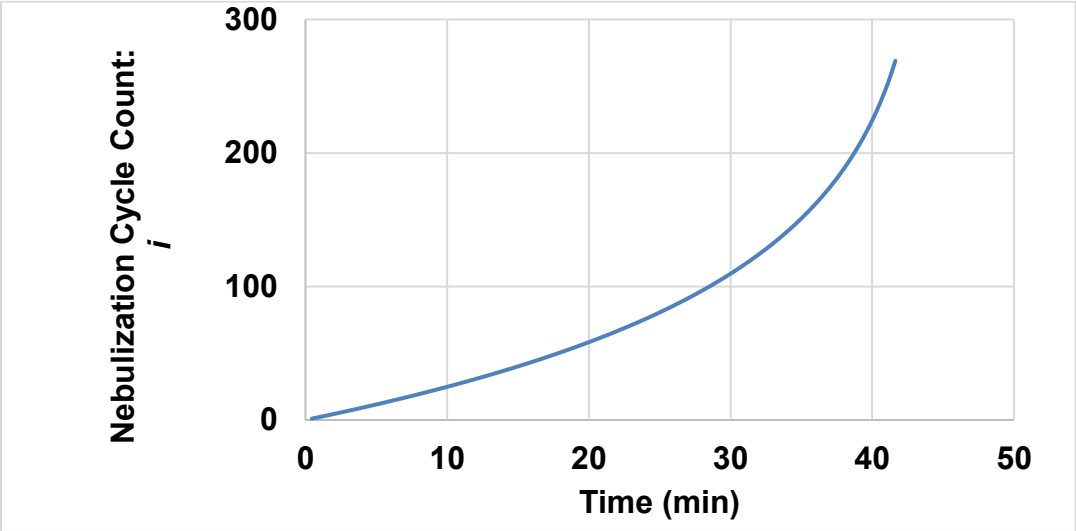

Figure C.2: Mathematical prediction for the relationship between nebulization cycle count and time.

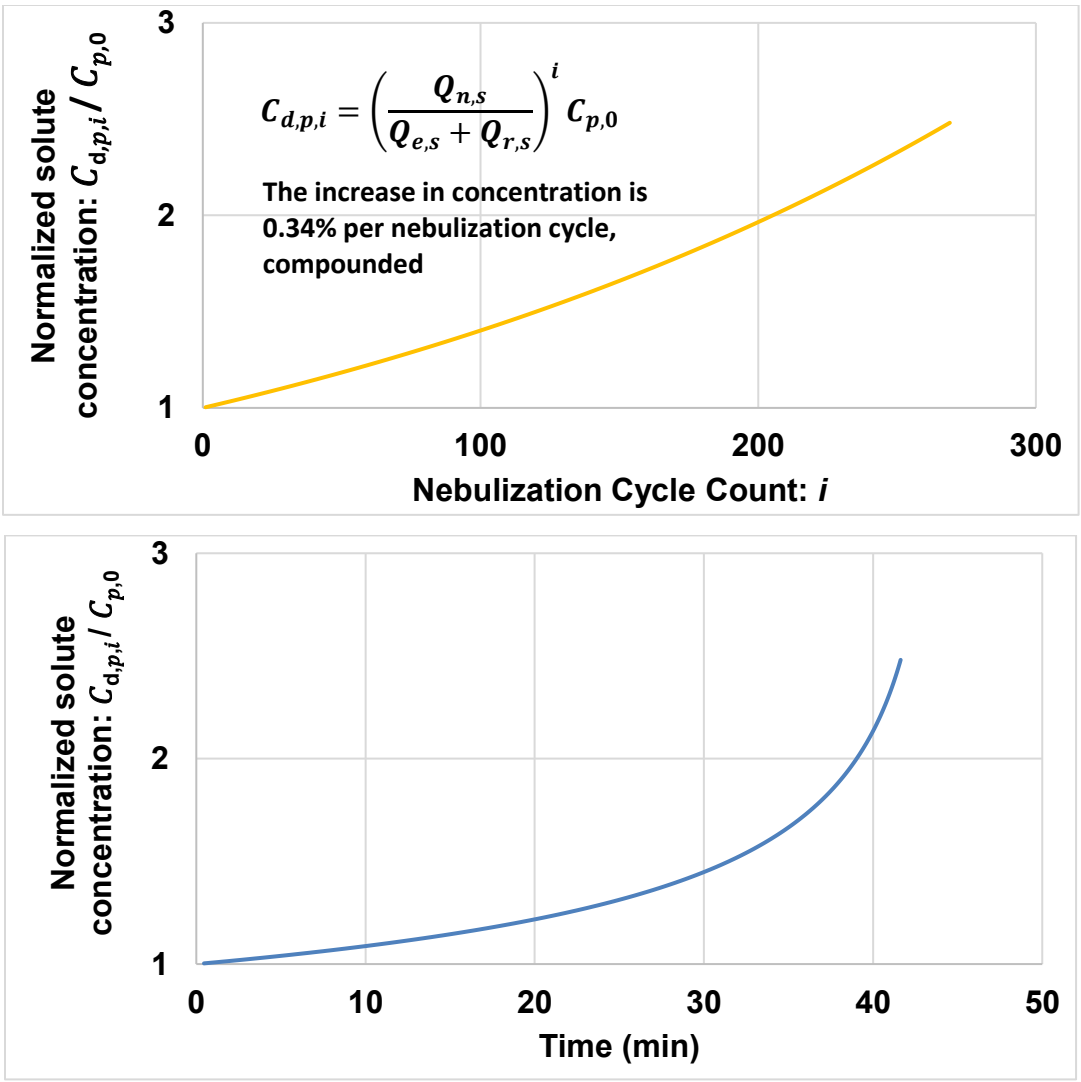

Figure C.3: Mathematical prediction of how the solute concentration increases with each cycle (top) or with time (bottom) in the jet nebulizer. The solute concentration is normalized by the initial value. Note that for phage as the solute, this includes both inactive and active phage.

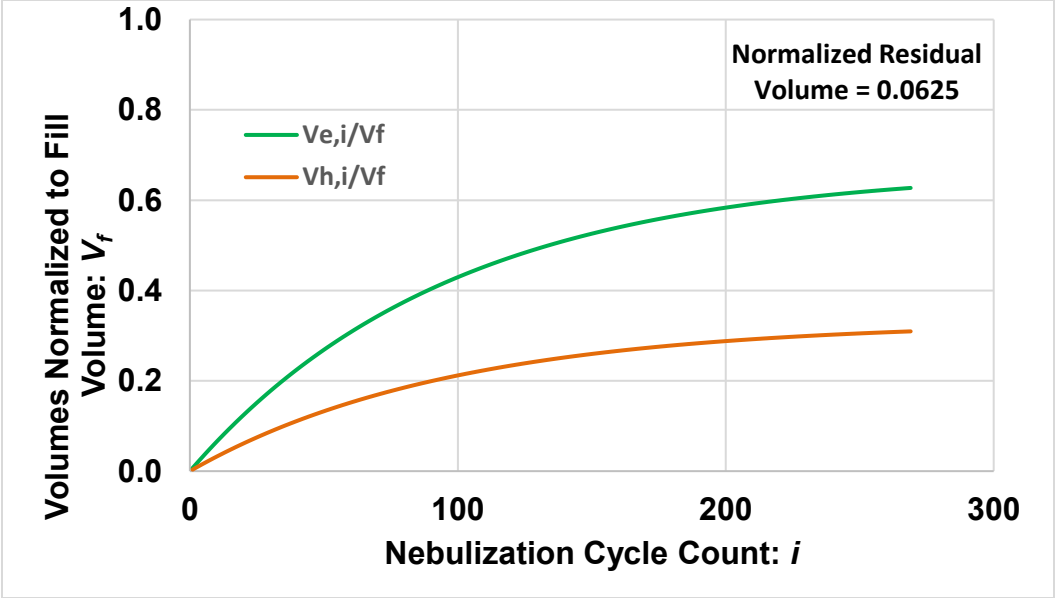

Figure C.4: Mathematical prediction of the volumes of solvent exiting the nebulizer through the mouthpiece as aerosol droplets or by losses due to humidification of the compressed gas. Roughly two-thirds of the solvent mass exited the mouthpiece as aerosol droplets and one-third by humidification of the compressed gas, while a small amount remained as residual volume in the reservoir of the device.

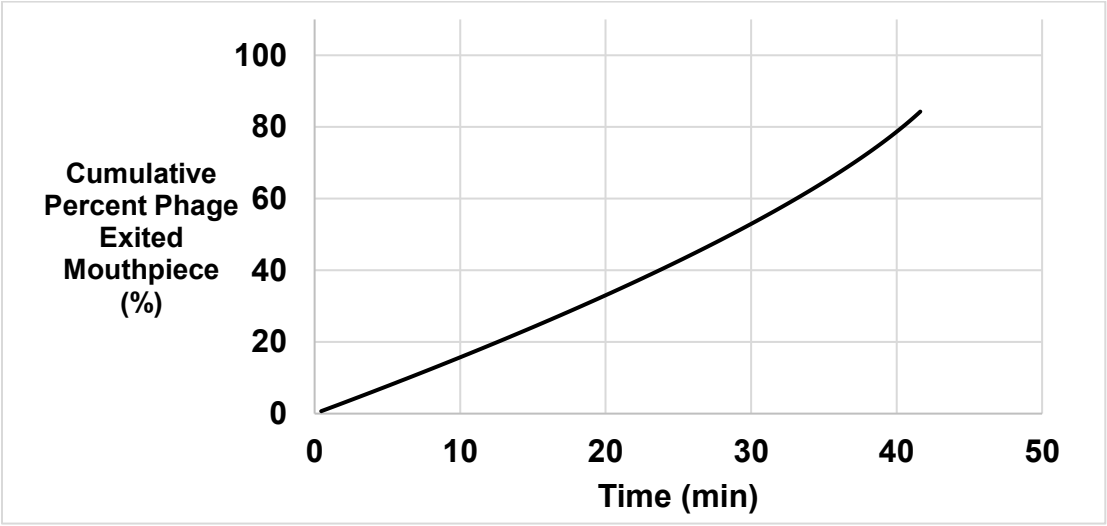

Figure C.5: The cumulative percent phage, either active or inactive, that exited the mouthpiece over time, relative to the initial amount of phage filled into the reservoir of the device. Not all phage exited the mouthpiece as some remained in the residual volume. It is expected that the concentration in the residual volume would be higher than initially filled.

Data on nebulization of phage D29 and DLP2 in different formulations

Measurements were performed to determine the titer of phage D29 during nebulization tests with different formulations that may be suitable for spray drying. The formulations tested were TTB (3 mg/mL trileucine, 25.5 mg/mL trehalose, 1.5 mg/mL trisodium citrate) and LTC (6 mg/mL leucine, 23.4 mg/mL trehalose, 0.6 mg/mL casein sodium salt). The latter formulation is similar to that which successful spray dried phages in the study by Matinkhoo *et al.* [550]. The nebulizer used was the same Aerogen Solo model tested in Chapter 4. The different assays performed are described in Table C.1.

Table C.1: Description of the different assays performed for titer reduction measurements with vibrating mesh nebulization of phage D29 in TTB and LTC formulations.

<table>
<tr><th>Test #1 - Stock titer over time</th><th>Test #2 - Control titer in filter</th><th>Test #3 - Control titer in nebulizer</th><th>Test #4 - Titer after nebulization</th></tr>
<tr><td>Initial titer (measured)</td><td>Place 6mL diluted lysate in separate filter at same time as start of Test #4</td><td rowspan="3">Take ~1mL (measure with micropipette) non-nebulized solution from nebulizer inlet in Test #4 (Assay #4)</td><td>Place 6mL diluted lysate in nebulizer with micropipette</td></tr>
<tr><td>Initial titer / 100 (Assay #1)</td><td rowspan="2">Measure titer in filter after completion of Test #4 (Assay #3)</td><td>Nebulize until complete except ~1mL for Test #3</td></tr>
<tr><td>Diluted control titer after kept at room temperature for duration of Test #4 (Assay #2)</td><td>Measure titer after nebulization by removing from filter with micropipette (Assay #5)</td></tr>
</table>

The results of the study described in Table C.1 are given in Figure C.6.

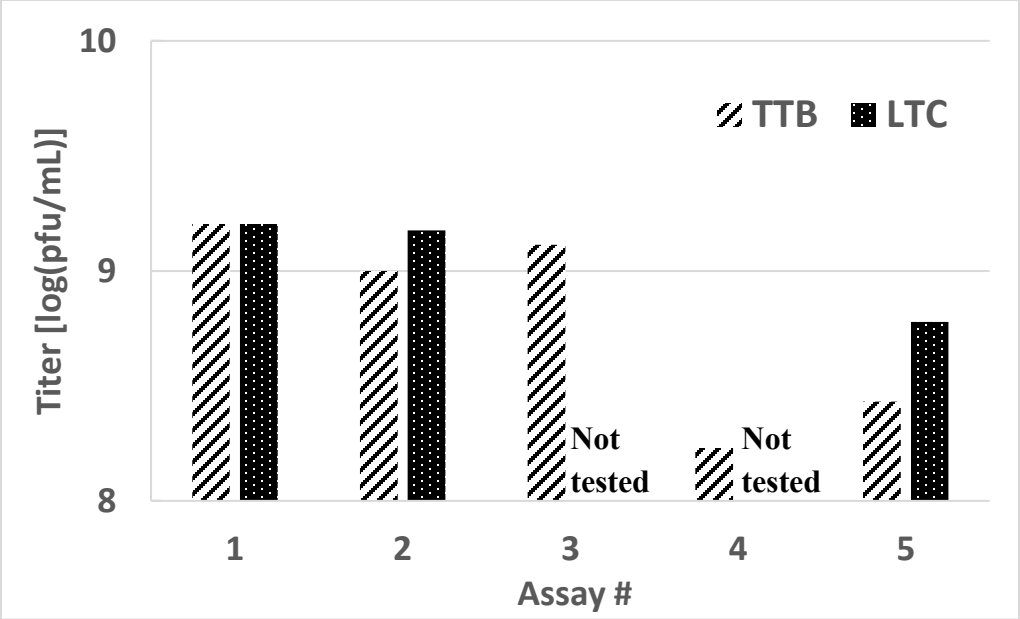

Figure C.6: Results of the study described in Table C.1.

The results indicate no phage D29 binding to the filter and liquid stability at room temperature for the duration of the run. Less than 1 log(pfu/mL) titer reduction was observed in each case. Slightly greater titer reduction due to vibrating mesh nebulization occurred for TTB, ~0.99 log(pfu/mL), than LTC, ~0.43 log(pfu/mL), perhaps associated with bubbling in the nebulizer, associated with the surface activity of trileucine. The titer reduction being large in the reservoir of the vibrating mesh nebulizer for the TTB case may indicate that the bubbles which formed in the reservoir due to the surface activity of trileucine are inactivating D29 due to contact with the air-liquid interface. The result with LTC, for which bubbles did not form, was similar to that for isotonic saline shown in Chapter 4. Spray drying with these formulations was discussed further in Appendix A.

Similar measurements were performed with phage DLP2 in trileucine and trehalose, water, and buffer, and in each case zero titer was observed, indicated that phage inactivation is dependent on the strain tested.

Imaging of phage D29

Helium ion microscopy was performed to view phages with and without the TEM staining method described in Chapter 4. The images are shown in Figure C.7.

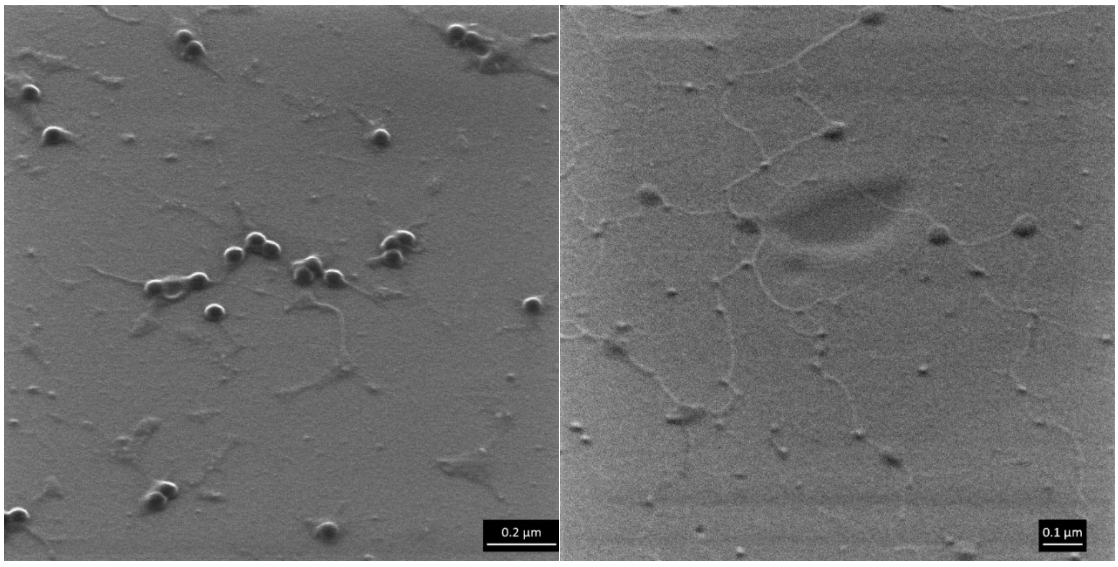

Figure C.7: Helium ion microscopy images of phage D29 without stain (left) and with stain (right).

Additional TEM images of phage D29 were performed and are shown in the following figures. These figures demonstrate the many ways phage D29 may be inactivated. Note that phage capsids are highly pressurized (~60 atm) due to high density packing (~500 mg/mL) of DNA and this confinement causes electrostatic repulsion of the negatively-charged DNA phosphate groups, which can be decreased by binding with divalent cations such as calcium and magnesium commonly used in phage buffer; typically, the outside of phage capsids are negatively charged as phage buffers are designed to be above the isoelectric point of the phage proteins and divalent cations will also bind to and stabilize the exterior of the capsid; phage capsids have a Young's modulus similar to Nylon (~1.8 GPa); some phages are subject to inactivation by osmotic pressure while others are not, depending on salt permeability [556-558]. Therefore, further formulation work to optimize salt content may affect titer reduction of phages during spray drying. Indeed, salt concentration will increase rapidly during solvent evaporation from atomized droplets and then decrease upon precipitation or when a phage is desiccated at the surface. The concentrations of spray dried phages were too low to view under TEM.

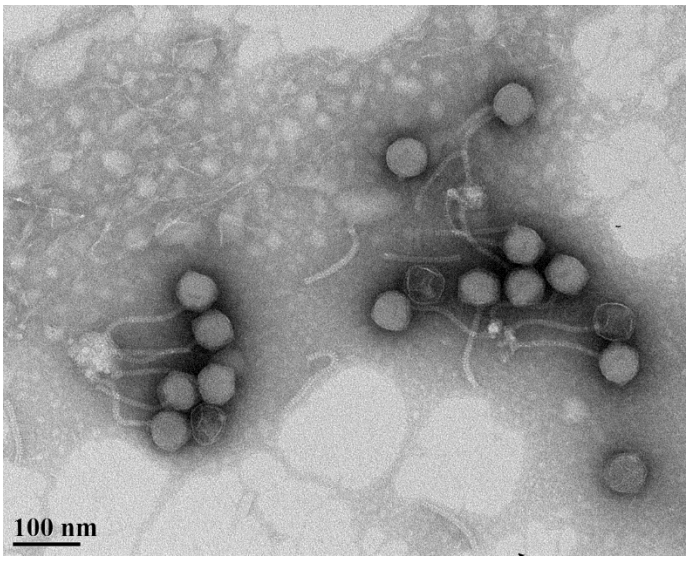

Figure C.8: TEM showing phage D29 binding to disintegrated bacterial cell wall, potentially leading to a titer reduction due to loss of binding capacity.

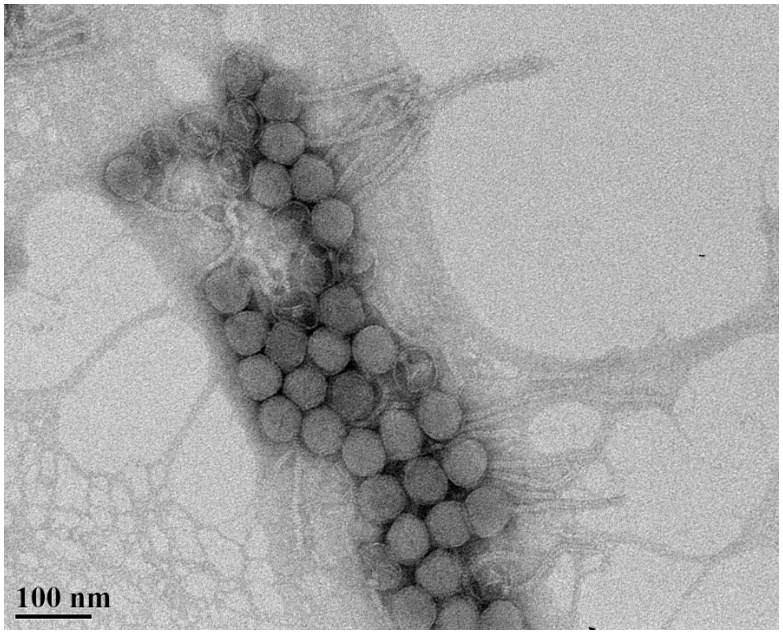

Figure C.9: TEM showing phage D29 clumping after centrifugation at high speeds potentially leading to titer reduction due to inability of some of the phages to access bacteria.

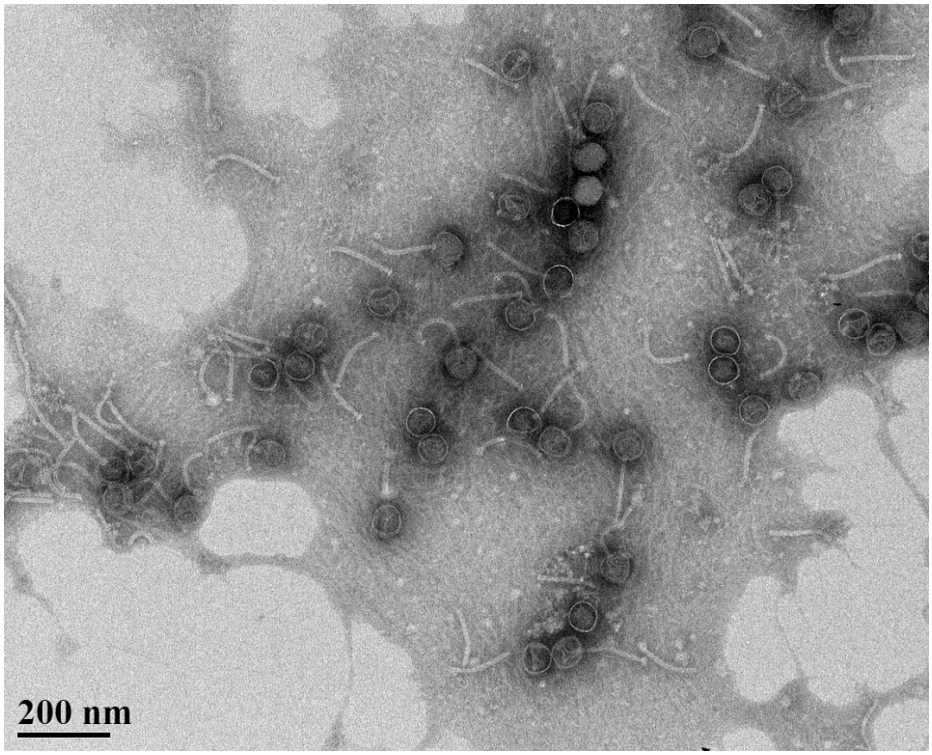

Figure C.10: TEM showing inactive phage D29 with detached tails and empty capsids.

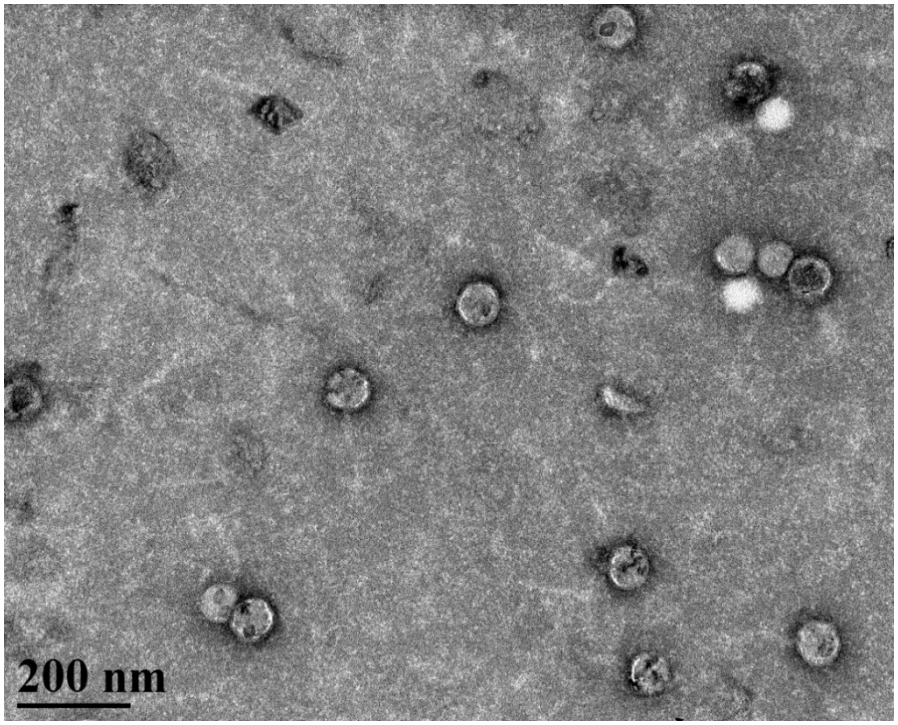

Figure C.11: TEM showing phage D29 from a lysate kept in the fridge for months for which a large titer reduction was observed; apparently there are degraded capsids.

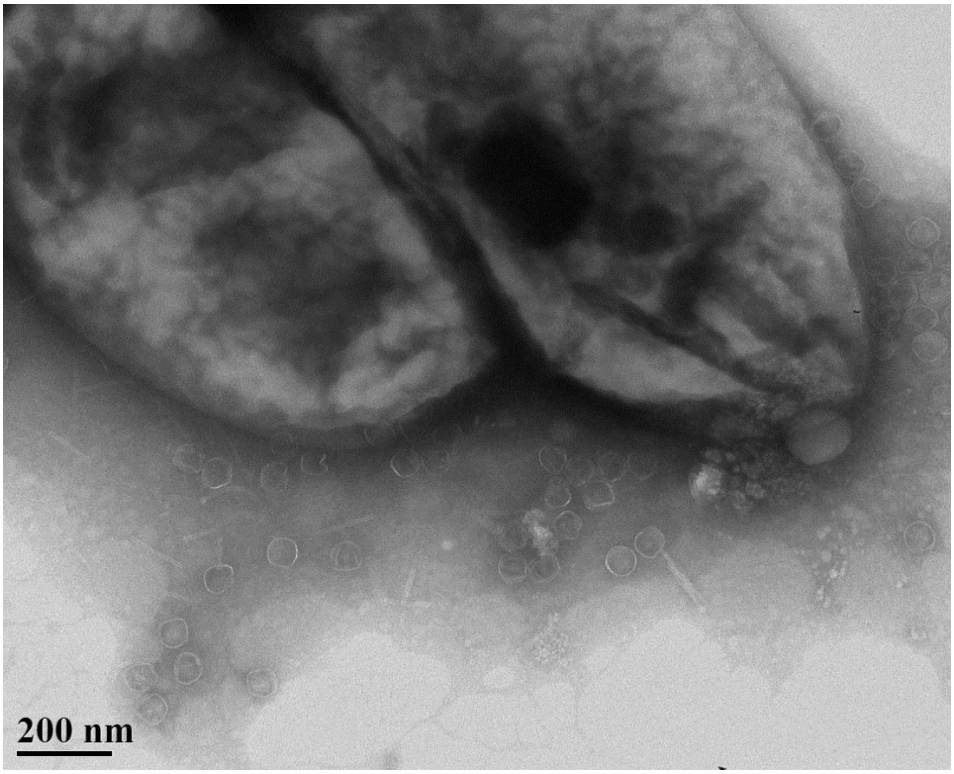

Figure C.12: TEM showing inactive phage D29 near bacteria which made it through the 0.22 µm filter.

Appendix D

HN878 bacterial challenge results

An attempt was made to provide prophylactic protection against hypervirulent *Mtb* strain HN878. This strain rapidly grows to high numbers and is more efficient at killing mice than *Mtb* strain H37Rv. A total of 7.4 ± 0.1 log(pfu/mL) was delivered to the lungs of mice (n=3 mice received phage only). The results of bacterial levels in the lungs 24 hours post-challenge are given in Figure D.1. The pre-treatment was not effective. It was not tested whether HN878 is susceptible to lysis by phage D29. It is possible that the bacteria grows too quickly relative to the time required for lysis, but this requires further experimental verification.

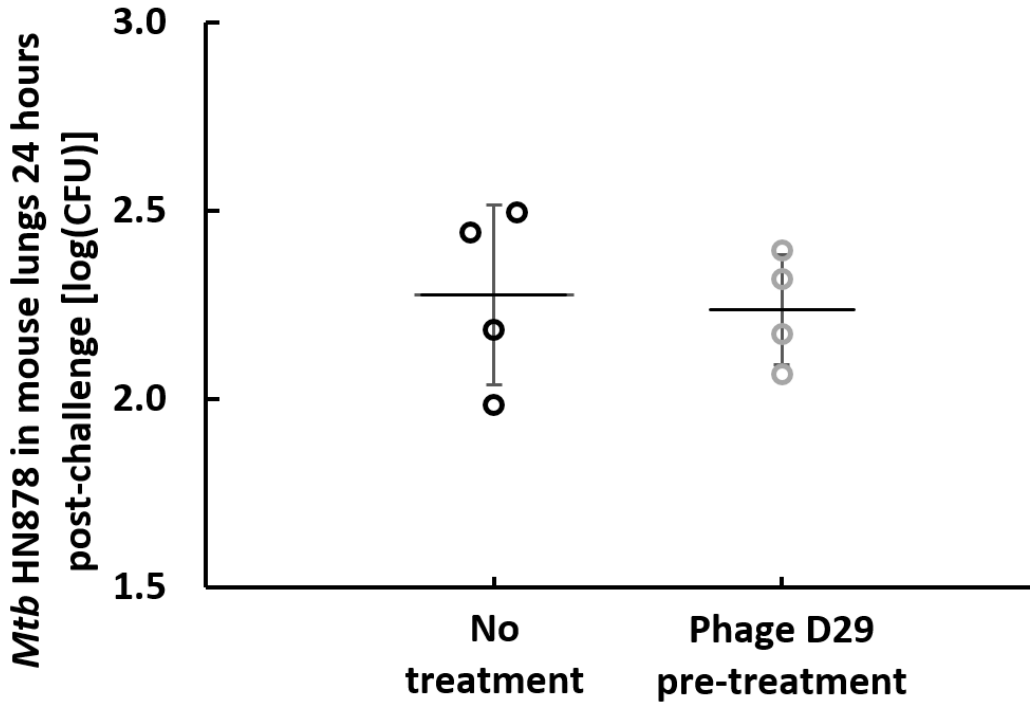

Figure D.1: Results of bacterial challenge against *Mtb* HN878.

NOID setup

A picture of the NOID set up for dose simulation experiments is given in Figure D.2.

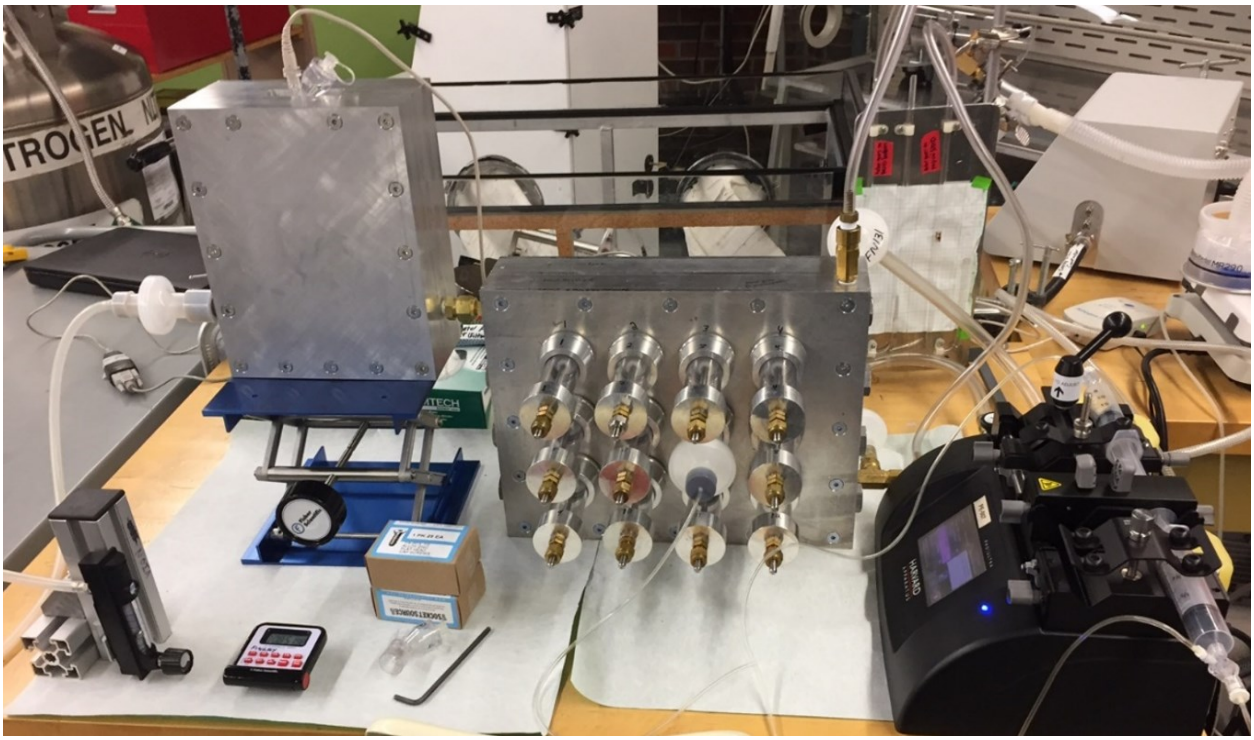

Figure D.2: Picture of NOID setup for dose simulation experiments.

Custom mouse restraint tubes were fitted to the nosepieces by In-Tox Products, LLC (Moriarty, NM, USA). The drawing package for the designed first plenum described in Chapter 5 and shown in Figure D.2 is available at (note that the o-rings were changed to 3/32”): https://www.dropbox.com/sh/rc9zhy4rpluvqlx/AACUkCKnZQvfCOSzCYgOeCNNa?dl=0

Modelling influence of plenum flow rate on deposition in NOID

Some modelling efforts were undertaken to understand how the deposition within the NOID would change with plenum flow rate. The aerosol first enters the first plenum where impaction is likely the dominant deposition mechanism. It may then undergo sedimentation in the mixing tube which may be modelled as a straight, horizontal, circular pipe. Deposition will then occur in the back plenum. The remaining aerosol is assumed to either be inhaled by the mice or convected by their noses. The effect of increasing plenum flow rate on changes in droplet size due to hygroscopic size changes is small (calculation performed as per Chapter 5). However, droplet size will change as the aerosol transits through the device due to preferential deposition of larger droplets by the aforementioned mechanisms.

The fraction of aerosol impacting in the first plenum, $f_{imp,1}$, was assumed to follow an empirical quadratic fit to preliminary deposition data. This value was approximate based on only one measurement at three flow rates and further experiments would increase the accuracy. The mixing tube has a diameter of 12 mm, which for a plenum flow rate of 500 mL/min corresponds to a Reynold's number of 60 (laminar flow), and a development length (0.06 × Reynold's number × tube diameter) of 43 mm, which is smaller than the mixing tube length of 250 mm. The fraction of aerosol entering the mixing tube that deposits due to sedimentation in the mixing tube, f_{sed}, was thus calculated according to the equation for laminar, Poiseuille flow [559],

$$f_{sed} = \frac{2}{\pi}\left[2\sqrt{1-\kappa^{\frac{2}{3}}} - \kappa^{\frac{1}{3}}\sqrt{1-\kappa^{\frac{2}{3}}} + arcsin\left(\kappa^{\frac{1}{3}}\right)\right] \quad \text{(D.1)}$$

in which [559],

$$\kappa = \frac{3}{4}\frac{v_s}{v_{tube}}\frac{L}{D} \quad \text{(D.2)}$$

where v_s is the settling velocity, v_{tube} is the velocity in the tube, L is the length of the tube, and D is the diameter of the tube. Note that calculation using equations for well-mixed plug flow gave a similar result, and diffusional deposition was calculated to be negligible using equations given by Finlay [559]. Also note that a droplet size of 2.7 μm results in a match of sedimentation deposition in the mixing tube to experimental tryptophan results, which is similar but a bit smaller than the 3.1 μm mass median aerodynamic diameter specified in the manufacturer pamphlet and

much smaller than measured at the exit of a T-piece by laser diffraction [536]. The 2.7 µm value was used for generating the curve in Figure D.3. The fraction of aerosol exiting the mixing tube that deposits in the back plenum, $f_{imp,2}$, was assumed based on initial data and a curve characterizing how it changes with flow rate was formed. The fraction of aerosol entering the nosepieces that convects by the noses of the mice, f_{conv}, was calculated according to

$$f_{conv} = 1 - \frac{\#mice \times Q_{1\ mouse} \times \frac{t_{inh}}{t_{exh}}}{Q_{plenum}} \tag{D.3}$$

where $\#mice$ is the number of mice (12 in this case), $Q_{1\ mouse}$ is the inhalation flow rate of one mouse, $\frac{t_{inh}}{t_{exh}}$ is the ratio of time a mouse spends inhaling to exhaling, and Q_{plenum} is the air flow rate into the plenum. Then, the total fraction of aerosol not inhaled by the mice, f_{tot}, was calculated according to

$$\begin{aligned} f_{tot} = f_{imp} + \left(1 - f_{imp}\right) \times f_{sed} + \left(1 - \left(f_{imp,1} + \left[\left(1 - f_{imp}\right) \times f_{sed}\right]\right)\right) \\ \times f_{imp,2} \\ + \left[1 - \left(\left(1 - \left(f_{imp,1} + \left[\left(1 - f_{imp}\right) \times f_{sed}\right]\right)\right) \times f_{imp,2}\right)\right] \\ \times f_{conv} \end{aligned} \tag{D.4}$$

The results are plotted in Figure D.3. Note that one mouse inhales 1/12 of the available aerosol. This model is not meant for quantitative purposes but rather for a qualitative illustration of how deposition may vary with plenum flow rate, in particular demonstrating changing the flow rate would not substantially change the amount of aerosol the mice inhale. Increasing the amount of aerosol the mice inhale is difficult as, for example, if less aerosol deposits in the first plenum, more aerosol will deposit in the mixing tube and back plenum and convect by the mice.

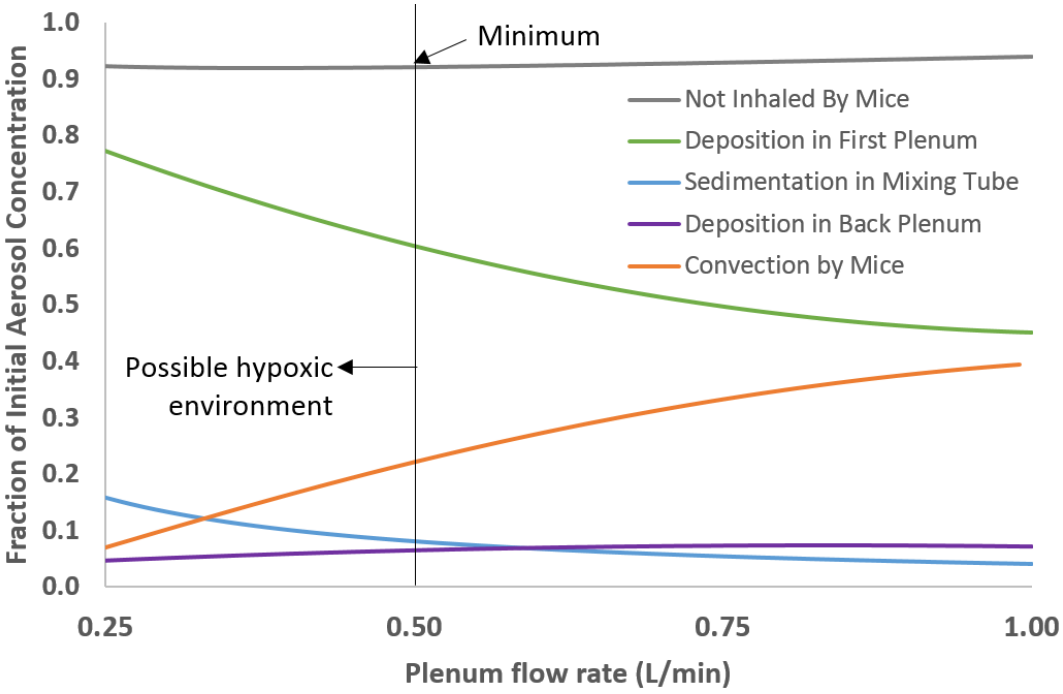

Figure D.3: Approximations of deposition within different areas of the plenum and the fraction of aerosol convecting and not inhaled by the mice.

Further NOID modifications that could be implemented

Further optimization of the NOID design and development of a better high titer phage purification process may help increase the amount of phage aerosol reaching the lungs of mice and enhance efficacy of protection. Note that not every phage will remain active to a greater extent with a vibrating mesh nebulizer as compared to a jet nebulizer, and hence the optimal NOID design may be phage-specific. Further design iterations may involve desiccation towers to decrease aerosol size and impaction in the first plenum (noting that mice don't like inhaling dry air) [560], a honeycomb design to deliver laminar air flow through the device from the bottom of the first plenum to decrease settling or delivering the aerosol upwards from the bottom of the device, the use of multiple nebulizers to deliver more phage per unit time, the use of more mice to allow for higher flow rates that potentially lower upstream deposition, the use of higher titer phage preparations or the use of a more purified lysate such that dilution into saline is not required to eliminate mesh clogging, the use of a nebulizer producing smaller aerosol droplets, potentially delivering the aerosol directly into a circular plenum with noseports [561-563], training the mice to remain in the restraint tubes for longer periods of time [564], and computational fluid dynamics to better understand the effects of design changes on aerosol deposition within the device. Furthermore, in-line droplet sizing and biologic viability in NOIDs is possible [560,564-567], and sizing of the TB aerosol and the D29 aerosol at the location the mice inhale may help determine whether similar deposition patterns in the lungs are expected. The D29 aerosol size at the location of inhalation could potentially be adjusted to be the same size as the TB aerosol at the location of inhalation, to increase the chance the phage come into contact with the TB bacteria in the lungs; however, a controlled amount of incomplete particle evaporation would be difficult with a polydisperse aerosol, and coughs generally produce a wide droplet size distribution [568]. It would be necessary to check whether the additional evaporation leads to phage inactivation at the air-liquid interface. Switching to rats or guinea pigs rather than mice would allow for higher plenum flow rates to be safely used.

Delivery of dry powder phage D29 aerosol to mice

Rather than nebulization, a potential alternative for delivering active phage is via a dry powder inhaler. A nose-only exposure system for dry powder has been developed and uses a rotating brush generator to disperse the aerosol into the device [569], and the present NOID could be modified in a similar manner. A commercial option termed PreciseInhale is also available from Inhalation Sciences (Sweden). The use of atmospheric spray freeze drying with trehalose and mannitol excipients has been explored for the production of phage D29 powder [570]. Additionally, my recent study demonstrated that phage D29 can be spray dried to a powder titer of 6.7 log(pfu/mg) using trileucine and trehalose as excipients [547; Appendix A]. At this titer, ~8 mg of powder would need to be delivered to the lungs of a mouse to achieve 1 pfu/alveolus, which is a large amount considering the rather large size of spray dried powders for deep lung deposition in mice, the low delivery efficiency, the labour and materials required to generate high titer lysate, the high cost of trileucine, and the 3 mg/L aerosol concentration maximum at the noseports to prevent suffocation. Further work to increase powder titer, e.g. by not requiring dilution of the lysate during the formulation step, may result in this also becoming a viable option. Measuring the titer during particle size measurements could be difficult since some phage have been demonstrated to be inactivated by silicone grease used to mitigate particle bounce [571].